Dissertation

submitted to the
Combined Faculties for the Natural Sciences and for Mathematics
of the Ruperto-Carola University of Heidelberg, Germany
for the degree of Doctor of Natural Sciences

Presented by
Diplom-Biologin Caroline Berger
born in Karlsruhe

Oral examination:

Blockade of endothelial Notch signaling in cellular systems and adult mice

Referees:

Prof. Dr. rer. nat. Ilse Hofmann

Prof. Dr. med. vet. Hellmut Augustin, PhD

The presented work was performed between October 2008 and December 2012 at the Joint Research Division Vascular Biology of the German Cancer Research Center Heidelberg (DKFZ) and the University Hospital Mannheim (UMM) at the Center for Biomedicine and Medical Technology Mannheim (CBTM).

1. I hereby declare that I have written the submitted dissertation myself and in this process have used no other sources or materials than those expressly indicated.
2. I hereby declare that I have not applied to be examined at any other institution, nor have I used the dissertation in this or any other form at any other institution as an examination paper, nor submitted it to any other faculty as a dissertation.

Heidelberg, 13. November 2012,

.....
Signatur

Danksagung

Ich möchte mich bei allen bedanken, die zum Gelingen dieser Arbeit beigetragen haben.

Großer Dank gilt Prof. Dr. Ilse Hofmann und Prof. Dr. Hellmut Augustin, die sich bereiterklärt haben, meine Arbeit wissenschaftlich zu begleiten und es mir ermöglicht haben, an der Ruprecht-Karls-Universität Heidelberg zu promovieren. Danke!

Ein besonderer Dank gilt meinem Betreuer Dr. Andreas Fischer, der mir und meinem Projekt stets wissenschaftlich zur Seite stand und maßgeblich zur stetigen Weiterentwicklung meines Projektes beigetragen hat.

Danke an meine motivierten Kollaborationspartner für eure Expertise: Dr. Philipp Koch, Prof. Dr. Sergej Goerdt, Dr. Jihong Lin, Prof. Dr. Hans-Peter Hammes, Dr. Carolin Mogler, Dr. Alexander Schering, Tjeerd Sijmonsma und Prof. Dr. Stephan Herzig.

Mein Dank gilt auch dem Stipendienprogramm des GRK880, welches mich während meiner Dissertation wissenschaftlich begleitet und zu meiner wissenschaftlichen Weiterbildung maßgeblich beigetragen hat, und dessen Organisator Prof. Dr. Hans-Peter Hammes, der für mich immer ein motivierender und interessierter Ansprechpartner war.

Vielen Dank an alle Gruppenmitglieder der Vaskulären Biologie sowie der Vaskulären Onkologie und Metastasierung für eure zahlreichen wissenschaftlichen Hilfestellungen und konstruktive Kritik, welche zum Gelingen der Arbeit beigetragen haben. Danke an Dr. Andreas Fischer, Dr. Alexander Schering und Dr. Daniel Epting für das Korrekturlesen meiner Arbeit.

Ein besonderer Dank gilt dem gesamten Funky Bunch der Arbeitsgruppe Fischer. Danke Anja, Anja2, Elle, Gerald, Gordian, Jen, Jossi, Julian, Markus, René, Steffi und Sven. Ihr wart von Anfang an mehr als nur Kollegen. Die Zeit mit euch bleibt unvergesslich!

Zudem danke ich meinen Freunden, die mir neben der Arbeit stets Auftrieb gegeben haben und immer ein offenes Ohr hatten. Ein besonderer Dank gilt meiner Familie, die mich unentwegt bestärkt hat und auf die ich immer zählen kann!

Für meine Eltern

Contents

Zusammenfassung

Angiogenese ist ein grundlegender Prozess während der Embryonalentwicklung, bei Entzündungsreaktionen und der Wundheilung. Die Entstehung neuer Gefäße wird von Proteinen der VEGF- und der Notch-Familie gesteuert. Störungen der präzise abgestimmten Kommunikation zwischen der Notch- und der VEGF-Signalkaskade haben die Entstehung eines nicht funktionellen vaskulären Netzwerkes zu Folge und tragen maßgeblich zum Krankheitsverlauf von Atherosklerose und Tumorwachstum bei. Eine Blockade der Notch Signaltransduktion durch niedermolekulare Hemmstoffe oder DLL4-spezifische Antikörper verringert die Perfusion von Tumoren und führt zu einer Hemmung des Tumorwachstums in Versuchstieren.

Das Ziel dieser Studie war es, einen besseren Einblick in die komplexe Funktion der Notch Signalkaskade im Endothel zu gewinnen. Um dieses Ziel zu erreichen, wurden kurze lösliche Peptide hergestellt, ausschließlich bestehend aus der jeweiligen Interaktionsdomäne von Notch-Liganden mit ihrem Rezeptor. Zudem wurden die Auswirkungen einer Deletion der endothelialen Notch-Signaltransduktion in adulten Mäusen untersucht.

Die Behandlung von endothelialen und myogenen Zellen mit den löslichen DLL1-, DLL4- und JAG1-Liganden sowie dem löslichen NOTCH1-Rezeptor hatte eine Blockade des Notch-Signalweges zur Folge. Alle löslichen Liganden übten pro-angiogene Effekte *in vitro* aus. Die Wirkungen der DLL1- und DLL4-Liganden waren deutlich effektiver als die des JAG1-Liganden und führten zu einer gesteigerten Aussprossung von Blutgefäßen während der Gefäßentwicklung in der Retina neugeborener Mäuse. Die Behandlung von Endothelzellen mit löslichem NOTCH1-Rezeptor reduzierte die Aussprossung neuer Blutgefäße *in vitro,* wohingegen die Anwendung *in vivo* eine gesteigerte Aussprossung von Blutgefäßen in der Retina zur Folge hatte. Die löslichen Liganden agierten somit als Kompetitoren um endogen exprimierte membranständige Rezeptoren. Die löslichen Rezeptoren hingegen unterbanden die Notch-Signaltransduktion, indem sie verschiedene Liganden blockierten.

Untersuchungen von genetisch veränderten Mäusen mit endothelspezifischem Verlust der Notch-Signalkaskade wurden durchgeführt. Ein Verlust dieser endothelialen Notch-Signalaktivität in Mäusen hatte bereits nach wenigen Monaten die Entstehung einer Kardiomyopathie zur Folge und resultierte nach einem Jahr in der Entstehung vaskulärer Tumore. Der Verlust der endothelialen Notch-Signalaktivität in einem ApoE-defizienten Hyperlipidämiemodell führte zu einer Verbesserung der Glukosetoleranz, verursachte jedoch die Entstehung einer Steatohepatitis. Demzufolge konnte die Notch-Signaltransduktionskaskade in ausgereiften Blutgefäßen als entscheidender Regulator der Organhomöostase sowie des Glukose- und Fettmetabolismus identifiziert werden.

Summary

Angiogenesis is a fundamental process during embryogenesis, inflammation and wound healing. The formation of new vessels is coordinated by proteins of the VEGF and the Notch signaling cascades. Dysfunction of the precisely balanced crosstalk between Notch and VEGF signaling entails the formation of a non-functional vascular network. These imbalances play a critical role during progression of many diseases including atherosclerosis and tumor growth. Blocking of Notch signaling, by small molecule inhibitors or DLL4-specific antibodies, perturbs tumor perfusion and inhibits tumor growth in animal models.

This study aimed to gain deeper insight into the complex function of Notch signaling in the endothelium. For this purpose, small soluble Notch ligand and receptor peptides were generated, which consist of the respective interaction domains only. Furthermore, the effects of deleting endothelial Notch signaling in adult mice were investigated.

Application of the designed soluble DLL1, DLL4, and JAG1 ligands, as well as, the soluble NOTCH1 receptor blocked Notch signaling in endothelial and myogenic cells. All soluble ligands consistently exerted pro-angiogenic effects *in vitro*. The effects of DLL1 and DLL4 were markedly stronger than that of the JAG1 ligand and could also evoke elevated sprouting angiogenesis in the retina of newborn mice. Treatment with the soluble Notch receptor reduced endothelial sprouting *in vitro*. However, *in vivo* application of soluble NOTCH1 receptor protein resulted in increased retinal sprouting with elevated numbers of tip cells. Thus, the soluble ligands suppressed Notch receptor activity by acting as competitors for endogenous membrane-bound ligands; whereas the soluble receptor acted as a decoy for the different Notch ligands.

Genetic studies with adult mice after endothelial-specific deletion of Notch signaling were performed. These mice developed cardiomyopathy within a few months; whereas vascular tumors developed after one year. In an ApoE-deficient model of hyperlipidemia, the deletion of endothelial Notch signaling improved the glucose tolerance of mice, but caused development of steatohepatitis. Thus, Notch signaling in the adult vasculature could be identified as a critical regulator of organ homeostasis as well as glucose and fat metabolism.

Abbreviations

α	Anti
ƛ	Wavelength
µ	Micro
AGS	Allagile syndrome
Ang	Angiopoietin
APS	Ammonium persulfate
bp	Base pair(s)
BrdU	Bromodeoxyuridine
BSA	Bovine serum albumin
CADASIL	Cerebral autosomal dominant arteriopathy with subcortical infarcts and leukoencephalopathy
CAR	coxsackie and adenovirus receptor
cDNA	Copy-DNA
CMV	Human cytomegalovirus
CO_2	Carbon dioxide
COUP-TFII	Orphan nuclear receptor
ctrl	Control
DAPT	*N*-[(3,5-Difluorophenyl)acetyl]-L-alanyl-2-phenyl]glycine-1,1-dimethylethyl ester
DLL1	Delta-like 1
DLL4	Delta-like 4
DMEM	Dulbecco's Modified Eagle Medium
DMSO	Dimethyl sulfoxide
DNA	Deoxyribonucleic acid
dsDNA/RNA	Double stranded DNA/RNA
dNTP	Equal molar mix of the decoy-nucleotides dATP, dCTP, dGTP and dTTP
DSL	Delta/Serrate/Lag2 domain; common domain of Notch ligands
DTT	1,4-Dithiothreitol
E	Embryonic day of development
EC	Endothelial cell
ECBM	Endothelial Cell Basal Medium
ECGM	Endothelial Cell Growth Medium
ECL	Enhanced chemiluminescence solution; detection reagents for western blots
ECM	Extracellular matrix
EDTA	Ethylenediaminetetraacetic acid
ELISA	Enzyme-linked immunosorbent assay

EPC	Endothelial precursor cells
EtOH	Ethanol
Fc	Fc portion of human IgG1
FCS	Fetal calf serum
FGF	Fibroblast growth factor
g	Constant of the gravity of earth; acceleration that the earth imparts to objects near its surface; 9,81 m * $s^{-}1$
FITC	Fluorescein thioisocyanate
GAPDH	Glyceraldehyde 3-phosphate dehydrogenase
GFP	Green fluorescent protein
H&E	Hematoxylin and eosin, dyes for histological staining
HCl	Hydrochloric acid
Hek293	Human embryonic kidney 293 cell(s)
HIF	Hypoxia-inducible factor
HUVEC	Human umbilical cord venous endothelial cells
H_2O	Water
HPRT	Hypoxanthine-guanine phosphoribosyltransferase
HRP	Horse radish peroxidase
HUAEC	Human umbilical arterial endothelial cell
HUVEC	Human umbilical vein endothelial cell
ICD	Intracellular domain
Ig	Immunoglobulin
IgG	Immunoglobulin G
IP	Immunoprecipitation
JAG1	Jagged-1
LSEC	Liver sinusoidal endothelial cells
M	Molar; Mol * $Liter^{-1}$
MACS	Magnetic cell separation
MOI	Multiplicity of infection
M_r	Molecular mass, measured in g/mol
mRNA	Messenger RNA
NLS	Nuclear localization sequence
NO	Nitric oxide
NP40	Nonidet P-40
Nrp	Neuropilin
O_2	Oxygen
ON	Over night
OD	Optical density

P	Probability-value
PAGE	Polyacrylamide gel electrophoresis
PBS	Phosphate buffered saline; phosphate buffer
PBS-T	Phosphate buffered saline with 0.05 % Tween 20
PCR	Polymerase chain reaction
PDGFB	Platelet derived growth factor
PDGFR	Platelet-derived growth factor receptor-B
PEI	Polyethyleneimmine, a transfection reagent
PFA	Paraformaldehyde
Pfu	Pyrococcus furiosus; thermophilic bacterium, source of thermostable DNA polymerase
PFU	Plaque forming units; measure of viral plaques
pH	Negative decimal logarithm of the hydrogen ion activity in a solution
PIGF	Placental growth factor
P/S	Penicillin/Streptomycin (antibiotics supplement for cell culture media)
PVDF	Polyvinylidene fluorid
qPCR	Quantitative Realtime PCR
RBP-J	Recombining binding protein suppressor of hairless
RIPA	Radioimmuno-precipitation assay lysis buffer
RNA	Ribonucleic acid
RNase	Ribonuclease
rpm	Revolutions per minute
RPMI	Roswell Park Memorial Institute Medium
RT	Room temperature
RT-PCR	Reverse transcriptase PCR
SDS-PAGE	Sodium dodecyl sulphate polyacrylamid gel electrophoresis
siRNA	Small interfering RNA
SI	Système International d'Unités; International System of Units
SMA	Smooth muscle actin
SMC	Smooth muscle cell(s)
ssDNA/RNA	Single stranded DNA/RNA
stdev	Standard deviation
TAE	Tris-EDTA-acetic acid buffer
Taq	Thermus aquaticus; thermophilic bacterium, source of thermostable DNA polymerase
TBS-T	Tris-Buffered Saline with 0.05 % Tween 20
TGFß	Transforming growth factor-ß
Tie	Tyrosine kinase with immunoglobulin and epidermal growth factor (EGF) homology domains
TNFα	Tumor necrosis factor alpha

TRIS	Tris(hydroxymethyl)-aminomethane
Triton X-100	[4-(1,1,3,3-Tetramethylbutyl)-phenol]ethoxylate
Tween 20	Polysorbate 20, polyoxyethylen(20)-sorbitan-monolaurate
U	Voltage
VE-cadherin	Vascular endothelial cadherin
VEGF	Vascular endothelial growth factor
VEGFR	Vascular endothelial growth factor receptor
v/v	Volume fraction per volume
w/v	Mass fraction per volume

Units

A	Ampère, SI base unit of electric current
°C	Degree celsius, unit of measurement for temperature
Da	Dalton, atomic mass unit
g	Gram, SI derived unit of mass
h	Hour, unit of time
m	Meter, SI base unit of length
M_r	Molecular mass, measured in g/Mol
min	Minute, unit of time
mol	Mol, SI base unit of the amount of substance
s	Second, SI base unit of time
S	Svedberg, unit of sedimentation coefficients (technically a measure of time, $1S=10^{-13}$ s)
U	Enzyme unit; the amount of enzyme that is needed to catalyze the conversion of 1 µmol substrate per minute under standard conditions
V	Volt, SI derived unit for absolute electric potential

1. Introduction

1.1 The vascular system

The vascular system in vertebrates consists of a complex network of branched tube-like blood and lymphatic vessels. These vessels regulate the exchange of gases, transport of nutrients, immune cells and other signaling cues between tissues distant organs. Blood and lymphatic vessels are formed by endothelial cells (ECs). ECs line the inner surface of blood and lymphatic vessels and exert unique functions, including inter-cellular communication, active participation in vascular homeostasis and molecular regulation. The formation of these vessel networks is highly dependent on the interaction of intra- and inter-cellular mechanisms such as migration, adhesion, differentiation and proliferation. The development of several diseases including tumor angiogenesis during cancer progression is due to aberrant regulation of such physiological mechanisms (Adams and Alitalo, 2007; Michiels, 2003).

The lymphatic system consists of blind-ended lymphatic capillaries, larger vessels and lymph nodes. It supports the immune system and controls the removal of waste products, pathogens or cellular debris as well as the absorption of lipids and fat-soluble vitamins from the digestive tract. The lymphatic vascular network develops after the formation of the blood vasculature and carries lymph originating from extravasated blood plasma into the tissue, unidirectional toward the neck. Lymph enters the blood circulation through the large lymphatic vessel, the thoracic duct, and forms a link between both vascular networks (Adams and Alitalo, 2007).

The cardiovascular system is formed during early embryonic development. Blood is transported from the heart through arteries and smaller arterioles into small capillaries. A close network of capillaries enables the cellular exchange of molecules and metabolic products. Since the cardiovascular system is a circulatory system, oxygen-depleted blood is transported through small venules and larger veins back to the heart. The oxygen-depleted blood is then transported from the heart to the lung for oxygen enrichment.

The structure of arteries is adapted to high pressure. The inner layer of mature arteries, called *tunica intima*, forms the vessel lumen and consists of ECs surrounded by elastic tissue. ECs are covered by one or more alternating layers of vascular smooth muscle cells (vSMCs), called *tunica media*, which provide stability of the arterial blood vessels. The outer *tunica externa* consists of one or more layers of connective tissue (Cleaver and Melton, 2003) (Figure 1, A). Veins have less vSMC in their *tunica media.* Furthermore, venous valves prevent a back flow of blood that constitutes a unique feature of veins.

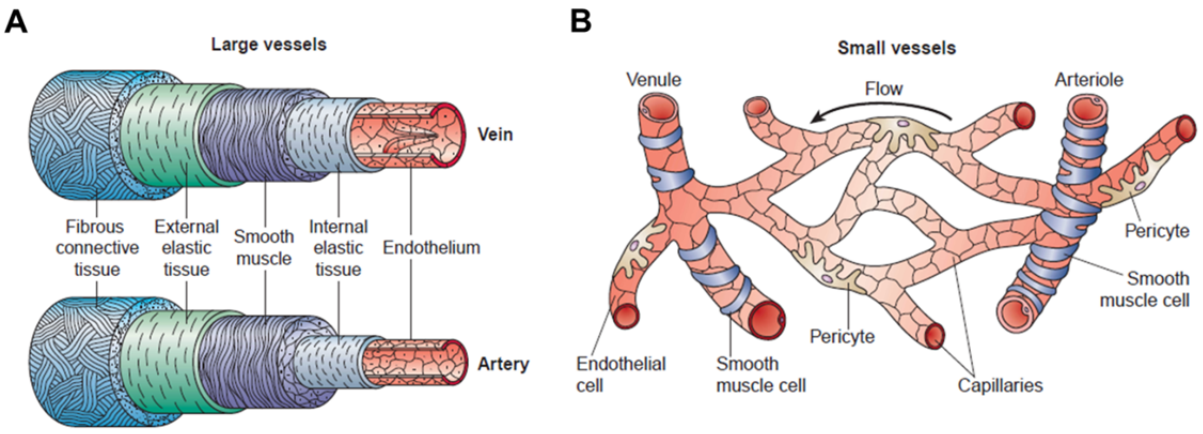

Figure 1: Structure of blood vessels

(A) The wall of arteries and veins consist of the *tunica intima* (EC lining, basement membrane and internal elastic layer), followed by the *tunica media* (layers of vSMC). The *tunica media* is thicker in arteries than in veins. The outer layer, the *tunica externa,* consists of connective tissue with collagenous and elastic fibers. (B) Venules, arterioles and capillaries are small vessels with a thin vascular wall and display partial coverage by mural cells, pericytes or vSMCs. Reprinted by permission from Macmillan Publishers Ltd: Nature Medicine (Cleaver and Melton, 2003), copyright (2003).

Small capillaries located at the transition from arteries to veins are sparsely covered by pericytes (Figure 1, B). The capillary wall and the lining of blood vessels by ECs display high morphological and functional heterogeneity and thus is categorized as continuous, discontinuous or fenestrated endothelium. In addition, further criteria such as shape, orientation and adhesion between ECs are used to classify these categories in detail. Depending on the particular tissue, smaller capillaries show endothelial phenotype variability. Capillaries in muscle and lung have a continuous endothelial lining without openings in the vascular wall. Intestinal capillaries, on the other hand, display a fenestrated phenotype characterized by gaps, which are covered by a permeable diaphragm of radially oriented fibrils, allowing an exchange of macromolecules. However, the basement membrane is still continuous in fenestrated capillaries. Capillaries having many fenestrations without diaphragm and a discontinuous basement membrane are grouped as discontinuous endothelium, also referred to as sinusoids. In the liver, hepatic sinusoids regulate detoxification and mediate metabolite exchange.

Beside structural differences, arteries and veins can be further distinguished by differences in their gene expression pattern, which already exist before the first blood flow starts (Roca and Adams, 2007). The Delta-Notch signaling pathway was identified as a key player of the arterial fate (section 1.1.3). Thus, early embryonic endothelial cells are already committed to the venous or arterial fate by a genetic program. Beside molecular distinctions, epigenetic factors such as blood pressure were shown to be involved in the determination of arteriovenous patterning.

1.1.1 Blood vessel formation

During embryonic development, the formation of blood vessels includes two major processes: vasculogenesis, defined as *de novo* formation of vessels, and angiogenesis, defined as growth of new capillary vessels from preexisting ones (Risau, 1997). Vasculogenesis is restricted to embryonic development and the first major vessels are formed *de novo* from endothelial precursor cells (EPCs) known as angioblasts. Most angioblasts derive from mesodermal cells, which are progressively restricted to the endothelial cell lineage in response to signaling molecules such as fibroblast growth factor (FGF2) and vascular endothelial growth factor (VEGF). Some ECs may be derived from bipotent hemangioblasts, which can differentiate into angioblastic cells or hematopoietic cells. Angioblasts scatter throughout the mesoderm and start to form small aggregates. The aggregates merge into cords and angioblasts subsequently differentiate into ECs (Figure 2, A). ECs are connected by adherens, gap and tight junctions. The vascular cords start to acquire a luminal structure and form the primary capillary plexus (Conway et al., 2001; Kurz et al., 1996).

The primary vascular network undergoes extensive remodeling in a process called angiogenesis, which completes the circulatory connections formed during vasculogenesis (Adams and Alitalo, 2007). During angiogenesis, the vascular wall of primitive blood vessels is structurally stabilized by mural cells, vSMCs for larger vessels and single pericytes around smaller vessels. During sprouting angiogenesis, ECs migrate towards the source of a pro-angiogenic stimulus and subsequently start to proliferate to form new lumenized blood vessels that connect neighboring vessels (described in detail in section 1.1.2) (Figure 2, B). In contrast, intussusceptive angiogenesis splits an existing single vessel in two parallel vessels by extending the capillary wall into the vessel lumen (Figure 2, B). Opposing capillary walls protrude into the lumen of a vessel and build an inter-endothelial zone of contact. Perforation of the endothelial bilayer as well as the basement membrane allows the invasion of growth factors or cells such as fibroblasts leading to the formation of a pillar in the vessel that enlarges over time and finally splits the vessel into two (Burri et al., 2004). A new biomechanical hypothesis of angiogenesis in the adult organism, called looping angiogenesis, describes a directed translocation of preexisting and functional blood vessels by biomechanical forces to sites of injury or tissue remodeling in situations with urgent need of fast revascularization. Thereby, myofibroblasts mediate a contraction of the extracellular matrix thus inducing a relocation of preexisting vessels closer to the avascular area in response to the mechanical stress (Benest and Augustin, 2009; Kilarski et al., 2009).

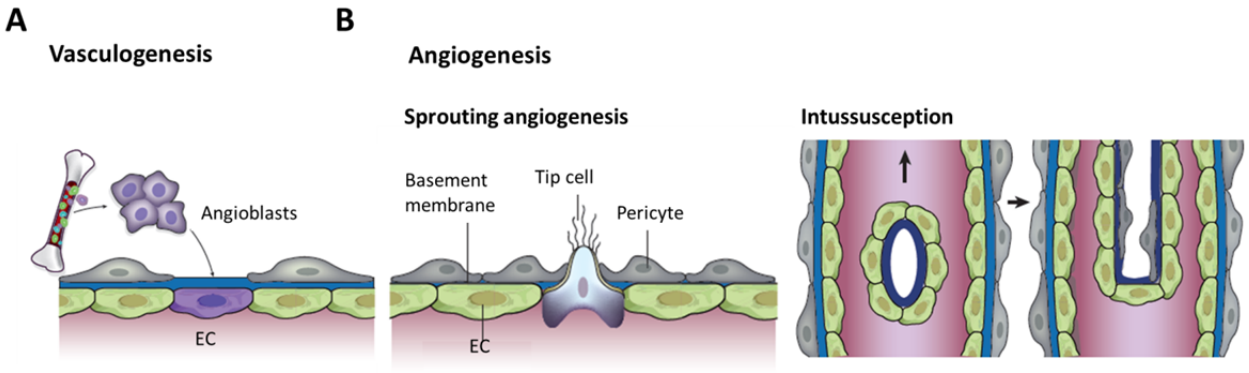

Figure 2: Mechanisms of blood vessel formation
(A) Angioblasts are recruited from the bone marrow and differentiate into ECs, which gives rise to a primary vascular network. (B) The vascular network is processed during angiogenesis by formation of new vessels from preexisting ones (sprouting angiogenesis) or splitting of an existing vessels into two (intussusception). Modified by permission from Macmillan Publishers Ltd: Nature Medicine (Carmeliet and Jain, 2011), copyright (2011).

1.1.2 Sprouting angiogenesis

During embryonic development, sprouting angiogenesis of blood vessels is induced by an inadequate supply of oxygen of distant avascular tissues and organs (Semenza, 2008). In response to hypoxia, cells accumulate the oxygen-sensitive hypoxia-inducible factor 1-alpha (HIF1α), which initiates subsequent expression and secretion of pro-angiogenic molecules including VEGF, angiopoietin-2 (ANG-2), fibroblast growth factor (FGF) and placental growth factor (PlGF) (Pugh and Ratcliffe, 2003).

The VEGF signaling pathway is the most important molecular regulator of sprouting angiogenesis. The five VEGF ligand family members (VEGF-A to -D, and the placental growth factor (PlGF)) interact differentially with corresponding cell surface receptor tyrosine kinases, VEGFR-1, VEGFR-2 and VEGFR-3 (Dixelius et al., 2003). VEGF-A, simply referred to as VEGF, interacts with VEGFR-2 and was reported to be the main regulator of sprouting angiogenesis (Ferrara et al., 2003).

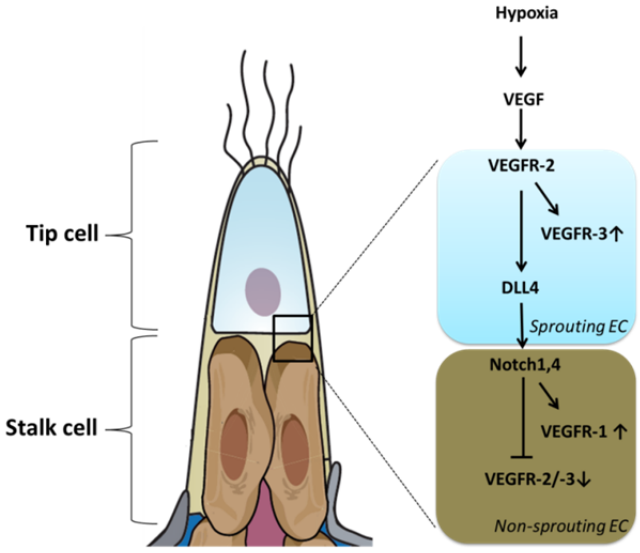

Figure 3: Tip cell selection and molecular control
VEGF/VEGFR-2 signaling initiates the selection of an endothelial tip cell. VEGF signaling in the tip cell causes an increased expression of VEGFR-3 and DLL4. Signaling of DLL4 through NOTCH receptors expressed in adjacent stalk cells causes a downregulation of VEGFR-2 and VEGFR-3 expression, thus maintaining the stalk cell phenotype. Notch-induced VEGFR-1 expression competes with VEGFR2-induced signaling in the stalk cell. Modified from Carmeliet and Jain, 2011, with permission.

Sprouting angiogenesis is initiated by VEGF-induced selection of one EC, so called tip cell, which is located close to the VEGF source (Carmeliet and Jain, 2011). Tip cells are lumenless highly motile cells at the front of a sprout and guide the developing sprout towards the angiogenic stimulus (Gerhardt et al., 2003). The cells are characterized by long filipodial extensions, which induce movement of the tip cell towards the stimulus. These filopodia anchor the cytoskeleton to focal points of the extracellular matrix followed by contraction of intracellular stress fibers (De Smet et al., 2009). Hypoxia-induced VEGF/VEGFR-2 signaling leads to activation of intracellular signaling cascades such as mitogen activated protein kinase (MAPK) and phosphatidyl-inositol-3 kinase (PI3K) but furthermore induces the expression of VEGFR-3 as well as DLL4, a transmembrane ligand of the Notch signaling pathway. VEGFR-3 expression facilitates fusion of vessels by downregulation of VEGFR-2. DLL4-induces activation of the NOTCH-1 or -4 receptor on neighboring cells called stalk cells. Stalk cells then proceed to downregulate VEGFR-2 and VEGFR-3 expression thereby making them less susceptible to VEGF and suppressing the sprouting phenotype (Figure 3) (Gerhardt et al., 2003; Phng and Gerhardt, 2009). Additionally, VEGFR-1 expression is enhanced in stalk cells. Thus, VEGFR-1 competes with the remaining VEGFR-2 for VEGF and thereby competitively inhibits the VEGFR-2 downstream pathway (Figure 3). The transient migratory, exploratory phenotype of the tip cell is thereby perpetuated. Thus, Delta-Notch signaling between tip and stalk cells constricts the number of migrating tip cells in order to prevent the formation of a disorganized vascular network. Initiation of sprouting angiogenesis by VEGF-induced tip cell selection is additionally influenced by several pro-angiogenic molecules regulating matrix remodeling, pericytes detachment, loosening of cell-cell junctions and permeability to enable sprout formation (Figure 4, A). Nevertheless, it has been shown that the formation of tip and stalk cells act dynamically and thus, the invasive nature of a tip cell represents only a transient state, which is induced and maintained by VEGF, but can be reverted when cells start to connect and build up new vessels (Leslie et al., 2007).

Elongation of a sprout is mediated by stalk cells, which are highly proliferative cells, connected by adherens and tight junctions to ensure the integrity of new vessels. Furthermore, establishment of luminal polarity followed by basal lamina deposition and mural cell recruitment stabilizes the new vessels (Figure 4, B) (Dejana et al., 2009). Lumen formation in elongated sprouts occurs by fusion of growing vacuoles of a single EC with vacuoles of adjacent cells. It was also reported that stalk cells start to polarize by which the apical sides lose their adhesion or even reject the opposing cells to create a luminal space (Strilic et al., 2009). Another hypothesis claims that budding of endothelial cells from existing vessels maintains the original lumen of the vessel (Figure 4, B) (Lubarsky and Krasnow, 2003).

Sprout formation and elongation is followed by a second crucial step towards the formation of a functional vascular network, the vessel anastomosis. Fusion of vessels occurs when tip cells of sprouting vessels come in close contact and fuse to create a new circuit that expands the existing vascular network.

The fusion process is mediated by tissue macrophages bridging neighboring tip cells and thus acting as cellular chaperones (Ruhrberg and De Palma, 2010). During fusion of the tip cells of two sprouts a gap is formed at the point of contact. Cells reorganize to enable fusion of the vessel lumens to ensure blood flow (Figure 4, C) (Herwig et al., 2011). The formation of a single one new tip cell is achieved by DLL4-Notch mediated lateral inhibition. The tip cell, having elevated expression of DLL4, is selected as the new tip cell and the angiogenic sprouting process starts anew.

After establishment of the blood flow, which ensures oxygen delivery to distant tissue paracrine VEGF production is downregulated. The reduced availability of VEGF, together with the increased distance to the growing front of a sprout, leads to the formation of endothelial cells with a quiescent, immotile and non-proliferative phenotype, named phalanx cells (Mazzone et al., 2009). Phalanx cells form a tight endothelial cell monolayer and attract pericytes, which together secrete protease inhibitors to produce a basement membrane (Figure 4, D) (Carmeliet and Jain, 2011).

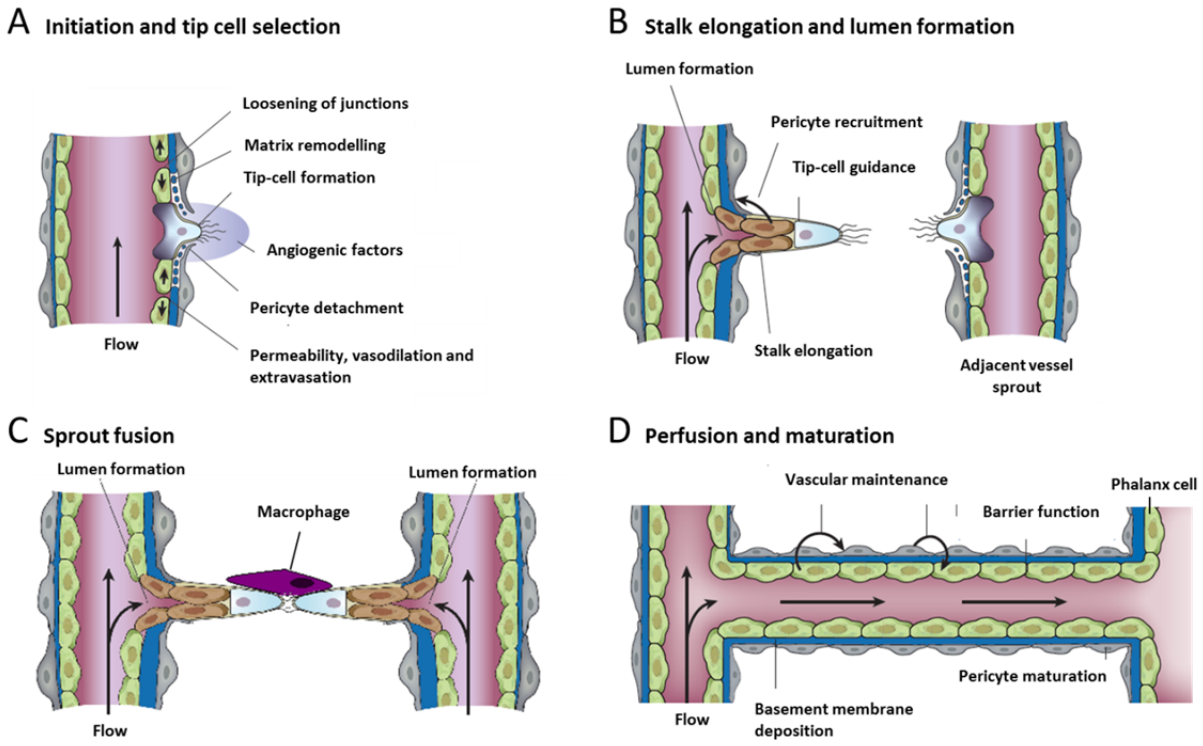

Figure 4: Steps in sprouting angiogenesis

(A) A pro-angiogenic stimulus induces the tip cell selection. Several cellular processes facilitating the migratory behavior of the tip cell: loosening of the endothelial cell-cell junctions, matrix remodeling, pericyte detachment and increased permeability. (B) Sprouts migrate towards pro-angiogenic stimuli. Elongation of the sprout is characterized by proliferation of stalk cells (brown), recruitment of pericytes and lumen formation. (C) Fusion of two sprouts is mediated by macrophages acting as bridging cells to generate a perfused vessel. (D) Stalk cells with high distance to the tip cell adopt a quiescent non-proliferative phalanx cell phenotype, which is accompanied by pericyte maturation, re-organization of junctions, basement membrane deposition, as well as, signals to maintain the phalanx cells in a quiescent state. Modified from Carmeliet and Jain, 2011, with permission.

1.1.3 Vessel maturation

Formation of a functional vessel with circulatory blood flow implies maturation processes such as differentiation of vessels in arteries or veins and stabilization of the vessels by recruitment of mural cells.
Arteriovenous differentiation is induced by high amounts of VEGF signaling through VEGFR-2 and the co-receptor neuropilin-1 (NRP1), which results in an activation of the Notch receptors through DLL4 and the expression of Notch target genes such as the transcription factors HES (hairy/enhancer of split), HEY (hairy/enhancer-of-split related with YRPW motif), and ephrin-B2 (Adams and Alitalo, 2007; Torres-Vazquez et al., 2003). Expression of the transcription factors HES and HEY strengthens the arterial cell fate by transcriptional repression of venous-specific genes (Zhong et al., 2001). Deletion of Notch components such as the ligand DLL4, the transcription factor RBP-J or Notch target genes HEY1 and HEY2 cause embryonic lethality in mice due to major defects in arterial differentiation. This emphasizes the importance of Notch signaling during arteriovenous differentiation (Fischer et al., 2004; Gale et al., 2004; Krebs et al., 2004). Members of the forkhead box transcription factor family, FoxC1 and FoxC2, further increase the DLL4 expression thus promoting the arterial cell fate (Seo et al., 2006). Determination of the venous endothelial cell fate is predominantly regulated by the nuclear orphan receptor chicken ovalbumin upstream transcription factor II (COUP-TFII) (You et al., 2005). COUP-TFII inhibits the Notch signaling cascade thereby promoting the expression of the ephrin-B2 receptor EphB4, which is a molecular marker for the venous cell fate. Beside a genetic regulation of arteriovenous identity, hemodynamic forces such as blood pressure and the direction of blood flow can additionally influence the identity of a vessel (Swift and Weinstein, 2009).

Maturation of a vessel implies the transition from an active growing stalk cell into a quiescent endothelial phalanx phenotype and requires the attachment of mural cells. Pericytes as well as vSMC are mural cells with a fibroblast-like morphology. However, it still stays controversial if pericytes and vSMC are variants and thus are interconvertible or if they derive from distinct progenitor cells. Secretion of platelet-derived growth factor B (PDGF-B) by the stalk cell attracts mural cells expressing the corresponding PDGF-B receptor (PDGFRß). Coverage of vessels with mural cells is crucial to keep ECs in a non-proliferative, quiescent state and maintain the endothelial integrity (Hellstrom et al., 2001).
Pericytes were reported to loosely cover small blood vessels and form the basement membrane of the microvasculature together with ECs. Thereby, they act as scaffolds stabilizing the structure of vessels (Mandarino et al., 1993). Pericytes interact with ECs by direct cell-cell contact and paracrine signaling (Rucker et al., 2000). Gap junctions allow the exchange of small molecules. On venous capillaries, pericytes are sparsely separated; on arterial capillaries they form a tight external cell layer supporting the endothelial inner lining. Medium-sized vessels, such as arterioles and venules, are covered with pericytes and vSMCs (Swift and Weinstein, 2009).

The lack of pericyte coverage causes hyperdilated and leaky vessels with impaired blood flow, which causes edema or even embryonic lethality (Hellstrom et al., 2001).
vSMCs prevalently cover large-diameter vessels, however venules and veins are only irregularly covered by vSMC, whereas many layers of elastic fibers and vSMCs are present in arterioles and arteries. This enables the arterial blood vessels to withstand high blood pressure (Cleaver and Melton, 2003; Swift and Weinstein, 2009). The function of vSMCs is to support blood flow by coordinated contraction and thereby facilitating tissue perfusion. Increased vSMC proliferation was reported during the process of vessel enlargement, called arteriogenesis (Schaper, 2009). In contrast to pericytes, vSMCs are not integrated into the basement membrane and do not signal directly to ECs (Gerhardt and Betsholtz, 2003).

1.1.4 Key regulatory signaling pathways during vascularization

The formation of vessels depends on a complex control system with a precise balance between pro-angiogenic and anti-angiogenic factors. Several intercellular signaling pathways have been linked to the coordinated control of vasculogenesis and angiogenesis, including the Angiopoietin/Tie receptor-, the fibroblast growth factor (FGF)-, the platelet-derived growth factor (PDGF)-, the transforming growth factor-ß (TGF- ß)-, and the vascular endothelial growth factor (VEGF) receptor pathways. During the last years, Delta-Notch signaling was added to this numeration and is described in more detail in section 1.2.

VEGF signaling

One of the most important regulators of blood vessel formation is the VEGF signaling pathway. VEGF signaling regulates cellular processes such as proliferation, migration and permeability (Bergers et al., 2000; Ferrara and Keyt, 1997). The five VEGF family members VEGF-A to -D and PlGF interact differentially with corresponding cell surface receptor tyrosine kinases, VEGFR-1, VEGFR-2, VEGFR-3 and with non-signaling co-receptors neuropilins NRP1 and NRP2 (Hoeben et al., 2004). Homo- or heterodimerization of the receptors leads to the expression of several target genes (Dixelius et al., 2003). All VEGFs participate during the angiogenic process mostly as pro-angiogenic stimuli (Adams and Alitalo, 2007).
VEGF-A is the most important key regulator during vessel formation and exists as seven homodimeric isoforms, which differ in the presence or absence of heparin-binding domains. The effects on angiogenesis are influenced by the balance of the different splice variants. VEGF signals through VEGFR-2, which has a high tyrosine kinase activity and can be weakly activated by VEGF-C and VEGF-D. VEGFR-1 has a low tyrosine kinase activity but high affinity for VEGF-A and constitutes a decoy receptor for VEGF-A. Soluble splice variants of VEGFR-1 and VEGFR-2 can inhibit VEGF-A signaling by acting as VEGF traps (Ebos et al., 2004; Kendall et al., 1996). VEGF-A/VEGFR2 interactions were reported on the one hand be the main regulator during vasculogenesis by stimulating the migration of angioblasts during the formation of blood islands and on the other hand during sprouting angiogenesis (Ferrara et al., 2003).

Sprouting angiogenesis, described in detail in section 1.1.2., is a cross-talk between VEGF and Notch signaling and acts to define and maintain the tip and stalk cell fate (Gerhardt et al., 2003). The important role of VEGF during vascularization is emphasized by the fact that VEGF null, as well as, VEGF heterozygous mice are embryonically lethal (E8.5 and E12) (Carmeliet et al., 1996; Ferrara et al., 1996).
Signaling is induced by homo- or heterodimerization of the corresponding receptors and autophosphorylation at the intracellular tyrosine residues following VEGF binding. The phosphorylated residues create a binding site for signal transduction molecules and thus causing the activation of several kinases and target genes (Dixelius et al., 2003; Hoeben et al., 2004). VEGF induced phosphorylation of VEGFR-2 causes endothelial proliferation by activation of PLCγ1, as well as, vascular permeability and cellular migration by activation of the phosphatidylinositol 3´-kinase (PI3K) (Fulton et al., 1999). Maintenance of ECs in mature blood vessels is mainly dependent on autocrine VEGF secretion to enhance cell survival. However, excessive VEGF secretion causes an activation of single ECs to induce sprouting angiogenesis and increases permeability (Ferrara et al., 2003).

PDGF signaling

Maturation of vessels is dependent on the coverage by mural cells. Growth-factors such as the TGF-β superfamily, angiopoietins and the PDGF family mediate this process (Jain and Booth, 2003). PDGFß receptor-positive pericytes are attracted by the release of PDGF-B ligand from ECs to stabilize the newly formed vessels (Gaengel et al., 2009; Hellberg et al., 2010). Loss of pericytes due to deletion of PDGF-B causes aneurisms and vascular leakage (Lindahl et al., 1997).

TGF-ß signaling

The TGF-beta superfamily consists of several molecules such as bone morphogenetic proteins (BMPs), activin, nodal and TGF-βs interacting with different receptors. Thus, TGF-ß signaling exert diverse functions during embryonic development, as well as, during homeostasis in adult tissues. TGF-ß ligands bind to heteromeric TGF-ß receptor complexes to induce the activation of different receptor-activated smad (R-smad) proteins. This initiates changes in proliferation, migration and maturation of cells. The diversity of ligand-receptor combinations, co-receptors and inhibitors makes TGF-ß signaling complex. Depending on the context, TGF-ß ligands exert pro- as well as anti-angiogenic effects. TGF-ß1 promotes the differentiation of precursor cells into mural cells, such as pericytes and vSMCs (Armulik et al., 2005; Bergers and Song, 2005; Chen and Lechleider, 2004). Deletion of different components of the TGF-ß signaling like TGF-ß1 or SMAD5 causes arteriovenous malformations in mice (Armulik et al., 2005; Bergers and Song, 2005). In humans, mutations in the HHT-1 or -2 genes, which encode endothelial receptors of the TGF-β superfamily, can cause hereditary hemorrhagic telangiectasia (HHT). HHT is an autosomal dominant vascular dysplasia characterized by nose bleeding, spidery red skin lesions and the formation of arteriovenous malformations in internal organs (Fernandez et al., 2006).

Angiopoietin-Tie signaling

The molecular communication between the endothelium and surrounding perivascular cells is mainly mediated by the Angiopoietin/Tie system. Angiopoietin/Tie signaling regulates maturation and maintenance of ECs (Benest and Augustin, 2009). The angiopoietin family consists of two tyrosine kinase receptors, TIE1 and TIE2, as well as, four growth factor ligands, ANG-1 to -4. ANG1 is secreted by pericytes, vSMCs and fibroblasts. It activates the TIE2 receptor expressed on ECs in a paracrine manner in order to induce cell survival and vessel maturation via recruitment of mural cells (Armulik et al., 2005; Eklund and Olsen, 2006; Thurston, 2003). In contrast, ANG-2 is produced by ECs and stored in Weibel Palade bodies so that it can quickly act in an autocrine manner as an antagonist of ANG-1/TIE2 signaling during angiogenesis. ANG-2-induced TIE2 activation primes endothelial cells for other cytokines during vessel destabilization. Furthermore, binding of ANG-2 to specific integrins in activated ECs with low TIE2 expression suggest a pro-angiogenic role of ANG-2 (Felcht et al., 2012).

FGF signaling

The FGF superfamily consists of highly redundant pro-angiogenic proteins which act directly on ECs expressing FGF receptors. In addition, FGF was shown to exert pro-angiogenic effects by inducing the secretion of ANG-2 and VEGF-B. Signaling of FGFs at low level is crucial to maintain endothelial quiescence in mature vessels (Murakami et al., 2008). However, elevated FGF signaling causes increased tumor angiogenesis and furthermore mediates the escape of tumors to anti-VEGF treatment (Bergers and Hanahan, 2008).

Guidance signals

Sprouting angiogenesis makes use of several attractive and repulsive guidance cues, which are also involved in the navigation of axons. The repulsive action of EphrinB4 and its ligand ephrin-B2 cause a segregation of ephrin-B2-positive arterial and EphrinB4-positive venous cells during vasculogenesis and thus represent a crucial event in the isolation of arteries and veins (Herbert et al., 2009). Moreover, the ephrin signaling pathway was shown to cooperate with VEGF signaling during vessel guidance. EphB4-induced reverse signaling through ephrin-B2 ligand, which is expressed in the tip cell, induces an internalization of VEGFR-2 and thus exert pro-angiogenic effects including proliferation, migration and cell survival (Sawamiphak et al., 2010).

Neuropilins (NRP) and its soluble or membrane-bound semaphorin ligands diverge in their effect on angiogenesis. SEMA3A and SEMA3B were shown to exert repulsive effects on angiogenic sprouts, whereas SEMA3C exerts attractive effects (Carmeliet and Jain, 2011). Secreted netrin proteins were reported to elicit attractive effects on the navigating sprout after binding to receptors of the DCC (deleted in colorectal cancer) family. Yet, they promote repulsive effects after interaction with receptors of the Unc5 (uncoordinated-5) family. The Unc5b receptor is expressed in endothelial tip cells. *Unc5b* deficiency causes increased endothelial sprouting during vascular growth (Lu et al., 2004).

Retraction of vessels could also be observed for interactions between secreted SLIT proteins with ROBO (roundabout) receptors (Carmeliet and Jain, 2011). Signaling pathways such as the Wnt pathway and further factors including the expression of endothelial intergrins, cell-junction molecules, and chemokines are not mentioned but also exert angiogenic effects.

1.2 Notch signaling

1.2.1 The Notch signaling pathway

The evolutionary conserved Notch signaling pathway regulates tissue homeostasis, maintenance of stem cell properties and cell fate decisions in a wide range of tissues in vertebrates and invertebrates (Artavanis-Tsakonas et al., 1999; Egan et al., 1998; Greenwald, 1998; Miele and Osborne, 1999).

Conservation of Notch signaling

The name of the signaling pathway is derived from a *Drosophila melanogaster* mutant with 'notched' wings, which was first described by Thomas Hunt Morgan in 1917. Molecular sequencing efforts of the mutated gene identified the Notch receptor, which was reported to regulate cell fate of equipotent neuroepidermal cells and the development of the wings (Artavanis-Tsakonas et al., 1991; Kidd et al., 1986; Wharton et al., 1985).
Notch receptors as well as ligands are transmembrane proteins. Notch signaling is initiated by a ´signal sending cell´ producing the ligand and transactivating the Notch receptor on a receiving cell through direct cell-cell contact. Varying numbers of paralogues of the Notch receptors and its ligands have been identified in invertebrates and vertebrates. *Caenorhabditis elegans* has two Notch receptors (LIN-12 and GLP-1) and four Notch ligands (APX-1, LAG-2, ARG-1 and DSL-1). *Drosophila melanogaster* has one Notch receptor (dNotch) which can be bound by the two transmembrane ligands (Delta and Serrate). Vertebrates have four Notch receptors (NOTCH 1–4) and five canonical ligands, subdivided in two classes, the Delta/Delta-like class with Delta-like1 (DLL1), Delta-like3 (DLL3) and Delta-like4 (DLL4) and the Serrate/Jagged class with Jagged1 (JAG1) and Jagged2 (JAG2) (Artavanis-Tsakonas et al., 1995; Bray, 2006). Despite the varying number of Notch receptors and ligands the domain organization of Notch receptors and the appropriate ligands between different species is highly conserved (Figure 5).

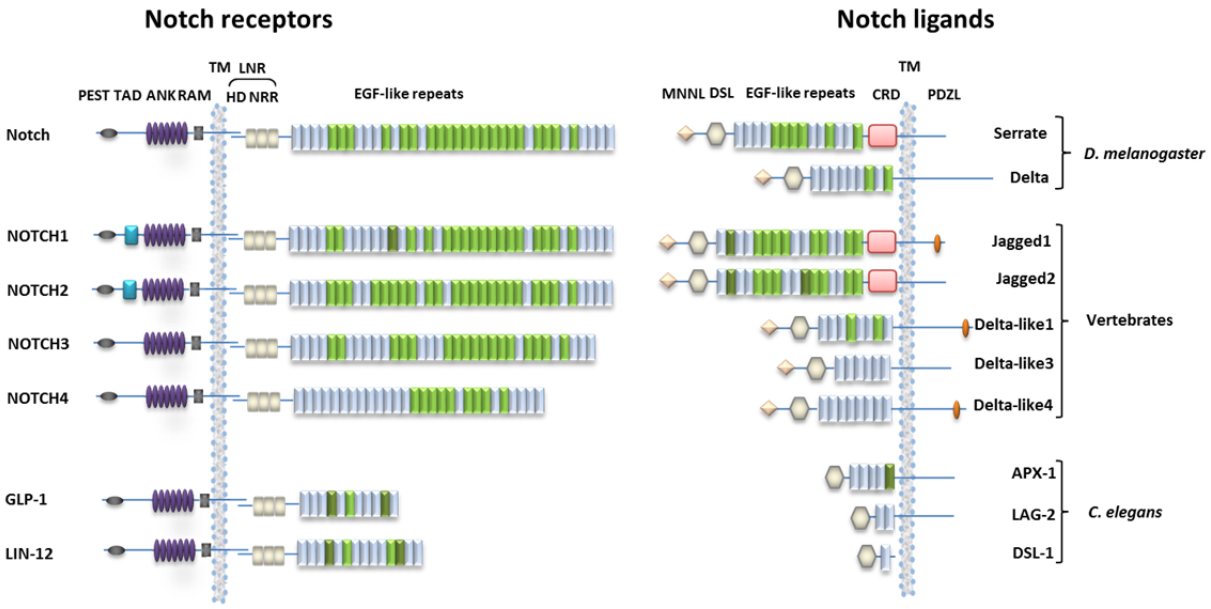

Figure 5: Notch receptors and ligands

D. melanogaster possess one Notch receptor (dNotch), which can be bound by two transmembrane ligands (Delta and Serrate). Vertebrates contain four Notch receptors (NOTCH1-4) and five ligands (Delta-like1, -3, -4, and Jagged1, -2. *C. elegans* has two Notch receptors (GLP-1, LIN-12) and three ligands of the Delta class (APX-1, LAG-2, DSL-1). The domain organization of the receptor and ligands is highly conserved between *D. melanogaster*, *C. elegans* and vertebrates and described in detail in Figure 6 and 7. Transcription activation domain (TAD); ankyrin repeats (ANK); transmembrane domain (TM); LIN12-Notch repeats (LNR); heterodimerization domain (HD); negative regulatory region (NRR); module at the N-terminus of Notch ligands domain (MNNL); Delta, Serrate, LAG-2-domain (DSL); Epidermal growth factor-like repeats (EGF), cysteine rich domain (CRD), PDZ ligand motif (PDZL).

Vertebrate Notch receptors

Notch receptors are single-pass transmembrane proteins consisting of a noncovalently linked Notch extracellular- (Notch-ECD) and Notch intracellular-domain (Notch-ICD).The N-terminal part of the Notch-ECD contains a series of epidermal growth factor (EGF)-like repeats, some of which contain Ca^{2+}-binding sites. The number of repeats varies among different Notch receptors of the particular species (Roca and Adams, 2007). Vertebrate Notch receptors consist of 29-36 EGF-like repeats (Fleming, 1998). The EGF-like repeats 11-13 were shown to be required for ligand binding (Cordle et al., 2008). A negative regulatory region (NRR), located close to the cell membrane, consists of a cluster of three LIN12-Notch repeats (LNR) and a heterodimerisation domain (HD) (Figure 6). The NRR has been shown to prevent ligand-independent Notch receptor activity by protecting the receptor against proteolytic cleavage (Hurlbut et al., 2007). The Notch intracellular domain consists of a RAM domain, seven tandem ankyrin repeats (ANK), a TAD and a C-terminal PEST domain (Figure 6). RAM domain together with the ANK repeats were shown to be involved in the interaction with RBP-J transcription factors (Tamura et al., 1995). The transcription activation domain (TAD) is a unique feature of the vertebrate NOTCH1 and NOTCH2 receptors. The C-terminal PEST domain accelerates proteolytic degradation of the protein thereby preventing excessive intracellular Notch signaling activity (Figure 6).

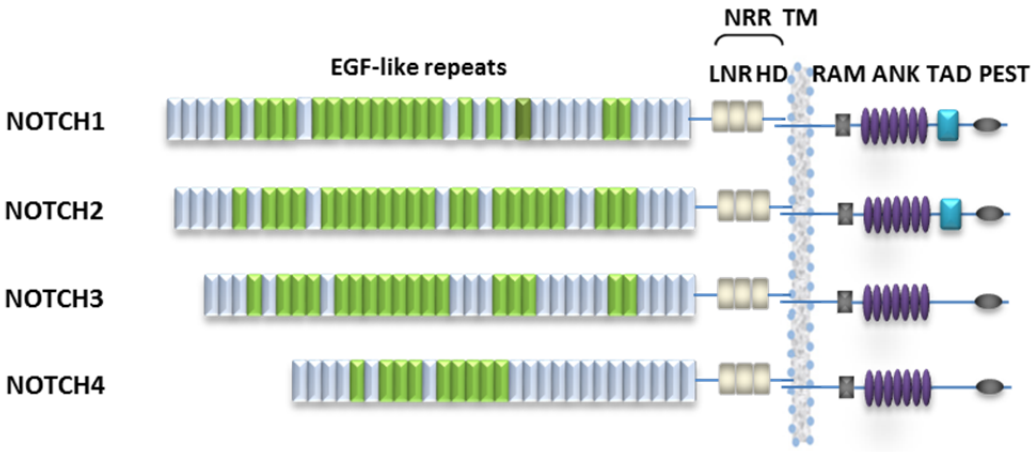

Figure 6: Domain organization of vertebrate Notch receptors

Vertebrate Notch receptors are represented with annotated domains. The Notch-ECD consist of EGF-like repeats with Ca^{2+} binding EGF domains colored in green, non-Ca^{2+} binding EGF domain in blue, atypical EGF domains in dark green, as well as, a negative regulatory region (NRR) comprising three LNR repeats and the heterodimerisation domain (HD). The RAM domain, seven tandem ankyrin repeats (ANK) and a C-terminal PEST domain are characteristics of the Notch-ICD domain. The TAD domain is only present in the NOTCH1 and NOTCH2 receptor. Transcription activation domain (TAD); ankyrin repeats (ANK); transmembrane domain (TM); LIN12-Notch repeats (LNR); heterodimerisation domain (HD); negative regulatory region (NRR).

Vertebrate Notch ligands

All vertebrate Notch ligands are single-pass transmembrane proteins. A common structural feature of canonical ligands is the presence of a highly conserved cysteine-rich Delta, Serrate, LAG-2-domain (DSL) domain. The DSL domain was reported to represent the binding region of the Notch receptor and thus is indispensable for activation of Notch signaling (Bray, 2006; Cordle et al., 2008; Roca and Adams, 2007) (Figure 7).

The extracellular domain of the ligands (ligand-ECD) contains a MNNL motif (module at the N-terminus of Notch ligands) with unknown structure at the N-terminus, followed by the conserved DSL domain and varying numbers of EGF-like repeats; 8 in Delta-like ligands and 15 to 16 in Jagged ligands. The Serrate/Jagged class with JAG1 and JAG2 differs from the Delta/Delta-like class with DLL1, DLL3 and DLL4 ligands by an additional cysteine rich domain (CRD) adjacent to the transmembrane domain (Artavanis-Tsakonas et al., 1995; Bray, 2006).

The intracellular domains (ligand-ICD) of the canonical Notch ligands are relatively short. A PDZ ligand (PDZL) binding motif at the C-terminal intracellular domain of the JAG1, DLL1 and DLL4 ligands promote cell-cell adhesion by interaction with proteins at the adherens junction (Figure 7) (Mizuhara et al., 2005).

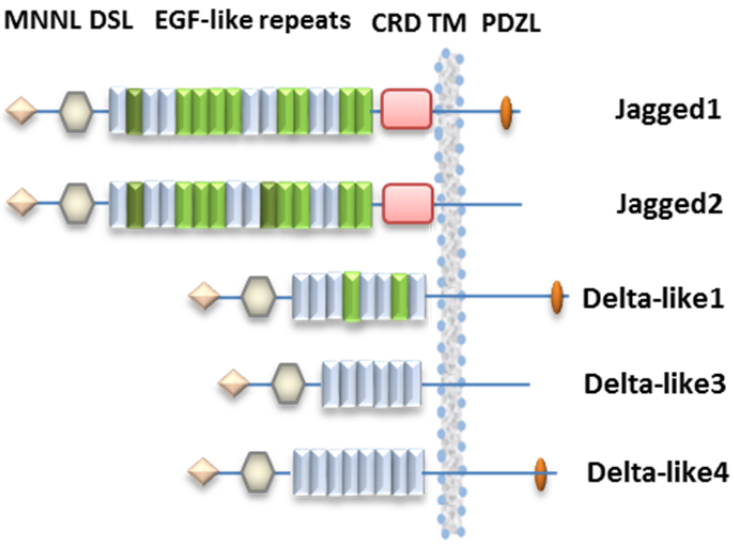

Figure 7: Domain organization of vertebrate canonical Notch ligands
Vertebrate canonical Notch ligands are represented with annotated domains. Ligand-ECD consists of a DSL domain preceded by a MNNL domain at the N-terminus of Notch ligands. Similar to the Notch receptors, the ligand-ECD comprises several EGF-like repeats. EGF-like repeats with Ca^{2+} binding EGF domains are colored in green, non-Ca^{2+} binding EGF domain in blue and atypical EGF domains in dark green. CRD represents the cysteine-rich region in juxtamembrane position, which is present in the Serrate/Jagged class of ligands. A C-terminal PDZL domain was identified in JAG1, DLL1 and DLL4. Module at the N-terminus of Notch ligands domain (MNNL); Delta, Serrate, LAG-2-domain (DSL); Epidermal growth factor-like repeats (EGF), cysteine rich domain (CRD), PDZ ligand motif (PDZL).

Noncanonical activation of the Notch signaling pathway can occur independently of the five canonical Notch ligands. Noncanonical ligands interact with the Notch-ECD such as the EGF-like dlk1 protein or the ubiquitin ligase Deltex, or with the Notch-ICD such as components of the β-catenin-dependent Wnt signaling pathway and enhance or inhibit Notch signaling. These ligands lack the DSL domain, which is specific for canonical Notch ligands, whereas other noncanonical ligands can have a completely different structure with lack of all typical Notch ligand domains (Baladron et al., 2005; Bray et al., 2008; Eiraku et al., 2005; Nueda et al., 2007).

Expression pattern of Notch receptors and ligands

The dynamic expression of Notch receptors and ligands makes it difficult to exactly determine a fixed expression pattern of Notch signaling components. Several reports attest to a role for the ligands DLL4 and JAG1 as well as the receptors NOTCH 1, -3 and -4 during the development of the vascular system. Thereby, DLL4, NOTCH-1, and NOTCH-4 were shown to be restricted to the endothelium. JAG1 was reported to be expressed in ECs and vSMCs while NOTCH3 displayed an exclusive expression in the vSMC lineage. The prevalent expression of Notch signaling components was restricted to arterial ECs and/or vSMCs, strengthening the role of Notch signaling during arteriovenous differentiation (Iso et al., 2003).

Canonical Notch signaling

Notch receptors are synthesized as single-chain precursors in the endoplasmatic reticulum (ER) (Figure 8). Before being transported and integrated into the cell membrane, the receptors undergo post-translational modifications including glycosylation by the enzyme POFUT (Protein O-fucosyl transferase) in the ER and proteolytic (S1) cleavage by the protease Furin in the Golgi network. This forms a receptor in which the Notch extracellular (Notch-ECD) and the intracellular domain (Notch-ICD) are noncovalently linked (Roca and Adams, 2007). The receptors can be further modified in the Golgi apparatus by the glycosyltransferase Fringe to increase the affinity for ligands of the Delta/Delta-like class (Bray, 2006; Haines and Irvine, 2003).

Receptor-ligand interaction of adjacent cells induces Notch trans-activation followed by a two-step cleavage of the Notch receptor. The action of an extracellular protease of the ADAM/TACE/Kuzbanian family (S1 cleavage) releases the Notch-ECD with the bound ligand attached to it and leaves a membrane bound intermediate. The release of the Notch-ECD causes a conformational change, which enables γ-secretase (S2 cleavage) for an intramembrane cleavage and subsequently releasing the NOTCH-ICD from the membrane (Figure 8) (Koo et al., 2005; Nichols et al., 2007; Parks et al., 2000; Song et al., 2006; Vollrath et al., 2001). NOTCH-ICD translocates to the nucleus where it interacts with the DNA-binding protein RBP-J (recombination signal-binding protein Jκ; also named CSL: Mammalian CBF1, *D. melanogaster* Su(H) and *C. elegans* LAG-1). RBP-J is the key transducer of the Notch signaling pathway and consists of two Rel-homology regions separated by a BTD-domain. Both structures were shown to be necessary for DNA contacts (Bray, 2006). The BTB domain was additionally supposed to mediate the interaction with the Notch intracellular domain. Notch-ICD binds to RBP-J leading to detachment of co-repressors including SMRT, SHARP and CtBP. The recruitment of the co-activator Mastermind (MAML) is part of the trimeric complex with RBP-J and Notch-ICD and converts RBP-J into a transcription activator initiating the expression of Notch target genes (Figure 8) (Roca and Adams, 2007). Other co-activators such as chromatin-remodeling complexes and histone acetyl transferases are recruited to the complex and contribute to the transcription of Notch target genes such as HES and HEY. These genes encode transcription factors, which induce the expression of further downstream genes (Fischer and Gessler, 2003; Lai, 2002). To avoid excessive Notch signaling, Notch-ICD is modified by kinases such as CDK8 and the SEL10 E3 ligase to make it accessible for proteosomal degradation. Thus, every Notch molecule signals only once. The absence of signal amplification by secondary messengers allows a fast downregulation of signaling capacity. However, receptor-ligand interaction of Notch components expressed in the same cell results in inhibition of Notch signaling (cis-inhibition).

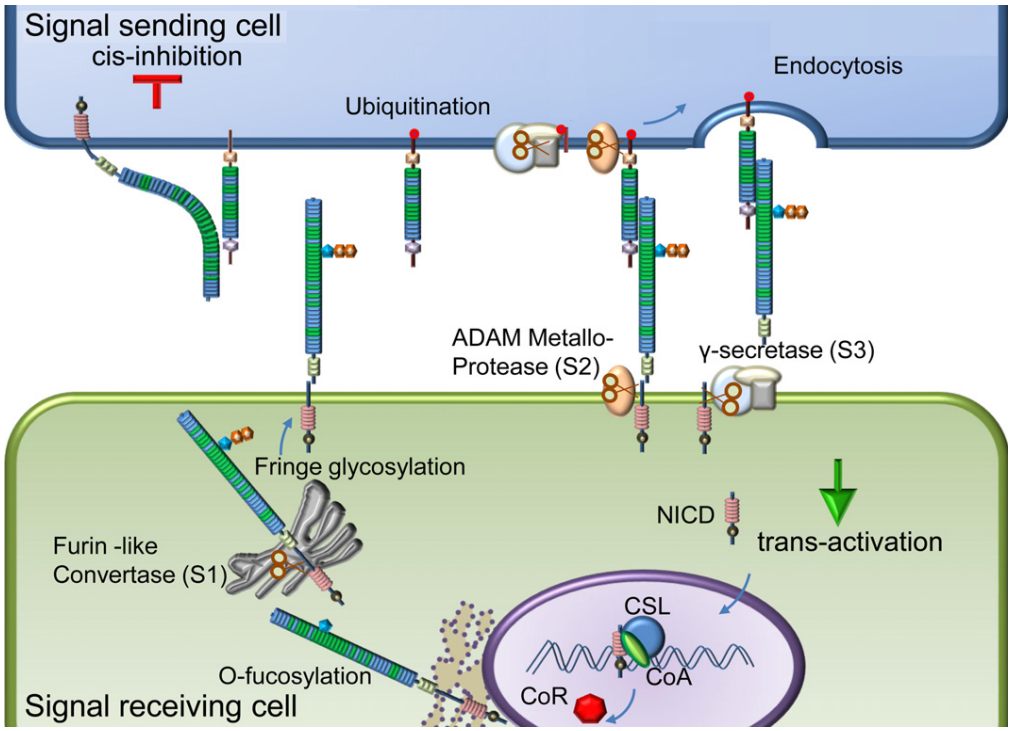

Figure 8: Canonical Notch signaling

The Notch receptor is modified by glycosylation and proteolysis (S1) before being transported and integrated into the cell membrane. Notch trans-activation is induced in response to receptor-ligand contact of adjacent cells. The ligand is expressed on the surface of the signal sending cell and activates the Notch receptor expressed on the signal receiving cell. The release of the Notch-ECD due to proteolytic cleavage by an ADAM metalloprotease (S2) together with the ubiquitylation-mediated endocytosis of the ligand–receptor complex initiates γ-secretase activity (S3) for an intramembrane cleavage of the Notch receptor. The Notch-ICD is released and translocates into the nucleus. Notch-ICD interacts with CSL, also named RBP-J, and the co-activator (CoA) MAML to form a transcription activation complex on promoter regions of Notch target genes, thereby removing transcriptional co-repressors (CoR). Interactions between ligands and receptors present on the same cell results in inhibition of Notch signaling (cis-inhibition). Adapted from Chillakuri et al. (2012). © 2012 Elsevier Ltd.

Molecular Notch receptor-ligand interaction

The molecular basis for Notch trans-activation or cis-inhibition is only partly understood. Cordle and Hambledon have demonstrated the interaction of the human NOTCH1 EGF-like repeats 11-13 with the DSL domain and the EGF-like repeats 1-3 of the JAG1 ligand in a Ca^{2+} dependent manner by nuclear magnetic resonance (NMR) and X-ray structural analysis (Cordle et al., 2008; Hambleton et al., 2004). The crystal structure of the EGF-like repeats 11–13 revealed a linear arrangement (Figure 9, A). Although, the EGF-like repeat 12 of the Notch-ECD was demonstrated to be sufficient for Delta binding in *D. melanogaster*. It showed no functionality *in vivo* since neighboring EGF-like repeats are necessary for effective binding (Rebay et al., 1991).

Structural analysis of the DSL domain of JAG1 was shown to display a unique protein folding with conserved residues towards one front of the DSL domain thus representing the main site for receptor binding (Figure 9, B) (Bray, 2006; Chillakuri et al., 2012; Cordle et al., 2008; Gordon et al., 2008). Furthermore, the DSL region was shown to be involved in trans-activation and cis-inhibition of the Notch receptor by formation of distinct complexes involving the same regions (Becam et al., 2010). Further work is needed to clarify the interfaces involved during Notch receptor-ligand binding.

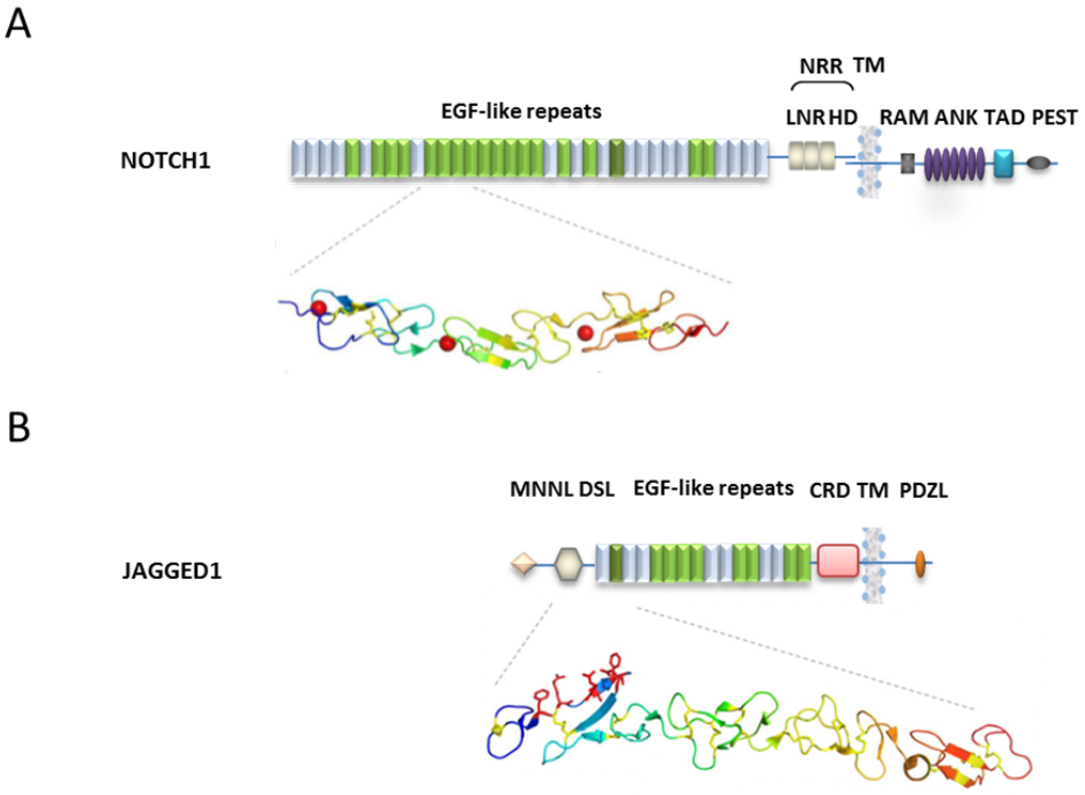

Figure 9: Architecture of the human NOTCH1 receptor and the JAG1 ligand

(A) The NOTCH1 receptor is illustrated with annotated domains in Figure 6. Crystal structure analysis of the ligand binding EGF-like repeats 11-13 (PDB ID: 2VJ3) of the NOTCH1-ECD with bound Ca^{2+} (red spheres) revealed an elongated calcium-stabilized characteristic EGF conformation consisting of three two-stranded, antiparallel ß-sheet, which were linked by disulfide bonds. (B) JAG1 is illustrated with the domains annotated in Figure 7. Crystal structure of human JAG1 DSL-and EGF-like repeats 1-3 (PDB ID: 2VJ2) reveales an arrangement with a linear conformation. The DSL domain (blue) displays a unique fold with highly conserved residues (red appendices) towards one front representing the main site for receptor interaction. Disulfide bonds are illustrated as yellow bridging structures. TM: transmembrane domain. Adapted from Chillakuri et al. (2012). © 2012 Elsevier Ltd.

Post-transcriptional modifications of Notch receptors and ligands

The activity of Notch signaling is influenced by post-transcriptional modifications of the receptor, as well as, the ligands including proteolytic processing, ubiquitylation and glycosylation.

The EGF-like repeat 12 of the Notch-ECD was reported to a key site for post-transcriptional glycosylation (Lei et al., 2003). The affinity of the Serrate/Jagged class of ligands to the fucosylated Notch receptor is higher compared to further glycosylation of the receptor by the glucosaminyl-transferase Fringe (Chillakuri et al., 2012). Thus, glycosylation of the Notch receptor alters the capability of the different Notch ligands to induce Notch signaling. Fringe-mediated modifications of the Notch receptor were reported to enhance DLL4-induced signaling, predominantly from tip to stalk cells, but impair Notch signaling activity upon JAG1 binding. Thus, the Notch ligands DLL4 and JAG1 have opposing roles in the regulation of endothelial sprouting once Notch receptors are glycosylated by Fringe (Figure 10) (Benedito et al., 2009).

In addition, ubiquitylation of Notch components influences Notch signaling activity. Notch ligands need to exert an endocytosis-mediated pulling force on the Notch-ECD in the ligand-expressing cell to achieve receptor dissociation and thus signaling activity (Meloty-Kapella et al., 2012). Ligand endocytosis is thereby initiated by intracellular ligand ubiquitylation. Consequently, soluble ligands are not capable of receptor activation. However, clustered or immobilized ligands may activate Notch receptors under certain conditions (Meloty-Kapella et al., 2012).

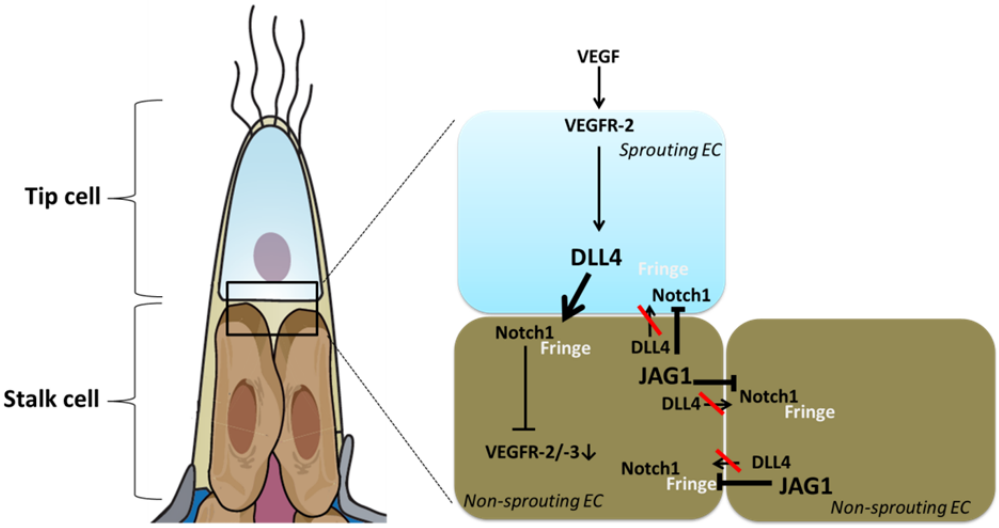

Figure 10: Antagonistic roles of DLL4 and JAG1 during sprouting angiogenesis

The tip cell (blue) guides a vascular sprout towards a VEGF stimulus. Signaling through VEGF receptors in the tip cell leads to upregulation of DLL4. DLL4-mediated activation of Notch receptors present on the adjacent cell induces a downregulation of VEGF receptor expression and thus promotes endothelial stalk cell fate (brown). Glycosylation of Notch receptors by Fringe enhances Notch signaling induced by DLL4 but suppresses signaling induced by JAG1. This ensures that Notch receptors in the tip cell do not get activated by JAG1 on the stalk cells. Modified from Carmeliet and Jain, 2011, with permission.

1.2.2 Notch signaling during development

Mutations in the Notch receptor were described to cause the 'notched' wing in *D. melanogaster.* In mice, deletion of Notch signaling by genetic inactivation of diverse Notch components results in severe abnormalities in many tissues. Null mutations of DLL1, DLL4, JAG1, NOTCH1, NOTCH2 and RBP-J led to embryonic lethality at E 9.5 -12 in mice, due to vascular remodeling defects (Iso et al., 2003). Even a haploinsufficiency of a single DLL4 allele causes severe vascular abnormalities with defective arterial differentiation, which again results in embryonic lethality (Gale et al., 2004). Notch4 is strongly expressed in the arterial endothelium, but the knock-out mice did not display any vascular phenotype most likely due to redundancies with Notch1. Conversely, a severe vascular phenotype is observed for mice lacking DLL1 or NOTCH2, which are not expressed in the vasculature (Hrabe de Angelis et al., 1997; Krebs et al., 2000; McCright et al., 2001; Xue et al., 1999).
Inducible transgenic mouse models were generated to avoid embryonic lethality. An endothelial-specific overexpression of a constitutive active NOTCH4 caused lethality accompanied by aberrant vessel structures and arteriovenous malformations (Murphy et al., 2008; Uyttendaele et al., 2001). Endothelial disruption of RBP-J in a conditional mouse model induces spontaneous angiogenesis in multiple tissues including the retina (Dou et al., 2008).

1.2.3 Notch signaling in human disease

A variety of human genetic disorders are linked to aberrant Notch signaling including the autosomal dominant Alagille syndrome (AGS) caused by mutations in the JAG1 or NOTCH2 gene (Penton et al., 2012). Mutations in the NOTCH3 gene lead to cerebral autosomal dominant arteriopathy with subcortical infarcts and leukoencephalopathy (CADASIL). CADASIL is a hereditary vascular disorder accompanied by migraine headaches and transient ischemic attacks or strokes. Its pathology is characterized by an angiopathy due to progressive degeneration of vSMCs. (Joutel et al., 1996).
Another Notch-related genetic disorder is the Hajdu-Cheney syndrome; an autosomal dominant multisystem disorder characterized by severe and progressive bone loss. It is caused by mutations in the NOTCH2 gene leading to disruption or loss of the C-terminal proteolytic recognition sequence and thereby increased Notch signaling (Simpson et al., 2011). Recent findings revealed an involvement of noncanonical Notch signaling during the development and progression of multiple sclerosis (MS). MS is accompanied by inflammatory and demyelinating lesions around the axons of the brain and the spinal cord. The NOTCH1 receptor was shown to build cytoplasmic aggregates containing a pro-apoptotic factor, which inhibits nuclear transport and NOTCH1-mediated differentiation of oligodendrocytes, thus causing a demyelination of axons (Nakahara et al., 2009).

Additionally, several cardiac diseases like the Tetralogy of Fallot (TOF) are linked to mutations in Notch signaling. TOF is a heart defect involving 3 to 4 anatomical cardiac abnormalities. A mutation in the JAG1 ligand as well as in the NOTCH1 receptor has been shown to be involved in the development of TOF (Eldadah et al., 2001; Greenway et al., 2009; Kola et al., 2011; Le Caignec et al., 2002).
Beside developmental defects and genetic diseases, many kinds of human cancers were also shown to have perverted Notch signaling (section 1.1.3).

1.3 Angiogenesis in health and disease

During embryonic development, the primitive capillary plexus is remodeled by angiogenic processes into a mature vasculature (Yancopoulos et al., 2000). In adults, blood vessels are mainly in a quiescent and non-angiogenic state. Nevertheless, angiogenesis is indispensable to maintain physiological homeostasis, as well as, tissue integrity during cellular processes such as wound healing, inflammation, the menstrual cycle, exercise and in response to ischemia (Carmeliet, 2003).
Angiogenesis is regulated by proteins from the VEGF-, FGF-, TGFß-, the Angiopoietin family, as well as, several cytokines, integrins and junctional molecules. Depending on the context, these molecules can either elicit pro-angiogenic or anti-angiogenic responses (section 1.1.1., 1.1.2 and 1.1.4). A balance of these factors is crucial to ensure accurate angiogenesis since several diseases can be exacerbated through the formation of an aberrant vascular network.
Insufficient blood supply is a main symptom in several diseases such as diabetes or atherosclerosis and may lead to ischemia, myocardial infarction or stroke. While the cause of these diseases may be different, the consequences are based on the same problems. Namely, insufficient blood supply causing cell death.
Conversely, exuberant formation of blood vessels is involved in many diseases such as age-related macular degeneration (AMD), psoriasis or tumor progression. AMD is the leading cause of blindness among people at age 50 and older in the U.S. and Europe. The severe form of AMD, wet AMD, is characterized by invasion of new blood vessels from the macula into the retina. These vessels are often leaky and fragile resulting in irreversible loss of vision (Yang et al., 2008). Besides AMD, chronic inflammatory diseases such as psoriasis are associated with aberrant angiogenesis (Nickoloff, 1991). Psoriasis affects 3 % of the population. It is provoked by massive proliferation of epidermal keratinocytes, accumulation of inflammatory cells, which produce pro-angiogenic factors causing excessive angiogenesis in the dermis and the formation of psoriatic plaques (Nickoloff, 1991).
Finally, deregulated angiogenesis is a major contributor tumor formation, progression and metastasis (section 1.3.2).

1.3.1 Tumor angiogenesis

Vascular growth is indispensable during embryogenesis but also occurs during postnatal life. Dr. Judah Folkman hypothesized in the early 1970s that tumor growth is angiogenesis-dependent. The abusive use of angiogenesis by tumors supplies the cancerous tissue with nutrients and oxygen thus enabling the proliferation and distribution of tumor cells.

During the early phase, the size of a pre-angiogenic tumor is nourished by diffusion and consequently is restricted to a volume of approximately 0.2 mm to 2 mm diameter. The tumor persists in an avascular state (tumor dormancy), in which proliferation and apoptosis are equalized, and remains clinically undetectable (Fang et al., 2000; Holmgren et al., 1995). Further tumor growth is dependent on neovascularization. Dormant tumors, which lack the expression of pro-angiogenic factors, rely on physiologically induced angiogenesis by external factors or further mutations to supply the necessary pro-angiogenic signals.

Metabolic demands force tumor cells to induce an ´angiogenic switch´. Tumors recruit their own vascular network from the preexisting vasculature in a process that mimics normal angiogenesis. This facilitates massive tumor expansion, as well as, metastasis (Hanahan and Folkman, 1996).

Hypoxia in the center of the pre-angiogenic tumor induces the secretion of pro-angiogenic factors, including VEGF, in order to attract proximate vessels. VEGF-stimulated angiogenesis induces vascular sprouting towards the nutrient-deprived tumor areas resulting in a connection of the tumor to the vascular system. Pathological angiogenesis results in a disorganized, tortuous, and irregularly shaped vascular network with vessels of an abnormal size and chaotic branching (Hanahan and Folkman, 1996). As the function of the aberrant vasculature is impaired, the inner mass of tumors still suffers from hypoxia due to the insufficient oxygen supply. This perpetuates the persistent release of diffusible pro-angiogenic factors.

Irregularities of the vascular structure and permeability are hallmarks of the tumor vasculature (McDonald and Baluk, 2002). Tumor vessels consist of disorganized and overlapped endothelial cells with intercellular openings resulting in an impairment of the endothelial barrier function and vascular leakage (Hashizume et al., 2000; McDonald and Foss, 2000). Leakiness is further increased by a loosened contact between endothelial cells, pericytes and the basement membrane (McDonald and Baluk, 2002).

In addition to secretion of pro-angiogenic factors to induce tumor neovascularization from the host, human tumors make use of several other evasion mechanisms to ensure their survival. For instance, vessel co-option is a mechanism by which the tumor cells cover their nutrient supply by occupying adjacent vessels (Folkman and Kalluri, 2003). The connection to the blood system enables the tumor to proliferate and metastasize. For metastasis, some tumor cells undergo an epithelial-to-mesenchymal transition (EMT). The mesenchymal phenotype enables high motility und less adhesion, facilitating the access to the blood stream and the dissemination through the body (Folkman and Kalluri, 2004). The extravasation of metastatic cells through the capillaries and the subsequent infiltration into surrounding tissues is dependent on the interaction of tumor cells with adhesion molecules.

The extravasated tumor cells modify the surrounding tissue to create a more suitable microenvironment. However, only a few extravasated tumor cells are capable of forming secondary tumors and inducing angiogenesis in the target organ (Folkman and Kalluri, 2004).
The abuse of angiogenic processes by tumors, as hypothesized by Dr. Folkman, in resulted in the development of agents inhibiting angiogenesis. The first anti-angiogenic agents were targeting VEGF signaling as the key pathway during angiogenesis. Bevacizumab (Avastin®, Genentech, San Francisco, CA) is a recombinant humanized antibody against VEGF-A inhibiting receptor binding of all isoforms of human VEGF. Bevacizumab has been approved by the Food and Drug Administration (FDA) for treatment of colorectal cancer or advanced lung cancer combined with a conventional chemotherapy and showed beneficial results concerning the overall survival of patients (Kerbel, 2008). Combinatory therapy for patients suffering from metastatic breast cancer resulted in prolonged progression-free survival (PFS) but did not alter the overall survival of patients (Miller et al., 2007). In combination with chemotherapy, Bevacizumab induced tumor growth inhibition and even tumor regression. This may in part be due to 'normalization' of tumor vessels and thus improved chemotherapeutic drug transport to the tumor cells (Carmeliet and Jain, 2011).
As an alternative to targeting VEGF, drugs have been developed to target its receptor instead. Sorafenib (Nexavar®, Bayer and Onyx, Emeryville, CA) and Sunitinib (Sutent®, Pfizer, New York City, NY) are FDA-approved tyrosine kinase inhibitors inhibiting the signaling of several receptor tyrosine kinases such as VEGF and PDGF receptors. Monotherapy with these VEGF receptor tyrosine kinase inhibitors prolonged the progression-free survival of patients with renal cancer carcinoma and the overall survival of patients with hepatocellular carcinoma (Loges et al., 2010).
Unfortunately, blockage of the VEGF signaling pathway is not devoid of severe side effects. Side effects observed for anti-VEGF and anti-VEGFR inhibitors include hypertension, intestinal toxicity, proteinuria, coagulation disorders and neurotoxicity (Roodhart et al., 2008). Late-stage tumors of most cancer types acquire resistance to anti-VEGF therapy, as tumors regrew during treatment after an initial period of growth suppression. The resistance of tumors against an anti-angiogenic therapy can be acquired by processes such as vessel co-option and secretion of other pro-angiogenic factors. Thus, the benefit of progression-free survival is only moderate and the overall cancer survival of patients is negligible and inconsistent. Since Sorafenib and Sunitinib target other receptor tyrosine kinases beside VEGF and PDGF receptors, restricting tumor growth comes at the cost of disrupting other receptor tyrosine kinase-dependent signaling pathways (Weis and Cheresh, 2011).
Due to the complications with anti-VEGF therapy, drugs have been developed targeting other important pathways of angiogenesis such as the Notch signaling pathway.

1.3.2 Notch signaling and tumor angiogenesis

The role of Notch signaling in human cancer started to be recognized after Ellisen et al., demonstrated in 1991 a connection between T-cell acute lymphoblastic leukemia and mutations in the NOTCH1 gene. Activating mutations in the NOTCH1 gene occur in more than 50 % of human T-cell acute lymphoblastic leukemia (T-ALL) patients (Staal and Langerak, 2008; Weng et al., 2004). Nowadays, aberrant Notch signaling is linked to several types of cancer. For example, a gain-of-function mutation after a pro-viral insertion in the Notch4 gene causes mammary tumors in mice (Imatani and Callahan, 2000; Orlandi et al., 2002). However, Notch signaling in human breast cancer has not been sufficiently investigated ((Imatani and Callahan, 2000; Orlandi et al., 2002). Due to its role in T-cell leukaemia and mammary tumors, activating mutations in the Notch receptors have been associated with an oncogenic role of Notch signaling during pathogenesis of tumors.
Further studies with skin tumors indicate that Notch signaling also exerts tumor suppressor functions (Thelu et al., 2002). The data are supported by high susceptibility for basal-cell-carcinoma-like tumors in mice, which are deficient for the Notch1 gene in the epithelium (Nicolas et al., 2003). Impaired Notch signaling has also been linked to the pathogenesis of small-cell lung cancer (SCLC). These conflicting functions of Notch as oncogene or tumor-suppressor are supposed to be highly dependent on the cellular context (Allenspach et al., 2002).
Ligand-mediated activation of the Notch pathway was also shown to promote tumor progression. The Notch ligand DLL4 is strongly expressed in the vasculature of human tumors, presumably as a consequence of high VEGF levels (Patel et al., 2006). High DLL4 expression was demonstrated in the vasculature of tumors from bladder, brain, breast, colon and kidney (Kuhnert et al., 2011). Furthermore, the progression of breast cancer correlates with the level of vascular DLL4 expression (Jubb et al., 2010).
Furthermore, the paracrine action of JAG2 has been linked to the pathogenesis of squamous cell head and neck carcinoma (Zeng et al., 2005). JAG2 promotes epithelial-to-mesenchymal transition (EMT) as an early event in lung adenocarcinoma metastasis by suppression of miR-200 and thereby accelerates the development and progression of lung adenocarcinoma (Yang et al., 2011). Expression of JAG1 correlates with poor outcome in clinical breast cancer (Dickson et al., 2007). Thus, Notch has become an interesting target for cancer therapy.

Blocking Notch signaling as cancer therapy

Reducing Notch signaling activity by either a DLL4-specific neutralizing antibody or a soluble DLL4-Fc fusion protein impairs blood perfusion and inhibits tumor growth due to formation of a non-productive excessive vessel network (Ridgway et al., 2006; Yan et al., 2010). However, chronic administration of these agents can cause vascular tumor formation in mice, rats and monkeys (Yan et al., 2010).
Forced activation of endothelial Notch signaling by overexpression of DLL4 or DLL1 inhibits angiogenesis (Li et al., 2011; Segarra et al., 2008; Zhang et al., 2011). Surprisingly the

outcome on tumor growth was different for distinct tumors. Data by Li et al. suggest that DLL4-mediated stimulation of Notch signaling in glioblastoma reduces tumor angiogenesis but promoted tumor growth by improving the function of blood vessels (Li et al., 2011). In contrast, Segarra and colleagues reported that DLL4-induced Notch activation in lymphoma cells results in less vascularized and significantly smaller tumors (Segarra et al., 2008).
Despite the controversial effects, the Delta-Notch pathway still represents an attractive target for tumor therapy. Further investigations are necessary to unravel the context-dependent role of the Notch signaling pathway during tumor angiogenesis.

1. 4 The endothelium and metabolism

The endothelium is the interface between blood and tissue. Metabolic changes can damage the endothelium and thus impair the crucial function of endothelial cells. For example, metabolic homeostasis is deregulated in patients suffering from Diabetes mellitus due to insulin-deficiency or insulin-resistance. Exposure of vascular endothelial cells to hyperglycemia triggers endothelial dysfunction. Endothelial cells lose their quiescent phenotype and their normal function is impaired. Enhanced proliferation, increased expression of adhesion molecules, reduced vasorelaxation, overproduction of growth factors and enhanced vascular permeability are hallmarks for endothelial dysfunction. Type2 diabetes-associated vascular modifications including diabetic nephropathy and retinopathy emerge as consequence of endothelial dysfunction (Popov and Simionescu, 2006).
Beside elevated glucose levels, other pathological alterations influence signaling pathways that subsequently may cause endothelial activation or dysfunction.
The angiogenic activity of endothelial cells can be influenced by VEGF-secreting metabolic regulators including peroxisome proliferator activated receptor ß (PPARß). PPARs belong to a family of transcription factors and contribute to lipid utilization, energy homeostasis and insulin sensitivity (Rosen and MacDougald, 2006). Additionally, PPARs were shown to influence angiogenesis. PPARß stimulates; whereas PPARα and PPAR-γ inhibit angiogenesis (Fraisl et al., 2008). Besides PPARs, several other regulatory molecules of metabolism affect angiogenesis such as forkhead transcription factors (FoxO). FoxO family members, in particular FoxO1, are involved in energy metabolism (Barthel et al., 2005). FoxO1 expression is induced in the liver during fasting in order to promote the expression of gluconeogenic enzymes. Furthermore, FoxO1 mediates the metabolic switch from carbohydrate to fatty acid oxidation as the major energy source during starvation. In endothelial cells, FoxO1 acts anti-angiogenic (Paik et al., 2007; Potente et al., 2005).
In return, metabolism can be regulated by the endothelium itself. For example, the endothelium functions as barrier to aberrant muscle lipid uptake (Hagberg et al., 2010). Decreased VEGF-B levels maintain this barrier function. Furthermore, decreased VEGF-B signaling restores insulin sensitivity and improves glucose tolerance (Hagberg et al., 2012).
However, studying the link between the endothelium and metabolism has only started to be unraveled.

1.4.1 Notch signaling and metabolism

Several reports suggest a role for the Notch pathway in metabolism. FoxO1, a key regulator of insulin action, together with Notch signaling regulate hepatic glucose metabolism (Pajvani et al., 2011). In consequence, haploinsufficiency of FoxO1 and Notch1 increases insulin sensitivity in mice (Pajvani et al., 2011). Thereby, Notch regulates hepatic glucose production in a FoxO1-dependent manner and genetic inhibition of Notch signaling suggests a potential benefit in diabetes treatment (Pajvani et al., 2011). The data were supported by another study reporting aberrant Notch signaling as driver of glycolysis in response to hypoxia (Landor et al., 2011). Surprisingly, Notch overexpression, as well as, inhibition causes the same phenotype.

Further data suggest a regulatory cooperation of Notch and PPAR-γ in fatty acid transport through ECs and thereby ensure fatty acid supply to distant organs (Iso et al., 2008). PPAR-γ is a lipid-activated nuclear receptor, necessary for adipocyte differentiation from pluripotent stem cells into mature adipocytes (Fernyhough et al., 2007; Rosen et al., 2000; Wu et al., 1999). Notch signaling causes an endothelial-specific activation of the fatty acid binding protein 4 (FABP4) via the peroxisome proliferator activated receptor- γ (PPAR-γ) (Iso et al., 2008). These studies provide an indication of Notch signaling as a molecular regulator of cellular glucose and fat metabolism.

1.5 Aim of the study

Angiogenesis is a highly regulated process, which is indispensable during embryogenesis but also involved in processes such as wound healing, inflammation, the menstrual cycle, exercise and in response to hypoxia in the adult. An imbalanced regulation of angiogenesis is linked to the pathogenesis of several diseases including cancer. Delta-Notch and VEGF signaling are key pathways in the regulation of angiogenesis. Notch signaling regulates endothelial activation, proliferation, migration, anastomosis, and maturation. Thus, Notch signaling constitutes an interesting target for anti-tumor therapy. Consequently, it is of high importance to better understand the molecular regulation of Notch in the vascular system.

The aim of the study was to characterize the complex functions of the Notch signaling pathway in the vasculature by investigating the molecular crosstalk of Notch receptors with different ligands. Therefore, soluble DLL1, DLL4, and JAG1 ligands or the soluble NOTCH1 receptor, consisting of the respective interaction domain for ligand-receptor interaction, were designed and investigated for their effect on VEGF-induced angiogenesis. Secondly, the generation of a mouse model with an inducible deletion of endothelial Notch signaling should help to define the role of Notch signaling in the adult vasculature.

Both approaches should contribute to a better understanding of the Notch signaling pathway and may be helpful for the development of future therapeutic strategies.

2 Materials and methods

2.1 Materials

2.1.1 Chemicals

Chemical	Manufacturer
Acetic acid	Carl Roth GmbH, Karlsruhe, Germany
Acid Fuchsin	Carl Roth GmbH, Karlsruhe, Germany
Agarose	Carl Roth GmbH, Karlsruhe, Germany
Ammonium persulphate (APS)	Sigma-Aldrich GmbH, Seelze, Germany
Anilin Blue	Carl Roth GmbH, Karlsruhe, Germany
Biebrich Scarlet	Sigma-Aldrich GmbH, Seelze, Deutschland
Bromphenol blue	Serva Electrophoresis GmbH, Heidelberg, Germany
Bovine serum albumin (BSA)	Sigma-Aldrich GmbH, Seelze, Deutschland
Collagenase	Sigma-Aldrich GmbH, Seelze, Deutschland
Coomassie Blue R250 disodium salt	Sigma-Aldrich GmbH, Seelze, Germany
DAPT N-[N-(3,5-Difluorophenacetyl)-L-alanyl]-S-phenylglycine t-butyl ester	Merck KGaA, Darmstadt, Germany
DAPI 4',6-diamidino-2-phenylindole	Carl Roth GmbH, Karlsruhe, Germany
Dimethyl sulfoxide (DMSO)	Sigma-Aldrich GmbH, Seelze, Germany
Disodium hydrogen phosphate	Sigma-Aldrich GmbH, Seelze, Germany
Disodium phosphate	Sigma-Aldrich GmbH, Seelze, Germany
1,4-Dithiothreitol (DTT)	Serva Electrophoresis GmbH, Heidelberg, Germany
EDTA disodium salt	Merck KGaA, Darmstadt, Germany
Ethanol 100%	Carl Roth GmbH, Karlsruhe, Germany
Ethanol 96%	Carl Roth GmbH, Karlsruhe, Germany
Ethylenediaminetetraacetic acid (EDTA)	Fisher Scientific, Southborough, UK
Ethidium bromide	Sigma-Aldrich GmbH, Seelze, Germany
Ferric chloride	Carl Roth GmbH, Karlsruhe, Germany
Gelatine Typ B	Sigma-Aldrich GmbH, Seelze, Germany
Glutaraldehyde	Sigma-Aldrich GmbH, Seelze, Germany
Glycerol/Glycerin	Carl Roth GmbH, Karlsruhe, Germany
Glycine	Carl Roth GmbH, Karlsruhe, Germany
Hematoxylin	Carl Roth GmbH, Karlsruhe, Germany
Heparin sodium salt	Sigma-Aldrich GmbH, Seelze, Germany
Hydrochloric acid (37%)	Sigma-Aldrich GmbH, Seelze, Germany

Isopentane 2-Methylbutan	Carl Roth GmbH, Karlsruhe, Germany
Ketamine (Ketanest 50)	Pfizer Inc., New York, USA
2-mercaptoethanol	Carl Roth GmbH, Karlsruhe, Germany
Methanol	Sigma-Aldrich GmbH, Seelze, Germany
Methyl cellulose	Sigma-Aldrich GmbH, Seelze, Germany
MTT Thiazolyl blue	Sigma-Aldrich GmbH, Seelze, Germany
Nycodenz	Axis-Shield PoC AS, Oslo, Norway
Nonidet-P40	Amresco LLC, OH, USA
Oil Red O	Sigma-Aldrich GmbH, Seelze, Germany
Paraffin	McCormick scientific, Maryland Heights, USA
Paraformaldehyde	Sigma-Aldrich GmbH, Seelze, Germany
Peanut oil	Sigma-Aldrich GmbH, Seelze, Germany
Periodic acid	Carl Roth GmbH, Karlsruhe, Germany
Phenol	Carl Roth GmbH, Karlsruhe, Germany
Phosphomolybdic acid	Sigma-Aldrich GmbH, Seelze, Germany
Phosphtungstic acid	Sigma-Aldrich GmbH, Seelze, Germany
Picric acid	Sigma-Aldrich GmbH, Seelze, Germany
Polyethylenimmine (PEI)	Sigma-Aldrich GmbH, Seelze, Germany
Ponceau S	AppliChem GmbH, Darmstadt, Germany
2-propanol	Merck KGaA, Darmstadt, Germany
Propylene glycol	Sigma-Aldrich GmbH, Seelze, Germany
Rotiphorese Gel 30	Carl-Roth GmbH, Karlsruhe, Germany
Schiff reagent	Carl-Roth GmbH, Karlsruhe, Germany
Sodium acetate	Sigma-Aldrich GmbH, Seelze, Germany
Sodium chloride	Mallinckrodt Baker, Griesheim, Germany
Sodium citrate dihydrate	Sigma-Aldrich GmbH, Seelze, Germany
Sodium deoxycholate	Sigma-Aldrich GmbH, Seelze, Germany
Sodium dodecyl sulphate (SDS)	Carl Roth GmbH, Karlsruhe, Germany
Sodium hydroxide	Carl Roth GmbH, Karlsruhe, Germany
D(+)-sucrose	AppliChem BioChemica, Darmstadt, Germany
Tamoxifen $C(C_6H_5)C_6H_4OCH_2CH_2N(CH_3)_2$	Sigma-Aldrich GmbH, Seelze, Germany
N,N,N,N-Tetramethylendiamin (TEMED)	Sigma-Aldrich GmbH, Seelze, Germany
TRIS	Carl Roth, Karlsruhe, Germany
Triton X-100	Sigma-Aldrich GmbH, Seelze, Germany
Trypan blue	Sigma-Aldrich GmbH, Seelze, Germany
Tween-20	Sigma-Aldrich GmbH, Seelze, Germany
Xylazine (Rampun 2 %)	Bayer AG, Leverkusen, Germany
Xylene	Sigma-Aldrich GmbH, Seelze, Germany

2.1.2 PCR reagents and buffers

Reagents	Manufacturer
Deoxynucleotide triphosphates (dNTPs, 10 mM)	Eurofins MWG|operon, Ebersberg, Germany
Taq polymerase	Peqlab Biotechnology GmbH, Erlangen, Germany
Taq polymerase buffer	Peqlab Biotechnology GmbH, Erlangen, Germany
High Capacity cDNA RT Kit	Life Technologies GmbH, Darmstadt, Germany
Power SYBR Green PCR Mix	Life Technologies GmbH, Darmstadt, Germany
Oligonucleotidesł	Eurofins MWG|operon, Ebersberg, Germany

ł Oligonucleotides used for PCR were listed separately in section 2.1.3.

2.1.3 Primers

All primers were constructed unsing the Primer3 software and synthesized by Eurofins MWG|operon, Ebersberg, Germany. The following oligonucleotides were used:

Human primers	Oligonucleotide sequence 5´→ 3´	Annealing temperature
DLL1-DSL-5Nco-for	GCGCCATGGACTCCTACCGCTTCGTGTGT	60°C
DLL1-DSL-3BglII-rev	GCGAGATCTGCAGATCGGCTCTGTGCAGTA	60°C
DLL4-DSL-5Nco-for	GCGCCATGGTAGCTGTGGGTCAGAACTGGT	60°C
DLL4-DSL-3BglII-rev	GCGAGATCTACAGCCCGAAAGACAGATAGG	60°C
DLL4-ex9early-for	CTTGCCATGACCTGGAGAAT	60°C
DLL4-Fc-Nco-rev	GAGCCATGGCCCAGGGGAAGCTGGGCGGCAA	60°C
Fc-SacI-for	GCGGAGCTCGATATCGGCCATGGTTAG	60°C
Fc-XhoI-rev	GCGCTCGAGATGTCTGGCCAGCTAGCACT	60°C
HES5-ex1/2-for	AGAAAAACCGACTGCGGAAG	60°C
HES5-ex3-rev	TAGTCCTGGTGCAGGCTCTT	60°C
HEY1-ex3-for	GAGAAGGCTGGTACCCAGTG	60°C
HEY1-ex5-rev	CGAAATCCCAAACTCCGATA	60°C
HEY2-ex3-for	CTTGTGCCAACTGCTTTTGA	60°C
HEY2-ex5-rev	GCACTCTCGGAATCCTATGC	60°C
HPRT-3-for	GTCAAGGGCATATCCTACAACAA	60°C
HPRT-5-rev	AAGATGGTCAAGGTCGCAAG	60°C
JAG1-DSL-5Nco-for	GCGCCATGGGCGTTGCCCACTTTGAGTAT	60°C
JAG1-DSL-3BglII-rev	GCGAGATCTGAGTTTGCAAGACCCATGCTT	60°C
NOTCH1-EGF-Eco-for	GCGGAATTCACAGGACGTGGATGAGTGCT	60°C
NOTCH1-EGF-Bgl-rev	GCGAGATCTCACATCGTACTGGCACAGATG	60°C
pENTR-for	TGGCCTTTTTGCGTTTCTAC	60°C
pENTR-rev	GTAACATCAGAGATTTTGAGACAC	60°C
pINFUSE-rev	AGGAGTTCAGGTGCTGAGGA	60°C
pINFUSE-for	CCACCATGTACAGGATGCAA	60°C

Murine primers	Oligonucleotide sequence 5´→ 3´	
ApoE-for1	GCCGCCCCGACTGCATCT	55°C
ApoE-for2	TGTGACTTGGGAGCTCTGCAG	55°C
ApoE-rev	GCCTAGCCGAGGGAGAGCCG	55°C
Rbp-j-for	GTGGAACTTGCTATGTGCTTTG	60°C
Rbp-j-rev1	CTGCCATATTGCTGAATGAAAA	60°C
Rbp-j-rev2	CACATTCCCATTATGATACTGAGTG	60°C
VE-Cad-Cre-for	GCCTGCATTACCGGTCGATGCAACGA	70°C
VE-Cad-Cre-rev	GTGGCAGATGGCGCGGCAACACCATT	70°C

2.1.4 Plasmids

Individually designed plasmids are described in section 2.2.1.

Following commercially available plasmids were used:

pENTR™ 2B Dual Selection Vector and pENTR™ 3C

Source: Life Technologies GmbH, Darmstadt, Germany
Entry vector for Gateway destination cloning (section 2.2.2)

pCMV-ENTR-hJAG1
Source: OriGene Technologies, Inc., Rockville, USA.
Plasmid for production of JAG1-DSL-Fc and Jag1-ECD-Fc overexpression constructs (section 2.2.1)

pINFUSE-hIgG1-Fc2
Source: InvivoGen, San Diego, USA
Plasmid designed for construction of Fc-Fusion proteins

pAd/CMV/V5-DEST™ vector
Source: Life Technologies GmbH, Darmstadt, Germany
Destination vector for Gateway cloning (section 2.2.2); used for Adenovirus production

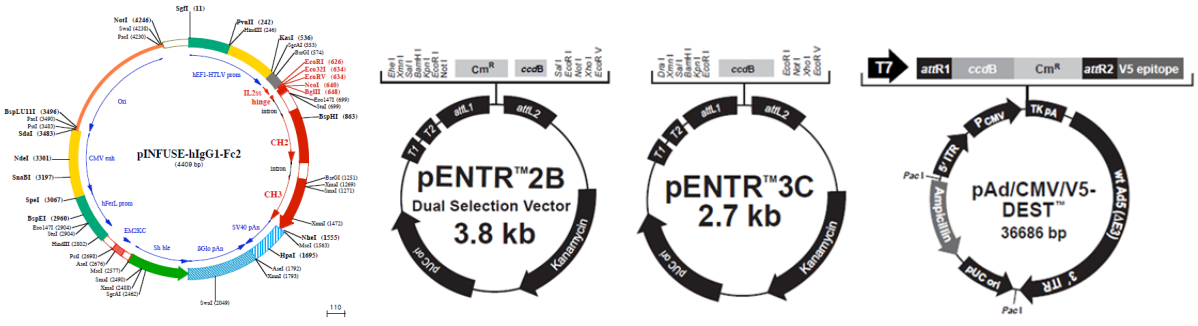

Figure 11: Vector maps
pINFUSE-hIgG1-Fc2 was used for construction of Fc-Fusion proteins; pENTR™2B or 3C were used as entry vectors; pAd/CMV/V5-DEST was used as destination vector for Gateway cloning. Reprinted by permission from Life Technologies, copyright (2011).

2.1.5 Enzymes, enzyme buffers and antibiotics

Compound or solution	Manufacturer
Ampicillin-sodium salt	Carl Roth GmbH, Karlsruhe, Germany
Gateway LR ClonaseTM II Enzyme Mix	Life Technologies GmbH, Darmstadt, Germany
Kanamycin	Carl Roth GmbH, Karlsruhe, Germany
Penicillin/Streptomycin	Life Technologies GmbH, Darmstadt, Germany
Pfu polymerase (5000 U/m)	Bioron GmbH, Ludwigshafen, Germany
Pfu polymerase buffer	Bioron GmbH, Ludwigshafen, Germany
Restriction enzymes and buffers *	New England Biolabs GmbH, Frankfurt, Germany
Zeocin	Life Technologies GmbH, Darmstadt, Germany

* all enzymes and buffers for restriction were purchased from NEB and are listed in corresponding section.

2.1.6 Antibodies

Target	Species & clonality	Company	Application
Primary antibodies:			
human GAPDH	mouse, monoclonal	Abcam	1:5000, 1 h, RT
murine CD11b	rat, monoclonal	BD Pharmingen™	1:100, 1 h, RT PE-conjugate
murine CD31	rat, monoclonal	BD Pharmingen™	1:100; FITC-conjugate
murine Desmin	rabbit, polyclonal	Thermoscientific	1:100, 1 h, RT
murine Glut1	rabbit, polyclonal	Millipore	1:50, 1 h, RT
murine stabilin-2		from Prof. Dr. Sergij Goerdt	1:500; biotinylated
rabbit skeletal myosin	mouse, monoclonal	Sigma-Alderich	1:500, 1 h, RT
Secondary antibodies:			
Alexa Fluor 488 α-rabbit IgG	donkey, polyclonal	Life Technologies	1:200, 1h, RT
Alexa Fluor 488 α-mouse IgG	goat, polyclonal	Life Technologies	1:200, 1h, RT
Alexa Fluor 546 α-rabbit IgG	goat, polyclonal	Molecular Probes	1:200, 1h, RT
α-goat IgG-HRP	rabbit, polyclonal	Dako	1:2000, 1h, RT4°C
α-human IgG (Fc)-HRP	rabbit, polyclonal	Pierce	1:500, ON, 4°C

2.1.7 Cell lines

Cell line	Source
Human umbilical vein endothelial cells (HUVEC)	Laboratory stock
Human embryonic kidney A (HEK) 293A	Life Technologies GmbH, Darmstadt, Germany
Human embryonic kidney T (HEK) 293T	Laboratory stock
C2C12	Laboratory stock

2.1.8 Cell culture media and supplements

Cell culture medium or supplement	Company
DMEM with Glutamax	Life Technologies GmbH, Darmstadt, Germany
Endothelial Cell Basal medium	PromoCell, Heidelberg, Germany
Endothelial Cell Growth medium	PromoCell, Heidelberg, Germany
Fetal bovine serum (FCS), heat inactivated	PAA laboratories GmbH, Cölbe, Germany
Horse serum, heat inactivated	Life Technologies GmbH, Darmstadt, Germany
Medium-199	Sigma-Aldrich GmbH, Seelze, Germany
Optimem	Life Technologies GmbH, Darmstadt, Germany
Penicillin/Streptomycin	Life Technologies GmbH, Darmstadt, Germany
RPMI	Life Technologies GmbH, Darmstadt, Germany
Supplemental Mix C-39215 for ECGM	PromoCell, Heidelberg, Germany
Trypsin-EDTA 0.05%	Life Technologies GmbH, Darmstadt, Germany
VEGF-A (165) (human, rec. protein)	RELIA Tech, Wolfenbüttel, Germany
Williams´E medium	Life Technologies GmbH, Darmstadt, Germany

2.1.9 Consumables

Consumable material	Company
BD U100-Insuline Micro-Fine + (0.5 ml)	BD Bioscience, Heidelberg, Germany
Cell culture plates CELLSTAR® (6-, 12-, 24-, 48- and 96-well)	Greiner Bio-One GmbH, Frickenhausen, Germany
Cell culture petri dishes CELLSTAR® (10 cm, 15 cm diameter)	Greiner Bio-One GmbH, Frickenhausen, Germany
Cell scraper, BD Falcon™	BD Bioscience, Heidelberg, Germany
Chromatography paper, Whatman, 3mm	GE Healthcare, Little Chalfont, UK
Conical tubes, Falcon BlueMax™ (15ml, 50 ml)	BD Bioscience, Heidelberg, Germany
Cryo Tube™ Vials	Thermo Scientific GmbH, Schwerte, Germany
Laboratory paraffin film, Parafilm "M"	Pechiney Plastic Packaging, Chicago, USA
Microcentrifuge Safelock Tubes (0.5 ml, 1.5 ml, 2.0 ml)	Eppendorf AG, Hamburg, Germany
Microscope slides 76 x 26 mm	R. Langenbrincken, Teningen, Germany
PCR tubes nuclease-, DNA- and RNA-free	Brand GmbH, Wertheim, Germany
Pipettes (1 mL, 200 µL, 100 µL and 10 µL)	Eppendorf AG, Hamburg, Germany
Pipettes (2 ml, 5 ml, 25 ml, 50 ml)	BD Bioscience, Heidelberg, Germany
Pasteur pipettes (glass)	John Pulter LTD, Essex, UK
Pasteur pipettes (plastic)	MBT Brand, Gießen, Germany
PVDF membrane Immobilion™-P	Merck-Millipore, Billerica, USA
Tissue culture flasks 75 cm^2 CELLSTAR®	Greiner Bio-One GmbH, Frickenhausen, Germany
Sterile filters Rotilabo®, CME	Carl Roth GmbH, Karlsruhe, Germany

2.1.10 Kits and ready-to-use solutions

Kit or solution	Manufacturer
AceGlow chemiluminescence substrate	Peqlab Biotechnology GmbH, Erlangen, Germany
ECL Western Blot Detection Kit	GE Healthcare, Littler Chalfont, UK
Cell Proliferation ELISA, BrdU	Roche Applied Science, Mannheim, Germany
DNA ladder Mix	Fermentas GmbH, St. Leon-Rot, Germany
DPX mounting medium, non-aqueous medium	Sigma-Aldrich GmbH, Seelze, Germany
Dry milk powder	Carl Roth GmbH, Karlsruhe, Germany
Eosin ready to use solution	Carl Roth GmbH, Karlsruhe, Germany
Fetal goat serum (10 %, ready-to-use)	Life Technologies GmbH, Darmstadt, Germany
Fluorescence mounting medium, aqueous medium	Dako Deutschland GmbH, Hamburg, Germany
Giemsa Stain Accustain	Sigma-Aldrich GmbH, Seelze, Germany
Anti-CD146-MACS MicroBeads	Miltenyi Biotec, Bergisch Gladbach, Germany
Isolectin B_4 (BSI-B_4), FITC conjugate, lyophilized powder	Sigma-Aldrich GmbH, Seelze, Germany
Hämalaun ready to use solution	Carl Roth GmbH, Karlsruhe, Germany
Luria Bertani Agar	Sigma-Aldrich GmbH, Seelze, Germany
Luria Bertani medium, LB Broth	Sigma-Aldrich GmbH, Seelze, Germany
MACS magnetic columns	Miltenyi Biotec, Bergisch Gladbach, Germany
NucleoSpin Extract II	Macherey-Nagel GmbH, Düren, Germany
Oligofectamin	Life Technologies GmbH, Darmstadt, Germany
PageRuler™Plus prestained (prot. ladder)	Fermentas GmbH, St. Leon-Rot, Germany
Phosphate buffer (PBS)	Life Technologies GmbH, Darmstadt, Germany
Protease Inhibitor Cocktail	Roche Diagnostics GmbH, Mannheim, Germany
Protein G sepharose	GE Healthcare, Littler Chalfont, UK
PureYield Plasmid Midiprep System	Promega GmbH, Mannheim, Germany
PureYield Plasmid Miniprep System	Promega GmbH, Mannheim, Germany
pENTR™/D-TOPO® system	Life Technologies GmbH, Darmstadt, Germany
Quick Ligase Kit	New England Biolabs GmbH, Frankfurt, Germany
RD Western Diet D12079B	Open Source Diets™, New Brunswick, US
RNeasy Lipid Tissue Mini Kit	Qiagen N.V., Hilden, Germany
RNeasy Mini Kit	Qiagen N.V., Hilden, Germany
Tissue Tek™ mounting media	Sekura Finetek Europe B.V. KvK, Stauffen, Germany

2.1.11 Buffers and solutions

Aniline Blue solution
2.5 g Aniline blue
2 ml Glacial acetic acide
100 ml ddH_2O

Biebrich Scarlet-Acid Fuchsin solution
90 ml Biebrich scarlet 1 % in ddH_2O
10 ml Acid fuchsin 1 % in ddH_2O
1 ml Glacial acetic acid

Blocking buffer
3 % BSA
Dissolved in PBS-T

Blotting buffer (10x)
106.6 g glycine (1.42 M)
30.28 g Tris (250 mM)
ad 1 l ddH_2O

Bouin's solution
75 ml Picric acid
25 ml Formaldehyde (37 %)
5 ml Glacial acetic acid

Glycerin jelly
10 g Gelatin; 60.0 ml ddH_2O
Stir and heat until melting
70.0 ml Glycerin; 1.0 ml Phenol;
Store at 4°C

Hanks buffer (1l)
8.0 g NaCl; 3.05 g Hepes
400 mg KCl
60 mg Na_2HPO_4 x2 H_2O
60 mg KH_2PO_4
adjust pH to 7,4
add ddH_2O to 1l, autoclave

Hanks I buffer
400 ml Hanks buffer
152 mg EGTA (1 mM)
4 ml Glucose solution (10 %)
Buffer has to be prepared freshly
adjust pH to 7,4
sterile filtrate (0,22 µm)

Hanks II buffer
400 ml Hanks buffer
100 mg Collagenase CLS II (0,3 mg/ml); 389 mg $CaCl_2x2H_2O$
4 ml Glucose (10 %)
Buffer has to be prepared freshly
adjust pH to 7,4; sterile filtrate

Laemmli buffer (4x)
62.5 mM Tris (pH 6.8)
2 % SDS; 10 % Glycerol
5 % 2-mercaptoethanol
0.001 % bromophenolblue in ddH_2O

Loading dye for nucleic acids (6x)
0.25% bromophenol blue
0.25% xylene cyanol
50% sucrose
0.1 M EDTA (in ddH_2O)

Oil Red O solution (0.5 %)
0.5 g Oil Red O; 100 ml Propylene
Solution has to be heated to 95 - 100°C for solubility, filtered and stored at 60°C

PAGE electrophoresis buffer (10 x)
144 g glycine (1.92 M)
30 g Tris (248 mM)
10 g SDS (35 mM); ad 1 l ddH_2O

PBLEC
1 % Triton-X-100; 0.1 mmol $CaCl_2$
0.1 mmol $MgCl_2$; 0.1 mmol $MnCl_2$
Adjust in 1 x PBS to pH 6.8

PBS (10x)
400g NaCl; 10 g KCl
57 g Na_2HPO4; 10 g KH_2PO4
6 ml ddH_2O, adjust to pH 6.8

PBS-T (10x)
PBS (1x)
0.05 % Tween-20

PFA (10%)
50g Paraformaldehyd and
1g NaOH were dissolved in 400 ml prewarmed H_2O. Adjust pH to 7.2 by addition of 4.2 g NaH_2PO_4.
Ad 500 ml ddH_2O

Phosphomolybdic-Phosphotungstic Acid solution:
25 ml Phosphomolybdic acid (5 %)
25 ml Phosphotungstic acid (5%)

Protein Lysis buffer (RIPA buffer)
50 mM Tris-HCl (pH 7.6)
150 mM NaCl; 1 mM EDTA
1 % Nonidet P40; 1 % SDS
0.25 % Natriumdesoxycholat
20 % Glycerol
4 µl/ml Proteinase Inhibitor (PIC) (1 PIC tablet for 2 ml ddH_2O)
DTT (1 mM)
DTT and PIC were added freshly.

Soerensen Buffer
Soerensen buffer A
9 g KH_2PO_4 (66 mM) ad 1l ddH_2O
Soerensen buffer B
11.8 g Na_2HPO_4 (83 mM) ad 1l ddH2O

TAE (50x)
242 g Tris (2 M)
57.1 ml acetic acid (1 M)
100 ml of 500 mM EDTA (pH 8.0) solution (50 mM); ad 1 l ddH_2O

Stripping solution
62.5 mM Tris (pH 6.8); 2 % SDS
0.75 % 2-mercaptoethanol

Tissue lysis buffer (50x
1.25 M NaOH
10 mM EDTA

Tissue neutralization buffer (50x)
400 mM Tris-HCl (pH 5)

Weigert's Iron Hematoxylin solution
Solution A: 1 g Hematoxylin + 100 ml Alcohol (95 %)
Solution B: 4 ml Ferric chloride (29% in ddH_2O) + 95 ml ddH_2O + 1ml absolute Hydrochloric acid
Working Solution: Equal parts of solution A+B were mixed.
Working solution is stable for 3 months

1 x working solutions were prepared by diluting the 10 x stock solutions 1:10 and the 50 x stock solutions 1:50 in ddH_2O. If not mentioned, 1 x solutions of the listed buffers were used for experiments.

Preparation of Methocel

Before use, the carboxymethylcellulose (12 g/l) was autoclaved. Subsequently, 250 ml of pre-heated ECGM was added to the solution and stirred for 20 min. Afterwards, another 250 ml of ECGM was added. The solution was then stirred at 4°C ON. The solution was aliquoted in 50 ml reaction tubes and centrifuged at 3500 x g at 4°C for 4 h. The supernatant was used for experiments.

Production of type I collagen from rat tail tendons

Frozen rat tails were defrosted in 70 % ethanol for 20 min. The entire length of the tails were skinned and the vertebrae were broken in order to expose the tendons. The tendons were then dissected and incubated in 70 % ethanol for 15 min and air-dried. To isolate type I collagen, the tendons were incubated in 250 ml 0.1 % acetic acid for 48 h. The resulting viscous solution was centrifuged at 24000 x g for 2 h to precipitate debris. Supernatants were aliquoted and stored at 4°C. Dilutions of the stock solution were adjusted to the needed viscosity using 0.1 % acetic acid.

2.1.12 Lab equipment and software

Equipment	Manufacturer
Absorbance Reader	Sunrise V3.21 Tecan
Autoclave	Systec GmbH, Wettenberg, Germany
Balance, PC 2200	Mettler Toledo GmbH, Giessen, Germany
Blot detector Chemi-SMART 5100	Peqlab Biotechnology GmbH, Erlangen, Germany
Boyden chamber	Neuroprobe, Gaithersberg, USA
Centrifuge 5415 R	Eppendorf AG, Hamburg, Germany
Centrifuge, Rotina 420R	Andreas Hettich GmbH, Tuttlingen, Germany
Cryotom	Thermo Scientific GmbH, Schwerte, Germany
Confocal microscope (LSM710)	Carl Zeiss AG, Oberkochen, Germany
ELISA Reader, Sunrise V3.21	Tecan GmbH, Crailsheim, Germany
Embedding machine STP120	Microm International GmbH Walldorf, Germany
Fluorescence microscope Axiovision Z1	Carl Zeiss AG, Oberkochen, Germany
Fluorescence microscope Ctr 6000	Leica, Wetzlar, Germany
Fluorescence microscope IX50	Olympus Europa GmbH, Hamburg, Germany
Freestyle Lite Set blood glucose measure system	Abbott GmbH & Co. KG, Wiesbaden, Germany
Freestyle blood glucose measure strips	Abbott GmbH & Co. KG, Wiesbaden, Germany
Freezer, -20°C	Liebherr GmbH, Ochsenhausen, Germany

Freezer, -80°C	Thermo Scientific GmbH, Schwerte, Germany
Gel electrophoresis chambers	Cti GmbH, Idstein, Germany
Heating block	Carl Roth GmbH, Karlsruhe, Germany
Incubator (cell culture)	Hera cell 250 Thermo scientific, Schwerte, Germany
Incubator (bacterial culture)	Memmert GmbH, Schwabach, Germany
Light microscope 090-135.001	Leica, Wetzlar, Germany
MACS separator ®	Miltenyi Biotec, Bergisch Gladbach, Germany
Magnetic stirrer	IKA GmbH, Staufen, Germany
Micro balance	Kern & Sohn GmbH, Bahlingen, Germany
Microtome HM355S	Microm International GmbH, Walldorf, Germany
Neubauer Cell Counting Chamber	Paul Marienfeld GmbH
PCR Cycler, MyCycler	Bio-Rad GmbH, München, Germany
pH-meter	Metrohm AG, Herisau, Switzerland
Photometer, Biophotometer	Eppendorf AG, Hamburg, Germany
Power supplies for electrophoresis	Biocom Direct, Bridge of Weir, UK
Quartz cuvette	Hellma GmbH, Müllheim, Germany
Real-time cycler StepOnePlus	Life Technologies GmbH, Darmstadt, Germany
Refrigerator	Liebherr GmbH, Ochsenhausen, Germany
Shaker, Silent rocker	Cti GmbH, Idstein, Germany
Sterile hood, Hera Safe	Thermo Scientific GmbH, Schwerte, Germany
Tank electro blotter, Perfect Blue	Peqlab Biotechnology GmbH, Erlangen Germany
Vortex mixer	Scientific Industries, New York, USA
Water bath SW20	Julabo, Seelbach, Germany
Water treatment plant Milli-Q	Merck-Millipore, Billerica, USA

Software	Manufacturer
Axiovision	Carl Zeiss AG, Oberkochen, Germany
Bioedit 7.1.3	Ibis Biosciences, Carslbad, USA
Cell^P	Olympus Europa GmbH, Hamburg, Germany
ClustalW	European Bioinformatics Institute 2012, Heidelberg, Germany
Endnote X4	Thomson Reuters, New York, USA
Fiji	http://fiji.sc
ImageJ	National Institutes of Health, Bethesda, USA
IrfanView 4.3	Irfan Skiljan
Leica Application Suite	Leica Microsystems, Wetzlar, Germany
Microsoft Office package 2003-2010	Microsoft Corp., Redmond, USA
Photoshop CS4	Adobe Systems Inc., San Jose, USA
Primer3	Whitehead Institute for Biomedical Research, Cambridge, USA
StepOne™ V 2.0	Life Technologies GmbH, Darmstadt, Germany

Microscopy software (Cell^P, Fiji, Axiovision and Leica Application Suite) was used to take images. For further procession of pictures IrfanView and Fiji were used. Changes in color or brightness were done for the whole experiment with the same intensity.

2.2 Biochemical and biomolecular methods

2.2.1 Molecular cloning

Oligonucleotide sequences of the primers used for cloning are listed in section 2.1.3. Commercially plasmids (described in section 2.1.4.1) served as basis for the following cloning procedures:

pENTR3C-pIRES-DLL4full-eGFP

DLL4 full length overexpression construct cloned by Dr. rer. nat. Seven Liebler

pENTR2b-IL2ss-Fc construct:

The 1kb hIgG1 Fc sequence containing IL2ss, MCS, hinge, CH2 and CH3 with introns and STOP codon was digested out from pINFUSE-hIgG1-Fc2 vector with the enzymes KasI and NheI and blunt ended with Klenow fragment. The pENTR2b entry vector was digested with EcoRI and EcoRV and blunt ended with Klenow fragment. The hIgG1 Fc sequence was ligated into the pENTR2b vector and the generated vector served as an entry vector containing the IL2ss-Fc sequence for Gateway cloning (section 2.2.2).

DLL1-DSL-Fc expression construct:

DLL1-DSL was amplified from human umbilical venous endothelial cell (HUVEC) cDNA with a PCR using the primers DLL1-DSL-5Nco and DLL1-DSL-3BglII. The 179bp amplificate was purified by gel extraction, digested with the enzymes NcoI and BglII. The fragment was cloned upstream of the hIgG1 Fc sequence into the pINFUSE-hIgG1-Fc2 vector digested with the same enzymes. The DLL1-DSL-hIgG1-Fc fragment with 1179 bp was digested with the enzymes KasI and NheI and blunt ended with Klenow fragment. The pENTR2b entry vector was digested with EcoRI and EcoRV and blunt ended with Klenow fragment. The DLL1-DSL-hIgG1 Fc sequence was ligated into the pENTR2b vector and Gateway cloning (section 2.2.2) was performed to transfer the DLL1-DSL-hIgG1 Fc construct into the pAD/CMV/V5-DEST destination vector for the production of adenovirus (section 2.4.5).

DLL4-DSL-Fc expression construct:

DLL4-DSL was amplified from human umbilical venous endothelial cell (HUVEC) cDNA with a PCR using the primers DLL4-DSL-5Ncoand DLL4-DSL-3BglII. The 249bp amplificate was purified by gel extraction, digested with the enzymes NcoI and BglII. The fragment was cloned upstream of the hIgG1 Fc sequence into the pINFUSE-hIgG1-Fc2 vector digested with the same enzymes. The DLL4-DSL-hIgG1 Fc fragment with 1249 bp was digested with the enzymes KasI and NheI and blunt ended with Klenow fragment. The pENTR2b entry vector was digested with EcoRI and EcoRV and blunt also ended with Klenow fragment. The DLL4-DSL-hIgG1 Fc sequence was ligated into the pENTR2b vector and Gateway cloning (section 2.2.2) was performed to transfer the DLL4-DSL-hIgG1 Fc construct into the pAD/CMV/V5-DEST destination vector for the production of adenovirus (section 2.4.5).

JAG1-DSL-Fc expression construct:

JAG1-DSL was amplified from human umbilical venous endothelial cell (HUVEC) cDNA with a PCR using the primers JAG1-DSL-5Nco and JAG1-DSL-3BglII. The 236 bp amplificate was purified by gel extraction, digested with the enzymes NcoI and BglII. The fragment was cloned upstream of the hIgG1 Fc sequence into the pINFUSE-hIgG1-Fc2 vector digested with the same enzymes. Because of problems with the entry vector, specific primers were designed corresponding to the pENTR™/D-TOPO® system protocol to amplify the JAG1-DSL-IL2ss-Fc region by PCR. The flanking sequences of the primers enabled directional cloning of the amplified construct into the pENTR™/D-TOPO® vector to generate an entry clone. Gateway cloning (section 2.2.2) was performed to transfer the JAG1-DSL-hIgG1 Fc construct into the pAD/CMV/V5-DEST destination vector for the production of adenovirus (section 2.4.5).

JAG1-ECD-Fc expression construct:

The pCMV-ENTR-hJAG1 plasmid was digested with the enzymes SacI and XhoI to delete the transmembrane- and intracellular domain of JAG1. The 1kb hIgG1 Fc sequence containing IL2ss, MCS, hinge, CH2 and CH3 with introns and STOP codon was amplified by PCR from pINFUSE-hIgG1-Fc2 vector as template with the primers Fc-SacI-for and Fc-XhoI-rev. The amplification product was digested with the enzymes SacI and XhoI and ligated in the modified pCMV-ENTR-hJAG1 digested with SalI and EcoRV. Gateway cloning (section 2.2.2) was performed to transfer the 4kb JAG1-ECD-hIgG1 Fc fragment into the pAD/CMV/V5-DEST destination vector for production of adenovirus (section 2.4.5).

DLL4-ECD-Fc expression construct:

The sequence of human full length DLL4 was digested out of the plasmid pENTR3C-pIRES-DLL4full-eGFP with the enzymes SalI and SmaI. The DLL4 full length fragment of 2 kb was ligated in the pENTR3c-IL2ss-Fc digested with SalI and EcoRV. The DLL4-ECD domain fused to IL2ss-Fc was amplified by PCR with the primers DLL4-ex9early-for and DLL4-Fc-Nco-rev using the new created pENTR3c-pIRES-DLL4full-IL2ss-Fc as template. The amplification product was digested with the enzymes XhoI and NcoI and ligated into the pENTR3c-pIRES-DLL4full-IL2ss-Fc vector digested with the same enzymes to delete the transmembrane- and the intracellular domain of DLL4. Gateway cloning (section 2.2.2) was performed to transfer the 2.5 kb DLL4-ECD-IL2ss-Fc fragment into the pAD/CMV/V5-DEST destination vector for the production of adenovirus (section 2.4.5).

NOTCH1-EGF11-13-Fc expression construct:

NOTCH1-EGF11-13 was amplified from human umbilical venous endothelial cell (HUVEC) cDNA with a PCR using the primers NOTCH1-EGF-Eco-for andNotch1-EGF-Bgl-rev. The 370 bp amplification product was purified by gel extraction, digested with the enzymes EcoRI and BglI and ligated into pENTR2b-IL2ss-Fc vector upstream of the hIgG1 Fc sequence digested with the same enzymes. The NOTCH1-EGF11-13-Fc 1370 bp fragment was transferred by Gateway cloning (section 2.2.2) into the pAD/CMV/V5-DEST destination vector for the production of adenovirus (section 2.4.5).

All enzymes were purchased from New England Biolabs GmbH, Frankfurt, Germany. The sequence of cloned plasmids was verified by the Sequencing Core Facility of the DKFZ, Heidelberg, Germany.

2.2.2 Gateway cloning

The gateway cloning technology enables the transfer of DNA-fragments between plasmids. The technique is based on site-specific *att* recombination used by bacteriophage ƛ to integrate DNA sequences into the genome of *E. coli*. Gateway cloning technology requires an initial insertion of the DNA fragment of interest into an entry vector such as a pENTR vector, containing two flanking attL recombination sequences. The gateway destination vector, usually a pAdeno vector, contains a ccdB sequence, which is flanked by attR sequences. The enzymes Int (Integrase) derived from the bacteriophage ƛ and the protein IHF (Integration Host Factor) derived from *E. coli* induce homologous recombination of attL with attR sequences, while maintaining the reading frame. The sequence of interest is then transferred into the destination vector, which can be used for the production of adenovirus. The ccdB sequence of the destination vector, which encodes a protein that is toxic for standard *E. coli* strains, is excised during homologous recombination and integrated into a by-product (section 2.2.1).

The pENTR^{TM}2B and pENTR^{TM}3C vectors (Life Technologies, Darmstadt, Germany) were chosen as entry vectors. Positive clones were selected based on kanamycin resistance. The attL flanked DNA was transferred by homologous recombination into an adeno-Gateway vector (pAd/CMV/V5-DEST) containing attR sites (Figure 12). Expression clones containing the DNA sequence of interest were positively selected based on their ampicillin resistance.

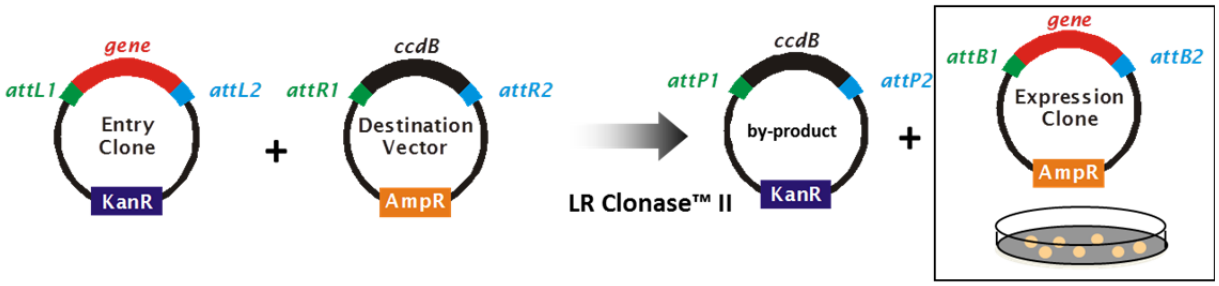

Figure 12: Gateway cloning technology

LR Gateway recombination resulted in the production of an ampicillin-resistant expression clone and a by-product. Reprinted by permission from Life Technologies, copyright (2011).

The Gateway® LR Clonase™ Kit was used as described in the manufacturers manual (Life Technologies, Darmstadt, Germany). In short, 150 ng of the pENTR™ entry clone and 300 ng of the pAdeno-DEST-V5 were mixed with 1µl of Gateway LR Clonase II Mix in a total volume of 4 µl TE buffer. After an 1h incubation at RT, the recombination process was stopped by addition of 0.5 µl proteinase K and an additional 10 min incubation at 37°C.

The destination vector containing the DNA sequence of interest was transformed into an *E.coli* strain as described in section 2.2.4. IN order to select positive clones, the transformed bacteria were plated on plates containing ampicillin.

2.2.3 DNA preparation

Depending on the volume of the bacterial cultures (2-6 ml or 100-250 ml), isolation of plasmid DNA from those cultures was performed using either the PureYield Plasmid Miniprep System or the PureYield Plasmid Midiprep System (Promega GmbH, Mannheim, Germany). Isolations were performed according to the manufacturer's protocol. The procedure is based on an alkaline bacterial lysis, which is neutralized after addition of acetic acid. Silica-membrane columns bind the plasmid DNA with high affinity and allow washing, endotoxin removal and elution of purified DNA with H_2O or TE buffer. Purified Plasmid DNA was stored at -20°C. For isolation of murine DNA a small piece of tissue, predominantly tail, was lysed in 200 µl Tail Lysis solution (1 x) under constant shaking at 95°C for 45 min. The samples were cooled down to RT and neutralized by addition of 200 µl Tris-HCl pH 5 (1 x). Then, 1 µl of the suspension was used for genotyping by PCR.

Concentration of isolated nucleic acids such as DNA and RNA was determined by measuring of the optical density at 260 nm using a photo-spectrometer (Eppendorf AG, Hamburg, Germany). Samples were diluted 1:100 in ddH_2O and transferred in a silica glass cuvette with a total volume of 100 µl. In order to remove background signals, the blank values of ddH_2O were subtracted from the sample values. The extinction of nucleic acids was measured at 260 nm, while proteins were measured at 280 nm. The ratio between the extinctions at 260 nm and 280 nm reflects the purity of the isolated nucleic acids. DNA preparation was successful resulting in a ratio of $E_{260}/E_{280} \geq 1.8$.

2.2.4 Transformation of competent *E.coli*

Plasmid constructs generated by molecular cloning were transformed into the DH5α or Stbl3 *E.coli* strains. The latter was used for transformation of Gateway plasmids. Briefly, competent bacteria were thawed on ice, mixed with differing amounts of plasmid-DNA and incubated for 20 min on ice. Transformation of bacteria was performed by heat shock at 42°C for 90 sec directly followed by cooling on ice for 1 min. Bacteria were incubated with 200 µl LB medium under constant shaking at 37°C for 45 min. Bacteria were plated on LB plates containing appropriate antibiotics and incubated at 37°C and 5 % CO_2 ON. Positive clones were picked, amplified in 6 ml LB medium and tested by analytical PCR analysis for the presence of the transformed plasmids. Plasmid-DNA was then purified as described in section 2.2.3. Sequencing was performed at the Sequencing Core Facility of the German Cancer Research Center Heidelberg (DKFZ). The BioEdit software package was used to analyze the obtained sequences (Ibis Biosciences, Carlsbad, USA).

2.2.5 RNA preparation and reverse transcription

RNA from human or murine cells and tissue was isolated using the RNeasy Mini kit (Qiagen, Hilden, Germany). Cultured cells were washed twice with PBS and lysed in a cell culture tissue plate by addition of 600 µl RLT buffer containing 1 % β-mercaptoethanol. ß-mercaptoethanol denatures proteins such as RNases by reducing disulfide bonds thus eliminating enzyme activity and preventing RNA degradation. Depending on the size of the cell culture plates, the amount of RLT buffer was adjusted accordingly. Cells were scraped off and vortexed to homogenize the cell lysate. RNA isolation was performed as described in the manufacturer´s protocol. In short, RNA was precipitated by addition of 70 % ethanol, bound by a silica-based membrane-column, washed and eluted in 30 µl nuclease-free H_2O. Isolated RNA was stored at -80°C.

RNA isolation from fat accumulating cells or fatty tissue such as liver sinusoidal endothelial cells isolated from Rbp-$j^{\Delta EC/EC}$; $ApoE^{-/-}$ and $ApoE^{-/-}$ control mice (section 2.3.1) was performed using the RNeasy Lipid Tissue Mini Kit (Qiagen N.V., Hilden, Germany).

For RNA isolation from murine tissue, following organ dissection, the samples were immediately minced on ice and frozen in liquid nitrogen. The frozen tissue was lysed with RLT buffer including 1 % β-mercaptoethanol. The tissue was homogenized by flushing the tissue 3 times through a 20-gauge needle on top of a sterile syringe. After centrifugation at 14000 rpm at 4°C for 5 min, the supernatant was processed as described for cultured cells. RNA concentration and purity was determined by measurement of the optical density of nucleic acids at 260 nm using a photo-spectrometer (Eppendorf AG, Hamburg, Germany), as described for DNA in section 2.2.3. RNA preparation was successful at a ratio of $E_{260}/E_{280} \geq 2$.

Reverse transcription polymerase chain reaction was performed to reverse transcribe mRNA into its complementary DNA, referred to as cDNA. The mechanism of reverse transcription originated from retroviruses. These viruses transcribe their RNA-coded genome with help of the enzyme RNA-dependent DNA polymerase, a so called reverse transcriptase, into DNA before integrating it into the eukaryotic genome.

Isolated RNA was transcribed into cDNA with the High Capacity cDNA Reverse Transcription Kit (Life Technologies GmbH, Darmstadt, Germany). The kit was used as described in the manufacturer's manual. Briefly, 1 µg of RNA was diluted in 10 µl of ddH_2O and mixed with 10 µl of a transcription mix. The transcription mix contained 2 µl RT buffer (10 x), 0.8 µl dNTPs (2.5 mM per nucleotide), 2 µl random primers, 1 µl reverse transcriptase (200 U/ml) and 4.2 µl ddH_2O. Amplification of cDNA was performed by polymerase chain reaction (PCR) in a thermocycler with the following program:

Reverse transcription PCR program	**Time**	**Temp.**
1. Incubation	10 min	25°C
2. Reverse transcription	120 min	37°C
3. Inactivation of the enzyme	5 sec	85°C

Samples were diluted to a volume of 100 µl with ddH_2O and stored at -20°C.

2.2.6 Polymerase chain reaction

The polymerase chain reaction (PCR) is a method to amplify a DNA sequence of interest (Mullis et al., 1986). The principle is based on thermal cycles of alternating heating and cooling steps. Reagents for a PCR reaction include DNA for amplification, dNTPs for the elongation of DNA molecules, a heat-stable DNA polymerase, and short single stranded DNA oligonucleotides, so called primers, which are complementary to both ends of the target sequence.

An initial heating step at ≥ 90°C was necessary to heat-activate the polymerase. The thermal cycling started with the separation of double-stranded DNA strands into single strands at high temperature, referred to as DNA denaturation. In the following step, the temperatures were lowered in order to allow the primers to anneal to the complementary target sequence. The exact temperature depended on the nucleotide composition of the specific primers and varied between 50°C to 65°C. After annealing, the temperatures were increased up to the activity optimum of the DNA polymerase. During this phase, the polymerase elongated the DNA single strands under consumption of dNTPs. The duration of elongation was dependent on the size of the DNA fragments to be amplified. The thermal cycles of heating and cooling were repeated 30-40 times and led to an exponential amplification of the specific DNA molecules. A final elongation step after the last cycle ensured a complete extension of the remaining single DNA strands.

Analytical PCR

Analytical PCR was used for the verification of cloning results and mouse genotyping. Primers were designed using the Primer3 software. Most primers were designed for an annealing temperature of 60°C in order to simplify the PCR procedure (Primers are listed in section 2.1.3). The duration of the elongation step was proportional to the product length and thus varied between 30 and 120 sec. Each PCR reaction contained the following components:

DNA template (20 - 100 ng/µl):	1 µl
forward primer (10 pM/µl):	1 µl
reverse primer (10 pM/µl):	1 µl
10x PCR buffer:	2 µl
dNTPs (25nM):	0.4 µl
Taq Polymerase (5U/µl):	0.2 µl
ddH_2O:	ad 20 µl

The cycling program was performed for 30-40 cycles in a thermo cycler:

	Time	Temp.	
1. Initiation	5 min	95°C	
2. Denaturation	30 sec	95°C	} 30-40 times
3. Annealing	30 sec	58°C-60°C	
4. Elongation	30-120 sec	72°C	
5. Final elongation	2 min	72°C	
Hold	∞	8°C	

DNA amplification and purity was confirmed by separation of the amplification products via agarose gel electrophoresis.

Quantitative PCR (qPCR)

In contrast to the analytical PCR, the quantitative PCR (qPCR) determined the copy number of cDNA templates in a PCR reaction by an intercalator-based method. A reporter DNA dye intercalates between base pairs of newly synthesized double-stranded cDNA. The intensity of its fluorescent emission are proportional to the DNA amount. The fluorescence of the labeling dye correlated with the amount of PCR product and thereby allowed to track the PCR reaction in real-time. The concentration of mRNA can be calculated by the amplification of the particular cDNA received from this mRNA. SYBR green was used as the fluorescent reporter dye and applied as POWER SYBR Green Master Mix (Life Technologies GmbH, Darmstadt, Germany), which also includes dNTPs, buffer and polymerase for qPCR reaction.

qPCR reaction components were mixed as follows:

cDNA template solution:	1 µl
forward primer (10 pM/µl):	1 µl
reverse primer (10 pM/µl):	1 µl
SYBR Green Master Mix:	12.5 µl
ddH_2O:	ad 20 µl

The samples were directly pipetted into 96-well plates. Forward and reverse primers were predominantly designed to be located on two neighboring exons. This excluded possible contaminations with genomic DNA, since genomic DNA, in contrast to cDNA, contains introns. While this short elongation time necessary is sufficient for cDNA amplification, the majority of genomic DNA remains single stranded. Quantitative PCR was performed with a StepOnePlus realtime cycler (Life Technologies GmbH, Darmstadt, Germany) using the following cycling program and subsequent analysis of the melting curve:

	Time	Temp.	
1. Initiation	10 min	95°C	
2. Denaturation	30 sec	95°C	} 35 times
3. Annealing	30 sec	60°C	
4. Elongation	30 sec	72°C	
5. Final elongation	6 min	72°C	
Calculation of the melt curve	30 sec	55°C → 95°C	↓ Increasing temperature; 1°C each step
Hold	∞	8°C	

Light emitted by the reporter dye during qPCR was quantified using the StepOne™ V2.0 software and indicated as Ct values. A normalization to the housekeeping genes hHPRT1 (Hypoxanthin-Phosphoribosyl-Transferase1) or mOAZ1 (Ornithine decarboxylase) was performed to calculate the fold change of expression. Significance was calculated using the two-tailed Student's t-test with * $p \leq 0.05$ regarded as significant.

2.2.7 Gel electrophoresis

SDS polyacrylamide gel electrophoresis

SDS polyacrylamide gel electrophoresis (SDS-PAGE) was used to separate proteins according to their electrophoretic mobility, which depends on the size and charge of a protein. SDS linearizes and adds a uniform negative charge to proteins and thus enables separation of proteins according to their size. The concentration ratio of acrylamide to bis-acrylamide in the gel determined the pore size and thus the separation rate of the proteins.

After proteins had been separated, they were transferred onto a nitrocellulose membrane and detected with appropriate antibodies during Western blot analysis (section 2.2.10). In short, cells or tissue were lysed as described in section 2.2.8 in RIPA buffer, which contained DTT to dissolve disulfide bonds and SDS. The secondary and tertiary structure of proteins was destroyed by heating the protein-buffer mixture for 10 min at 95°C. Gels for SDS-PAGE consisted of a separating gel and a stacking gel, in which the proteins were retained before entering the separating gel during the electrophoresis. Both gels consisted of acrylamide, bis-acrylamide, SDS, ammonium persulfate (APS), TEMED, and pH adjusted Tris buffer. APS and TEMED were stabilizers and initiators of polymerization. Separating gels were prepared with an acrylamide concentration of 10 %. The acrylamide concentration can be increased for higher separation efficiancy of small proteins. Electrophoresis chambers were used for the preparation of gels as described in the manufacturer´s manual. Gels were prepared with following compositions:

Separating gel (10 %)	**Stacking gel**
4 ml Rotiphorese Gel 30	1 ml Rotiphorese Gel 30
3 ml Tris buffer 1.5 M, pH 8.8	525 µl Tris buffer 1.5 M, pH 6.8
4.8 ml H_2O	4.3 ml H_2O
120 µl SDS 10 %	60 µl SDS 10 %
120 µl APS 10 %	60 µl APS 10 %
30 µl TEMED	15 µl TEMED

Electrophoresis chambers including the gels were filled with electrophoresis buffer (1 x). Protein samples were mixed 1:4 with Laemmli buffer (4 x) and applied to the wells. In addition, a pre-stained protein ladder that separates into bands with a defined size was loaded as well. Electrophoresis was performed at 100 - 120 V at RT for 2h. Next, proteins were transferred from the gel onto a nitrocellulose membrane and detected with appropriate antibodies by Western blot analysis (section 2.2.10).

Agarose gel electrophoresis

Agarose gel electrophoresis was used for separation of DNA or RNA fragments according to their size. Experiments were performed with 1 % agarose gels. Therefore, 1 % (w/v) agarose was dissolved in TAE buffer (1 x) and heated in the microwave until completely dissolved. The agarose solution was supplemented with 0.1 µg/ml ethidium bromide and poured into a casting tray with inserted combs. The gels were allowed to harden. The comb was carefully removed and the electrophoresis chamber containing the gel was filled up with TAE buffer (1 x). Samples were mixed 1:6 with loading dye (6 x) and applied to the wells. In addition, a Gene Ruler DNA ladder, which separates into bands with defined sizes, was loaded as well. Electrophoresis was performed at 100 - 120 V and bands were detected with UV light (254 nm).

2.2.8 Isolation of proteins from cell lysates

Proteins from cultured cells were isolated by addition of RIPA buffer (section 2.1.11). Cells were washed with ice cold PBS (1 x) and lysed in RIPA buffer. 200 µl RIPA buffer were added per well of a 6-well cell culture plate. Depending on the size of other cell culture plates, the amount of buffer was adjusted accordingly. After a short incubation on ice, cells were removed with a cell scraper. The cell lysate was then transferred into an Eppendorf tube. In order to remove the cell debris, the cell lysates were centrifuged at full speed and 4°C for 5 min. The supernatant was diluted 1:4 with 4 x Laemmli buffer. Protein samples were denaturated by heating at 95°C for 5 min and stored at -20°C until usage.

2.2.9 Immunoprecipitation of Fc-coupled constructs

The technique of immunoprecipitation (IP) is widely used to isolate and thereby purify specific proteins from samples such as cell crude lysates, extracts or animal tissues. Samples were treated with an insoluble resin, called Sepharose, which is bound to Protein G. Protein G is a ~60 kDa surface protein of the bacterium *S. aureus* and captures antibody complexes by binding to the Fc region of immunoglobulins. High affinity of Protein G was shown for human IgGs. HUVECs were transduced with adenovirus expressing Fc or DLL1-DSL-Fc. Cells were cultured at 37°C and 5 % CO_2 for 48 h. The amount of ECGM was reduced to 5 ml per tissue culture petri dish with a diameter of 10 cm. Sepharose G beads were used and diluted according to the manufacturer's protocol. The beads were washed twice with PBS and restored to 50 % slurry with PBS. 200 µl of the slurry was added to 5 ml of the HUVEC supernatant. The mixture was incubated at 4°C on a rocker ON. Beads were collected by centrifugation at 4°C and 14.000 x g for 10 min. The supernatant was discarded, the beads washed with PBS and the centrifugation step was repeated. Afterwards, Sepharose G beads were resuspended in 120 µl 4 x Laemmli buffer and boiled at 95°C for 5 min in order to remove the immune-complexes from the beads. Beads were collected by centrifugation and SDS-PAGE (section 2.2.7) was performed with the supernatant. Proteins were transferred onto nitrocellulose membranes and detected with an α-Fc antibody as described in the following section 2.2.10.

2.2.10 Western blot analysis

Western blot analysis is an analytical technique to detect proteins in a tissue homogenate or cell extract. Protein samples were separated by SDS-PAGE gel electrophoresis according to their size (section 2.2.7). Proteins were transferred to a nitrocellulose membrane and were detected immunohistochemically by antibodies, which were specific for the target protein. For transferring the proteins, the membrane was positioned close to the cathode (-) and covered by the SDS polyacrylamide gel, which in turn was positioned close to the anode (+). Gel and membrane were arranged in a semi dry blot system in between Whatman papers as lower and upper layer. The sandwich was wetted with 1 x blotting buffer. Peptides were transferred from the gel onto the membrane at 100 V and 4°C for 2 h. After blotting, the

membrane was blocked with 3 % BSA in PBS-T for 1 h at RT to prevent nonspecific binding of the antibodies to the surface of the membrane. Since the generated soluble Notch-constructs were already fused to an Fc-region of an antibody, the usage of a secondary HRP-coupled antibody was sufficient for detection. Blocking solution was replaced by the secondary α-human Fc-HRP antibody diluted in 1 % BSA/PBS-T at RT for 2h. The antibody solution was subsequently removed and the membrane was washed at least 3 times with PBS-T. Proteins were visualized by a ECL chemiluminescence solution. The ECL solution contains luminol, which was oxidated by the peroxidase of the secondary antibody. The luminescence was measured and analyzed using a Chemi-SMART 5100 system. To detect other proteins with the same molecular weight, the membrane was stripped with stripping solution at 60°C for 30 min and washed 3 times for 10 min with PBS at RT. To detect the housekeeping protein hGAPDH as loading control, the membrane was stripped, followed by blocking for 1h and incubated afterwards with α-GAPDH antibody (1:1000 in 1 % BSA in PBS-T) for 1 h. Next, the membrane was washed three times for 5 min with PBS-T and incubated at RT for 1 h with the corresponding HRP-labeled secondary antibody (1:2000). The membrane was washed and proteins were detected as described above.

2.2.11 Microarray analysis

Microarray analysis was performed in cooperation with the Genomics and Proteomics Core Facility of the German Cancer Research Center Heidelberg (DKFZ). The microarray analysis was performed using the Illumina's BeadArray™ technology, in which pre-synthesized oligonucleotides were coupled to beads as array elements. Each bead was coupled to a specific oligonucleotide acting as a probe for complementary sequences in the sample and an address code. Sentrix-6 BeadChips encompassed the sequences of 47000 murine genes on one chip, which were represented by approximately 47000 different oligonucleotide-coupled beads. For immobilization, the bead suspension was loaded randomly on the surface of a chip. A read-out of the address codes allocated the beads and their sequences to the position on the chip.

Liver sinusoidal endothelial cells (LSEC) were isolated from livers of 16 week old Rbp-j$^{\Delta EC/EC}$; ApoE$^{-/-}$ and ApoE$^{-/-}$ control animals 4 weeks after Tamoxifen injection (n=4; n=2). RNA was isolated using the RNeasy Lipid Tissue Mini Kit. 500 ng of total RNA at a concentration >50 ng/µl was quality controlled using an Agilent 2100 Bioanalyzer (Agilent Technologies GmbH, Böblingen, Germany). Complementary stable cDNA was produced by reverse transcription. Before usage the cDNA was transcribed back to RNA (cRNA), in which uracil-bases were labeled with biotin. cRNA samples were loaded to the chip and bound to complementary oligonucleotide sequences of the beads. Reporter RNAs lacking murine RNA sequences were added in different concentrations for background subtraction. Following washing to remove unbound RNA, Biotin was labeled with fluorescent molecules (Cy3-coupled Streptavidin). As a read-out, the amount of fluorescent signal per spot was scanned with a laser and quantile normalization across each chip was performed.

The significance (p) of the results was analyzed by comparison of one probe on the array with the negative beads. The fold change of gene expression was calculated by subtraction of the averaged signals of the control samples from the averaged signals received by hybridization with the Rbp-$j^{\Delta EC/EC}$; $ApoE^{-/-}$ samples. A fold change ≤ 1 represented a down-regulation of the transcript in LSECs from Rbp-$j^{\Delta EC/EC}$; $ApoE^{-/-}$ compared to the $ApoE^{-/-}$ control; whereas a fold change ≥1 represents an up-regulation. A fold change of 1 indicated no change of expression.

2.2.12 Histological stainings

Haematoxylin and eosin stain

The staining procedure was performed in glass racks. For paraffin embedded sections, microscope slides were rehydrated as described in section 2.3.6. Slides were rinsed in ddH_2O for 4 min. The sections were stained with filtered Mayer's hemalaun solution for 4 min and rinsed afterwards in running tap water for 3-5 min. Eosin solution was mixed with 2 % acetic acid. Slides were stained in Eosin solution and were rinsed in running tap water for 3-5 min. Sections were dehydrated (section 2.3.7) and mounted in non-aqueous DPX mounting medium.

Masson´s trichrome staining

Masson´s trichrome staining was used for the detection of collagen fibers in paraffin-embedded tissue sections. Sections were prepared, deparaffinized and rehydrated as described in 2.3.6. Sections were washed in ddH_2O, re-fixed in Bouin's solution at 56°C for 1 h and rinsed in running tap water for 5 min until removal of the yellow color. Slides were stained in Weigert's Iron Hematoxylin Solution for 4 min and afterwards rinsed in warm running tap water for 3-5 min. Sections were transferred in ddH_2O followed by staining in Biebrich scarlet-acid fuchsin solution for 10 min. After washing in ddH_2O, sections were differentiated in phosphomolybdic-phosphotungstic acid solution for 10 min. Microscope slides were then transferred immediately to aniline blue solution for 5 min, rinsed in ddH_2O and differentiated in 1 % acetic acid solution for 2min. After a last washing in ddH_2O, sections were dehydrated as described in section 2.3.6 and mounted in non-aqueous mounting medium. Collagen fibers were stained in blue and nuclei in black. Muscle, cytoplasm and keratin were coloured red.

Oil Red O staining

The fat-soluble diazo dye Oil Red O, also named Solvent Red 27 or Sudan Red 5B, was used for triglyceride and lipid staining. Staining was done on cryo-section since fixation with alcohol was described to cause a removal of lipids. Cryo-sections (5-10 µm) were prepared as described in 2.3.6. Sections were placed on a microscope slide, air-dried for 30 min at RT and fixed in freshly prepared ice cold formalin (10 %) for 10 min. Microscope slides were rinsed 3 times in ddH_2O followed by 2 incubation steps in absolute propylene glycol for 2 min. Sections were transferred in pre-warmed Oil Red O solution (60 °C) (0.5 % Oil Red O in

absolute propylene glycol) and stained for 8 min. Slides were differentiated in 85 % propylene glycol solution (dissolved in ddH_2O) for 3 min and rinsed twice in ddH_2O. Nuclei were stained with filtered Mayer's hemalaun solution for 4 min. Sections were rinsed in running tap water for 3-5 min and placed in ddH_2O. Finally, the sections were mounted in pre-heated glycerin jelly. Lipids were stained in red and nuclei in pale blue.

PAS staining

Periodic Acid Schiff (PAS) staining was used for detection of glycogen on paraffin-fixed tissue sections. Sections were deparaffinized and rehydrated as described in section 2.3.6. Slides were washed in ddH_2O and oxidized in 0.5 % periodic acid solution for 5 min. Following washing in ddH_2O microscope slides were transferred in Schiff´s reagent for 15 min, washed in warm running tap water for 5 min. Sections were washed in ddH_2O before being counterstained in Weigert's Iron Hematoxylin Solution for 2 min. Sections were rinsed in warm running tap water for 5 min and dehydrated (section 2.3.6) and mounted in non-aqueous mounting medium. Glycogen depositions were stained in purple and nuclei in blue.

2.2.13 Immunohistological stainings

Mouse skeletal myosin staining

C2C12 myogenic cells were cultured in high glucose (4.5 g/l) Dulbecco’s Modified Eagle Medium (DMEM) supplemented with 10 % FCS, 1 % Penicillin/Streptomycin solution (P/S) and GlutaMAX. Cells were transduced with adenovirus for the expression of DLL1-DSL-Fc, DLL4-DSL-Fc, JAG1-DSL-Fc, DLL4-ECD-Fc, JAG1-ECD-Fc and NOTCH1-EGF11-13-Fc or Fc control. Cells were cultured for 24h and seeded afterwards at high density on 15 mm cover slips coated with 0.2 % gelatine in PBS, in order to gain better adherence of cells. To induce myogenesis as positive control, C2C12 cells were cultured in differentiation medium consisting of DMEM supplemented with 2 % horse serum instead of 10 % FCS. After 48 h, cells were fixed and permeabilized with methanol at -20°C for 5 min. Unspecific binding sites were blocked by incubating the cells in blocking solution (3 % BSA in 0.1 % Tween in PBS) at RT for 30 min. Cells were incubated for 1h at RT with an anti-myosin antibody (1:500 in blocking solution) to detect fast-twitch skeletal myosin heavy chains. After 3 washes with PBS-T, cells were incubated for 1 h with a secondary Alexa Fluor 488-conjugated goat anti-mouse antibody (1:200 in blocking solution) followed by a washing step in PBS-T. Hoechst staining (DAPI, 1:5000 in PBS) of the nuclei was performed for additional 10 min followed by 2 washes in PBS-T. Cover slips were then mounted with fluoromount (Dako GmbH, Hamburg, Germany). Pictures were captured with a fluorescence microscope (Zeiss Axio Imager.Z1; AxioCam HRc camera).

Mouse IsolectinB$_4$ staining

Retinas of C57BL/6J mice were dissected as described in section 2.4.1. For immunohistological staining of retinal neovascularization, endothelial cells were stained with FITC-labeled *G. simplicifolia* I IsolectinB$_4$ (1mg/ml) (1:100 in PBLEC) at 4°C ON. After washing in PBS, the retinas were flat mounted in aqueous fluorescence mounting medium. Vascularization of the retinas was examined with a confocal microscope (Leica TCS SP2 Confocal Microscope, Leica, Wetzlar, Germany) and processed using Fiji software. Quantification of the vessel branches and outgrowth were performed. The numbers of sprouts at the growing front of the retina were counted on pictures captured with 100 x magnification. The mean value of sprouts per field was calculated.

Mouse CD31/Desmin/GLUT1 staining

Cryosections of murine liver, heart and tumor tissue were incubated in ddH_2O for 4 min. IN order to avoid unspecific antibody binding, the samples were incubated with 10 % goat serum (ready to use) for 1 h at RT. The slides were incubated with rat-anti mouse CD31 antibody (1:50 in PBS) at RT for 1 h. Hoechst staining (DAPI, 1:5000 in PBS) was performed for additional 10 min. Sections were washed with PBS-T and mounted in aqueous fluorescence mounting medium. The CD31 antibody was directly coupled to FITC. Images were taken with a fluorescence microscope (Leica Ctr 6000).

For CD31/Desmin co-staining of tumor tissue, sections were incubated in ddH_2O for 4 min and blocked with 10 % goat serum (ready to use) at RT for 1 h. A FITC-conjugated rat-anti mouse CD31 antibody (1:50 in PBS) and a rabbit-anti mouse desmin antibody (1:200 in PBS) were added for 1 h at RT. Following washing with PBS-T, slides were incubated with an Alexa546-conjugated secondary anti-rabbit antibody. Hoechst staining (DAPI, 1:5000 in PBS) was performed for additional 10 min. Sections were washed with PBS-T and mounted in aqueous fluorescence mounting medium.

For GLUT1/Desmin co-staining, tumor tissue was incubated in ddH_2O for 4 min and blocked with 10 % goat serum (ready to use) for 1 h at RT. Since the GLUT1 and the Desmin antibody were produced in the same species, staining was performed sequentially. Tumor sections were incubated with a rabbit-anti mouse desmin antibody (1:200 in PBS) for 1 h at RT. Slides were washed in PBS-T and incubated with an Alexa546-conjugated secondary anti-rabbit antibody at RT for 1 h. The rabbit anti-mouse Glut1 antibody was added to the sections (1:200 in PBS) at RT for 1 h. Slides were washed in PBS-T and incubated with an Alexa488-conjugated secondary anti-rabbit antibody at RT for 1 h. Hoechst staining (DAPI, 1:5000 in PBS) was performed for 10 min. Sections were washed with PBS-T and mounted in aqueous fluorescence mounting medium. Images were taken with a fluorescence microscope (Leica Ctr 6000).

2.3 Animal experimental methods

The mice were bred under specified-pathogen-free (SPF) barrier conditions, housed in individually ventilated cages and maintained in a temperature controlled room at the animal housing facility of the German Cancer Research Center (DKFZ) Heidelberg. All mice were tested in regular intervals in accordance with FELASA guiding principle for their health status. Mice were handled in accordance with guidelines of the Regierungspräsidium Karlsruhe and the approved protocol number: 35-9185.81/G-44/08 and 5-9185.81/G-77/11.

2.3.1 Generation of mouse models with conditional endothelial-specific deletion of Notch signaling

A transgenic mouse strain with Tamoxifen-inducible endothelial specific recombination of the Rbp-j gene was created by crossing Tg (Cdh5-cre/ERT2)1^{Rha} mice (MGI: 3848982) with $Rbpj^{tm1.1Rsch}$ (MGI: 3809244) mice (Nakhai et al., 2008; Sorensen et al., 2009).
Tg (Cdh5-cre/ERT2)1^{Rha} mice express a Tamoxifen-inducible cre fused to a modified estrogen receptor (ERT2) under control of the VE-cadherin (Cdh5) promoter, as well as, other regulatory sequences within the Cdh5 gene. $Rbpj^{tm1.1Rsch}$ transgenic mice carry loxP sites upstream of exon 6 and downstream of exon 7 of the Rbp-j gene. The generated mouse strain was officially referred to as B6-$Rbpj^{tm1Rsch}$ Tg(Cdh5-cre/ERT2)1Rha (short: $Rbpj^{flox/flox}$; VE-Cadherin-Cre^{ERT2}).
Some of the $Rbpj^{flox/flox}$; VE-Cadherin-Cre^{ERT2} transgenic mice were crossed with $ApoE^{tm1Unc}$ transgenic mice (MGI: 1857129), in which an insertion of a neomycin resistance cassette deleted parts of exon and intron 3 of the ApoE gene (Piedrahita et al., 1992). The generated strain was officially referred to as B6-Tg(Cdh5-cre/ERT2)1Rha $Rbpj^{tm1Rsch}$ $Apoe^{tm1Unc}$ (short: $Rbpj^{flox/flox}$; VE-Cadherin-Cre^{ERT2}; $ApoE^{-/-}$). Application of the estrogen analogue Tamoxifen caused an induction of Cre recombinase activity.
After Tamoxifen application and successful recombination, litters were referred to as $Rbpj^{\Delta EC/EC}$ or controls depending on the presence of the VE-Cadherin-Cre^{ERT2} transgene. Cre recombinase-mediated recombination causes a frame shift resulting in a non-functional Rbp-j protein. Tamoxifen application was performed as described in section 2.3.2.

2.3.2 Tamoxifen application and Western Diet

Transgenic mice were injected intraperitoneally with 1.5 mg Tamoxifen (in peanut oil) for 5 days. Tamoxifen treatment did not cause recombination of Rbp-j in mice lacking the VE-Cadherin-Cre^{ERT2} transgene. Subsequent to Tamoxifen application, food was changed to Western Diet (Open Source Diets) for the ApoE-deficient strain. The heath status was controlled in short intervals.

2.3.3 Genotyping

The mice were genotyped by PCR analysis (section 2.2.6) at an age between 2 and 3 weeks. Deletion of the Rbp-j gene was determined by PCR with the primers Rbp-j-for, Rbp-j-rev1 and Rbp-j-rev2. Deletion of the transgenic floxed Rbp-j sequence was verified by a 316 bp amplification product. The presence of the floxed sequence revealed a 211 bp PCR product. The existence of the VE-Cadherin-Cre gene was determined by PCR with the primer combination VE-Cad-Cre-for and VE-Cad-Cre-rev. A 166 bp amplification product indicates the presence of the transgene. ApoE genotyping was performed with ApoE-for1, ApoE-for2, and ApoE-rev primers. A 155 bp PCR product indicates a wildtype allele; whereas a 245 bp PCR product indicates a knock-out allele. Primer sequences are listed in section 2.1.3.

2.3.4 Dissection of laboratory animals

Mice were sacrificed by cervical dislocation according to FELASA guidelines. A cut from the neck to the lower abdomen was performed to open the body cavity. The organs of interest were dissected immediately and used for paraffin or cryo embedding (section 2.3.6). Small pieces of organs were collected and frozen quickly in liquid nitrogen for RNA isolation (section 2.2.5). DNA was isolated from tissue samples followed by tissue lysis as described in section 2.2.3.

2.3.5 Blood collection by cardiac puncture

Mice were sacrificed by cervical dislocation. Blood was immediately taken by insertion of a 22 gauge needle into the sternum into the heart. Blood was transferred in a heparin-coated Eppendorf tube to prevent blood agglutination. After centrifugation, the serum was diluted to a volume of 200 µl. Analyses of serum parameters were performed at the Zentrallabor of the University of Heidelberg.

2.3.6 Organ embedding and sectioning

Mice were sacrificed by cervical dislocation. Organs were dissected, washed in PBS and prepared for either paraffin or cryo-embedding.
For cryo-embedding, organs were transferred in cryo-molds and carefully surrounded with Tissue-Tek. The embedding molds were placed in a bowl filled with isopentane on top of liquid nitrogen to ensure slow freezing of the embedded organs. Cryo-embedded tissues were stored at -80°C. Cryo-sections of 4-5 µm thickness were cut with a cryotome. Resulting sections were transferred onto microscope slides and stored at -20°C until immunohistological stainings were performed (section 2.2.13).

For paraffin-embedding, organs were fixed in 10 % paraformaldehyde solution (PFA) at 4°C ON. Dehydration of embedded tissues was performed in an ascending ethanol series (70 %, 80 %, 90 %, 100 %, 100 %) for 2 h between each step. Organs were incubated in xylene for 2h followed by incubation in a mixture of xylene and liquid paraffin for additional 2 h before final embedding in paraffin. Paraffin embedded organs were stored at RT. Sections of ~6 µm thickness were cut with a microtome, transferred onto microscope slides and used for histological stainings (section 2.2.12). For histological stainings of paraffin embedded tissue, sections were deparaffinized according to the following protocol:

Xylene	5 min
Xylene	5 min
96 % Ethanol	2 min
80 % Ethanol	2 min
70 % Ethanol	2 min
ddH_2O	4 min

The particular staining was performed as described in section 2.2.12 followed by dehydration of the stained sections according to the following protocol:

ddH_2O	5 min
70 % Ethanol	2 min
80 % Ethanol	2 min
96 % Ethanol	2 min
Xylene	5 min
Xylene	5 min

Slides were covered with coverslips using non-aqueous DPX mounting medium.

2.3.7 Isolation of murine cells

Isolation of fibroblasts

Isolation of Rbp-$j^{flox/flox}$ lung fibroblasts was performed under sterile conditions. Lungs were minced and resuspended in 2 ml of 0.25 % trypsin/1mM EDTA solution for further dissociation of the cells. The cell suspension was heated for 4 min at 37°C while gently inverting the tube. Following sedimentation of the cell suspension the supernatant was mixed with 20 ml of Dulbecco's Modified Eagle Medium (DMEM) with high glucose (4.5 g/l) supplemented with 10 % FCS, 1 % Penicillin/Streptomycin solution (P/S) and GlutaMAX (D10 medium). Dissociation of the cells was enforced by repeating the addition of trypsin/1mM EDTA solution, followed by incubation at 37°C and three subsequent collections of supernatant. The collected supernatant was then centrifuged at 1000 rpm and RT for 10 min. The cell pellet containing lung fibroblasts was resuspended in 2 ml of D10 medium. Cells were seeded in 6 well tissue culture plates and incubated at 37°C and 5 % CO_2 in a humidified incubator. Treatment of fibroblasts with adenovirus expressing cre recombinase was described in section 2.5.4.

Isolation of hepatocytes

Hepatocytes of the adult livers from 16 week old Rbp-j$^{\Delta EC/EC}$; ApoE$^{-/-}$ and ApoE$^{-/-}$ control animals were isolated 4 weeks after Tamoxifen injection (n=2). Hepatocyte isolation was performed in collaboration with Tjeerd Sijmonsma (Research group of Prof. Dr. Stefan Herzig, German Cancer Research Center Heidelberg (DKFZ)).

The method was based on a two-step technique, which involved perfusion with EGTA and collagenase. Mice were anaesthetized by intraperitoneal injection with ketamine (100 mg/kg) and xylazine (10mg/kg). The peritoneal cavity was opened and a catheter was inserted into the portal vein. Liver was perfused using a peristaltic pump flushing the liver with a flow rate of (8ml/min) with pre-warmed (42°C) Hanks I buffer for 3 min. The vena cava was cut to avoid an increase of blood pressure. Perfusion buffer was switched to pre-warmed (42°C) Hanks II buffer for 5-6 min. The liver was removed and transferred into a 50 ml conical tube with 30 ml of adhesion medium (37°C). Livers of two animals per group were pooled and transferred under sterile conditions into a 10 cm cell culture dish. The liver capsules were opened with sterile forceps and cells were carefully released into the surrounding adhesion medium. The cell-rich medium was filtered with additional 10 ml of medium through a cell strainer (70 µm). The flow-through was collected in a 50 ml conical tube and filled up adjusted to 40 ml of medium. Isolated cells were centrifuged at 37xg and RT for 2 min. After removal of the supernatant containing endothelial cells and Kupffer cells, pelleted cells were resuspended in 40 ml adhesion medium. Subsequently, the centrifugation step was repeated and the cell pellet was resuspended in adhesion medium. Viable cells were enumerated via Trypan-blue staining. The number of isolated hepatocytes per liver was expected to be around 2 x 10^7 cells. 9 x 10^6 cells were cultured in 20 ml Williams´ medium supplemented with 10 % FCS, 1 % P/S, 2mM glutamine (1:100), 0.01 mg/ml Insulin (17.2µM), and 100 nM dexamethasone on collagen coated cell culture plates with a diameter of 15 cm. Cells were washed and medium was replaced after 4 h with Williams´ medium supplemented with 10 % FCS, 1 % P/S, 2mM glutamine (1:100), and 100 nM dexamethasone. Hepatocytes were used after 24 h for RNA and DNA isolation. Experiments were performed in the laboratory of Prof. Dr. Stefan Herzig at the German Cancer Research Center Heidelberg (DKFZ).

Isolation and purification of liver sinusoidal endothelial cells

Liver sinusoidal endothelial cells (LSECs) were isolated from Rbp-j$^{\Delta EC/EC}$; ApoE$^{-/-}$ mice and ApoE$^{-/-}$ control littermates 4 weeks after injection and purified as described by Diehl and colleagues (Diehl et al., 2008), with slight modifications. LSEC isolation was performed in collaboration with Dr. Philipp Koch and Dr. Cyrill Gerauld (Research group of Prof. Dr. Sergij Goerdt, Department of Dermatology, Venereology, and Allergy; University Medical Center and Medical Faculty Mannheim).

Briefly, mice were sacrificed by CO_2-asphyxation. The portal vein was perfused with a 0.05 % collagenase solution followed by removal of the liver. Liver tissues of one or two mice were pooled, minced and digested with 0.04 % collagenase solution followed by density gradient centrifugation with 35 % Nycodenz. The interface of the density gradient was subjected to Magnetic Cell Separation (MACS)-sorting with Anti-CD146-MACS MicroBeads. Purity was confirmed by FACS analysis with directly labelled antibodies against CD31 (FITC-conjugated), Stabilin-2 (biotinylated), and CD11b (PE-conjugated) and resulted in >80 % CD31+, >80 % Stabilin-2+ and <5 % CD11b+ cells. RNA was isolated using the RNeasy lipid tissue Mini Kit and used for microarray analysis. Gene expression analysis was performed at the Genomics and Proteomics Core Facility of the German Cancer Research Center Heidelberg (DKFZ) with 4 for independent samples of Rbp-$j^{\Delta EC/EC}$;$ApoE^{-/-}$ LSEC (n=6) and 2 of $ApoE^{-/-}$ control LSEC (n=4).

2.4 Functional *in vivo* assays

2.4.1 Analysis of retinal neovascularization

C57BL/6J mice were injected at postnatal days P1 and P3 with adenovirus expressing DLL1-DSL-Fc, DLL4-DSL-Fc, DLL4-ECD-Fc, NOTCH1-EGF11-13-Fc or Fc control. 30 µl of viral suspensions were administered intraperitoneally with a 500 µl syringe and a 30-gauge needle at a dose of 1×10^9 PFU/ml per neonate. Mice were monitored the following days and sacrificed at day 7 for analysis of retinal vessel growth and neovascularization. The eyes were enucleated and fixed in 4 % paraformaldehyde at 4°C for 1 h. Retinas were dissected, washed 3 times in PBS and incubated in blocking solution (1 % BSA, 0.5 % Triton-X-100 in PBS) at 4°C ON. Retinas were stained with $IsolectinB_4$ as described in section 2.2.13. Vascularization of the retinas was examined with a confocal microscope (Leica TCS SP2 Confocal Microscope, Leica, Wetzlar, Germany) and processed using the Fiji software.

2.4.2 Intraperitoneal glucose tolerance test

The intraperitoneal glucose tolerance test (IPGTT) was used to determine the clearance of glucose from the body. $Rbpj^{\Delta EC/EC}$; $ApoE^{-/-}$ and $ApoE^{-/-}$ control mice were used for IPGTT 6-9 weeks after Tamoxifen application. Following fasting for 6 h, the fasting blood glucose concentrations were measured by collecting 5 µl of blood extracted from the tail vein. Glucose solution (2 g/kg in 0.9 % NaCl) was intraperitoneal injected using a 20-gauge needle. Blood samples were collected 30, 60 and 120 min after glucose application and analyzed for glucose concentration [mg/dl] using a blood glucose meter.

2.5 Cell culture methods

2.5.1 Handling of cells

All cell culture work was performed in a sterile hood. Cells were cultured at 37°C and 5 % CO_2 in a humidified incubator. Cells were grown in tissue culture petri dishes with a diameter of 10 cm or in T75 tissue flasks in 10 ml medium. Depending on the size of other cell culture plates, the amount of medium was adjusted accordingly.

HEK 293A, HEK 293T, lung fibroblasts and C2C12 cells were cultured in Dulbecco's Modified Eagle Medium (DMEM) with high glucose (4.5 g/l) supplemented with 10 % FCS, 1 % Penicillin/Streptomycin solution (P/S) and GlutaMAX (D10 medium). Myogenic differentiation in C2C12 cells was induced by changing the medium to low-serum Dulbecco's Modified Eagle Medium (DMEM) supplemented with 2.5 % horse serum instead of 10 % FCS. HUVECs were grown in Endothelial Cell Growth Medium (ECGM) containing 10 % FCS, 1 % penicillin/streptomycin and Supplemental Mix C-39215. Cells were split at a density of ~ 80 - 90 %. For this purpose, cells were washed with PBS. After the PBS has been aspirated, Trypsin/EDTA solution was added dropwise onto the cells. Furthermore, cells were incubated at 37°C until the cells started to detach from the plate. Trypsinization was stopped by addition of 10 % FCS in PBS. The cell suspension was then centrifuged at 200xg for 5 min and the pellet was resuspended in an appropriate amount of fresh medium. Cells were transferred into a new cell culture flask or plate. Since HUVECs are primary cells, cells from passage 2 to 6 were used for the experiments. The amount of trypsinized cells was counted with a hemocytometer. The cell numbers from 4 large squares was averaged and multiplied by 10^4 to receive the number of cells/ml. Adenoviral work was performed in a biosafety level 2 laboratory.

2.5.2 Freezing and thawing cells

Cryoconservation of cells was used to store cell lines for further usage. Cells were trypsinized as described in section 2.5.1. The cell suspension was centrifuged at 200xg for 5 min to sediment the cells. The cell pellet was resuspended in the appropriate cell culture medium supplemented with 20 % FCS and 10 % DMSO. Cryo tubes were filled with 1 ml of the cell/DMSO solution. The tubes were cooled down in a freezer box filled with isopropanol at -80°C ON. Cells were transferred to liquid nitrogen for long term storage.

Cells were thawed rapidly by warming the cryo tubes at 37°C in a water bath. DMSO was removed by addition of 1 ml of warm medium and centrifugation of the cell suspension at 200xg for 5 min. The cell pellet was resuspended in fresh medium and transferred into appropriate cell culture plates. Cells were cultured as described in section 2.5.1.

2.5.3 Isolation of human umbilical vein endothelial cells

Human umbilical vein endothelial cells (HUVECs) were isolated from the vein of human umbilical cords donated by the University Hospital Mannheim. HUVEC isolation was accepted by the ethics commission of the University Hospital Mannheim.
In short, umbilical cords were washed in sterile PBS. In order to induce a dissociation of endothelial cells, veins were flushed with PBS and incubated with collagenase solution (0.1 %) at 37°C for 15 min. Collagenase solution was collected in a 50 ml tube. The veins were rinsed again with PBS. The flow-through was added to the collagen solution. After centrifugation for 5 min at 37°C the pellet containing the HUVEC was resuspended in 10 ml Endothelial Cell Growth Medium (ECGM), supplemented with 10 % FCS, 1 % P/S and supplemental mix. The cell suspension was then cultured in a T75 flask at 37°C and 5 % CO_2. The medium was refreshed after 4 h. 24 h later the HUVECs were trypsinized for cryo-conservation or split into ECGM for experimentation. To exclude vSMC contaminations, endothelial lineage was confirmed by staining of isolated HUVECs for CD31 and α-smooth muscle actin. Experiments were performed with HUVECs pooled from 3 different donors.

2.5.4 Gene transfer into eukaryotic cells

Transfer of nucleic acids into eukaryotic cells with chemical, physical or biological methods is referred to as transfection, whereas virus-mediated DNA transfer is called transduction.

Plasmid transfection with Polyethylenimine

Chemical transfection of HEK 293A cells with diverse plasmids was performed with Polyethylenimine (PEI) to force cells to express the encoded proteins. PEI is a cationic polymer of ethylenimine, which complexes with anionic DNA. In general, 3 µl PEI (1 x; 1 µg/ml dissolved in 150 nM NaCl) were used for the transfection of 1 µg DNA. Depending on the amount of DNA to be transfected, the corresponding amount of PEI (1x) was mixed with Optimem to a final volume of 100 µl. Simultaneously, DNA to be transfected was suspended in 100 µl Optimem and solutions were allowed to incubate at RT for 20 min. The PEI- and DNA-containing solutions were mixed, incubated for an additional 20 min at RT and added dropwise to the cells. Medium was changed after 24 h. Plasmid transfection with PEI was used for the production of adenovirus as described in section 2.5.5.

Adenoviral transduction

An adenovirus-mediated system was used for DNA transfer into cells. Replication deficient adenoviruses were created with the help of the ViraPower Adenoviral Expression System according to the manufacturers manual (Life Technologies GmbH, Darmstadt, Germany). Adenoviral transduction enables overexpression of DNA sequences of interest in many cell lines due to a strong CMV promoter. The replication-deficient adenoviruses cause a transient gene expression since no integration into the genome takes place. Cells were transduced at a confluency of 90 % with adenovirus expressing Fc, DLL1-DSL-Fc, DLL4-DSL-Fc, JAG1-DSL-Fc, DLL4-ECD-Fc, JAG1-ECD-Fc or NOTCH1-EGF11-13-Fc. Cell culture work was performed under biosafety level 2 conditions. 2.4 x 10^5 cells were seeded in a 6 well cell culture plate and incubated at 37°C and 5 % CO_2 ON. HUVECs were transduced by addition of 50 µl of adenovirus lysate with a concentration of 1x 10^8 PFU and a corresponding multiplicity of infection (MOI) of 200. MOI describes the number of virus particles per cell. C2C12 cells were transduced with a MOI of 400, since cells exhibited a lowered binding activity of adenoviral particles to the cell surface (Nalbantoglu et al., 1999)**.** Transduced cells were incubated ON. Cells were washed twice with PBS and fresh medium was added. Since the highest gene expression was reached 48-96 h after transduction, experiments including functional assays, qPCR or Western blot analysis were performed 48 h post transduction.

2.5.5 Production of Adenovirus

Adenovirus production was performed using the ViraPower Adenoviral Expression System according to the manufacturer's manual. The system is based on Gateway cloning technology. The pAd/CMV/V5-DEST vector was used for adenovirus production and encoded the adenovirus genome except for the E1 and E3 proteins. The E1 proteins are involved in virus replication. Adenoviruses lacking these proteins are incompetent for replication. The DNA sequences of interest were cloned into the pAd/CMV/V5-DEST vector via Gateway cloning technology as described in section 2.2.2. The adenoviral vector containing the DNA sequence of interest also contained bacterial sequences for amplification in *E.coli*. An ampicillin resistance gene enabled positive selection of bacteria expressing the construct. The amplified vector construct was linearized by the enzyme PacI to expose the viral Inverted Terminal Repeats (ITR), which were crucial for virus replication and packaging, and excise bacterial sequences. In detail, 5 µg of the generated pAd/CMV/V5-DEST plasmid was mixed with 1 µl PacI enzyme (1x10^4 U/ml), 5 µl NEB buffer 4 (10 x), 5 µl BSA (10 x) and adjusted with H_2O to a final volume of 50 µl. The reaction was incubated for 4 h at 37°C. The digested plasmid DNA was purified by precipitation with 5 µl sodium acetate solution (3 M) and 150 µl ethanol (96 %). Following centrifugation at 24100 x g for 15 min the supernatant was discarded and the pellet was washed by addition of 300 µl ethanol (70 %). The DNA suspension was centrifuged at 24100 x g for 1 min. The pellet was then air-dried and resuspended in 110 µl Optimem to a final concentration of 0.4 µg/µl.

10 µl of the plasmid solution were tested for successful PacI digestion via agarose gel electrophoresis resulting in a 2kb fragment.
Production of adenovirus was performed with PEI (1x) reagent in HEK 293A cells, a cell line expressing the E1 proteins. One day before transfection, 5×10^5 cells were seeded per well of a 6-well cell culture plate in order to reach 90 % confluency on the day prior to transfection. Cell culture medium was replaced with 800 µl of medium without antibiotics. 12 µl of the PEI (1x) transfection reagent were dissolved in 88 µl Optimem and incubated for 20 min at RT. The solution was mixed with the PacI-digested and linearized plasmid (~4 µg in 100 µl Optimem). After 20 min of incubation at RT, the solution was added dropwise to the cells. Cells were then incubated at 37°C and 5 % CO_2 ON. Since cells started to produce virus, cell culture work with adenovirus was performed in a biosafety level 2 laboratory. 24 h after transfection, the medium was replaced with DMEM supplemented with 10 % FCS, 2 mM L-glutamine, and 1 % P/S. Cells were trypsinized and transferred to 10 cm cell culture plates 48 h after transfection. The medium was replaced every 2-3 days until the formation of cell-free foci, referred to as plaques. Such foci were formed approximately 6-10 days post transfection due to virus multiplication and infection of cells. Adenovirus was harvested 10-12 days post transfection until 80 % of the cells were infected and started to detach from the cell culture plate. Adenovirus-containing cells and supernatant were collected in a 50 ml Falcon tube and subjected to 3 freeze-and-thaw cycles (-80°C for 30 min /+37°C for 15 min) in order to lyse the remaining cells and liberate intracellular virus. The adenoviral cell suspension was centrifuged for 15 min at 200 x g to remove cellular debris. The supernatant, or so called crude lysate, was stored at -80°C and enabled the re-production of virus particles. In order to increase the viral titer, 1 ml of the crude virus lysate was used for transduction of HEK 293A cells. Virus amplification was repeated as previously described. Initial plaques developed after 2-3 days post transduction. The virus-containing supernatant resulting from the virus re-amplification was stored in 500 µl aliquots at -80°C. Aliquots were used only 3 times due to the reduction of viral transduction efficiency caused by freezing and defreezing of viral aliquots.

2.5.6 Titration of adenovirus

The adenoviral titer was determined by analysis of the ability of the virus to induce plaque formation. The titer varied between 1×10^7 - 1×10^8 plaque-forming units (pfu)/ml. For this purpose, 1×10^6 HEK 293A cells were seeded in a 6-well cell culture plate and incubated at 37°C and 5 % CO_2 ON until 90 % confluency was reached on the day of infection. Adenoviral serial dilutions ranging from 10^{-3} to 10^{-9} in 1 ml of DMEM supplemented with 10 % FCS, 2 mM L-glutamine, and 1% P/S were prepared. Cell culture medium was aspirated and replaced by the serial virus dilutions. Cells were allowed to incubate ON. Medium was removed the following day and cells were overlayed with 2 ml pre-warmed agarose solution in order to prevent detachment of infected cells. For production of agarose overlay solution, 1.2 ml of 4 % pre-heated agarose (65°C) was mixed with 12 ml pre-heated plaquing medium (DMEM with 2 % FCS) (37°C).

To avoid hardening of the solution, overlay of cells had to occur immediately. After 15 min at RT cells were returned to the incubator. Cells were covered again with 1 ml of agarose overlay solution 48 h after the first overlay. Formation of plaques was detected 8-12 days after adenoviral infection. For a better visualization of the cell free areas, living cells were stained by addition of 300 µl MTT solution (5 mg/ml). MTT is a yellow dye, which is metabolized by living cells and turns blue. 3 h after MTT treatment, the number of plaques were enumerated for all dilutions. The number of plaques correlated with the number of virus particles, which are able to infect cells and was counted as PFU. The multiplicity of infection (MOI) for viral infection of cells was calculated by PFU per cell number.

2.6 Functional *in vitro* assays

2.6.1 Proliferation assay

The proliferation rate of cells was investigated using the Cell Proliferation ELISA, BrdU (colorimetric) Kit (MTT, Roche) according to the manufacturer's protocol.
5-bromo-2'-deoxyuridine (BrdU) incorporated into DNA as an analogue of thymidine during the S-Phase into DNA. BrdU incorporation correlated with the amount of newly synthesized DNA and thus provided information about the proliferation rate of examined cells. BrdU was labeled with a peroxide-coupled antibody. Addition of a substrate solution containing hydrogen peroxide caused a reaction, which resulted in the development of a dye. The absorbance of the substrate solution increased proportionally with the development of the dye and was directly measured as relative proliferation rate by an ELISA reader.
For the experiments, HUVECs were transduced with adenovirus expressing the soluble Notch ligands and receptors. 24 h post transduction, cells were trypsinized, counted and seeded with a cell number of 1000 cells/100 µl into a flat bottomed 96-well tissue culture plate. Cells were cultured at 37°C and 5 % CO_2 for 24 h. Every sample was performed in triplicates. 10µl BrdU labeling solution per well was added for an additional 24 h. The medium containing the BrdU labeling solution was aspirated, cells were fixed for 30 min with FixDenat solution and the medium was replaced with Anti-BrdU-POD working solution containing the peroxidase coupled BrdU antibody for 90 min at RT. Cells were washed in PBS followed by addition of the substrate solution. Subsequently, the cells were incubated until the color reaction started and then measured. The absorbance was measured at 400 nm. The reference was scanned at 492 nm and subtracted from the sample values. The relative proliferation rate was calculated by the absorbance ratio between control cells and sample cells. Each assay was performed in triplicates, which were normalized to respective controls and averaged.

2.6.2 Chemotactic migration assay

The modified 48-well Boyden chamber (Boyden, 1962) was used to measure the transmigration of HUVECs. To that end, HUVECs were transduced with adenoviruses expressing the soluble Notch ligands or receptors. 24 h post transduction, cells were starved in Endothelial Cell Basal Medium (ECBM) with 2.5 % FCS without any supplements ON. The lower wells of the Boyden chamber were loaded with 28.5 µl ECBM alone or supplemented with 25 ng/ml VEGF as an angiogenic stimulus. A type-I collagen-coated polycarbonate membrane with 8 µm pore diameter and a rubber gasket were carefully placed between the upper and lower part of the Boyden chamber. Wells of the upper part of the chamber were filled with 52 µl of 3 x 10^5 cells/ml HUVEC suspension. Samples were meassured in triplicates. The cells were allowed to transmigrate towards the VEGF stimulus in a humidified chamber at 37°C and 5 % CO_2 for 4 h. Afterwards the membrane-bound HUVECs were fixed in 100 % of ethanol for 10 min, washed twice in ddH_2O and stained in Giemsa solution at RT for 1 h. The membrane was washed in ddH_2O and transferred with the same orientation as on the chamber onto a cover slide. Non-migrated cells, which were located on top of the membrane, were removed with a cotton swab, while the remaining transmigrated cells were quantified on a standard microscope with 40 x magnification. Five randomly chosen fields of view were analyzed. The number of cells from 3 independent experiments was averaged.

2.6.3 3D-sprouting assay

Primary endothelial cells lost their quiescent status during cell culture in a 2-D monolayer. Culturing of endothelial cells as 3-D spheroids enabled cells to keep their quiescent stage (Korff and Augustin, 1998). The development of vessel-like structures of quiescent endothelial cells on the surface of the spheroid was investigated *in vitro* as sprouting angiogenesis. 8 x 10^4 HUVECs were transduced with adenoviruses expressing the soluble Notch ligands or receptors. 24 h post transduction, cells were trypsinized and resuspended in 5 ml of ECGM supplemented with 20 % methocel solution. The viscous cell suspension was placed as single 25 µl drops on square, non-adherent petri dishes. The cells were then incubated upside-down as hanging drops at 37°C and 5 % CO_2 ON. Due to gravity the cells accumulated at the bottom of the hanging drop and formed spheroids consisting of approximately 400 endothelial cells. Spheroids were washed and collected by carefully rinsing the petri dish with PBS, centrifuged at 1000 x g for 5 min at RT and resuspended in a mixture of 2 ml 80 % methocel and 20 % FCS. A type-I collagen solution with an optimal concentration, specific for every collagen isolation, was adjusted with 0.1 M acetic acid. In order to avoid an early polymerization of the collagen, the following steps were performed on ice. 2 ml of the collagen solution was mixed with 250 µl Medium-199 (10 x) and adjusted with 0.2 M NaOH to a pH of 7.4 until the indicator dye turned from orange to yellow (proportion 8:1:1).

The spheroid/methocel/FCS solution was mixed with the collagen solution in a proportion of 1:1 and pipetted into 3 wells of a non-adhesive 24-well cell culture plate with 1 ml/well. Gels were allowed to polymerize at 37°C and 5 % CO_2 for 30 min. To stimulate angiogenic sprouting of the spheroids, 25 ng/ml VEGF in 100 µl ECBM was added on top of the collagen gels. ECBM without stimulus was used as control. The spheroids were incubated for additional 24 h at 37°C and 5 % CO_2 and fixed with 1 ml/well 10 % paraformaldehyde.
In addition, the sprouting assay was applied to test the effect of secreted Notch ligands and receptors on endothelial sprouting. Therefore, HUVECs were transduced with adenoviruses expressing the Notch ligands or receptors. Cells were cultured in serum-reduced medium (ECBM + 1 % FCS) for 48 h. 100 µl of the conditioned medium containing the secreted proteins with or without addition of 25 ng/ml VEGF was applied onto the collagen gel containing untreated HUVEC spheroids. The spheroids were incubated for 24 h at 37°C and 5 % CO_2 and fixed with 1 ml/well 10 % paraformaldehyde, as described above.
Measurements of the cumulative sprout length per spheroid was performed with an Olympus IX50 microscope and the Cell^P and Microsoft Excel software. 10 spheroids per well and condition were analyzed. The cumulative sprout length was averaged. The experiment was repeated 3 times and significance was calculated using the two-tailed Student's t-test with * $p \leq 0.05$ regarded as significant.

2.7 Statistical analysis

All experiments were performed at least in triplicates. Averaged results were used to calculate the standard deviation. Assays with a high divergence in between the single experiments were normalized to control. The p-value was determined by application of the two-tailed Student's t-test using the software Microsoft Excel. *$p \leq 0.05$ was considered as significant. Statistical analysis for the microarray was described in section 2.2.11.

3 Results

3.1 Production and functional characterization of soluble Notch ligand and receptor constructs in endothelial cells

3.1.1 Production and testing of soluble Notch ligands and receptors

To improve benefits of Notch-blocking therapies, the crosstalk between Notch ligands and their receptors requires further investigation. Structural analysis revealed that the Delta/Serrate/LAG-2 (DSL) domain of the Notch ligand Serrate is required for receptor binding in *D. melanogaster*. Furthermore, it has been shown that the DSL domain is required for Notch trans-activation and cis-inhibition. Calculations of the electrostatic surface potential and nuclear magnetic resonance spectroscopy of human JAG1 and the NOTCH1 receptor uncovered a protein complex formation of the ligand DSL domain with the EGF-like repeats 11-13 of the NOTCH1 extracellular domain (ECD) (Cordle et al., 2008). The conservation of the DSL motif and the EGF-like repeats 11-13 was investigated in various species by amino acid sequence alignment. The comparison of protein residues of the DSL motif of *H. sapiens*, *D. melanogaster* and *C. elegans* revealed high conservation with short evolutionary distance (Figure 13, A, C). Amino acid sequence alignment of the Notch receptor EGF-like repeats 11-13 also displayed high conservation among *H. sapiens*, *D. melanogaster* and *C. elegans* (Figure 13, B, D).

In humans, the DSL domain is an exclusive characteristic for canonical Notch ligands including the Delta/Delta-like class with DLL1, DLL3 and DLL4 and the Serrate/Jagged class with JAG1 and JAG2. The DSL domain represents a short 45 aa motif within the ECD, which diverges among different ligands between 500 aa and 1000 aa due to varying numbers of EGF-like repeats.

Small soluble Notch ligand constructs were designed by PCR amplification of the DSL domain found in *DLL1, DLL4* and *JAG1*. In addition, constructs consisting of the complete ECD of the *DLL4* and *JAG1* were created to evaluate possible differences on Notch signaling activity. The effect of ligand constructs containing only the DSL domain, as well as, constructs containing the complete ECD was compared. The amplification product was subcloned into a vector construct containing the constant Fc-region of human immunoglobulin-G1 (IgG1), which resulted in solubility of the Fc-coupled constructs. In addition, fusion to the Fc portion of the IgG1 subclass from a human origin was reported to increase the protein half-life of the recombinant proteins and furthermore to enable the formation of covalent protein dimers. Application at low dosage helped to prevent increased effector functions such as antibody-dependent cellular and complement-dependent cytotoxicity (Salfeld, 2007). An IL2 signal sequence (IL2ss) enabled secretion of Fc-coupled proteins.

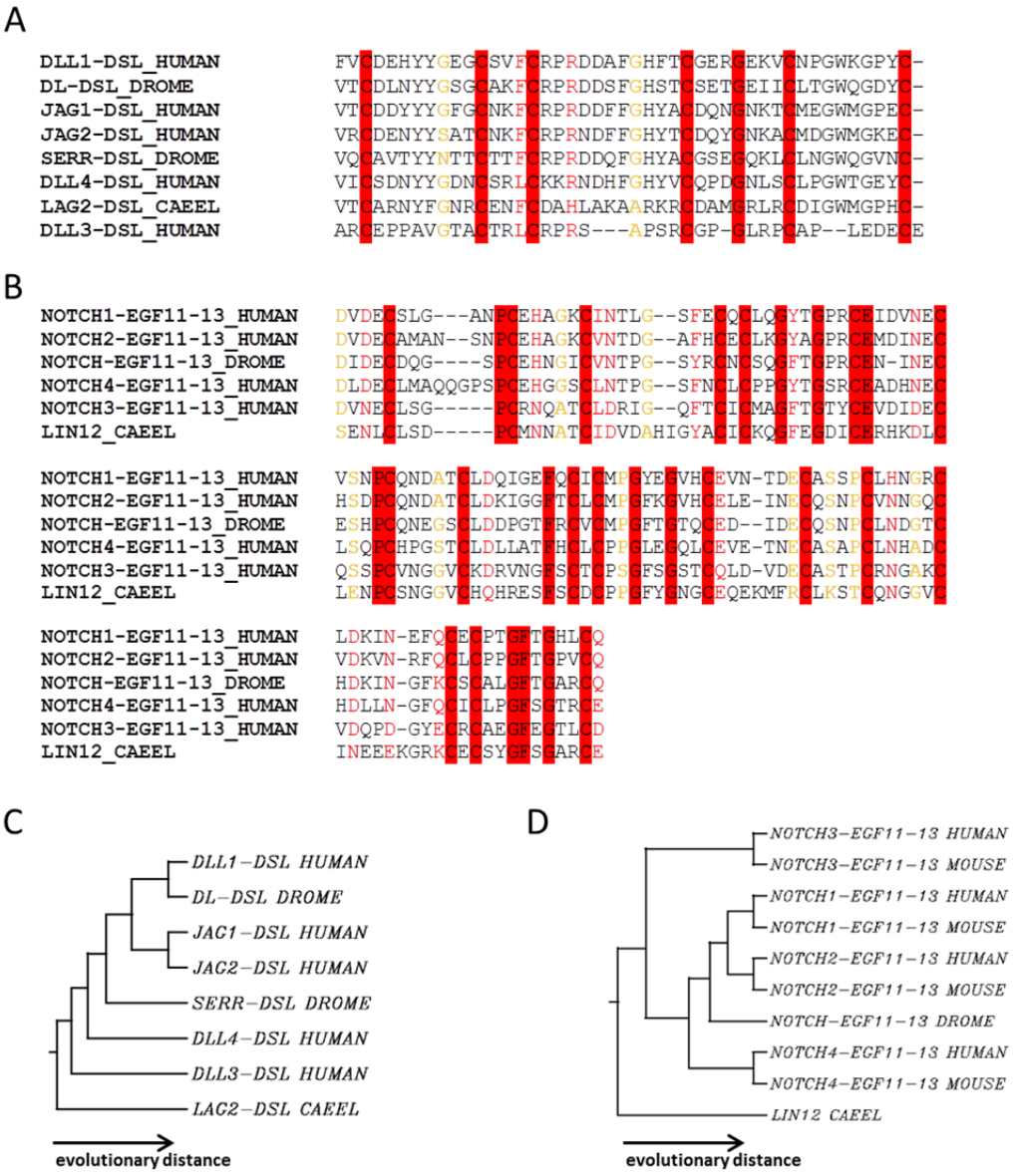

Figure 13: Protein alignment of ligand DSL motifs and Notch EGF-like repeats 11-13 revealed sequence homology between different species

(A, C) The Jagged/Delta family DSL domains of various species displayed a highly conserved sequence with short evolutionary distance (*H. sapiens* DLL1, residues 177-221; *D. melanogaster* Delta (DL), residues 182-226; *H. sapiens* JAG1, residues 185-229; *H. sapiens* JAG2, residues 196-240; *D. melanogaster* Serrate (SERR), residues 235-279; *H. sapiens* DLL4, residues 173-217; *C. elegans* LAG-2, residues 122-166; *H. sapiens* DLL3, residues 178-216). (B, D) Notch EGF-like repeats 11-13 displayed high sequence homology in various species with short evolutionary distance (*H. sapiens* NOTCH1, residues 412-526; *H. sapiens* NOTCH2, residues 415-530; *D. melanogaster* NOTCH, residues 449-562; *H. sapiens* NOTCH4, residues 432-549; *H. sapiens* NOTCH3, residues 431-541 ; *C. elegans* LIN12, residues 503-619). Identical residues were highlighted in red, conserved substitutions were labelled as red letters and semi-conserved substitutions as orange letters.

The designed soluble Notch ligands consisting of the DSL domain were designated as DLL1-DSL-Fc, DLL4-DSL-Fc and JAG1-DSL-Fc, whereas the soluble ligands consisting of the ECD domain were referred to as DLL4-ECD-Fc as well as JAG1-ECD-Fc (Figure 14). Adenoviruses expressing the different soluble ligand constructs were produced. Treatment of HUVECs with corresponding adenovirus caused an overexpression of the particular soluble Fc-coupled constructs.

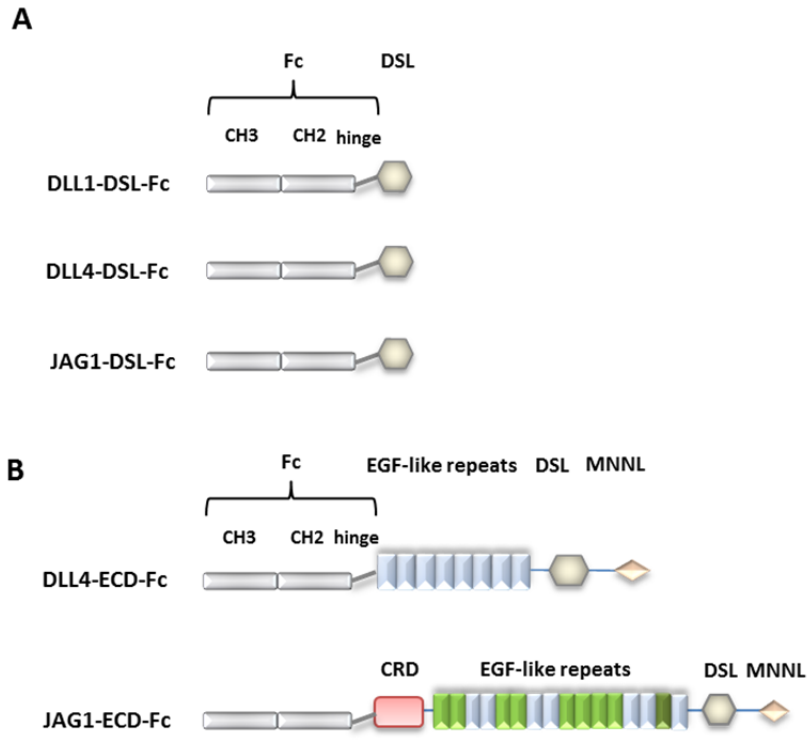

Figure 14: Architecture of soluble ligand-Fc constructs

(A) Recombinant proteins were created by fusion of the human IgG1 Fc (consisting of CH2, CH3 and hinge region) to the corresponding DSL region of the DLL1, DLL4 or JAG1 ligand. (B) Fc-coupled constructs were additionally created for the extracellular domain (ECD) of the DLL4 and the JAG1 ligand. DLL4-ECD-Fc and JAG1-ECD-Fc consist of the DSL domain preceded by a MNNL motif at the N-terminus and followed by several EGF-like repeats at the C-terminus of the Notch ligands. The number of EGF-like repeats varied depending on the ligand. EGF-like repeats with Ca^{2+} binding EGF domains were colored in green, non-Ca^{2+} binding EGF domains in blue and atypical EGF domains in dark green. A cysteine rich domain (CRD) in juxtamembrane position was only present in the Serrate/Jagged class of ligands.

As alternative to manipulating Notch signaling by soluble ligand-Fc constructs, a soluble Fc-coupled receptor was designed consisting of the NOTCH1 EGF-like repeats 11-13. The EGF-like repeats 11-13 display a 113 aa highly conserved motif of the large NOTCH1-ECD (1600 aa) and have been described to interact with the JAG1 DSL domain (Cordle et al, 2008). The Notch receptor construct, designated as NOTCH1-EGF11-13-Fc, was designed by PCR amplification of the NOTCH1 EGF-like repeats 11-13 followed by fusion to human IgG1-Fc and the IL2 secretion sequence (Figure 15). Subsequently, adenovirus expressing the soluble receptor construct was produced.

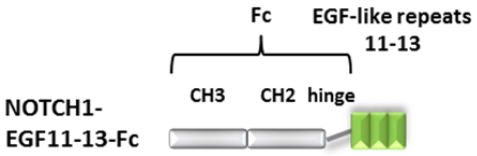

Figure 15: Architecture of a soluble NOTCH1 receptor-Fc construct

A soluble receptor construct was created by fusion of the human Fc-region (consisting of CH2, CH3 and hinge region) to the corresponding Ca^{2+} binding EGF-like repeats 11-13 of the NOTCH1 receptor.

The soluble ligand constructs were predicted to bind to the Notch receptors EGF-like 11-13 motif and thereby interfering with its signaling activity. The soluble receptor was supposed to interact with the DSL domain of the different ligands and thereby was expected to act as competitive inhibitor (Figure 16).

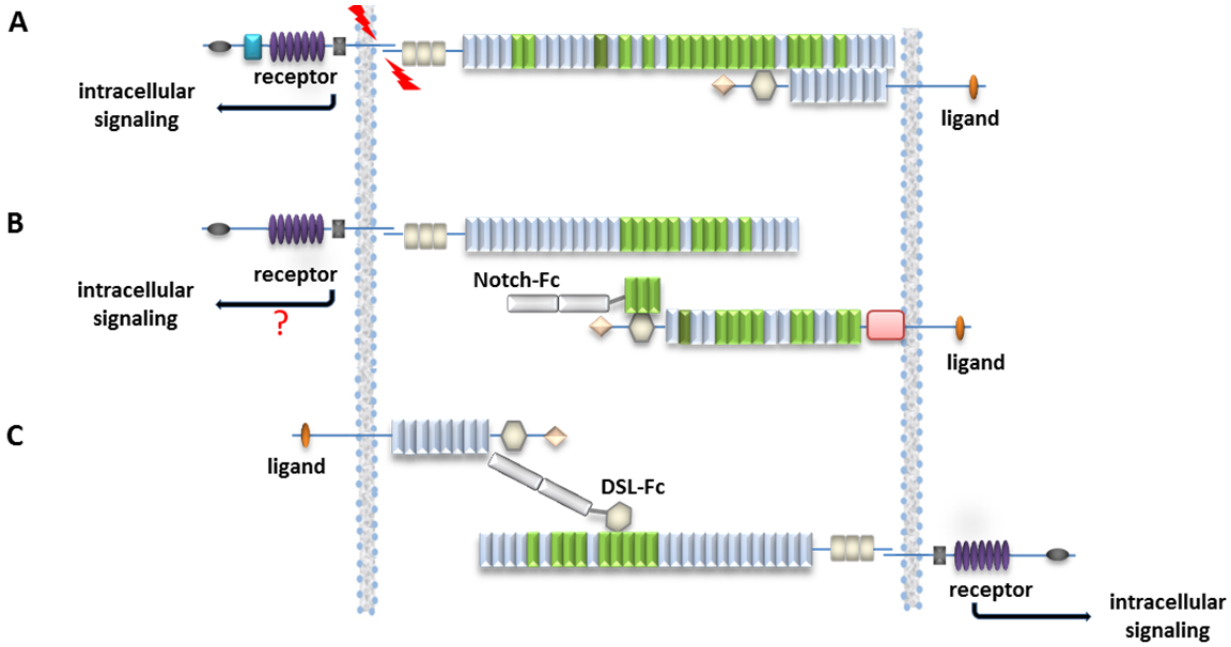

Figure 16: Supposed action of the Fc-coupled Notch interfering ligand and receptor constructs

Simplified depiction of Notch receptor and ligand expression in ECs. Notch receptors 1 and 4, denoted as ´receptor´, and Notch ligands Delta-like4 and Jagged1, denoted as ´ligands´, are broadly expressed on the EC surface with annotated domains in Figure 7 and 8. (A) Activation of the Notch receptor upon ligand binding triggers a proteolytic cleavage cascade, which results in the translocation of the Notch intracellular domain into the nucleus leading to an expression of Notch target genes. (B) Notch signaling can be interfered by a soluble Fc-fusion construct of the EGF-like repeats 11-13 of the NOTCH1 receptor, referred to as ´Notch-Fc´ that is supposed bind to the ligands´ DSL domains (grey). (C) Notch signaling can be interfered by soluble Fc-fusion constructs of the DSL domains of a DLL1, DLL4 or JAG1 ligand, referred to as ´DSL-Fc´ that supposed bind to the EGF-like repeats 11-13 of the Notch-ECD.

Secretion of soluble Notch constructs

The ligand and receptor constructs contain an IL2ss sequence, which should allow the secretion of the recombinant proteins. HUVECs were transduced with adenovirus to overexpress the Fc-coupled DLL1-DSL-Fc or Fc control construct in order to investigate the feasibility of their secretion. After 48 h, protein lysates and supernatants of the adenoviral treated HUVECs were taken for Western blot analysis. DLL1-DSL-Fc and Fc protein were detected by an α-Fc antibody and revealed specific bands with the size of 37 kDa for the Fc control and 43 kDa for DLL1-DSL-Fc in cell lysates, as well as, in conditioned supernatants. This confirmed the secretion of the constructs into the cell culture medium (Figure 17).

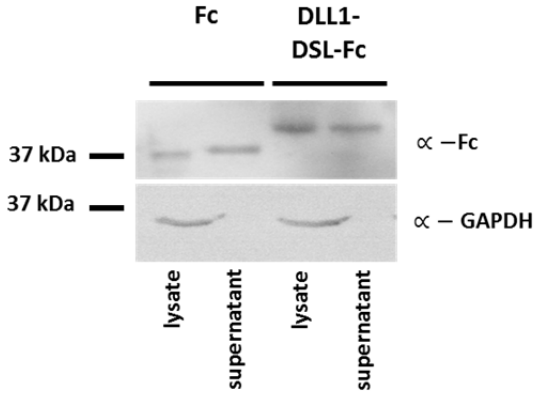

Figure 17: Secretion of the DLL1-DSL-Fc construct by HUVEC

Western blot analysis of HUVEC protein lysates and conditioned medium 48 h after adenoviral transduction revealed a strong expression of Fc and DLL1-DSL-Fc protein in cell lysates. Secretion of DLL1-DSL-Fc, as well as, Fc control into the supernatant was confirmed. Proteins were detected with an α-Fc antibody. GAPDH served as a loading control for the lysate fraction.

Purification of soluble Notch ligands

Large scale purification of the soluble Notch ligands from cell supernatants was performed by immunoprecipitation of the secreted proteins with Sepharose G beads. The high affinity of protein G to the Fc-region of immunoglobulins was exploited to precipitate and purify secreted Fc, DLL1-DSL-Fc or DLL4-DSL-Fc proteins from HUVEC supernatant. HUVECs were transduced with corresponding adenoviruses and then the proteins were immunoprecipitated 48 h later. Purified protein was detected by Western blot with an α-Fc antibody and revealed specific bands with the size of 37 kDa for the Fc control, 43 kDa for DLL1-DSL-Fc and 46 kDa for DLL4-DSL-Fc (Figure 18).

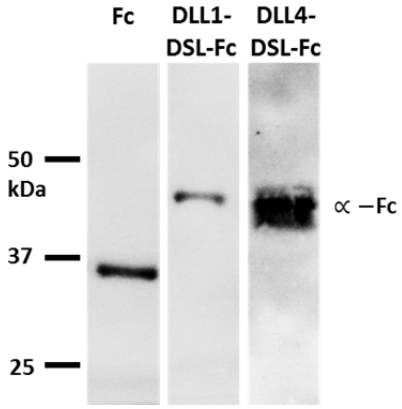

Figure 18: Immunoprecipitation of DLL1-DSL-Fc and DLL4-DSL-Fc

Western blot analysis of immunoprecipitated proteins from HUVEC supernatant 48 h after transduction with corresponding adenoviruses revealed specific bands for Fc (37 kDa), DLL1-DSL-Fc (43 kDa) and DLL4-DSL-Fc protein (46 kDa). Purified proteins were detected with an α-Fc antibody.

Soluble Notch constructs decreased the expression of Notch downstream genes in endothelial cells

Notch receptors along with the Notch ligands are known to be expressed in vascular ECs (Shutter et al., 2000; Uyttendaele et al., 2001). The effect of the Fc-coupled ligand- and receptor-constructs on Notch signaling was investigated in HUVECs. Even though the expression level of Notch components was higher in arterial cells, several components of the Notch signaling pathway including NOTCH1-3, DLL1, -3, -4, JAG1-2, as well as, Notch target genes HEY1 and HEY2 were reported to be expressed in cultured HUVEC (Harrington et al., 2008; Hu et al., 2011). Adenoviral transduction of HUVEC was performed with the particular vector overexpressing the ligand DSL-constructs DLL1-DSL-Fc, DLL4-DSL-Fc and JAG1-DSL-Fc, the ligand-ECD constructs JAG1-ECD-Fc and DLL4-ECD-Fc or the receptor construct NOTCH1-EGF11-13-Fc. mRNA levels of the classical downstream Notch target genes *HEY1, HEY2* and *HES5* were measured after 48 h by quantitative real-time PCR (qPCR).

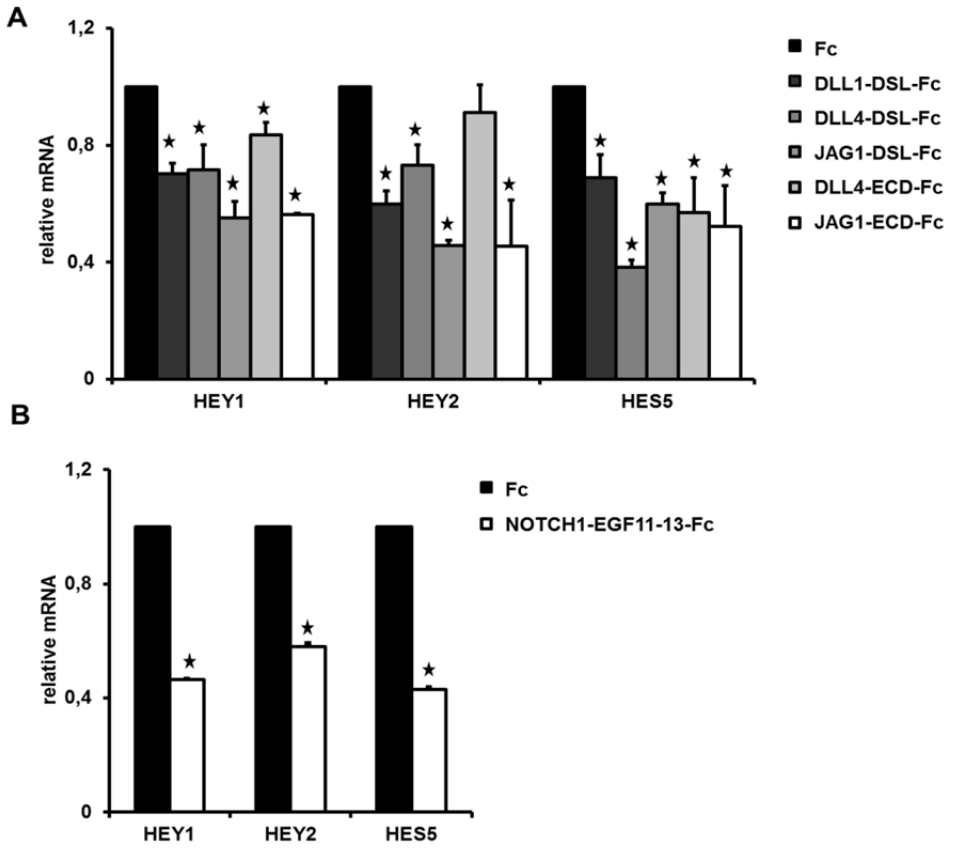

Figure 19: Fc-coupled ligand- and receptor-constructs decreased the expression of Notch downstream target genes

mRNA expression of Notch target genes *HEY1, HEY2* and *HES5* was analyzed by qPCR 48 h after adenoviral transduction of HUVEC. (A) *HEY1, HEY2* and *HES5* mRNA levels were significantly decreased in DLL1-DSL-Fc, DLL4-DSL-Fc, JAG1-DSL-Fc and JAG1-ECD-Fc expressing HUVECs. Transduction of cells with DLL4-ECD-Fc resulted in a significant decrease of *HEY1* and *HES5* mRNA expression. (B) HUVEC overexpressing NOTCH1-EGF11-13-Fc revealed significantly decreased mRNA levels of *HEY1, HEY2* and *HES5* compared to Fc control. Data is expressed as mean +SD. ★, $p<0.05$.

qPCR analysis revealed a significant decrease in *HEY1*, *HEY2* and *HEY5* mRNA expression in HUVECs expressing DLL1-DSL-Fc, DLL4-DSL-Fc, JAG1-DSL-Fc and JAG1-ECD-Fc (Figure 19, A). mRNA expression of the Notch targets *HEY1* and *HES5* were significantly decreased after expression of DLL4-ECD-Fc, while *HEY2* mRNA levels were not altered (Figure 19, A). HUVEC overexpressing the receptor construct NOTCH1-EGF11-13-Fc exhibited significantly decreased mRNA levels of all tested Notch target genes (Figure 19, B).

The effect of soluble ligands and receptors on Notch signaling activity was previously been described by several groups and revealed diverse results. A number of publications reported that soluble ECD-ligands were unable to activate Notch signaling (Funahashi et al., 2008; Hicks et al., 2002; Mishra-Gorur et al., 2002; Noguera-Troise et al., 2006; Sun and Artavanis-Tsakonas, 1997). Conflicting with these results, several other reports proposed an activation of Notch signaling by soluble Delta- or Jagged-ECD ligands in mammalian cells (Qi et al., 1999; Varnum-Finney et al., 1998). We could show that the ligand DSL-constructs DLL1-DSL-Fc, DLL4-DSL-Fc and JAG1-DSL-Fc, as well as, the NOTCH1-EGF11-13-Fc receptor construct are competitive tools to inhibit Notch signaling.

3.1.2 Functional characterization of soluble Notch constructs in endothelial cells

3.1.2.1 Functional Notch blockade induced myogenesis in C2C12 cells

C2C12 cells are murine myoblasts that are able to differentiate into contractile plurinucleated syncytia, so called myotubes (Yaffe and Saxel, 1977). Myotubes express proteins such as skeletal myosin isoforms, which are necessary for contractility. Skeletal myosin represents a marker of terminally differentiated myotubes. Since Notch signaling is well known to inhibit myogenic differentiation, soluble Notch ligand and receptor constructs were investigated for their capacity to block Notch signaling in differentiating C2C12 cells (Nofziger et al., 1999).

Myoblast differentiation was enhanced in response to adenoviral transduction of C2C12 cells with the different ligands, as well as, the NOTCH1-EGF11-13-Fc receptor. This was indicated by fused multinucleated skeletal myosin-positive cells (Figure 20, A, B). The increased myogenic differentiation suggests that the soluble Notch constructs counteract Notch signaling in myoblasts.

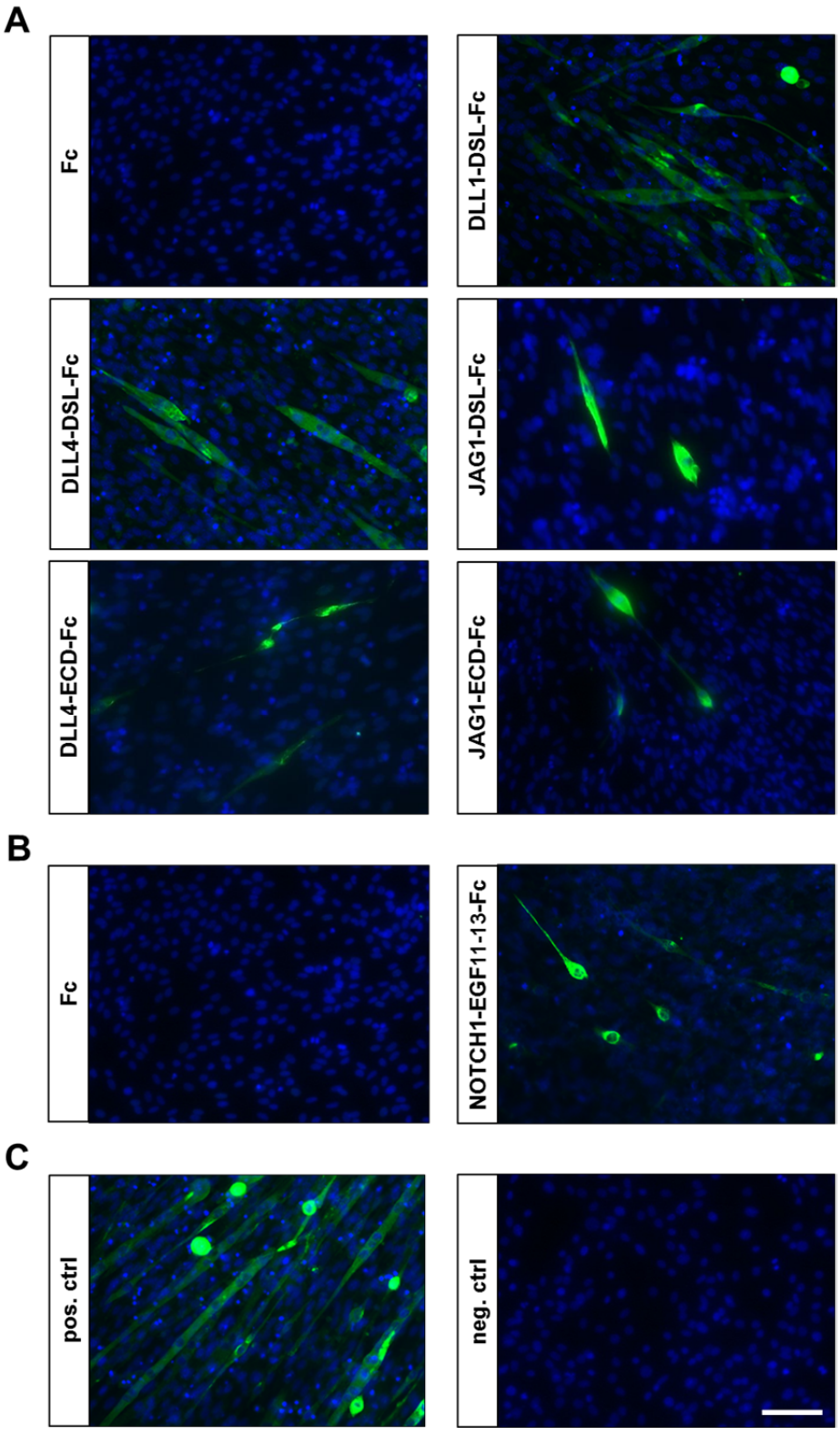

Figure 20: Expression of soluble Notch constructs promoted myogenic differentiation of C2C12 cells Cells were stained for skeletal myosin (green) and DAPI (blue) to investigate myogenic differentiation. (A) DLL1-DSL-Fc and DLL4-DSL-Fc strongly enhanced myoblast differentiation compared to Fc control. For JAG1-DSL-Fc, DLL4-ECD-Fc and JAG1-ECD-Fc a slight increase in myogenic differentiation was evaluated. (B) NOTCH1-EGF11-13-Fc caused a slight increase in myogenic differentiation compared to Fc control. (C) Untreated cells represented the negative control. C2C12 cells cultured under low-serum conditions to induce differentiation served as positive control. Representative pictures are shown. Scale bar: 100 µm

3.1.2.2 Soluble Notch constructs exerted diverse effects on endothelial proliferation and migration

Endothelial proliferation and migration are essential steps during sprouting angiogenesis (Gupta and Qin, 2003). Active Delta-Notch signaling was reported to reduce proliferation and migration of endothelial cells (Kuhnert et al., 2011).

An endothelial proliferation assay was performed to test if the Notch-mediated anti-proliferative endothelial phenotype could be reversed by a Notch blockade with soluble Notch constructs. BrdU incorporation of HUVEC was surveyed after adenoviral expression of DLL1-DSL-Fc, DLL4-DSL-Fc, JAG1-DSL-Fc, DLL4-ECD-Fc, JAG1-ECD-Fc or the NOTCH1-EGF11-13 receptor construct in order to study endothelial proliferation. The proliferation rate of HUVEC was significantly enhanced by the ligand DSL-constructs DLL1-DSL-Fc and DLL4-DSL-Fc (Figure 21, A). The JAG1-DSL-Fc construct in addition to the large DLL4-ECD-Fc and JAG1-ECD-Fc constructs had minor effects on endothelial proliferation. Also, NOTCH1-EGF11-13-Fc did not alter the proliferation rate of HUVEC *in vitro*.

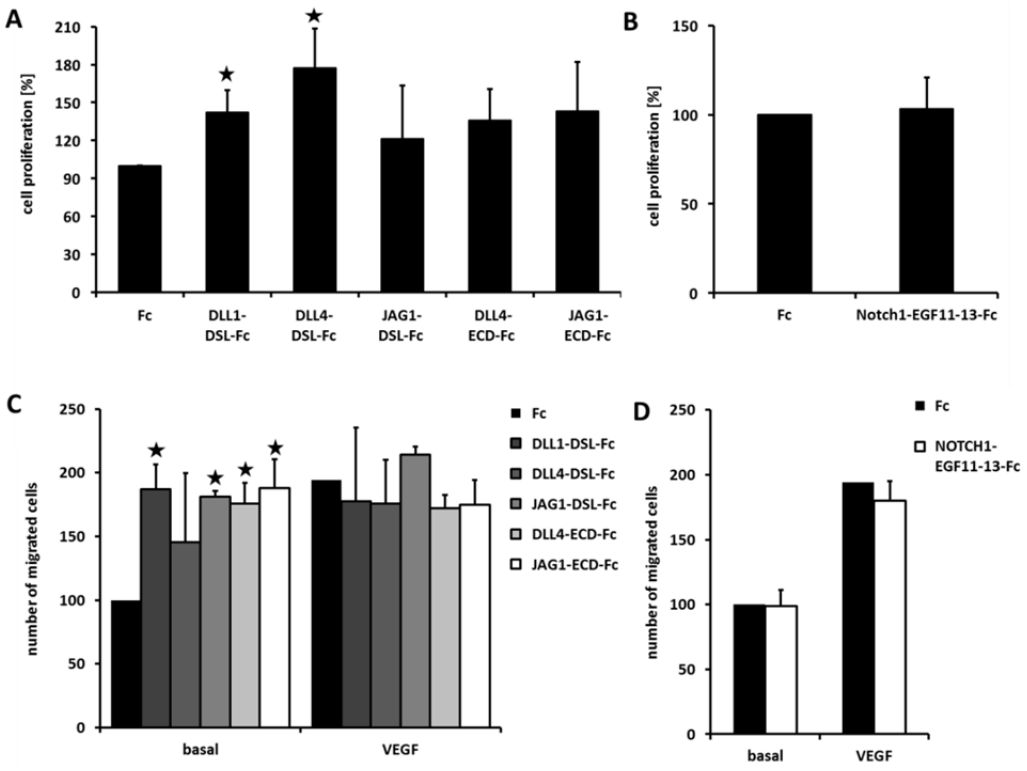

Figure 21: Expression of soluble Notch ligands and receptors exerted diverse effects on endothelial proliferation and chemotactic migration

HUVECs were transduced with adenovirus expressing the ligand constructs DLL1-DSL-Fc, DLL4-DSL-Fc, JAG1-DSL-Fc, DLL4-ECD-Fc, JAG1-ECD-Fc, the NOTCH1-EGF11-13-Fc receptor construct or Fc as control. Proliferation and chemotactic migration were assayed 48 h later. (A, B) BrdU incorporation was significantly increased after transduction of HUVEC with DLL1-DSL-Fc and DLL4-DSL-Fc. NOTCH1-EGF11-13-Fc exerted no effect on proliferation. (C, D) Transmigration of cells in a modified Boyden chamber was significantly increased by DLL1-DSL-Fc, JAG1-DSL-Fc, DLL4-ECD-Fc and JAG1-ECD-Fc under basal conditions. Chemotactic migration of ECs was unaltered under basal, as well as, stimulated conditions by the NOTCH1-EGF11-13-Fc construct, compared to Fc control. Data is expressed as mean +SD. ★, $p<0.05$.

Migration and chemotactic movement of ECs through a collagen coated filter towards a VEGF stimulus (25 ng/ml VEGF) was analyzed in a modified Boyden chamber assay (Figure 21, C, D). The number of transmigrated HUVECs after transduction with adenovirus expressing the soluble ligand constructs DLL1-DSL-Fc, JAG1-DSL-Fc, DLL4-ECD-Fc and JAG1-ECD-Fc was significantly increased even under unstimulated (basal) conditions. Migration of ECs was not further increased in response to VEGF stimulation. Increased basal migration induced by the previously mentioned ligand constructs negated the Notch-induced anti-migratory effect. No significant changes in endothelial cell migration were detectable for the DLL4-DSL-Fc and the NOTCH1-EGF11-13-Fc construct (Figure 21, C, D).

3.1.2.3 Soluble Notch ligands and receptors promoted basal sprouting angiogenesis

The Notch ligands DLL1, DLL4 and JAG1 along with Notch targets genes (*HEY1*, *HEY2*) have been described to be important regulators of sprouting angiogenesis (Roca and Adams, 2007). A 3D-sprouting assay (Korff and Augustin, 1998) was carried out in order to test the effects of the soluble constructs on sprouting angiogenesis. The expression of the soluble ligands DLL1-DSL-Fc, DLL4-DSL-Fc, JAG1-DSL-Fc, DLL4-ECD-Fc and JAG1-ECD-Fc or the NOTCH-EGF11-13-Fc receptor in HUVECs was achieved by adenoviral transduction. Fc was used as a control. Capillary sprouting was stimulated with 25 ng/ml VEGF.

All soluble ligands significantly increased endothelial sprouting under unstimulated (basal) conditions (Figure 22, A, B). Endothelial sprouts appeared narrow and short compared to the control. This phenotype was already reported in the literature for the DLL4-ECD-Fc construct (Noguera-Troise et al., 2006). Additional stimulation with 25 ng/ml VEGF caused no significant increase of sprouting behavior (Figure 22, A, B). Data revealed that all ligand constructs induced a pro-angiogenic sprouting behavior of EC. In contrast, ECs expressing the soluble NOTCH1-EGF11-13-Fc receptor revealed a significant decrease in basal as well as VEGF-stimulated sprouting behavior in the 3D-sprouting assay. Thus, soluble ligands and receptors exerted opposite effects on endothelial sprouting. This may arise due to the fact that the soluble receptor blocks multiple Notch ligands. During angiogenesis, JAG1 acts as an inhibitor of DLL4-mediated Notch signaling. Thus, the vascular phenotype after blockade of Notch ligands with NOTCH1-EGF11-13-Fc depends on the abundance of stimulatory or inhibitory Notch ligands.

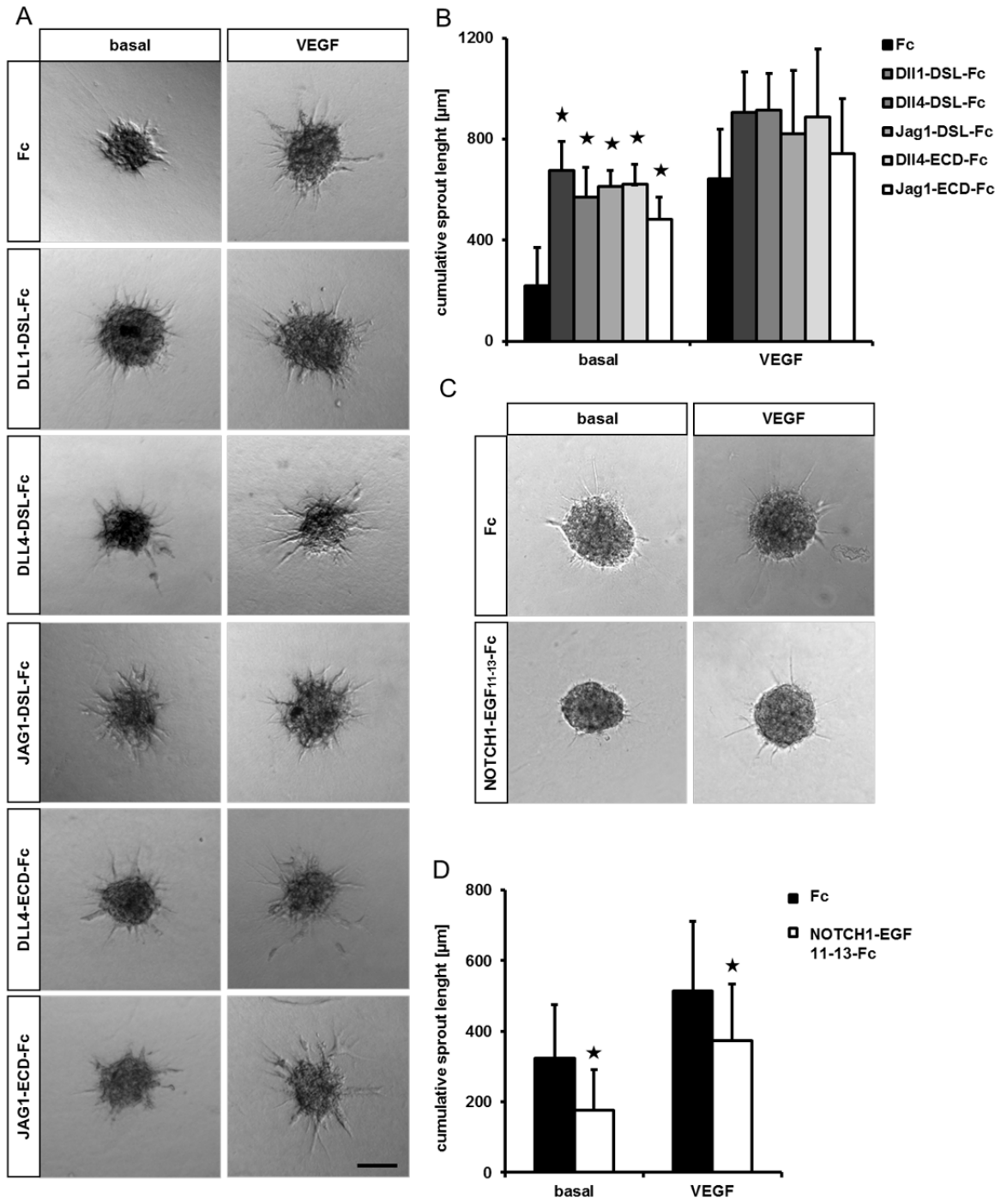

Figure 22: Blockade of Notch signaling by soluble ligands or receptors caused contradictory results on sprouting angiogenesis

(A-D) HUVEC were transduced with adenovirus expressing the soluble ligands or receptors DLL1-DSL-Fc, DLL4-DSL-Fc, JAG1-DSL-Fc, DLL4-ECD-Fc, JAG1-ECD-Fc, NOTCH-EGF11-13-Fc (n=2). HUVEC spheroids are cultured in a collagen matrix without growth factors (basal) or with VEGF (25 ng/ml). (A-B) Representative pictures (A) and quantification of the cumulative sprout length (B) of spheroids overexpressing the ligand constructs revealed an increase in endothelial sprouting under basal conditions. Endothelial sprouting was not significantly increased in response to VEGF. (C, D) Representative pictures (C) and quantification of the cumulative sprout length (D) revealed a significant reduction in capillary sprout formation under basal and VEGF-stimulated conditions in HUVEC expressing NOTCH1-EGF11-13-Fc. ★, $p<0.05$. Scale bar: 100 µm

3.1.2.4 Treatment with soluble Notch ligands enhanced endothelial sprouting

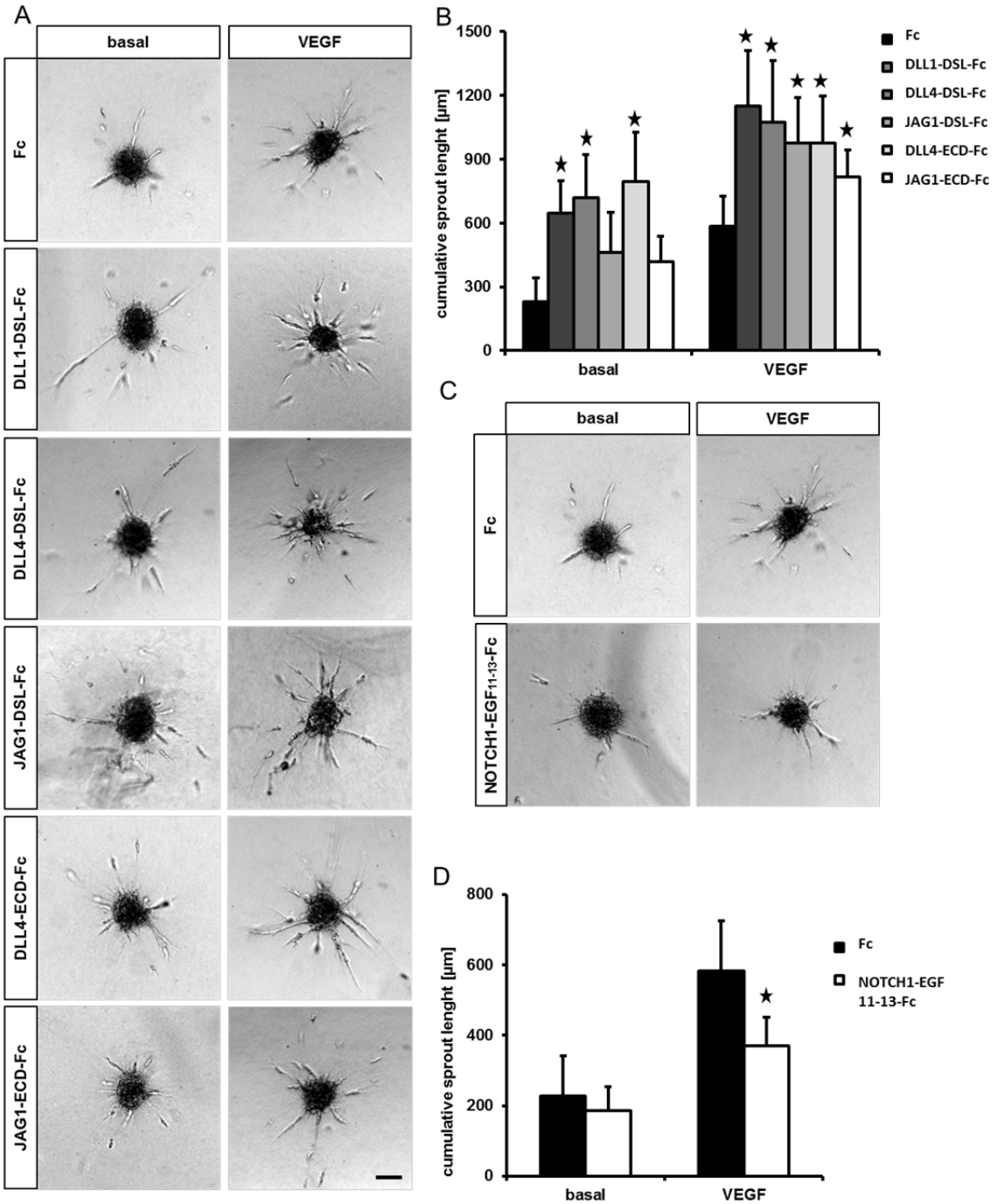

Figure 23: Application of Notch ligand- or receptor-proteins exerted diverse effects on endothelial sprouting
(A-D) HUVEC spheroids were treated with conditioned medium of adenoviral transduced HUVEC expressing the secreted proteins DLL1-DSL-Fc, DLL4-DSL-Fc, JAG1-DSL-Fc, DLL4-ECD-Fc, JAG1-ECD-Fc, NOTCH-EGF11-13-Fc or Fc as control. (A, B) Representative pictures (A) and quantification of cumulative sprout length (B) of HUVEC spheroids treated with conditioned medium containing DLL1-DSL-Fc, DLL4-DSL-Fc and DLL4-ECD-Fc protein caused a significant increase of basal endothelial sprouting. Treatment with JAG1-DSL-Fc and JAG1-ECD-Fc protein containing supernatant revealed no significant increase in basal sprouting. Conditioned medium containing DLL1-DSL-Fc, DLL4-DSL-Fc, JAG1-DSL-Fc, DLL4-ECD-Fc and JAG1-ECD-Fc protein potentiated the VEGF-induced angiogenesis significantly. (C, D) NOTCH1-EGF1-13-Fc revealed anti-angiogenic effects under VEGF-stimulated conditions. ★, $p<0.05$. Scale bar: 100 µm

The experiment described above relied on adenoviral infection of ECs with the different Notch blocking constructs. For many applications, however, it is necessary to treat cells, tissues or whole living organisms with secreted proteins. Since large-scale purification of most of the Fc-coupled proteins failed, further experiments were performed with conditioned medium. Conditioned medium of adenoviral transduced HUVECs overexpressing and secreting the recombinant ligand and receptor proteins was applied to HUVEC spheroids embedded in collagen gels (Figure 23, A-D). Addition of DLL1-DSL-Fc, DLL4-DSL-Fc or DLL4-ECD-Fc protein to HUVEC spheroids significantly increased basal angiogenic sprouting. However, HUVEC spheroids treated with conditioned medium containing JAG1-DSL-Fc or JAG1-ECD-Fc protein revealed no significant increase in basal endothelial sprouting. Furthermore, inhibition of Notch signaling by DLL1-DSL-Fc, DLL4-DSL-Fc, and DLL4-ECD-Fc soluble proteins significantly potentiated VEGF-induced sprouting angiogenesis *in vitro* (Figure 23, A, B). Conditioned medium containing NOTCH1-EGF11-13-Fc protein, on the other hand, revealed anti-angiogenic effects on VEGF-stimulated sprouting angiogenesis (Figure 23, C, D).

Taken together, Notch inhibition by the soluble ligand constructs DLL1-DSL-Fc, DLL4-DSL-Fc, JAG1-DSL-Fc and DLL4-ECD-Fc synergized with VEGF to induce angiogenesis, whereas the NOTCH1-EGF11-13-Fc receptor constructs exerts contrary effects.

3.1.2.5 Soluble Notch constructs induced vascular abnormalities in the retina

The mouse retina has become a well-characterized model for *in vivo* angiogenesis research. The retinal vasculature starts to develop at postnatal day P0 with the radial growth of vessels from the optic disc to the ora serrata within the nerve fiber layer. Starting at postnatal day P4, deeper retinal layers are formed. The postnatal development of the murine retinal vasculature makes it accessible for manipulations. During early retinal angiogenesis, tip cells navigate towards a gradient of VEGF to the outer front of the retina. The Delta-Notch signaling pathway orchestrates VEGF-mediated formation of a well-ordered retinal vasculature through determination of ECs to become tip or stalk cells (Hellstrom et al., 2007). Inhibition of Notch signaling via endothelial-specific NOTCH1 deletion, heterozygosity of DLL4 or by chemical inhibition of γ-secretase resulted in increased numbers of tip cells. This leads to the formation of a hyperdense vascular network (Hellstrom et al., 2007; Lobov et al., 2007; Ridgway et al., 2006; Suchting et al., 2007). Based on the data from *in vitro* experiments, the most consistent and efficient Notch blocking constructs were chosen to be investigated for their effects on murine retinal angiogenesis.

Consequently, C57BL/6 mice were injected intraperitoneal at postnatal day P1 and P3 with the soluble ligand constructs DLL1-DSL-Fc, DLL4-DSL-Fc and DLL4-ECD-Fc, the NOTCH1-EGF11-13-Fc receptor construct and the Fc construct as control. The highly conserved soluble Notch blocking constructs, which were based on human genetic sequences, were expected to also be functional in mice. Intraperitoneal injection of replication-deficient adenovirus primarily results in the infection of liver cells. The secreted proteins will then enter the blood stream to reach other organs including the retina. Mice were sacrificed at postnatal day P6 and changes in the retinal vascularization were assessed by immunohistological stainings with *G. simplicifolia* isolectin B_4 in order to visualize ECs (Figure 24, A, B). Retinal analysis was performed in collaboration with Dr. Alexander Schering (Research group of Prof. Dr. Hellmut Augustin, German Cancer Research Center Heidelberg).

The distance of vessel outgrowth towards the retinal outer front, the number of tips at the retinal periphery, as well as, the number of vascular branch points was quantified. The soluble ligands DLL1-DSL-Fc and DLL4-DSL-Fc and the receptor NOTCH1-EGF11-13-Fc significantly impaired the vessel outgrowth from the optic disc towards the VEGF stimulus at the retinal front (Figure 24, A-D). No significant difference was observed after application of the ligand DLL4-ECD-Fc construct. DLL1-DSL-Fc-, DLL4-DSL-Fc-, DLL4-ECD-Fc, and NOTCH1-EGF11-13-Fc increased the number of tips in the superficial retinal vasculature (Figure 25, A-D). Differences in density of the retinal network after adenoviral expression of the soluble Notch ligands or receptors were not observed (Figure 25, E-F).

In summary, decreased outgrowth of vessels but increased number of tips at the growing front of the retinal vasculature, following adenoviral administration of the DLL1-DSL-Fc, DLL4-DSL-Fc or the NOTCH1-EGF11-13-Fc constructs, had striking similarities to the phenotype described for genetic and chemical Notch blockage.

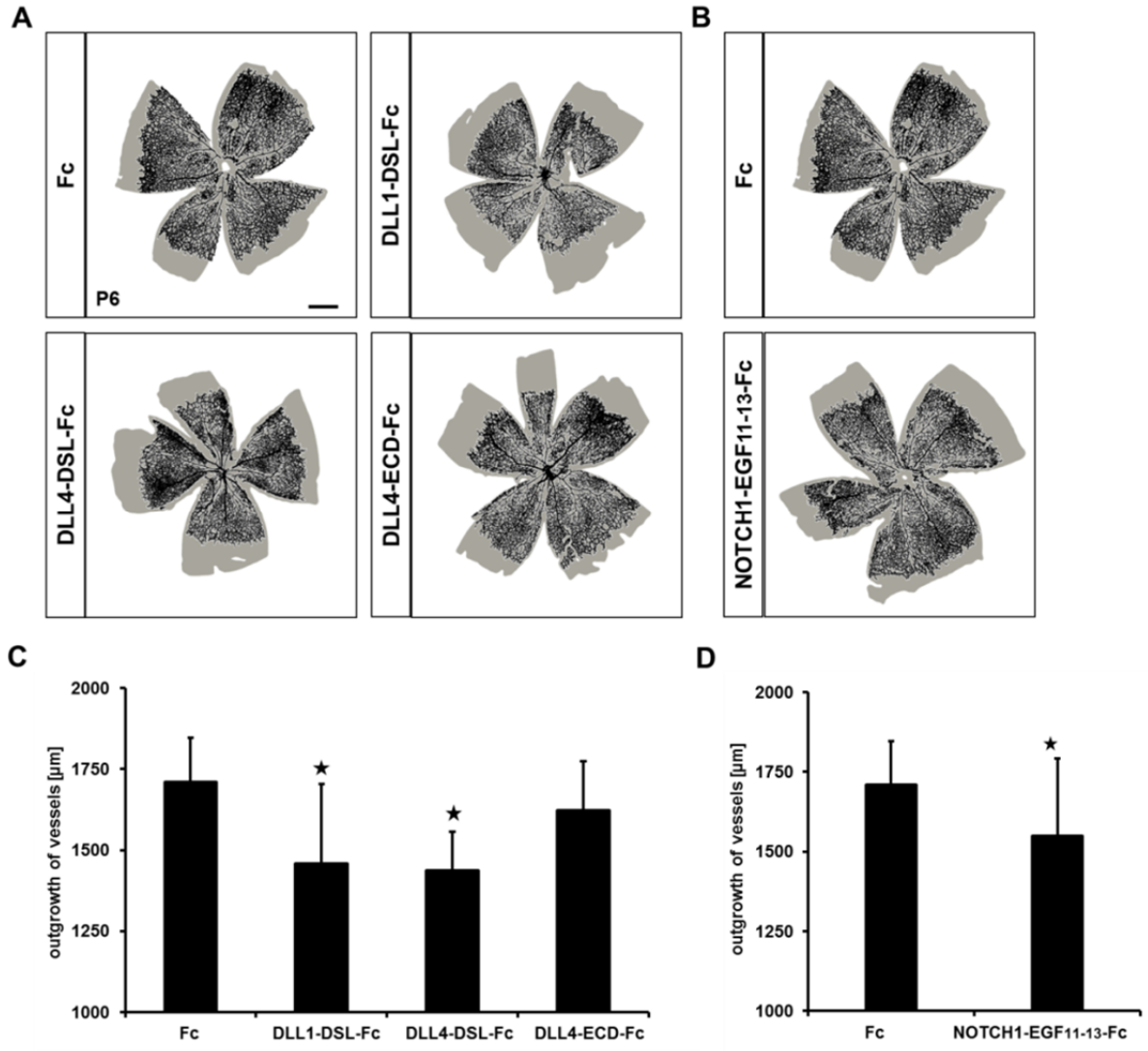

Figure 24: Vascular abnormalities in the retina after treatment with soluble Notch ligands and receptors

(A–D) Isolectin B_4 staining of developing retinal vasculature in C57BL/6 mice at day P6. Mice were injected i.p. at day P1 and P3 with adenovirus expressing DLL1-DSL-Fc, DLL4-DSL-Fc, DLL4-ECD-Fc, NOTCH1-EGF11-13-Fc or Fc as control. Mice were sacrificed at day P6 (n = 5), retinas were whole-mounted and vessels were stained with Isolectin B_4. Images were captured with a confocal microscope. Quantification of the vascular area and image processing was done using Fiji software. (A, C) A significant decrease in the vascularized area was observed for mice treated with DLL1-DSL-Fc and DLL4-DSL-Fc expressing virus whereas treatment with DLL4-ECD-Fc showed no significant difference to Fc-control. (B, D) Application of the NOTCH1-EGF11-13-Fc expressing virus significantly reduced vessel outgrowth. Error bars represent standard deviation. ★, $p<0.05$. Original magnification: ×40. Scale bar: 500 µm.

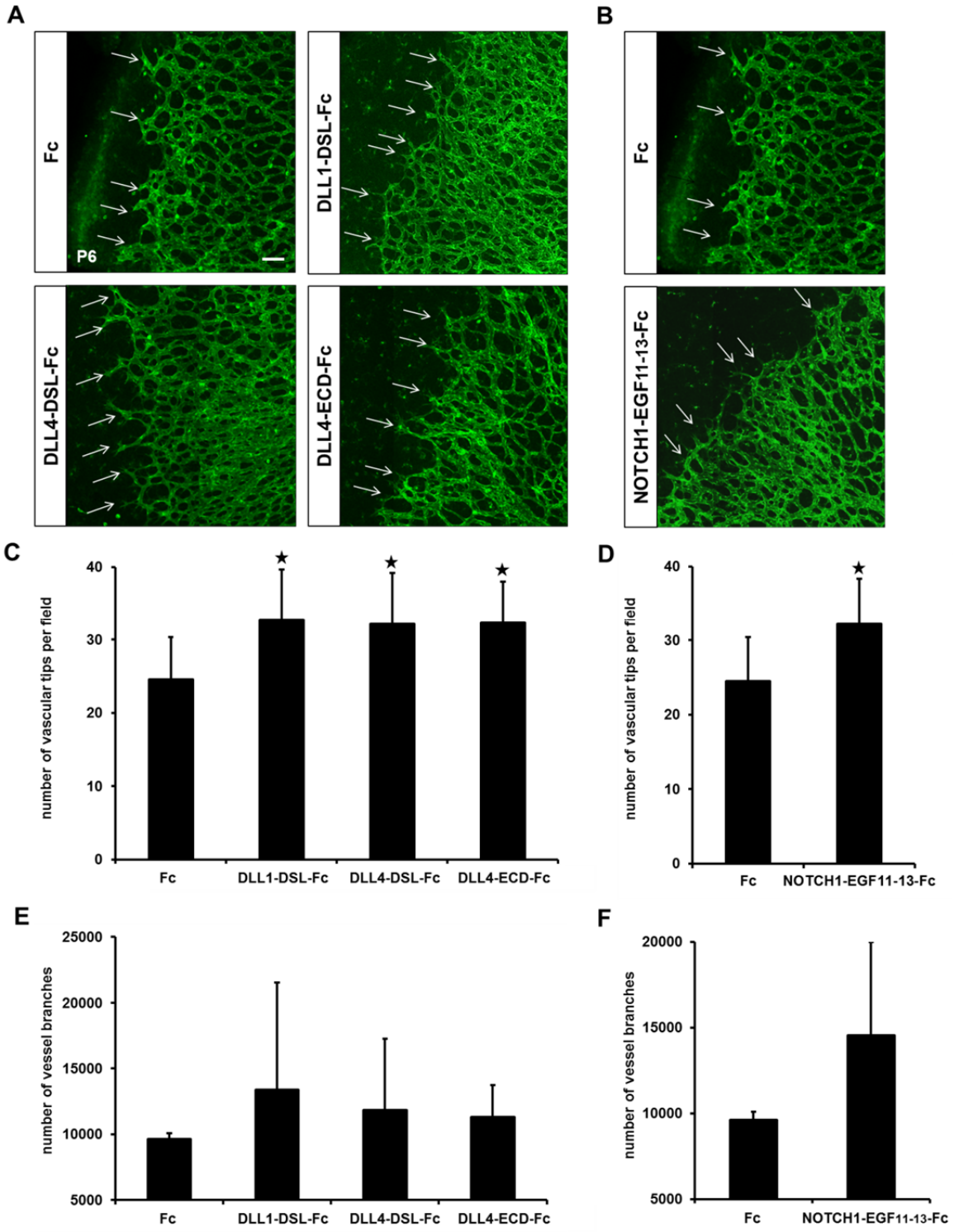

Figure 25: Blockade of Notch causes a change in tip numbers of the retinal vasculature

(A–F) C57BL/6 mice were injected at postnatal day P1 and P3 intraperitoneally with adenovirus expressing DLL1-DSL-Fc, DLL4-DSL-Fc, DLL4-ECD-Fc, NOTCH1-EGF11-13-Fc or Fc as control (n = 3). (A, B) Retinal vessels were stained with Isolectin B_4 at day P6. Images were captured by confocal microscopy and analyzed with Fiji software. (A-D) Representative retinal pictures and quantification of retinas from mice treated with virus expressing DLL1-DSL-Fc, Dll4-DSL-Fc, DLL4-ECD-Fc or NOTCH1-EGF11-13-Fc revealed more numerous tips with filopodial extensions at the growing front of the retinal vasculature (A- D). (E, F). The number of vessel branches was not changed for DLL1-DSL-Fc, DLL4-DSL-Fc, DLL4-ECD-Fc and NOTCH1-EGF11-13-Fc. c. Error bars represent standard deviation (C-F). ★, $p<0.05$. Original magnification: ×40. Scale bar: 100 µm.

3.2 Characterization of Notch signaling in the adult murine vasculature

The Notch pathway is one of the key regulatory signaling pathways during the development of the vascular system (Hofmann and Iruela-Arispe, 2007; Iso et al., 2003; Phng and Gerhardt, 2009; Roca and Adams, 2007). Mouse models with global knock-out or even haploinsufficiency of Notch components such as Notch1, Dll4, Rbp-j or Hey1/Hey2 suffer from severe vascular defects and early embryonic lethality (Duarte et al., 2004; Fischer et al., 2004 ; Gale et al., 2004; Krebs et al., 2004; Limbourg et al., 2005). The early lethality of mice demonstrates a crucial and indispensable role for Notch signaling during development but renders it impossible to study the role of Notch signaling in vascular maintenance during adulthood.

3.2.1 Generation of a mouse model with inducible endothelial-specific deletion of Notch signaling

An inducible transgenic mouse model with endothelial-specific loss of Notch signaling was generated in order to study the role of vascular Notch signaling during adulthood.
All Notch receptors signal through Rbp-j and its deletion causes a global loss of Notch signaling activity. Transgenic animals with endothelial-specific loss of Notch signaling were generated by crossing a Tamoxifen-inducible endothelial-specific Cre expressing transgenic strain (VE-Cadherin-Cre^{ERT2}) with a transgenic strain carrying a loxP-flanked (floxed) Rbp-j gene (Rbp-j$^{flox/flox}$) (Figure 26, A). Breedings of Rbp-j$^{flox/flox}$;VE-Cadherin-Cre^{ERT2} with Rbp-j$^{flox/flox}$ mice resulted in an offspring in which ~30 % of the mice carried the Cre-allele (Figure 26, A).
Both groups of litters, Rbp-j$^{flox/flox}$;VE-Cadherin-Cre^{ERT2} and Rbp-j$^{flox/flox}$, received 5 injections of Tamoxifen (1.5mg/day) at 12-16 weeks of age. Rbp-j$^{flox/flox}$;VE-Cadherin-Cre^{ERT2} mice with Cre recombinase-mediated endothelial-specific excision of Rbp-j were designated as Rbp-j$^{\Delta EC/EC}$ mice. Rbp-j$^{flox/flox}$ mice lacking the Cre-recombinase were considered controls.

Translation of Rbp-j is aborted due to excision of the loxP-flanked exons 6 and 7, encoding the DNA-binding domain. Feasibility of Cre-mediated Rbp-j excision was tested with fibroblasts isolated from lungs of floxed Rbp-j transgenic mice (Figure 26, B). Excision was verified via PCR analysis with a 316 bp amplification product in response to treatment with adenovirus expressing Cre recombinase (Figure 26, B). Successful excision of the floxed sequence, *in vivo*, was observed in tissue lysates of liver, lung, aorta and heart from Rbp-j$^{\Delta EC/EC}$ mice (Figure 26, C).

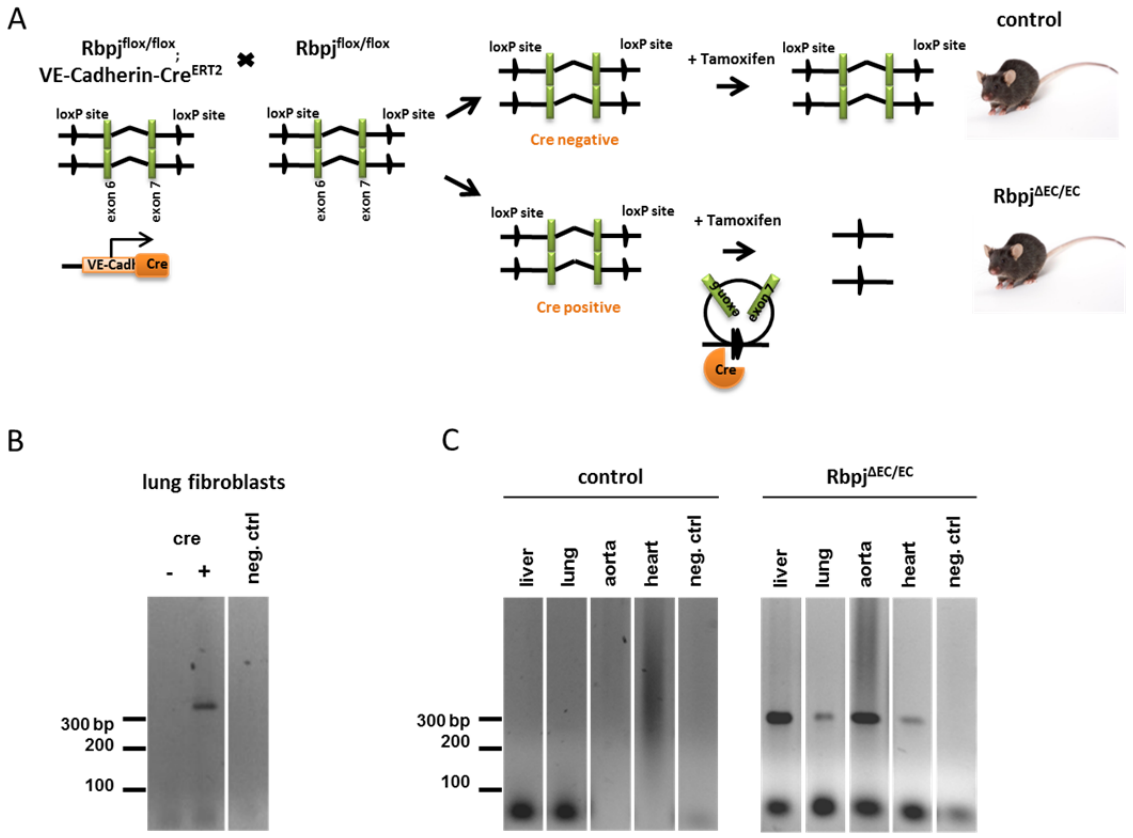

Figure 26: Endothelial-specific deletion of Notch signaling in a mouse model
(A) Mating scheme of Rbp-j$^{flox/flox}$; VE-Cadherin-Cre^{ERT2} mice with Rbp-j$^{flox/flox}$ mice. Tamoxifen application to litters induced an endothelial-specific activation of the Cre recombinase, which recombined floxed sequences upstream of Rbp-j exon 6 and downstream of exon 7 in mice expressing the VE-Cadherin-Cre^{ERT2} transgene (Rbp-j$^{\Delta EC/EC}$). (B) Excision of Rbp-j exons 6 and 7 was verified in cultured lung fibroblasts from Rbp-j$^{flox/flox}$ mice by transduction of an adenoviral cre recombinase. (C) Organ lysates of Tamoxifen-treated Rbp-j$^{\Delta EC/EC}$ and control mice were tested by PCR for successful excision of Rbp-j. Excision was validated by PCR analysis of liver, lung, aorta, and heart lysates from Rbp-j$^{\Delta EC/EC}$ mice resulting in a 311 bp amplification product. No amplification product was observed for control mice.

3.2.1.1 Endothelial specific deletion of Notch signaling caused a pathological heart and liver phenotype

Rbp-j$^{\Delta EC/EC}$ mice showed no obvious phenotypical changes during the first weeks after Tamoxifen treatment. A deterioration of the health status accompanied by loss of weight was recorded after 4-6 months. Internal organs of mice were subjected to morphological and histological investigations.

Massive enlargement of the heart and structural changes of the liver surface were observed in Rbp-j$^{\Delta EC/EC}$ mice (Figure 27, A, B). Histological investigation of the liver by H&E staining revealed no differences in liver architecture and lobular structures. However, livers of Rbp-j$^{\Delta EC/EC}$ mice were characterized by massive dilations and loss of radial arrangement of hepatic sinusoids (Figure 27, C). H&E staining of heart sections revealed no difference in size of cardiomyocytes (Figure 27, D). Yet, a loosening of the tight arrangement of cardiomyocytes and an accumulation of blood cells in the cellular interspace were observed in Rbp-j$^{\Delta EC/EC}$ mice (Figure 27, D).

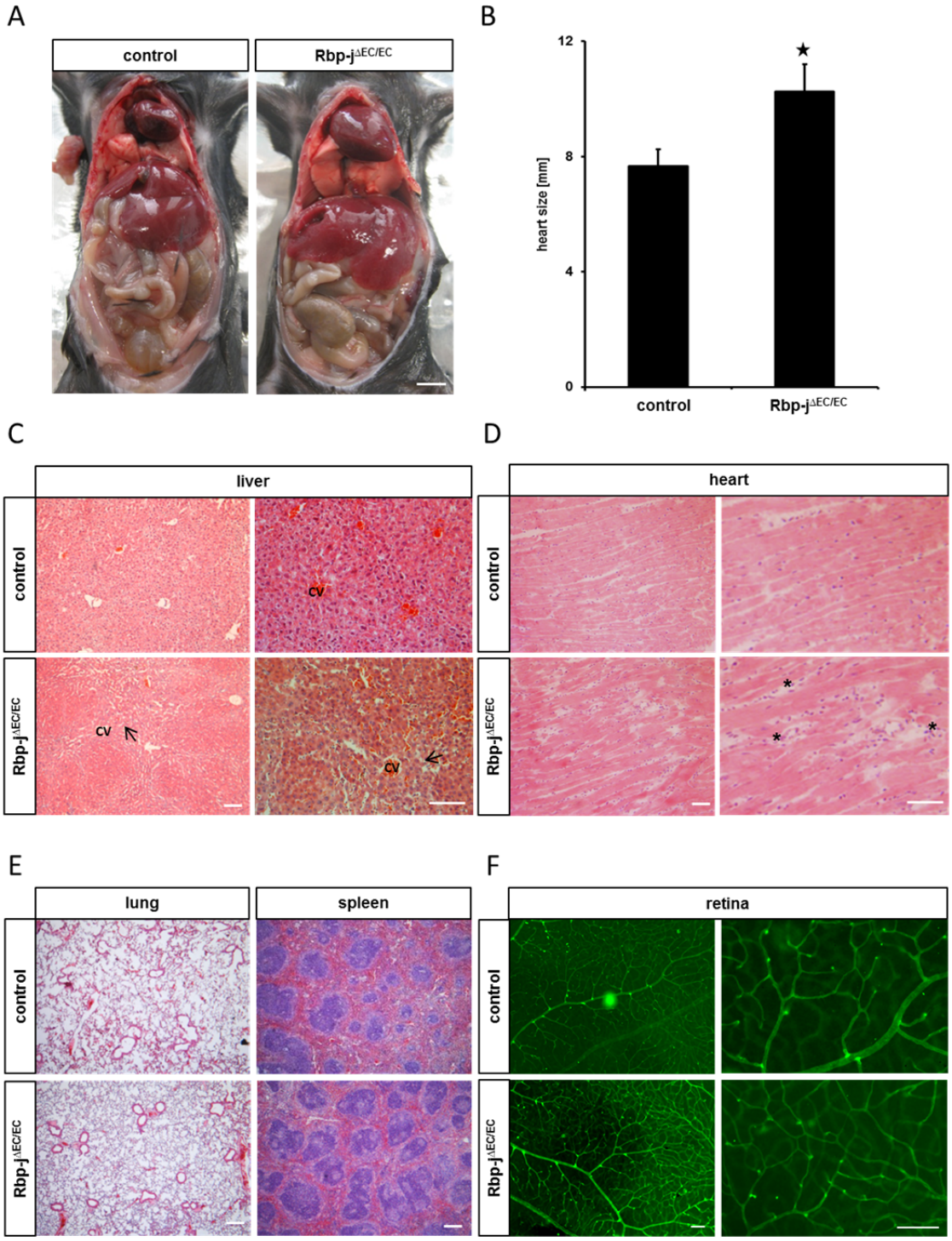

Figure 27: Deletion of Rbp-j resulted in morphological changes of heart and liver

(A) Rbp-j$^{\Delta EC/EC}$ mice displayed a massive enlargement of the heart and structural changes of the liver surface 4-6 weeks after Tamoxifen application. (B) Rbp-j$^{\Delta EC/EC}$ mice had a significantly increased heart size compared to controls. (C) Representative pictures of H&E stainings of liver sections from Rbp-j$^{\Delta EC/EC}$ mice revealed a pathologic liver phenotype with dilated liver sinusoids (arrows). Loss of sinusoidal radially arrangement towards the central vein (CV) became apparent in the higher magnification (right panel). (D) H&E staining of the heart revealed a loosening of cardiomyocyte structure accompanied by blood congestions indicated as asterisk (*). (E) Representative pictures of H&E-stained lung and spleen tissue. Staining did not reveal structural differences between Rbp-j$^{\Delta EC/EC}$ mice and controls. (F) The retinal vasculature did not reveal developmental defects in Rbp-j$^{\Delta EC/EC}$ mice as shown in a higher magnification (right panel). ★, $p<0.05$. Scale bars: 100 µm (C-F); 500 µm (A).

Lung and spleen as vascular-rich organs were investigated by H&E staining but did not manifest structural changes in Rbp-j$^{\Delta EC/EC}$ mice (Figure 27, E). Investigations of the Rbp-j$^{\Delta EC/EC}$ retinas revealed no evident alterations to the vasculature (Figure 27, F).
The heart and liver vasculature of Rbp-j$^{\Delta EC/EC}$ mice was studied by immuno-staining for the endothelial marker CD31. The cardiac vasculature was not altered for both groups. However, massively dilated hepatic vessels with discontinuous CD31 staining and accumulation of necrotic regions were observed on liver sections of Rbp-j$^{\Delta EC/EC}$ mice (Figure 28, B).

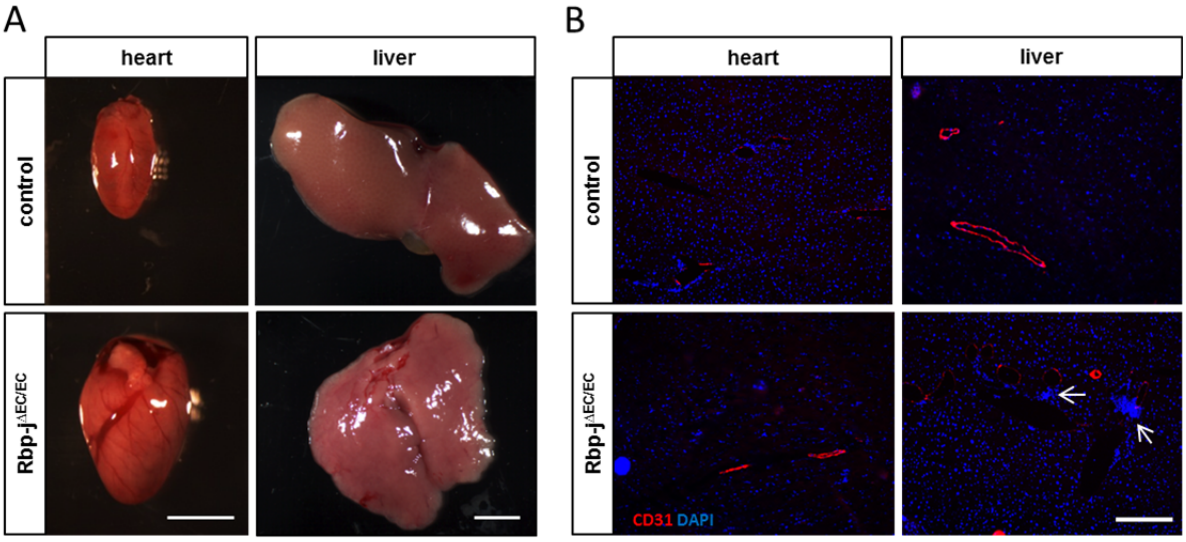

Figure 28: Deletion of endothelial Rbp-j resulted in enlargement of the heart and a pathological liver
(A) Pathological appearance of heart and liver of Rbp-j$^{\Delta EC/EC}$ mice. (B) Exemplary anti-CD31/DAPI stainings of heart and liver sections. The heart vasculature of Rbp-j$^{\Delta EC/EC}$ mice showed no abnormalities. Dilated vessels and an accumulation of cells (white arrows) were observed in livers of Rbp-j$^{\Delta EC/EC}$ mice. Scale bars: 200 µm (B); 500 µm (A).

3.2.1.2 Deletion of endothelial Notch signaling rendered mice susceptible to hemangioma development

Rbp-j$^{\Delta EC/EC}$ mice were monitored for a period of 12 months. The development of hemangiomas in the skin of Rbp-j$^{\Delta EC/EC}$ mice was observed one year after endothelial loss of Notch signaling (Figure 29, A). Hemangiomas are benign vascular tumors characterized by aberrant EC proliferation. The glucose transporter 1 (GLUT1) was described to be a specific immunohistochemical marker for juvenile hemangiomas (North et al., 2000).
Analysis of the hemangioma revealed a highly vascularized lesion, confirmed by a porous structure in H&E stained sections (Figure 29, B). Vessels were positive for endothelial CD31 and Desmin, which stains mural cells surrounding the vessels (Figure 29, C). Consistent with classification as hemangioma, GLUT1 was present in some vessels (Figure 29, D). The life expectancy of mice was not significantly reduced after chronic loss of endothelial Notch signaling.

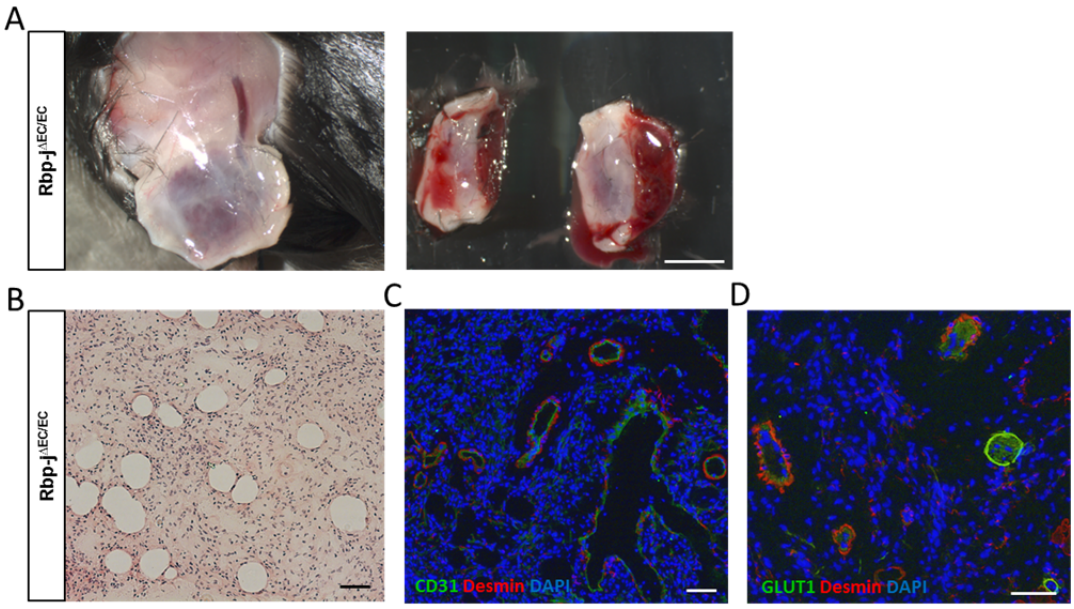

Figure 29: Loss of endothelial Notch signaling resulted in formation of vascular tumors
(A) Rbp-$j^{\Delta EC/EC}$ mice developed hemangiomas in the skin one year after loss of Notch signaling. (B) H&E staining of skin hemangioma. (C, D) Co-immunostaining of a skin hemangioma for CD31/Desmin (C) and GLUT1/Desmin (D). Scale bars: 500 µm (A); 200 µm (B-D).

3.2.2 Generation of a mouse model with endothelial loss of Notch signaling in an ApoE-deficient background caused a reduced life expectancy

Rbp-$j^{\Delta EC/EC}$ mice displayed an aberrant liver morphology (Figure 27, 28). Since the liver is an organ with high metabolic activity, microarray data of endothelial cells with blocked Notch signaling activity were examined for metabolism relevant genes. Data provided evidence, that endothelial loss of Notch causes alterations in lipid metabolism by transcriptional regulation of peroxisome proliferator activated receptor-γ (PPAR-γ) and fatty acid binding protein 4 (FABP4) (unpublished data, Dipl. Ing. Stefanie Herberich).
Rbp-$j^{flox/flox}$;VE-Cadherin-Cre^{ERT2} and Rbp-$j^{flox/flox}$ mice were crossed with mice lacking the Apolipoprotein E (ApoE) gene to challenge the endothelial-specific Notch deficient mice by hyperlipidemia and hypercholesterolemia. In response to Tamoxifen application at an age of 12-16 weeks, litters carrying the VE-Cadherin-Cre^{ERT2} transgene were designated as Rbp-$j^{\Delta EC/EC}$; $ApoE^{-/-}$ mice; Cre-negative litters were referred to as $ApoE^{-/-}$ controls.
ApoE is part of the very low density lipoprotein (VLDL), intermediate density lipoprotein (IDL) and high density lipoprotein (HDL) complexes. It mediates the transport of plasma lipids, such as triglycerides and cholesterol, to or from cells by facilitating binding of lipoproteins to LDL and LRP (LDL receptor-related protein) cell surface receptors. As a result of ApoE deficiency, the distribution of plasma cholesterol and triglycerides is shifted from HDL complexes to VLDL and IDL complexes (Kashyap et al., 1995; Zhang et al., 1992). Consequently, mice show dramatic alterations in lipid metabolism and develop atherosclerotic lesions. This can be provoked by feeding animals with fat-rich Western diet.

The Kaplan-Meier survival analysis revealed a 50 % survival rate for Rbp-j$^{\Delta EC/EC}$; ApoE$^{-/-}$ mice 6.5 weeks after deletion of Notch signaling activity (Figure 30, B).

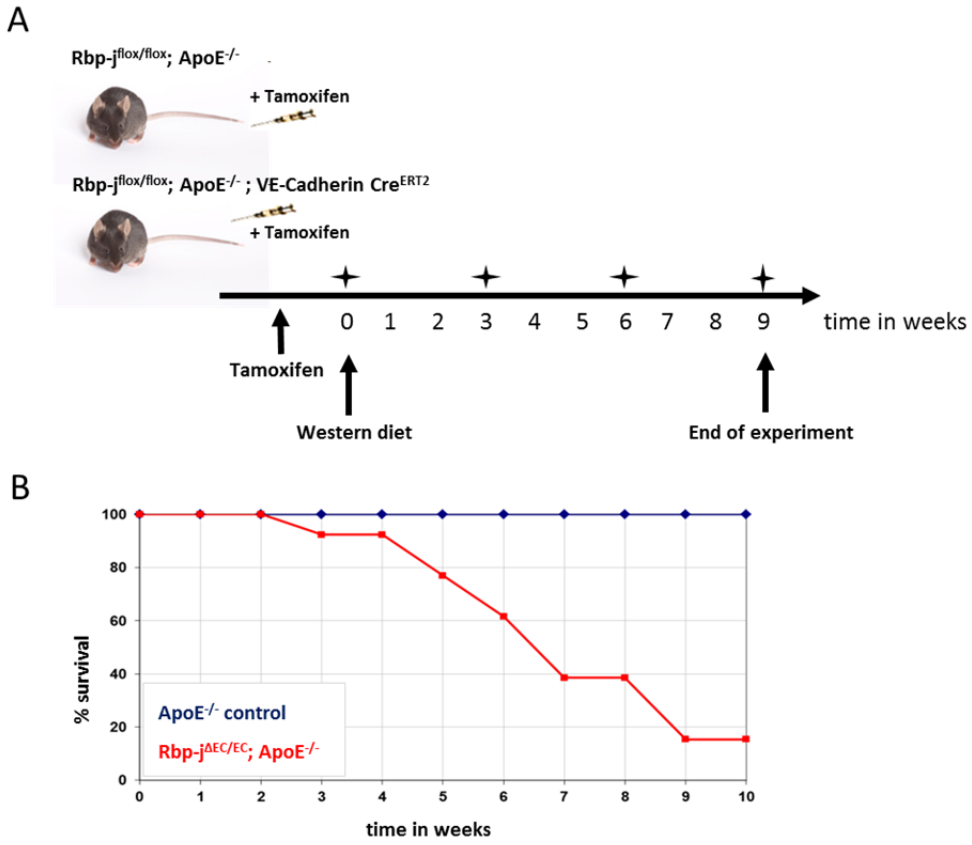

Figure 30: Rbp-j$^{\Delta EC/EC}$; ApoE$^{-/-}$ mice displayed increased mortality

(A) Experimental time schedule. Tamoxifen application to Rbp-j$^{flox/flox}$; ApoE$^{-/-}$; VE-Cadherin Cre^{ERT2} or Rbp-j$^{flox/flox}$;ApoE$^{-/-}$ control mice was subsequently followed by feeding of a fat-rich Western diet. Experimental investigations were performed 0, 3, 6, and 9 weeks after Tamoxifen application (+). (B) Kaplan-Meier survival analysis of 13 Rbp-j$^{\Delta EC/EC}$; ApoE$^{-/-}$ mutants and 17 ApoE$^{-/-}$ controls.

3.2.2.1 Rbp-j$^{\Delta EC/EC}$; ApoE$^{-/-}$ mice exhibited reduced body weight, organ-specific weight differences and elevated serum triglyceride levels

Metabolic parameters of Rbp-j$^{\Delta EC/EC}$; ApoE$^{-/-}$ mice were investigated and compared to ApoE$^{-/-}$ controls after being fed with Western Diet for 6-9 weeks. The average body weight was significantly decreased by 10 % for Rbp-j$^{\Delta EC/EC}$; ApoE$^{-/-}$ mice (Figure 31, A, B).

Measurements of organ weight revealed significant organ-specific differences. Heart and lung of Rbp-j$^{\Delta EC/EC}$; ApoE$^{-/-}$ mice exhibited an increased organ weight; while the weight of spleen, kidney and liver remained unchanged (Figure 31, C).

Serum analyses were performed after 6 weeks. Rbp-j$^{\Delta EC/EC}$; ApoE$^{-/-}$ and control mice exhibited massively elevated triglyceride, cholesterol and LDL levels (Figure 31, D). Total cholesterol, HDL and LDL levels were not significantly altered between both groups (Figure 31, D). However, triglyceride levels were significantly increased in Rbp-j$^{\Delta EC/EC}$; ApoE$^{-/-}$ mice (Figure 31, D).

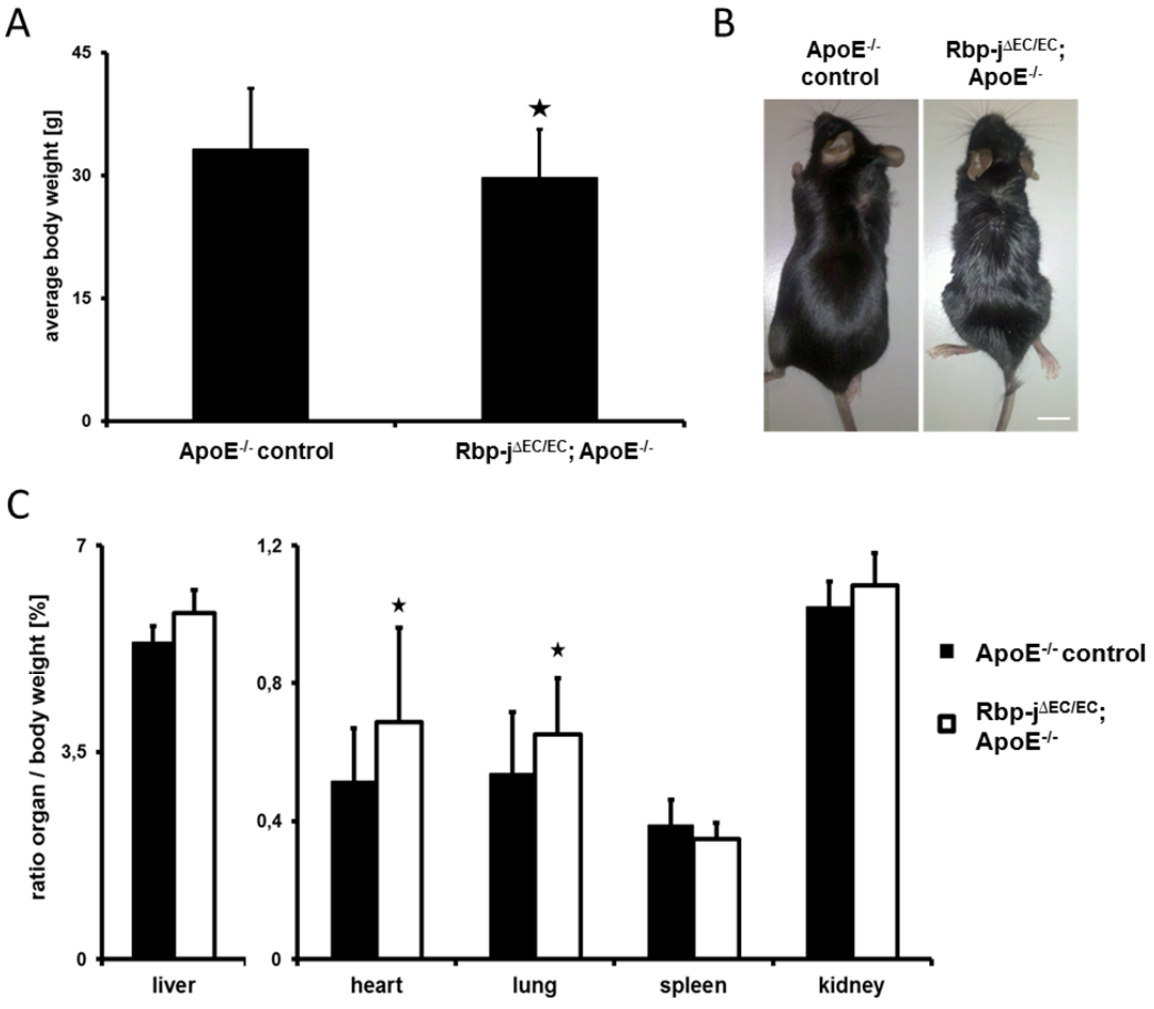

D

Serum analysis	Triglycerides (mg/dl)	Cholesterol (mg/dl)	HDL (mg/dl)	LDL (mg/dl)
ApoE$^{-/-}$ control	124.8 ± 76.3	935.8 ± 303.4	8.4 ± 3.8	895.7 ±283.4
Rbp-j$^{\Delta EC/EC}$; ApoE$^{-/-}$	384.4 ± 196.5	1128.7 ± 258.6	9.2 ± 3.6	1059 ± 286.4
t-test	p ≤ 0.05	NS	NS	NS

Figure 31: Endothelial deletion of Rbp-j in an ApoE deficient background resulted in reduced body weight, organ-specific weight differences, and increased triglyceride levels

(A) Averaged body weight of Rbp-j$^{\Delta EC/EC}$; ApoE$^{-/-}$ animals and ApoE$^{-/-}$ controls after 6-9 weeks of being fed with Western diet (n=17). (B) Representative picture of a Rbp-j$^{\Delta EC/EC}$; ApoE$^{-/-}$ mouse. (C) Organ-specific weight differences of mice were illustrated as ratio of organ to body weight [%] after 6-9 weeks of being fed with Western diet (n=7). (D) Serum analysis for triglycerides, cholesterol, HDL/LDL lipid levels after 6-9 weeks of mice being fed with Western diet (n=6). ★, $p<0.05$. NS: not significant; LDL, low-density lipoprotein; HDL, high-density lipoprotein. Scale bar: 1cm.

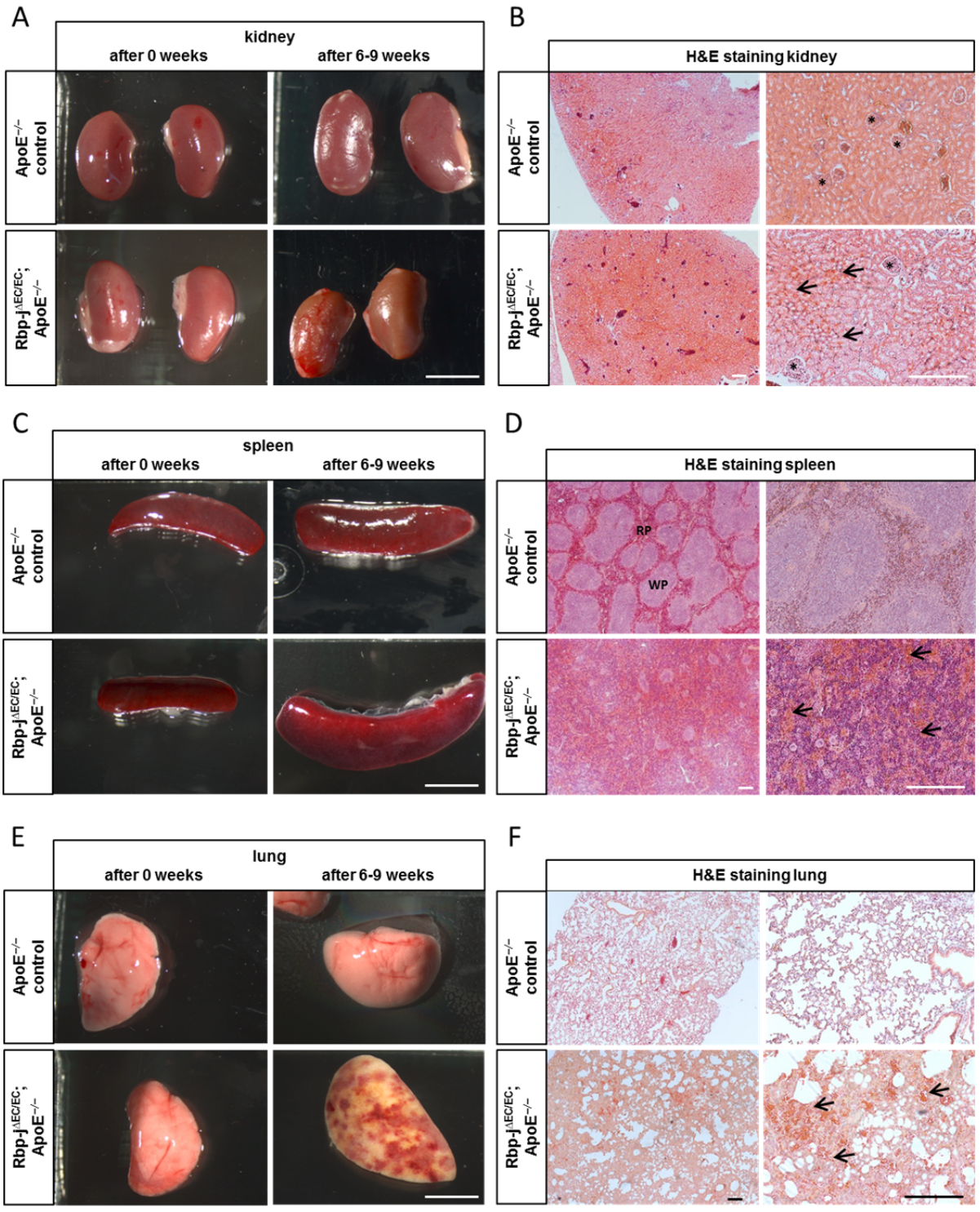

Figure 32: Endothelial deletion of Rbp-j in an ApoE$^{-/-}$ background caused blood congestions in several organs
(A, C, E) Photographs of organs of Rbp-j$^{\Delta EC/EC}$; ApoE$^{-/-}$ mice and ApoE$^{-/-}$ controls immediately after deletion of Notch signaling (0 weeks) and 6-9 weeks later. Mice were fed with Western diet. (B, D, F) H&E staining of organ sections. Hemorrhages are indicated by black arrows in higher magnifications (40 x; right panels). (B) H&E-stained sections of Rbp-j$^{\Delta EC/EC}$; ApoE$^{-/-}$ kidneys displayed no difference in size of the glomeruli (*) and the circumjacent subcapsular space. (D) H&E sections of spleen revealed an immunoreactive appearance in Rbp-j$^{\Delta EC/EC}$; ApoE$^{-/-}$ mice. (F) H&E staining of lung sections from Rbp-j$^{\Delta EC/EC}$; ApoE$^{-/-}$ mice 6-9 weeks after Tamoxifen application revealed severe blood congestion (black arrows) and thickening of the alveolar septa. RP, red pulp; WP, white pulp. Scale bars: 100 µm (B; D; F); 5 mm (A; C; E).

3.2.2.2 Rbp-j$^{\Delta EC/EC}$; ApoE$^{-/-}$ mice exhibited blood congestions in several organs

Post mortem surveys of several organs including kidney, spleen and lung from Rbp-j$^{\Delta EC/EC}$; ApoE$^{-/-}$ and control mice were performed immediately after Tamoxifen application (0 weeks) and 6-9 weeks later (Figure 32). Morphological investigations were performed in collaboration with Dr. Carolin Mogler (Institute of Pathology, University of Heidelberg; Vascular Oncology, German Cancer Research Center (DKFZ), Heidelberg).

Loss of ApoE was associated with lipoprotein glomerulopathy, which is characterized by dilated glomerular capillaries containing thrombi (Ando et al., 1999). However, H&E stainings of kidney sections revealed no obvious dilation or difference in size, cellularity and symmetry of the glomeruli and the circumjacent subcapsular space in Rbp-j$^{\Delta EC/EC}$; ApoE$^{-/-}$ mice (Figure 32, B). A congestion of blood cells was seen exclusively in kidney sections from Rbp-j$^{\Delta EC/EC}$; ApoE$^{-/-}$ mice (Figure 32, B).

Analysis of the spleen revealed no morphological difference immediately after Tamoxifen application (Figure 32, C). After 6-9 weeks, a few Rbp-j$^{\Delta EC/EC}$; ApoE$^{-/-}$ mice exhibited an enlarged spleen (splenomegaly) accompanied by an immunoreactive phenotype (Figure 32, C, D). Additionally, blood cells accumulated in the spleen of Rbp-j$^{\Delta EC/EC}$; ApoE$^{-/-}$ mice (Figure 32, D). Pathological changes with severe blood congestions and thickening of the alveolar septa were observed in lungs of Rbp-j$^{\Delta EC/EC}$; ApoE$^{-/-}$ mice 6-9 weeks after endothelial Notch deletion (Figure 32, E, F).

3.2.2.3 Loss of Notch signaling in Rbp-j$^{\Delta EC/EC}$; ApoE$^{-/-}$ mice caused development of dilated cardiomyopathy

Since blood congestion is a typical sign of heart failure, cardiac morphology was assessed in context of Notch signaling.

While Notch signaling in myocardial cells has been previously described, endocardial Notch signaling is not sufficiently elucidated. Deletion of Notch signaling in endothelial cells was reported to occur in the endocardium and endothelial cells of the myocardial capillaries. Successful recombination of Rbp-j in heart tissue was confirmed by PCR analysis (Figure 26, D). 6-9 weeks after deletion of endothelial Notch signaling, a significant enlargement of the heart was detectable (Figure 33, A). These findings were confirmed by an increased heart to body weight ratio (0.51 % ± 0.15; n=7) (Figure 33, C). Pathologic enlargement of the heart muscle was observed in 61.5 % of Rbp-j$^{\Delta EC/EC}$; ApoE$^{-/-}$ mice. A similar heart phenotype was seen in Rbp-j$^{\Delta EC/EC}$ mice (Figure 27, B). In Rbp-j$^{\Delta EC/EC}$; ApoE$^{-/-}$ mice, aberrant lipid metabolism accelerated the development of a heart muscle disease (cardiomyopathy). Cardiomyopathies are often linked to heart failure and sudden cardiac death. Diagnosis of cardiomyopathy was confirmed by an overall mortality of 85 % for Rbp-j$^{\Delta EC/EC}$; ApoE$^{-/-}$ mice 9 weeks after application of Tamoxifen (Figure 30, B).

Post-mortem measurements of the left (LVW) and right ventricular wall (RVW) revealed a significant increase in the thickness of both walls in Rbp-j$^{\Delta EC/EC}$; ApoE$^{-/-}$ mice (Figure 33, D; n = 4). H&E staining of heart sections did not reveal a change in size of endocardial endothelial cells or cardiomyocytes in Rbp-j$^{\Delta EC/EC}$; ApoE$^{-/-}$ mice (Figure 33, E). Therefore, concentric hypertrophy could be excluded as a reason for the cardiomyopathy (Figure 33, E).
However, the enlarged Rbp-j$^{\Delta EC/EC}$; ApoE$^{-/-}$ hearts displayed an excessive loosening of the tight cardiomyocytes arrangement (Figure 33, E). Loss of Notch signaling caused a massive dilation of myocardial capillaries as indicated by increased blood congestions (Figure 33, E). The expansion of capillaries due to endothelial dysfunction led to an overt structural change of myocardial fibers in both ventricles. Dilation of myocardium was described as hallmark for dilated cardiomyopathy (DCM), which is a non-ischemic form of cardiomyopathy causing a massive impairment of ventricular pumping efficiency. Endocardial necrotic areas were observed in Rbp-j$^{\Delta EC/EC}$; ApoE$^{-/-}$mice as result of ischemia due to cardiac failure (Figure 33, E).
The deficiency of the ApoE gene has been shown to increase the risk for coronary artery disease, which is a constriction of the arteries as a result of the accumulation of atherosclerotic plaques. Clinical studies linking ApoE polymorphism in humans to the development of DCM provide contradictory results (Jurkovicova et al., 2006; Ozhan et al., 2004). ApoE-deficient mice were reported to develop structural and functional ventricular alterations as a consequence of atherosclerotic lesions at one year of age (Cole et al., 2011). As cardiomyopathy can arise from dyslipidemia, mice lacking the ApoE gene were shown to exert physical, functional and histological markers of DCM, including fibrosis, which starts to develop at an age of 10 months (Cole et al., 2011). Our observations with mice at the age of 5-6 months did not uncover any evidence for the development of DCM in ApoE$^{-/-}$ control mice and thus linked the development of a DCM to endothelial loss of Notch signaling. Dilated cardiomyopathy is associated with complications including heart failure, fluid congestions and cardiac arrhythmia. Endothelial Notch signaling was thereby shown to be crucial for the maintenance of the adult cardiac function.

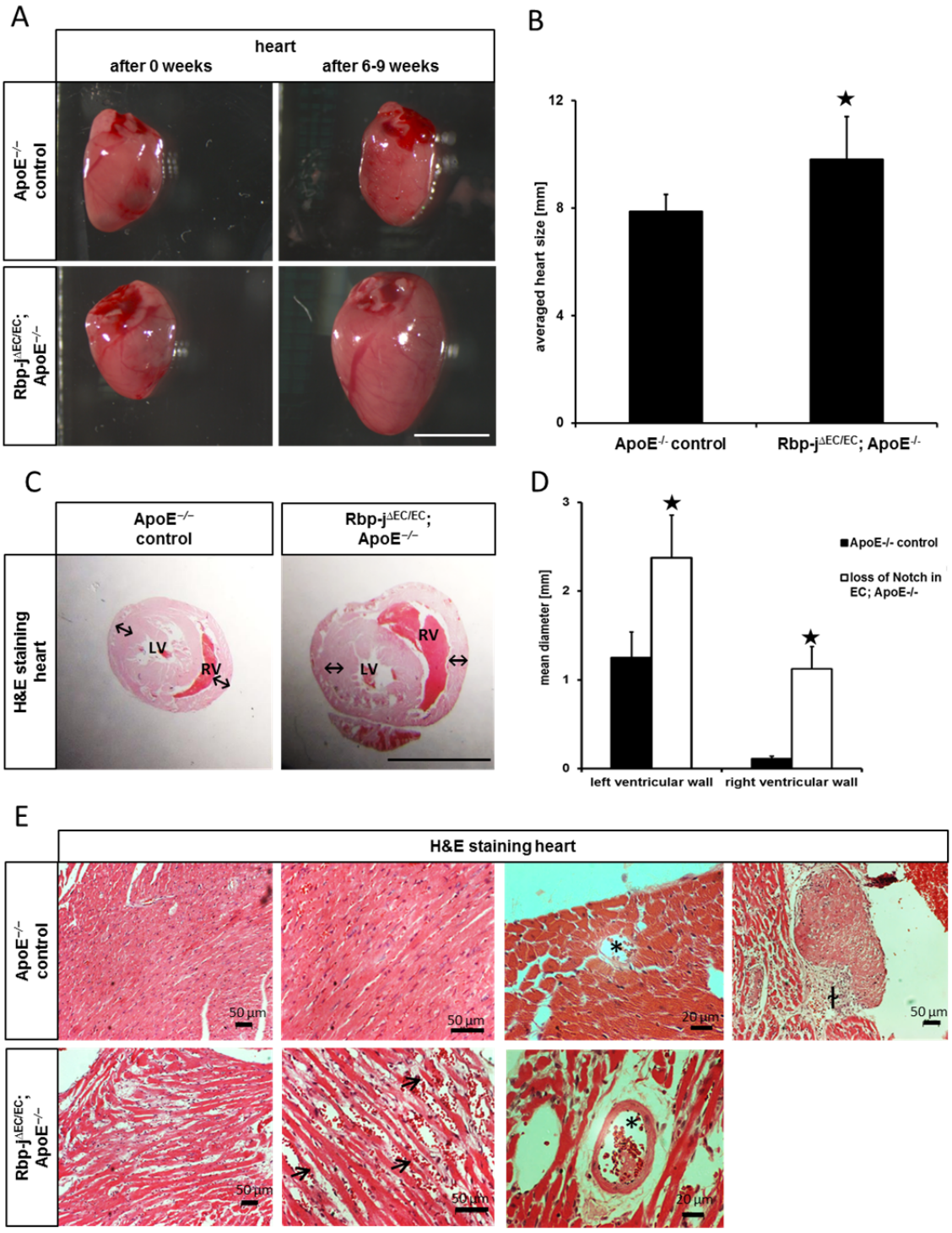

Figure 33: Loss of endothelial Notch activity caused an enlargement of ventricular walls

(A) Representative pictures of hearts from Rbp-j$^{\Delta EC/EC}$; ApoE$^{-/-}$ mice and ApoE$^{-/-}$ control animals immediately after Tamoxifen application (0 weeks) and 6-9 weeks later. Mice were fed with Western diet. (B) Rbp-j$^{\Delta EC/EC}$; ApoE$^{-/-}$ mice displayed an increased heart size 6-9 weeks after Tamoxifen application. (C, D) Loss of endothelial Notch signaling caused enlarged thickness of the left ventricle (LV) and the right ventricle (RV) wall (n=4). (E) H&E staining of heart sections 6-9 weeks after Tamoxifen application. Rbp-j$^{\Delta EC/EC}$; ApoE$^{-/-}$ mice displayed a dissociated cardiomyocyte structure and dilation of capillaries with accumulation blood cells (arrows). Larger vessels (*) are dilated in Rbp-j$^{\Delta EC/EC}$; ApoE$^{-/-}$ mice. Endocardial necrosis (ł) was present in Rbp-j$^{\Delta EC/EC}$; ApoE$^{-/-}$ mice. LV, left ventricle; RV, right ventricle. Scale bars: 20 µm; 50 µm; 5 mm (A; C).

3.2.2.4 Loss of Notch signaling in Rbp-j$^{\Delta EC/EC}$; ApoE$^{-/-}$ mice caused sinusoidal dilation, blood congestion, fibrosis and fat depositions in the liver

The liver is subdivided into functional units, called lobules. Blood flows through the hepatic vessels, the sinusoids, to supply cells with nutrients or oxygen and discharges into the central vein of a lobule.

A severe pathological liver phenotype was detected in 68 % of Rbp-j$^{\Delta EC/EC}$; ApoE$^{-/-}$mice (Figure 34, A, C). The livers displayed a high number of reddened spots, which were identified as blood congestions in H&E stainings. Spots appeared 3 weeks after deletion of Notch signaling (Figure 34, A, B). Liver morphology of Rbp-j$^{\Delta EC/EC}$; ApoE$^{-/-}$mice deteriorated over time and resulted in a pale appearance with nodule-like structures (Figure 34, A, right column). The outline of the liver lobes appeared irregular. However, no significant differences in liver-to-body-weight were observed between both groups (Figure 31, C).

In general, H&E-stained liver sections of Rbp-j$^{\Delta EC/EC}$; ApoE$^{-/-}$mice revealed no morphological changes of liver architecture (data not shown). However, an abnormal dilation of hepatic sinusoids was evident after loss of endothelial Notch signaling (Figure 34, B). This evidence is in line with previous reports using a DLL4-blocking antibody (Ridgway et al., 2006). Zonal necrosis surrounding the central vein was observed in Rbp-j$^{\Delta EC/EC}$; ApoE$^{-/-}$mice.

Furthermore, Rbp-j$^{\Delta EC/EC}$; ApoE$^{-/-}$mice exhibited severe blood congestions and increased accumulation of fat filled vacuoles in hepatocytes (Figure 34, B, D). Massive fat accumulations in the liver are described as fatty liver disease (FLD). 67 % of mice with endothelial deletion of Notch signaling in an ApoE-deficient background developed severe fatty livers (Figure 34, C). FLD is closely associated with metabolic diseases like diabetes, dyslipidemia, glycogen storage diseases, obesity and chronic medication. With increasing size of fat-containing vacuoles, hepatocytes shift their centrally located nucleus to the periphery of the cell. Fat accumulation in Rbp-j$^{\Delta EC/EC}$; ApoE$^{-/-}$ livers displayed zonal distribution patterns predominantly enclosing the central vein (data not shown). Staining of fibrotic tissues revealed no significant alterations to livers of Rbp-j$^{\Delta EC/EC}$; ApoE$^{-/-}$mice.

Massive intracytoplasmic lipid accumulations resulting in cell death and inflammatory or fibrotic processes are hallmarks of steatohepatitis. ApoE deficiency is known to protect from-diet-induced hepatic fat depositions (Karavia et al., 2011). Thus, aberrant endothelial Notch signaling was shown to provoke liver pathogenesis.

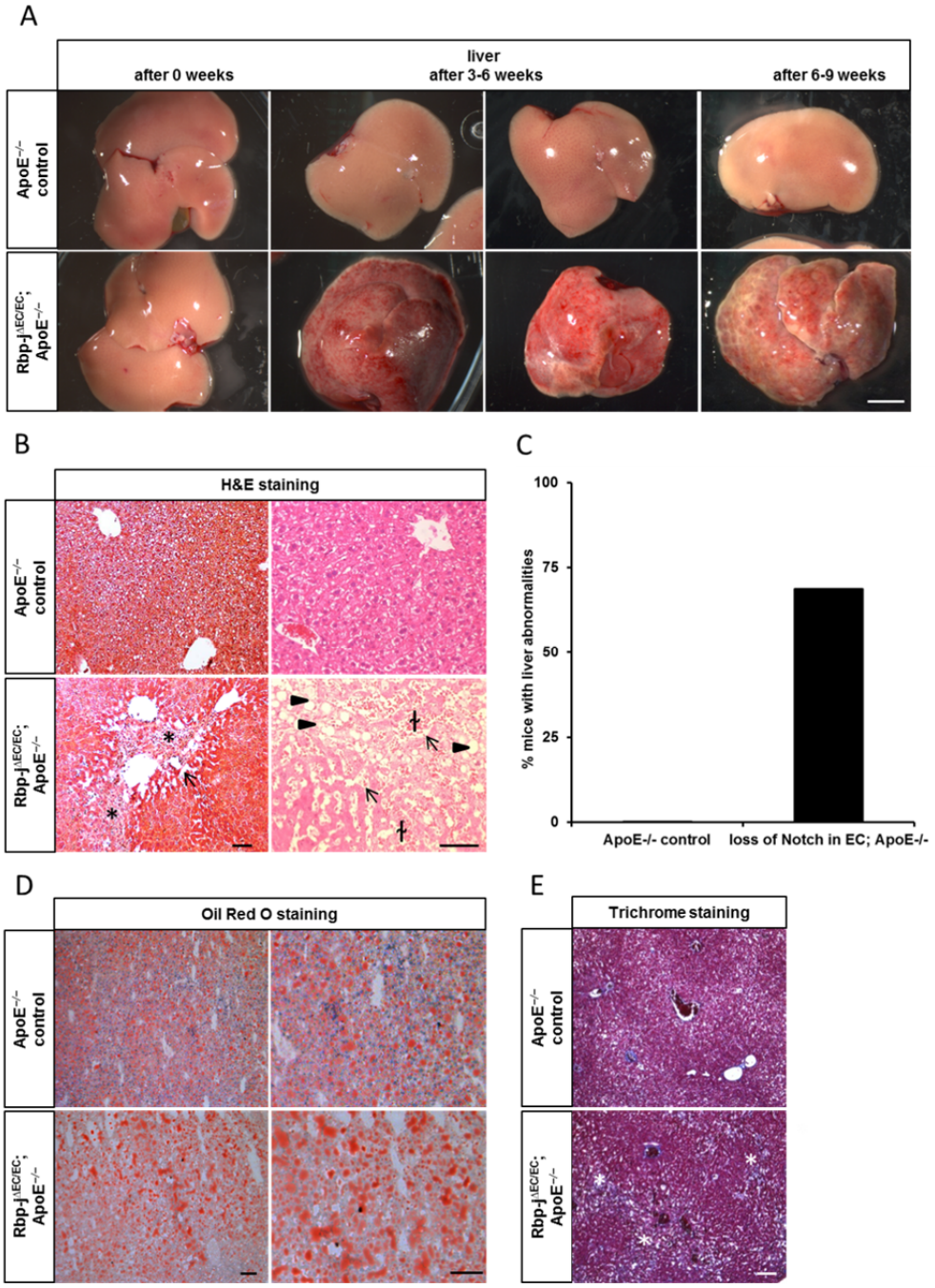

Figure 34: Loss of endothelial Notch activity caused sinusoidal dilation, blood congestion, fat depositions, and zonal fibrosis in the liver

(A) Representative pictures of livers from Rbp-j$^{\Delta EC/EC}$; ApoE$^{-/-}$mice and ApoE$^{-/-}$ controls immediately after Tamoxifen injection (0 weeks), 3-6 weeks, and 6-9 weeks. Rbp-j$^{\Delta EC/EC}$; ApoE$^{-/-}$mice displayed liver dysplasia with consistent impairment over time. Mice were fed with Western diet. (B, D, E) Histological stains of liver sections 6-9 weeks after Tamoxifen application. Left panels illustrated pictures captured with low magnification (10 x); right panels illustrated pictures with higher magnification (20 x). (B) Rbp-j$^{\Delta EC/EC}$; ApoE$^{-/-}$ mice displayed massive dilation of hepatic sinusoids (arrows) and congestion of blood cells (ŧ). Stars indicate necrotic areas surrounding the vessels. Fat depositions in hepatocytes (arrowheads) were increased in Rbp-j$^{\Delta EC/EC}$; ApoE$^{-/-}$ mice. (C) Liver pathogenesis was present in 68 % of Rbp-j$^{\Delta EC/EC}$; ApoE$^{-/-}$mice (n=16) compared to 0 % of ApoE$^{-/-}$ controls (n=19). (D) An increase in hepatic lipid accumulation was observed in Rbp-j$^{\Delta EC/EC}$; ApoE$^{-/-}$mice (lower raw). (E) Masson's trichrome staining indicated fibrotic areas (blue staining, marked by white stars) in Rbp-j$^{\Delta EC/EC}$; ApoE$^{-/-}$mice. CV, central vein. Scale bars: 50 µm (D); 100 µm (B; E); 5 mm (A).

3.2.2.5 Notch signaling in the liver endothelium was identified to be responsible for regulation of the hepatic fat metabolism

Dilation of liver sinusoids in Rbp-j$^{\Delta EC/EC}$; ApoE$^{-/-}$mice forces adjacent cubical hepatocytes to adopt a compressed, narrowed and elongated cellular phenotype (Figure 35, A). Hepatocytes constitutes over 70 % the main cellular mass of the liver and exert important metabolic functions including protein synthesis of lipoproteins and glycoproteins; transformation of carbohydrates, fat synthesis and detoxification.

To verify the indispensable function of endothelial cells as a critical cell type for the observed phenotype, hepatocytes and sinusoidal endothelial cells were isolated from Rbp-j$^{\Delta EC/EC}$; ApoE$^{-/-}$mice and ApoE$^{-/-}$ controls 4 weeks after Tamoxifen application. Primary cells were analyzed for Rbp-j mRNA expression by qPCR with primers detecting Rbp-j exons 6 and 7, which are deleted after recombination of Rbp-j. Hepatocytes from Rbp-j$^{\Delta EC/EC}$; ApoE$^{-/-}$mice did not reveal impaired Rbp-j mRNA expression, attesting regular Notch signaling (Figure 35, B). However, recombination was successful for sinusoidal endothelial cells (Data not shown), as the results confirmed that the severe liver pathology observed in Rbp-j$^{\Delta EC/EC}$; ApoE$^{-/-}$mice was provoked by an endothelial specific loss of Notch signaling. Thus, the liver endothelium was identified to act as critical regulator of hepatic fat metabolism.

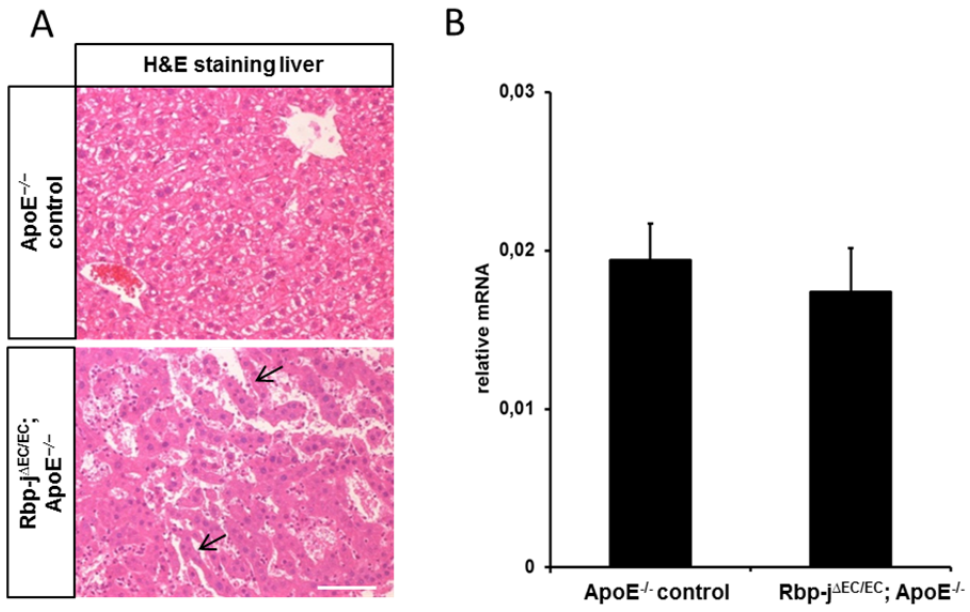

Figure 35: Hepatocytes of Rbp-jΔEC/EC; ApoE-/- mice adopted a narrowed cellular phenotype but were themselves not deficient for Notch signaling capacity

(A) Livers of Rbp-jΔEC/EC; ApoE-/- mice displayed a flattened and elongated shape of hepatocytes (arrows) compared to the natural cubical form in ApoE-/- controls 6 weeks after Tamoxifen injection and feeding with Western diet. (B) Rbp-j mRNA levels were determined by qPCR using cDNA generated from total hepatocyte RNA as template. GAPDH mRNA levels were used for normalization. The averaged Rbp-j mRNA level in isolated hepatocytes was not changed in Rbp-jΔEC/EC; ApoE-/- mice (n=2). Scale bars: 100 µm.

3.2.2.6 Loss of endothelial Notch signaling protected Rbp-j$^{\Delta EC/EC}$; ApoE$^{-/-}$ mice from diet-induced insulin insensitivity

Excessive alcohol consumption, lipid metabolism disorders and infections contribute to the development of steatohepatitis. Moreover, obesity, diabetes and elevated triglyceride levels display prevalent risk factors of fatty liver disease, elevated blood glucose levels, and insulin resistance. Since the liver exerts crucial metabolic functions in the control of glucose homeostasis, steatohepatitis is often associated with insulin resistance and the pathogenesis of diabetes.

Insulin promotes the cellular uptake of glucose in response to food digestion and absorption of glucose into the blood. Type 2 diabetes mellitus is caused by a decreased ability of insulin to stimulate glucose uptake and thereby failure to inhibit hepatic gluconeogenesis. In order to assess the association of steatohepatitis and glucose homeostasis, an intraperitoneal glucose tolerance test (IPGTT) was performed in Rbp-j$^{\Delta EC/EC}$; ApoE$^{-/-}$ mice and ApoE$^{-/-}$ controls 6-9 weeks after Tamoxifen injection. Mice were fasted for 6 h before blood glucose measurements. The clearance of an intraperitoneal injected glucose load (2g/kg) was measured before (0) and 30, 60 and 120 min after injection. Rbp-j$^{\Delta EC/EC}$; ApoE$^{-/-}$ mice revealed 16 % significantly lowered fasting blood glucose levels. In contrast, control mice exerted hyperglycemia (Figure 36, A). Glucose injection and measurements after 30, 60 and 120 min revealed an improvement after endothelial-specific deletion of Notch signaling.

Increased insulin-sensitivity in Rbp-j$^{\Delta EC/EC}$; ApoE$^{-/-}$ mice was accompanied by significantly lowered fasting blood glucose concentrations and increased hepatic storage of glucose as glycogen (violet color) (Figure 36, B). The spotted pattern of the PAS-stained liver sections identified deposition of polysaccharides such as glycogen encompassing the hepatic portal vein and arteries at the periphery during high-fat feeding periods.

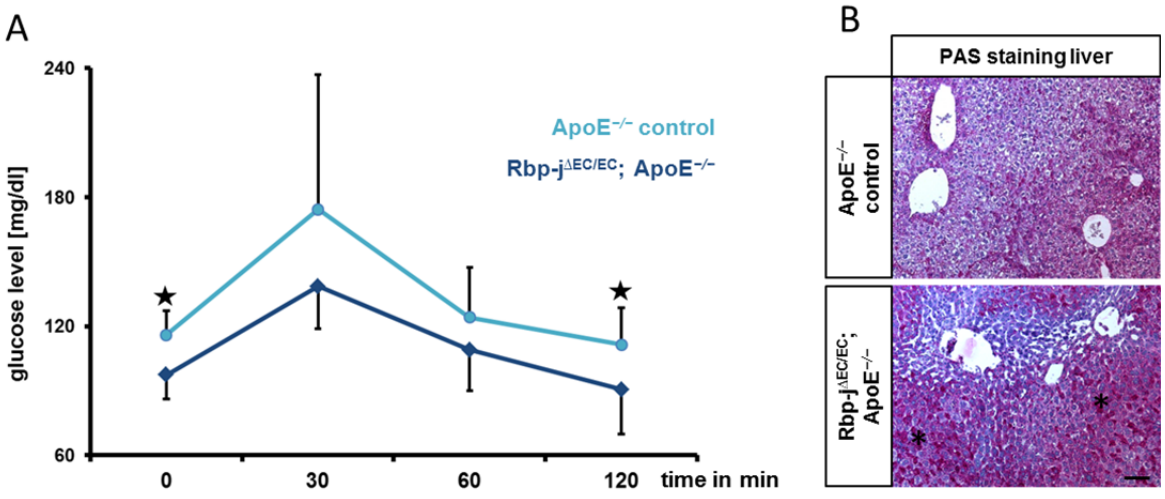

Figure 36: Endothelial loss of Notch signaling improved glucose tolerance and increased hepatic glycogen deposition

(A) IPGTT of Rbp-j$^{\Delta EC/EC}$; ApoE$^{-/-}$ and ApoE$^{-/-}$ control mice 6-9 weeks after Tamoxifen application followed by a Western diet. After 6 h of fasting, mice were injected with 2 g/kg glucose. Plasma glucose concentrations were assessed before (0) and 30, 60, and 120 min after glucose injection. Results represented mean blood glucose concentrations in mg/dl (n=7). (B) The intensity of PAS-stained polysaccharides (violet color) was increased in Rbp-j$^{\Delta EC/EC}$; ApoE$^{-/-}$ mice as indicated with stars. Scale bar: 100 µm (B).

3.2.2.7 Microarray analysis of livers sinusoidal endothelial cells isolated from Rbp-j$^{\Delta EC/EC}$; ApoE$^{-/-}$ mice and ApoE$^{-/-}$ controls

Chronic lack of endothelial Notch signaling in Rbp-j$^{\Delta EC/EC}$; ApoE$^{-/-}$ mice improved glucose tolerance but caused a steatohepatitis (Figure 34, A). To evaluate the underlying molecular mechanisms, global gene expression patterns of liver sinusoidal endothelial cells (LSEC) of Rbp-j$^{\Delta EC/EC}$; ApoE$^{-/-}$ and control mice were characterized by microarray analysis. LSEC isolation was performed in collaboration with Dr. Philipp Koch and Dr. Cyrill Geraud (Dermatology, Universitätsmedizin Mannheim). Purity of LSEC was determined by FACS analysis and resulted in high purity with >80 % CD31+ endothelial cells, >80 % Stabilin-2+ cells, a specific marker for LSEC, and < 5 % CD11b+ cells (representing macrophage contamination) for both groups (Figure 37, A). Microarray analysis was performed at the Genomics and Proteomics Core Facility of the German Cancer Research Center Heidelberg (DKFZ).

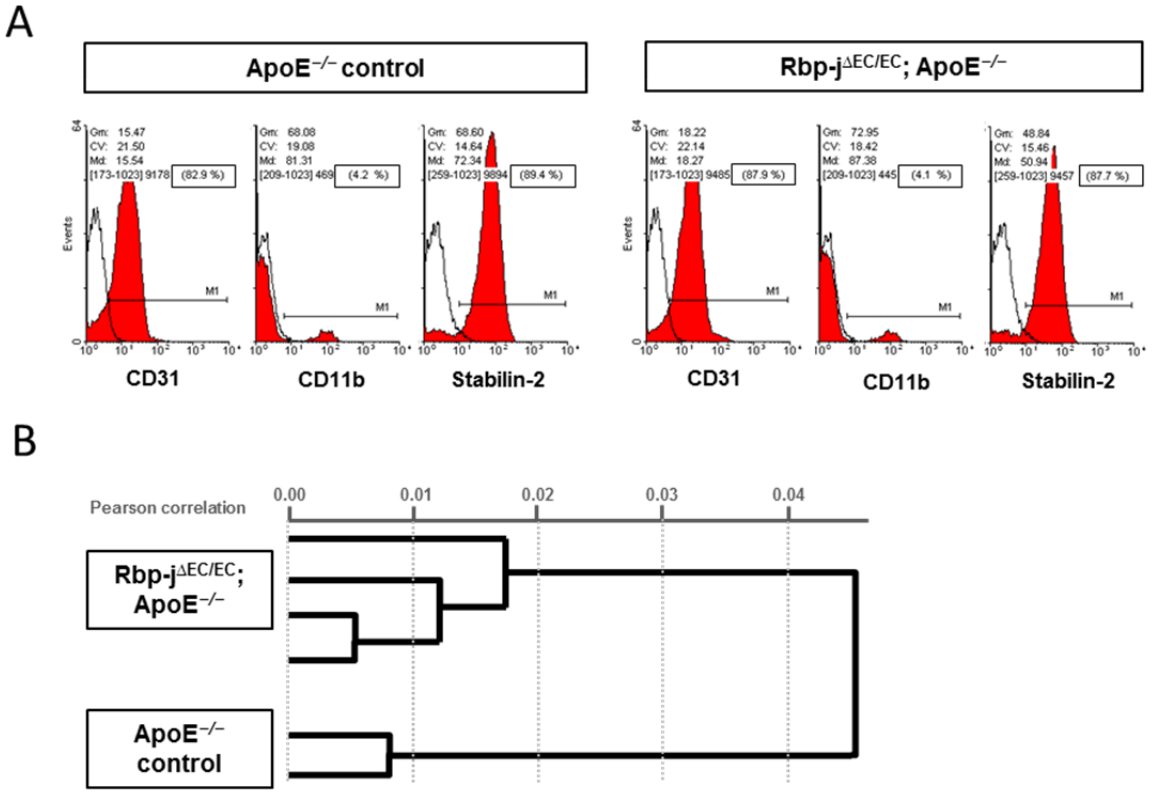

Figure 37: Microarray analysis of LSEC isolated from Rbp-j$^{\Delta EC/EC}$; ApoE$^{-/-}$ mice and ApoE$^{-/-}$ controls

(A) Representative diagrams of a FACS analysis of LSEC isolated from ApoE$^{-/-}$ controls (left) and Rbp-j$^{\Delta EC/EC}$; ApoE$^{-/-}$ mice (right) resulted in high purity of cells after staining against CD31, CD11b or Stabilin-2. FACS analysis revealed no difference in purity between LSEC isolated from Rbp-j$^{\Delta EC/EC}$; ApoE$^{-/-}$ mice or appropriate controls. (B) A dendrogram resulting from hierarchical clustering using the Pearson correlation coefficient revealed strong correlation in between the four samples from Rbp-j$^{\Delta EC/EC}$; ApoE$^{-/-}$ mice (n=6). Similar results were observed for two samples isolated from ApoE$^{-/-}$ control animals (n=4). Comparison of the Rbp-j$^{\Delta EC/EC}$; ApoE$^{-/-}$ and the ApoE$^{-/-}$ control group showed a week correlation.

The Pearson product-moment correlation coefficient (r) was used for computational sorting of the microarray data (hierarchical clustering). The hierarchical clustered values were illustrated within a dendrogram (Figure 37, B). The closer the different samples cluster to the value of 0, the more correlation in gene expression patterns they exert. The LSEC samples of Rbp-j$^{\Delta EC/EC}$; ApoE$^{-/-}$ mice displayed a strong correlation. However, samples from Rbp-j$^{\Delta EC/EC}$; ApoE$^{-/-}$ mice revealed no clustering with the ApoE$^{-/-}$ control samples, indicating differences in gene expression patterns between the investigated groups (Figure 37, B).

562 transcripts were found to be up- or down-regulated more than 50 % in LSEC from Rbp-j$^{\Delta EC/EC}$; ApoE$^{-/-}$ (Appendix; Table 1). Notch target genes including Hes1 and Nrarp were down-regulated with a fold change of 0.5, which confirmed a functional Notch signaling blockade. Microarray analysis revealed significant effects on the expression of genes of the Wnt pathway (R-spondin 3 homolog (Rspo), Dickkopf homolog 3 (Dkk3), Frizzled homolog 5 (Fzd5), and the Wnt ligands Wnt 9b and Wnt2). An effect on the transcriptional regulation of genes involved in Wnt signaling in response to Rbp-j deficiency was not surprising since the Notch and Wnt pathway were described to cross-talk in the endothelium (Dejana, 2010). Transcription of factors involved in angiogenesis including von Willebrand factor (Vwf), Vegf-A and -C, EphrinB2, Netrin 4 (Ntn4) and bone morphogenic protein 4 (Bmp4) were also influenced by endothelial Notch signaling.
Furthermore, the transcription of the endothelial tight junctional adhesion molecule B (JAM2) was impaired, impeding interendothelial adhesion and communication. Microarray data revealed changes in the expression of mRNA transcripts of several chemokines and receptors. In accordance with the microarray data, Notch signaling was described to regulate chemotaxis in endothelial cells (Chigurupati et al., 2007). Liver damage and inflammation in Rbp-j$^{\Delta EC/EC}$; ApoE$^{-/-}$ mice was indicated by a 3 fold increase of the nuclear pore glycoprotein-210 (Nup210) expression. Nup210 is a crucial trafficking regulator in nuclear pore complexes, and is associated with progression of end stage liver disease such as primary biliary cirrhosis (Nakamura et al., 2006). With regard to metabolism, a decreased transcriptional expression was revealed for the Forkhead box protein O1 (FoxO1), a transcription factor and effector for insulin signaling during hepatic gluconeogenesis and glycogenolysis. PPAR-γ transcription was found to be upregulated in microarray data of Rbp-j$^{\Delta EC/EC}$; ApoE$^{-/-}$ mice.

4. Discussion

The formation of the vascular system encompasses cellular processes such as endothelial cell activation, proliferation, migration and anastomosis. These processes are highly dependent on the VEGF and the Delta-Notch signaling pathways. Hypoxia-induced VEGF signaling initiates the formation and migration of tip-forming endothelial cells; whereas Notch signaling maintains the migratory tip cell versus a proliferatory stalk cell phenotype in growing vessels (Hellstrom et al., 2007). The feasibility of Notch signaling to control sprouting angiogenesis is dependent on a balanced differential regulation of the VEGF signaling pathway (Benedito et al., 2012). Dysregulated Notch signaling has been linked to several diseases including Alagille syndrome, Tetralogy of Fallot, CADASIL (Harper et al., 2003), and cancer (Chillakuri et al., 2012). In tumors, hypoxia-mediated induction of VEGF or paracrine VEGF secretion from tumor cells activates Notch signaling. Persistent activity of both pathways results in a high number of actively growing vascular sprouts, causing the formation of a tortuous and unorganized vessel network (Chung et al., 2010). Interference with tumor angiogenesis by VEGF-neutralizing antibodies prolongs the patients' progression-free survival rate in most studies. However, VEGF-neutralizing antibodies do not alter the overall survival. Severe side effects, resistance and drug tolerance enforce the search for alternative or additional treatment options to restrict tumor growth. The use of a combinatorial anti-angiogenic therapy with Notch and VEGF signaling-inhibitors in murine tumor models results in a synergistic inhibition of tumor expansion (Ridgway et al., 2006).

4.1 Soluble DLL1-DSL-Fc and DLL4-DSL-Fc ligands represent promising tools to block Notch signaling

Clinical trials with γ-secretase inhibitors reveal severe side effects including intestinal toxicity. This is due to the fact that the inhibitors block the intramembranous processing of the Notch receptor but also over 60 other substrates. In order to improve the specificity of Notch blockade, anti-Notch antibodies or Notch decoy molecules have been developed. Blocking Notch signaling by Notch decoy molecules, which prevent ligand-induced Notch activity, results in decreased angiogenesis and impaired tumor growth (Funahashi et al., 2008), whereas an anti-DLL4 therapy results in increased angiogenesis (Sainson and Harris, 2007). Surprisingly, the vessels are non-functional, which leads to the inhibition of tumor growth. In 2006, Ridgway and colleagues identified that chronic DLL4 blockade caused cellular toxicity and the development of vascular tumors (Liu et al., 2011; Ridgway et al., 2006).

Further investigations using X-ray structural analysis identified the DSL domain as the interacting motif with which the JAG1 ligand binds to the NOTCH1 receptor (Cordle et al., 2008). Additionally, the EGF-like repeats 11-13 of NOTCH1 have been identified to be crucial for ligand binding (Hambleton et al., 2004).

Based on the conservation of the ligand DSL and receptor EGF11-13 motifs (Figure 13), we generated soluble Notch ligands DLL1-DSL-Fc, DLL4-DSL-Fc and JAG1-DSL-Fc, and a receptor NOTCH1-EGF11-13, in which the particular potential ligand-binding domain was fused to IgG1-Fc. Soluble ligands comprised of the complete ECD-domain were designed for DLL4 and JAG1 (DLL4-ECD-Fc, JAG1-ECD-Fc) in order to compare the effects on receptor activity. The generated Fc-fused ligands and receptors are small in size. This facilitates the *in vivo* transport along with increased half-life in the blood stream (Salfeld, 2007). The use of the specific Notch ligand-receptor binding motifs for the generation of the soluble ligands and receptors is supposed to increase the specificity for interactions with Notch components. Consequently, unintentional interactions with proteins such as non-canonical Notch ligands, act inhibitory for canonical Notch signaling activity should be avoided. For example, uninflatable (uif) and Crumbs (Crb) are shown to antagonize canonical Notch signaling activity by interacting with the Notch extracellular domain during *Drosophila melanogaster* development (Herranz et al., 2006; Xie et al., 2012). In vertebrates, the non-canonical Notch ligand epidermal growth factor-like domain 7 (EGFL7) antagonizes JAG1-induced Notch signaling by interaction with the EGF-like repeats 7-12 of the endothelial receptors Notch1, -2 and -4 (Fitch et al., 2004; Parker et al., 2004). Surprisingly, EFGL7 interacts with DLL4 to potentiate Notch signaling. Beside EGFL7 further non-canonical Notch ligands including the soluble matrix thrombospondin (TSP2) enhance Notch trans-signaling (Meng et al., 2009). In summary, canonical ligand-induced Notch signaling can be influenced by a subset of non-canonical Notch ligands, which exert their effect by interaction with domains not involved in canonical ligand binding.

Application of the soluble Notch ligands to endothelial cells resulted in suppression of Notch target gene expression (Figure 19). The inhibitory effect on Notch signaling identifies the ligand DSL domain as being sufficient to exert blocking effects on Notch signaling activity. The inhibition of Notch signaling activity using soluble Notch ligands can be explained by the absence of endocytosis-mediated mechanical forces of membrane-integral ligands that normally dissociate the Notch receptor. During ligand-mediated Notch receptor activation endocytosis of the receptor-ECD-bound ligand generates a mechanical force, which causes a conformational change in the receptor (Meloty-Kapella et al., 2012). The conformational change provides access for proteases to exert ´site 2 cleavage´, enabling Notch heterodimer dissociation, which in turn is crucial for signal transduction. Several groups confirme the importance of ligand-induced receptor dissociation (Funahashi et al., 2008; Lin et al., 2010; Noguera-Troise et al., 2006; Urs et al., 2008). The dominant negative action of soluble ligands on Notch receptor activity strengthens the hypothesis of endocytosis-mediated signal induction. Even membrane-integral non-canonical Notch ligands exhibit ubiquitylation sites for facilitating ligand endocytosis. However, it has still not been clarified whether endocytosis induced by non-canonical ligands is necessary for induction of Notch signaling. Additionally, the mechanism by which soluble canonical ligands such as DSL-1 in *C. elegans* or soluble non-canonical ligands including MAGP2 exert activating effects on Notch signaling has yet to be unravelled (Kopan and Ilagan, 2009).

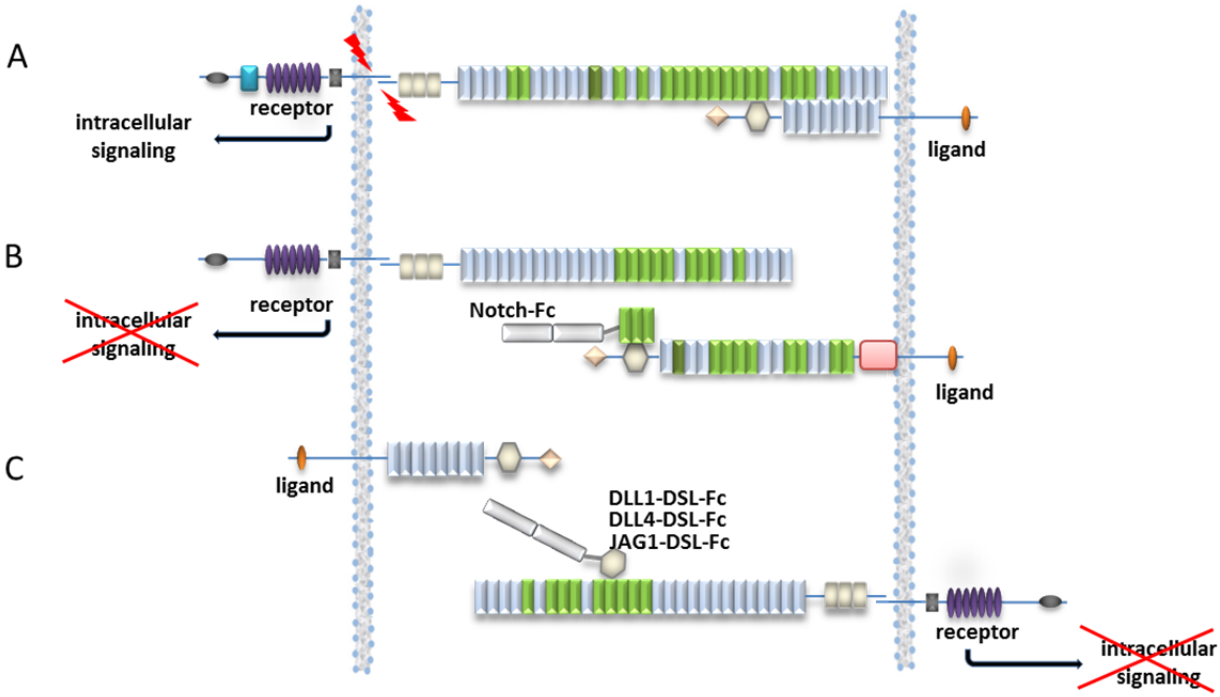

Figure 38: Action of the Fc-coupled Notch interfering ligand and receptor constructs

Simplified depiction of Notch receptor and ligand expression in ECs. Notch receptors 1 and 4, denoted as ´receptor´, and Notch ligands Delta-like4 and Jagged1, denoted as ´ligands´, are broadly expressed on the EC surface. (A) Activation of the Notch receptor upon ligand binding triggers a proteolytic cleavage cascade, which results in intracellular signaling and Notch target gene expression. (B) Notch signaling is impaired by the soluble receptor NOTCH1-EGF11-13-Fc, referred as ´Notch-Fc´, which functioned as a decoy for the different Notch ligands. Thereby, NOTCH1-EGF11-13-Fc disrupts the endogenous signal-transducing ligand-receptor interactions. (C) Notch signaling is impaired by the soluble ligand constructs DLL1-DSL-Fc, DLL4-DSL-Fc and JAG1-DSL-Fc, which function as non-signaling competitors for endogenous membrane-bound ligands.

The antagonistic effect of the soluble DLL1-DSL-Fc and DLL4-DSL-Fc ligands on Notch signaling activity was further confirmed by significantly increasing endothelial proliferation (Figure 21) and chemotactic migration under non-stimulative conditions. Under basal conditions, the number of endothelial sprouts was increased by DLL1-DSL-Fc and DLL4-DSL-Fc ligands in the 3D-sprouting assay (Figure 22). The formation of a `hyperdense´ vascular network with increased numbers of tip cells is consistent with the report of a similar phenotype following treatment of tumors with soluble DLL4-ECD constructs (Noguera-Troise et al., 2006). Experiments with myogenic cells also confirmed the dominant negative effect of soluble ligands (Figure 20). Studying DLL1-DSL-Fc and DLL4-DSL-Fc ligands in the postnatal mouse eye, *in vivo*, revealed an impaired radial outgrowth of the superficial vascular plexus from the optic nerve to the retinal periphery at postnatal day 7 (Figure 24). The resulting vascular networks displayed a profound increase in tip cell numbers. This is supported by the *in vitro* angiogenic sprouting data (Figure 25). The observed hypersprouting resembles the retinal phenotype described for inhibition of Notch signaling activity via chemical inhibition with γ-secretase or by genetic deletion of Dll4, Rbp-j or Notch1 (Hellstrom et al., 2007; Hu et al., 2009; Ridgway et al., 2006).

However, the number of vessel branches was not altered in response to DLL1-DSL-Fc and DLL4-DSL-Fc treatment (Figure 25) although it is reported for Notch blockade in the literature (Hellstrom et al., 2007; Ridgway et al., 2006). Taken together, the soluble DLL1-DSL-Fc and DLL4-DSL-Fc ligands efficiently suppress Notch signaling activity in different cell types and thereby enforce the formation of a tip cell-rich phenotype.

The soluble JAG1-DSL-Fc peptide inhibited Notch target gene expression (Figure 19). These results stand in contrast to a study, which also used a peptide, encompassing the JAG1 receptor-binding region, that revealed agonistic action on Notch signaling activity (Hellstrom et al., 2007; Weijzen et al., 2002). A hyperdense sprouting phenotype was observed in endothelial cells in response to JAG1-DSL-Fc expression under unstimulated conditions. Treatment with JAG1-DSL-Fc protein in combination with VEGF increased endothelial sprouting. Myogenic differentiation was slightly induced by JAG1-DSL-Fc (Figure 20). Yet, no significant effects on endothelial proliferation and migration were observed (Figure 21). The dominant-negative regulation of Notch signaling activity by the soluble JAG1-construct revealed inconsistent results. This might be explained in part by glycosylation at the ligand-binding region of the Notch receptor. This results in enhanced DLL4-induced but impaired JAG1-induced Notch signaling activity (Benedito et al., 2009). Thus, depending on the glycosylation status of the receptor, the soluble JAG1 ligands might compete with endogenous Delta-like ligands

The antagonistic effect of the soluble Notch ligands DLL4-ECD and JAG1-ECD on Notch signaling was confirmed by increased basal endothelial sprouting (Figure 22). This supports the data of Gavin Thurston's group, that reports enhanced angiogenic sprouting after application of the soluble DLL4-ECD ligand (Noguera-Troise et al., 2006). However, the antagonizing effects of DLL4-ECD-Fc and JAG1-ECD-Fc on Notch signaling were not consistent in *in vitro* studies since cellular processes such as endothelial proliferation were unaltered. Yet, *in vivo* investigation of DLL4-ECD-Fc in the murine retina revealed impaired vascular outgrowth of the superficial vascular plexus and an increased number of sprouting cells at the retinal periphery (Figure 24, 25). The data resemble the retinal phenotype of mice with heterozygous endothelial deletion of DLL4, which results in a dense vascular network and excessive vascular sprouting due to an increased tip cell number (Hellstrom et al., 2007). The differences between *in vitro* and *in vivo* experiments could arise due to participation of cofactors in the more complex *in vivo* cellular system.

The soluble NOTCH1-EGF11-13-Fc receptor blocked the expression of Notch target genes (Figure 19). *In vitro* experiments revealed no effects on endothelial proliferation and migration (Figure 21). However, NOTCH1-EGF11-13-Fc impaired the growth of the vascular plexus during retinal vascularization. Retinas displayed an increased number of tip cells at the vascular periphery (Figure 24, 25). These results confirm the notion that insufficient Notch signaling causes an increase in tip cell numbers (Hellstrom et al., 2007; Suchting et al., 2007). While both, the ligand and the receptor constructs, exerted dominant negative

effects on Notch target gene expression; they differed in their effect on endothelial sprouting. The soluble ligands induced a hypersprouting phenotype; whereas the soluble receptor induced a decrease in basal and VEGF-induced endothelial sprouting *in vitro* (Figure 22, 23). The data for the receptor construct are concordant with a study using soluble NOTCH1-ECD. NOTCH1-ECD-Fc acts as antagonist of ligand-induced signaling activity and leads to an impairment of VEGF-induced neoangiogenesis due to vascular disruption in a murine tumor model (Funahashi et al., 2008). The soluble NOTCH1-EGF11-13-Fc receptor may act as a decoy for several Notch ligands by blocking multiple endogenous ligand-receptor interactions. Depending on the ligand, the outcome on angiogenesis might be different since Delta and Jagged ligands are reported to exert different effects.

In summary, the soluble Notch receptors and ligands consisting of the respective interacting motifs exert antagonizing effects on Notch signaling activity. The soluble receptor is thought to act as a decoy for the different Notch ligands; however, the soluble ligands suppress Notch receptor activity by acting as competitors for endogenous membrane-bound ligands (Figure 38).

4.2 Notch signaling in the adult vasculature

Notch signaling is crucial during vascular development by restricting tip cell fate and arterio-venous specification (Adams and Alitalo, 2007). Several Notch ligands including DLL4, JAG1, JAG2 and receptors such as NOTCH1, -2 and -4 are described to be expressed in endothelial and supporting cells (Dou et al., 2008). Deletion of Notch1, Jag1, or Rbp-j in mice results in destroyed angiogenesis and embryonic lethality (Krebs et al., 2000; Xue et al., 1999). Thereby, the early embryonic death of the mice limits the feasibility of investigating the role of Notch signaling in the adult vascular system.
We generated an inducible mouse model with endothelial-specific inactivation of Rbp-j using the Cre-lox technology in order to investigate the role of the Notch signaling pathway in the adult vasculature. The Rbp-j gene encodes the key transducer of all four vertebrate Notch receptors. Inactivation of Rbp-j in the signal receiving cell chronically aborts signaling activity, which is induced by all Notch receptors and prevents redundancy. A few studies with other inducible Notch mouse models have been reported as well. Deletion of Rbp-j in bone marrow-derived EPC attenuates the capacity of homing and facilitates liver regeneration (Wang et al., 2009b). RBP-J deficiency in dendritic cells renders the cells unable to initiate specific immune responses in tumors (Feng et al., 2010). In addition, Rbp-j deficiency in hepatic, hematopoietic and endothelial cells increases endothelial proliferation followed by spontaneous angiogenesis in several organs and tissues (Dou et al., 2008; Kuhn et al., 1995; Leuker et al., 2001; Wang et al., 2009a).

Dysregulated endothelial Notch signaling acts as inducer of neoplasia

We observed a deterioration of the health status occurring 4-6 months after inactivation of endothelial Rbp-j (Rbp-$j^{\Delta EC/EC}$ mice). This is most probably a consequence of massive cardiac enlargement as well as structural changes to the liver (Figure 27). Long-term deletion of endothelial Notch signaling rendered mice susceptible to development of hemangiomas e. g. in the skin (Figure 29). Hemangiomas are benign vascular tumors characterized by aberrant EC proliferation of capillaries giving rise to the formation of enlarged vessels. Hemangiomas occur in newborns (3-5 %) but rarely develop in adults. The observation of hemangiomas following endothelial deletion of Notch signaling is in concordance with a report from the group of Prof. Dr. Kopan, which describes the formation of vascular tumors predominantly affecting the liver in response to sporadic endothelial loss of Notch1 heterozygosity (Liu et al., 2012). Aberrant Notch signaling is already linked to vascular malformations, since increased endothelial Notch1 and Notch4 expression are reported to cause arteriovenous malformations (Murphy et al., 2008; ZhuGe et al., 2009).

Loss of endothelial Notch signaling provoked development of dilated cardiomyopathy

The development of the pathological heart and liver phenotype was accelerated by additional ApoE deficiency and resulted in a 50 % survival rate after 6.5 weeks for Rbp-$j^{\Delta EC/EC}$; $ApoE^{-/-}$ mice (Figure 30). The decreased survival rate is not caused by the ApoE deficiency, since ApoE mutant mice have a life expectancy of 18 month (Moghadasian et al., 2001). Rbp-$j^{\Delta EC/EC}$; $ApoE^{-/-}$ mice developed a pathologic enlargement of the heart (cardiomyopathy), accompanied by a significantly increased ratio of heart to body weight (Figure 33). The cardiac pathology resembles the phenotype observed in Rbp-$j^{\Delta EC/EC}$ mice 4-6 months after gene deletion. It is well known that Notch signaling controls heart development (MacGrogan et al., 2010; Niessen and Karsan, 2008). Notch1 deficiency in mice causes calcification of the heart valves, which leads to the progressive development of aortic valve disease (Garg et al., 2005). However, the role of Notch signaling during adulthood is elusive. Cardiac endothelial cells exert direct cellular signaling by growth factors, auto- and paracrine mechanisms and act as an active trans-endothelial blood-heart barrier. Endothelial cells thereby affect cardiac growth, contractility and rhythm (Brutsaert, 2003). The data provide evidence for a function of Notch as a signal coordinator for heart homeostasis in addition to cardiac development.

Rbp-$j^{\Delta EC/EC}$; $ApoE^{-/-}$ mice suffered from dilated cardiomyopathy (DCM). DCC is a progressive cardiac disease characterized by a dilation of the left ventricle associated with systolic dysfunction. Left ventricular failure can be followed by an impairment of the right ventricular function and diastolic dysfunction. Massive impairment of ventricular pump efficiency leads to progressive cardiac enlargement accompanied by hypertrophy resulting in cardiac failure. Rbp-$j^{\Delta EC/EC}$; $ApoE^{-/-}$ mice displayed an increased thickness of both ventricular walls (Figure 33); however hyperplasia and hypertrophy were not pronounced. Blood congestions in multiple organs including lung, spleen and kidney were probably provoked as secondary

effects due to impaired pump activity (Figure 27). Deletion of endothelial Notch signaling caused a loosening of the tight cardiomyocyte fiber arrangement in both ventricle walls (Figure 33). This effect might be caused by a dilation of capillaries in response to loss of endothelial Notch activity. The mechanical dissociation of the myocardium might influence cellular communication, as well as, contractile activity of the heart resulting in heart failure. Therefore, endothelial Notch signaling activity seems to be crucial for maintaining the adult cardiac function.

DCC can be caused by viral myocarditis or a variety of toxic agents including alcohol and drugs. Genetic inheritance occurs in 25-35 % of patients. Genes that cause DCC encode proteins involved in contraction or cytoskeletal proteins such as α-cardiac actin (Jefferies and Towbin, 2010). The participation of Notch signaling in the pathogenesis of DCC has been suggested by the identification of a previously unknown non-canonical Notch ligand in *Drosophila melanogaster* that when mutated causes dilated cardiomyopathy (Kim et al., 2010). However, the cellular mechanism of endothelial Notch signaling for the pathogenesis of DCC remains to be investigated.

Loss of endothelial Notch signaling causes liver damage but protects from diet-induced insulin insensitivity

The liver exerts a wide range of functions, including metabolism, detoxification and synthesis of proteins. Notch signaling is implicated in the development of the liver since it was shown to induce the differentiation of hepatoblasts into progenitor cells that are necessary for the formation of the bile ducts (Tanimizu and Miyajima, 2004). Mutations in the Jag1 gene cause the hereditary Alagille syndrome, which is associated with paucity of intrahepatic bile ducts. Aberrant Jag1 expression has also been linked to autoimmune diseases of the liver such as primary biliary cirrhosis (PBC) and primary sclerosing cholangitis (PSC) (Kohler et al., 2004). Liver sinusoidal endothelial cells (LSECs) facilitate the access of hepatocytes to oxygen and macromolecules, participate in metabolism and maintain hepatic stellate cell quiescence (DeLeve, 2003). Damage of LSECs initiates the pathogenesis of vascular liver diseases including the sinusoidal obstruction syndrome, which is characterized by obstruction of small hepatic vessels, fluid retention and increased liver size (DeLeve, 2003). Deletion of Notch signaling in LSEC is shown to induce proliferation of LSEC and hepatocytes in resting livers indicating a role for Notch signaling in the maintenance of endothelial quiescence (Ridgway et al., 2006; Wang et al., 2009a).

We could demonstrate that inactivation of Notch signaling in LSEC of Rbp-j$^{\Delta EC/EC}$; ApoE$^{-/-}$ mice caused a pathologic liver phenotype characterized by massive dilation of the sinusoids (Figure 34) as it was also observed in a milder form in livers of Rbp-j$^{\Delta EC/EC}$ mice (Figure 27, 28). Hepatocytes of Rbp-j$^{\Delta EC/EC}$; ApoE$^{-/-}$ mice displayed a compressed, narrowed and elongated cellular morphology (Figure 35), which in turn might be caused by shrinkage or compression due to expansion of hepatic vessels. Increased hepatocyte proliferation could not be evaluated.

Our data are confirmed by a study that reports histopathological changes in the liver, accompanied by sinusoidal dilations and hepatocyte atrophy in response to chronic Notch blockade via application of Dll4- or Notch1-inhibitory antibodies in mice, rats and monkeys (Yan et al., 2010). However, spontaneous angiogenesis as described by the Dou and colleagues in multiple tissues and organs was not observed in organs of Rbp-j$^{\Delta EC/EC}$; ApoE$^{-/-}$ mice (Dou et al., 2008).

The pathological liver phenotype was extended by increased accumulation of lipid filled vacuoles (Figure 34) along with fibrosis (steatohepatitis). Steatohepatitis can be induced by either pathologically formed macromolecules, which cannot be broken down, or the blockage of metabolic pathways. In the latter, deficiency of ApoE resulted in increased plasma cholesterol and triglycerides levels (Figure 31), since Apolipoprotein-E is involved in the clearance of lipoprotein-packed triglycerides (VLDL and LDL remnants). Serum triglyceride levels were further increased in Rbp-j$^{\Delta EC/EC}$; ApoE$^{-/-}$ mice. However, massive accumulation of fat in the liver cannot be attributed to the hyperlipidemia caused by deficiency of ApoE, as ApoE$^{-/-}$ mice were shown to exert protective effects on diet-induced development of fatty liver disease (Karavia et al., 2011). These data confirm the low-grade fatty liver observed in ApoE$^{-/-}$ control mice. If the high grade fat storage in hepatocytes of Rbp-j$^{\Delta EC/EC}$; ApoE$^{-/-}$ mice results from increased lipid uptake from the intestine, endogenous factors such as inhibited lipid disposal, increased *de novo* synthesis of lipids, or reduced export of lipids in hepatocytes have to be evaluated.

Fatty liver disease often occurs in obese people with type 2 diabetes. However, Rbp-j$^{\Delta EC/EC}$; ApoE$^{-/-}$ mice displayed lowered fasting blood glucose levels and overall improved the glucose tolerance. Thus, diabetes mellitus as a reason for fatty liver pathogenesis can be excluded since deletion of endothelial Notch signaling protects from insulin-insensitivity or -resistance.

Gene expression analysis of LSEC in response to genetic endothelial Notch blockade identified the transcription factors and key regulators of metabolic functions PPAR-γ and FoxO1 as Notch regulated genes. FoxO1 mediates endothelial angiogenic quiescence and the metabolic homeostasis of the vascular endothelium by controlling lipid and glucose metabolism (Oellerich et al., 2012). In insulin-responsive tissues, FoxO1 is a key effector of insulin action and promotes hepatic glucose production when nutrient and insulin levels are low (Barthel et al., 2005). Deletion of Notch signaling in LSEC caused a decreased FoxO1 expression. This resulted in lowered blood glucose levels and increased insulin sensitivity.

The data are confirmed by a study reporting that haploinsufficiency of Notch1 along with FoxO1 regulate hepatic glucose metabolism and improve insulin sensitivity (Pajvani et al., 2011). A direct interaction of FoxO1 with Rbp-j strengthens the crosstalk between both signaling pathways (Pajvani et al., 2011). However, further investigations are necessary to clarify the role of the Notch pathway in insulin-responsive tissues.

The transcription factor PPAR-γ controls fatty acid oxidation and synthesis and thereby mediates lipid utilization. We could show that deletion of Notch signaling in LSEC induced a significantly increased expression of PPAR-γ.

A Notch-mediated induction of PPAR-γ expression is suggested to regulate fatty acid transport through the endothelial cell layer in cardiac microvessel endothelial cells (Goto et al., 2009). We argue that even deletion of Notch signaling causes an increase in PPAR-γ expression in liver sinusoidal endothelial cells. Thereby, a balanced cross-talk between Notch and PPAR-γ signaling might be crucial for a proper regulation of fat metabolism.

Since it is not a strictly black-or-white pattern, the balanced cross-talk between the Notch pathway and the metabolism regulators PPAR-γ and FoxO1 might be responsible for fatty liver pathogenesis and improved insulin-sensitivity. Thus, endothelial Delta-Notch signaling exerts an important role in adult liver homeostasis by interfering with metabolism.

4.3 Summary and outlook

We could demonstrate that endothelial-specific blockade of Notch signaling by soluble Notch constructs or genetic deletion of Rbp-j in mice results in vascular abnormalities. Blockade of endothelial Notch signaling in mice results in the formation of vascular neoplasms indicating that active Notch signaling acts as a repressor for endothelial neoplastic transformation. Inhibition of endothelial Notch activity improves diet-induced glucose tolerance; while on the other hand causing the development of a fatty liver and dilated cardiomyopathy. In conclusion, we hypothesize that endothelial Notch signaling maintains homeostasis of the heart and the liver. In line with these observations we identified the endothelium as a critical regulator of fat and glucose metabolism. Therefore, pharmaceutical strategies for a chronic Notch signaling blockade have to be reevaluated in order to avoid intolerable side effects.

Appendix

Microarray tables

Table 1: List of transcripts changed more than 50 % after deletion of Notch signaling in LSEC

gene	probeID	fold change	description
Stc1	ILMN_260319	6,361356	Mus musculus stanniocalcin 1 (Stc1), mRNA.
Gpx3	ILMN_219947	4,813587	Mus musculus glutathione peroxidase 3 (Gpx3), transcript variant 2, mRNA.
Angptl4	ILMN_259520	4,749956	Mus musculus angiopoietin-like 4 (Angptl4), mRNA.
2700060E02Rik	ILMN_216512	4,576394	Mus musculus RIKEN cDNA 2700060E02 gene (2700060E02Rik), mRNA.
Sox11	ILMN_211466	4,251528	Mus musculus SRY-box containing gene 11 (Sox11), mRNA.
Nid2	ILMN_211992	3,931822	Mus musculus nidogen 2 (Nid2), mRNA.
Hist1h2af	ILMN_196733	3,463107	Mus musculus histone cluster 1, H2af (Hist1h2af), mRNA.
Nol10	ILMN_238030	3,430936	Mus musculus nucleolar protein 10 (Nol10), mRNA.
LOC100048556	ILMN_317312	3,418496	PREDICTED: Mus musculus similar to monocyte chemoattractant protein-5, transcript variant 1 (LOC100048556), mRNA.
Ankrd37	ILMN_227116	3,389081	Mus musculus ankyrin repeat domain 37 (Ankrd37), mRNA.
Saa3	ILMN_254030	3,362551	Mus musculus serum amyloid A 3 (Saa3), mRNA.
Nup210	ILMN_211743	3,234737	Mus musculus nucleoporin 210 (Nup210), mRNA.
AI481316	ILMN_217742	3,200162	
Ccrn4l	ILMN_208982	3,139877	Mus musculus CCR4 carbon catabolite repression 4-like (S. cerevisiae) (Ccrn4l), mRNA.
Lmna	ILMN_209635	3,10046	Mus musculus lamin A (Lmna), transcript variant 2, mRNA.
Slc2a1	ILMN_215238	3,084898	Mus musculus solute carrier family 2 (facilitated glucose transporter), member 1 (Slc2a1), mRNA.
Agtrl1	ILMN_222383	3,08248	Mus musculus angiotensin receptor-like 1 (Agtrl1), mRNA.
Uhrf1	ILMN_193478	2,965724	Mus musculus ubiquitin-like, containing PHD and RING finger domains, 1 (Uhrf1), mRNA.
Hist1h2an	ILMN_214020	2,95872	Mus musculus histone cluster 1, H2an (Hist1h2an), mRNA.
Egln3	ILMN_210459	2,958417	Mus musculus EGL nine homolog 3 (C. elegans) (Egln3), mRNA.
Hist1h2ai	ILMN_196735	2,93698	Mus musculus histone cluster 1, H2ai (Hist1h2ai), mRNA.
Rab3b	ILMN_212366	2,908354	
3830612M24	ILMN_185370	2,884358	
Dctd	ILMN_219335	2,859729	Mus musculus dCMP deaminase (Dctd), mRNA.
Hist1h2ak	ILMN_196730	2,845266	Mus musculus histone cluster 1, H2ak (Hist1h2ak), mRNA.
Hist1h2ah	ILMN_196729	2,783756	Mus musculus histone cluster 1, H2ah (Hist1h2ah), mRNA.
4930502E18Rik	ILMN_210023	2,739659	
Tubb6	ILMN_220148	2,737016	Mus musculus tubulin, beta 6 (Tubb6), mRNA.
Tiam1	ILMN_221605	2,723037	Mus musculus T-cell lymphoma invasion and metastasis 1 (Tiam1), mRNA.
Ebi2	ILMN_223731	2,704802	
Smpdl3b	ILMN_210171	2,693354	Mus musculus sphingomyelin phosphodiesterase, acid-like 3B (Smpdl3b), mRNA.
Grb10	ILMN_195756	2,624307	
Ccl2	ILMN_211411	2,622508	Mus musculus chemokine (C-C motif) ligand 2 (Ccl2), mRNA.
Pparg	ILMN_212393	2,614471	Mus musculus peroxisome proliferator activated receptor gamma (Pparg), mRNA.
E2f1	ILMN_221662	2,595059	Mus musculus E2F transcription factor 1 (E2f1), mRNA.
Pcdh17	ILMN_236878	2,594398	Mus musculus protocadherin 17 (Pcdh17), mRNA.
Hist1h2ad	ILMN_196727	2,591686	Mus musculus histone cluster 1, H2ad (Hist1h2ad), mRNA.
Hist1h2ao	ILMN_196731	2,581015	Mus musculus histone cluster 1, H2ao (Hist1h2ao), mRNA.
Aprt	ILMN_212844	2,558331	
Csf2rb2	ILMN_222474	2,547294	Mus musculus colony stimulating factor 2 receptor, beta 2, low-affinity (granulocyte-macrophage) (Csf2rb2), mRNA.
LOC100044948	ILMN_325390	2,535754	PREDICTED: Mus musculus similar to macrophage migration inhibitory factor (LOC100044948), mRNA.
Mcm5	ILMN_221972	2,517568	Mus musculus minichromosome maintenance deficient 5, cell division cycle 46 (S. cerevisiae) (Mcm5), mRNA.
Hist1h2ah	ILMN_196729	2,516695	Mus musculus histone cluster 1, H2ah (Hist1h2ah), mRNA.

Lmna	ILMN_209635	2,50709	Mus musculus lamin A (Lmna), transcript variant 2, mRNA.
Uck2	ILMN_220523	2,480474	Mus musculus uridine-cytidine kinase 2 (Uck2), mRNA.
Kcnk5	ILMN_218669	2,470933	Mus musculus potassium channel, subfamily K, member 5 (Kcnk5), mRNA.
Prc1	ILMN_222947	2,470091	Mus musculus protein regulator of cytokinesis 1 (Prc1), mRNA.
Ddc	ILMN_225530	2,457435	Mus musculus dopa decarboxylase (Ddc), mRNA.
Hist1h2ad	ILMN_196727	2,450206	Mus musculus histone cluster 1, H2ad (Hist1h2ad), mRNA.
Ampd1	ILMN_259430	2,444153	Mus musculus adenosine monophosphate deaminase 1 (isoform M) (Ampd1), mRNA. XM_921992
Birc5	ILMN_210249	2,387904	
Lmna	ILMN_246563	2,37844	Mus musculus lamin A (Lmna), transcript variant 1, mRNA.
1190002H23Rik	ILMN_209224	2,377614	Mus musculus RIKEN cDNA 1190002H23 gene (1190002H23Rik), mRNA.
Nol5	ILMN_247488	2,374185	Mus musculus nucleolar protein 5 (Nol5), mRNA.
2310016C08Rik	ILMN_222570	2,373141	Mus musculus RIKEN cDNA 2310016C08 gene (2310016C08Rik), mRNA.
Mki67	ILMN_234804	2,359769	PREDICTED: Mus musculus antigen identified by monoclonal antibody Ki 67 (Mki67), mRNA.
Cdc2a	ILMN_215304	2,35473	Mus musculus cell division cycle 2 homolog A (S. pombe) (Cdc2a), mRNA.
Slc16a6	ILMN_233199	2,328384	Mus musculus solute carrier family 16 (monocarboxylic acid transporters), member 6 (Slc16a6), transcript variant 2, mRNA.
Trim69	ILMN_221473	2,297875	Mus musculus tripartite motif-containing 69 (Trim69), mRNA.
St8sia4	ILMN_216048	2,280993	Mus musculus ST8 alpha-N-acetyl-neuraminide alpha-2,8-sialyltransferase 4 (St8sia4), mRNA.
Hist1h2ag	ILMN_196728	2,270674	Mus musculus histone cluster 1, H2ag (Hist1h2ag), mRNA.
Mest	ILMN_212378	2,269025	Mus musculus mesoderm specific transcript (Mest), mRNA.
Anln	ILMN_209418	2,263487	Mus musculus anillin, actin binding protein (scraps homolog, Drosophila) (Anln), mRNA.
Cdca8	ILMN_208664	2,262016	Mus musculus cell division cycle associated 8 (Cdca8), mRNA.
Cd63	ILMN_214933	2,257796	
Dbp	ILMN_211471	2,25284	Mus musculus D site albumin promoter binding protein (Dbp), mRNA.
Lmna	ILMN_209635	2,249851	Mus musculus lamin A (Lmna), transcript variant 2, mRNA.
Hist1h2ai	ILMN_196735	2,242066	Mus musculus histone cluster 1, H2ai (Hist1h2ai), mRNA.
Mest	ILMN_212378	2,236438	Mus musculus mesoderm specific transcript (Mest), mRNA.
Adamts9	ILMN_189047	2,227893	
Ednrb	ILMN_208799	2,227297	Mus musculus endothelin receptor type B (Ednrb), mRNA.
Kif22	ILMN_223310	2,213389	Mus musculus kinesin family member 22 (Kif22), mRNA.
LOC100048556	ILMN_317312	2,207106	PREDICTED: Mus musculus similar to monocyte chemoattractant protein-5, transcript variant 1 (LOC100048556), mRNA.
1110038B12Rik	ILMN_224564	2,201965	PREDICTED: Mus musculus RIKEN cDNA 1110038B12 gene, transcript variant 6 (1110038B12Rik), mRNA.
Plaur	ILMN_208927	2,197833	Mus musculus plasminogen activator, urokinase receptor (Plaur), mRNA.
Plat	ILMN_220503	2,197558	
Odc1	ILMN_219842	2,187263	Mus musculus ornithine decarboxylase, structural 1 (Odc1), mRNA.
Gnl3	ILMN_250637	2,185508	Mus musculus guanine nucleotide binding protein-like 3 (nucleolar) (Gnl3), transcript variant 2, mRNA.
Ednrb	ILMN_208799	2,179752	Mus musculus endothelin receptor type B (Ednrb), mRNA.
Limch1	ILMN_249397	2,176761	Mus musculus LIM and calponin homology domains 1 (Limch1), mRNA.
2310016C08Rik	ILMN_222570	2,175855	Mus musculus RIKEN cDNA 2310016C08 gene (2310016C08Rik), mRNA.
C230093N12Rik	ILMN_217458	2,166302	Mus musculus RIKEN cDNA C230093N12 gene (C230093N12Rik), mRNA.
Tpi1	ILMN_186788	2,160657	Mus musculus triosephosphate isomerase 1 (Tpi1), mRNA.
Birc5	ILMN_210249	2,159148	Mus musculus baculoviral IAP repeat-containing 5 (Birc5), transcript variant 1, mRNA.
Reep1	ILMN_218368	2,135305	Mus musculus receptor accessory protein 1 (Reep1), mRNA.
LOC100043796	ILMN_311576	2,133395	PREDICTED: Mus musculus similar to macrophage migration inhibitory factor, transcript variant 1 (LOC100043796), mRNA.
Lmna	ILMN_209635	2,130628	Mus musculus lamin A (Lmna), transcript variant 2, mRNA.
Pbk	ILMN_222572	2,128768	Mus musculus PDZ binding kinase (Pbk), mRNA.
Cd63	ILMN_214933	2,127965	Mus musculus Cd63 antigen (Cd63), transcript variant 2, mRNA.
Ccrn4l	ILMN_208982	2,121579	Mus musculus CCR4 carbon catabolite repression 4-like (S. cerevisiae) (Ccrn4l), mRNA.
Tnfrsf12a	ILMN_185117	2,113429	Mus musculus tumor necrosis factor receptor superfamily, member 12a (Tnfrsf12a), mRNA.
Stmn1	ILMN_213714	2,111052	
Car13	ILMN_219489	2,110453	Mus musculus carbonic anhydrase 13 (Car13), mRNA.
Hist2h2ac	ILMN_233024	2,106779	Mus musculus histone cluster 2, H2ac (Hist2h2ac), mRNA.
Zfp703	ILMN_259956	2,10452	PREDICTED: Mus musculus zinc finger protein 703 (Zfp703), mRNA.

Nusap1	ILMN_249313	2,102256	Mus musculus nucleolar and spindle associated protein 1 (Nusap1), transcript variant 2, mRNA.
Vegfa	ILMN_224512	2,084426	Mus musculus vascular endothelial growth factor A (Vegfa), transcript variant 1, mRNA.
Gng2	ILMN_236937	2,083852	Mus musculus guanine nucleotide binding protein (G protein), gamma 2 (Gng2), transcript variant 2, mRNA.
Gna13	ILMN_202533	2,082814	
Srm	ILMN_211754	2,078196	Mus musculus spermidine synthase (Srm), mRNA.
Brrn1	ILMN_224166	2,077863	
Cd63	ILMN_214933	2,077001	Mus musculus Cd63 antigen (Cd63), transcript variant 2, mRNA.
EG667728	ILMN_310163	2,073104	PREDICTED: Mus musculus predicted gene, EG667728 (EG667728), misc RNA.
Erdr1	ILMN_221931	2,071128	Mus musculus erythroid differentiation regulator 1 (Erdr1), mRNA.
Cdc20	ILMN_211070	2,070189	Mus musculus cell division cycle 20 homolog (S. cerevisiae) (Cdc20), mRNA.
LOC641366	ILMN_253840	2,068983	PREDICTED: Mus musculus hypothetical ENV polyprotein (LOC641366), mRNA.
Errfi1	ILMN_246139	2,065192	Mus musculus ERBB receptor feedback inhibitor 1 (Errfi1), mRNA.
2810417H13Rik	ILMN_220915	2,062868	Mus musculus RIKEN cDNA 2810417H13 gene (2810417H13Rik), mRNA.
LOC219228	ILMN_197523	2,061984	
Ddx26b	ILMN_215260	2,05904	Mus musculus DEAD/H (Asp-Glu-Ala-Asp/His) box polypeptide 26B (Ddx26b), mRNA.
D930046M13Rik	ILMN_191508	2,056701	
Ddc	ILMN_195063	2,042517	
Mcm6	ILMN_218086	2,032503	Mus musculus minichromosome maintenance deficient 6 (MIS5 homolog, S. pombe) (S. cerevisiae) (Mcm6), mRNA.
Gtse1	ILMN_215955	2,027283	Mus musculus G two S phase expressed protein 1 (Gtse1), mRNA.
Emp1	ILMN_213976	2,027022	Mus musculus epithelial membrane protein 1 (Emp1), mRNA.
Tk1	ILMN_210465	2,023844	Mus musculus thymidine kinase 1 (Tk1), mRNA.
Kif23	ILMN_224124	2,021145	
Gprc5b	ILMN_211032	2,018147	Mus musculus G protein-coupled receptor, family C, group 5, member B (Gprc5b), mRNA.
Birc5	ILMN_210249	2,017172	Mus musculus baculoviral IAP repeat-containing 5 (Birc5), transcript variant 1, mRNA.
Ncaph	ILMN_229155	2,013412	Mus musculus non-SMC condensin I complex, subunit H (Ncaph), mRNA.
Cdca3	ILMN_222106	2,005385	Mus musculus cell division cycle associated 3 (Cdca3), mRNA.
Cdr2	ILMN_214090	2,004445	Mus musculus cerebellar degeneration-related 2 (Cdr2), mRNA.
Nus1	ILMN_257947	1,992477	Mus musculus nuclear undecaprenyl pyrophosphate synthase 1 homolog (S. cerevisiae) (Nus1), mRNA.
Mcm10	ILMN_217134	1,988338	Mus musculus minichromosome maintenance deficient 10 (S. cerevisiae) (Mcm10), mRNA.
LOC100048116	ILMN_312568	1,980411	PREDICTED: Mus musculus similar to Jmy-pending protein (LOC100048116), mRNA.
Mif	ILMN_207449	1,980032	Mus musculus macrophage migration inhibitory factor (Mif), mRNA.
Fkbp10	ILMN_212109	1,977086	Mus musculus FK506 binding protein 10 (Fkbp10), mRNA.
EG667190	ILMN_257408	1,976162	PREDICTED: Mus musculus predicted gene, EG667190 (EG667190), misc RNA.
Fzd5	ILMN_260431	1,975312	Mus musculus frizzled homolog 5 (Drosophila) (Fzd5), transcript variant 1, mRNA.
Cd34	ILMN_219848	1,967763	Mus musculus CD34 antigen (Cd34), mRNA.
Rgs4	ILMN_209130	1,95924	Mus musculus regulator of G-protein signaling 4 (Rgs4), mRNA.
B230312L03Rik	ILMN_204093	1,959192	
Cdkn1a	ILMN_209664	1,957833	Mus musculus cyclin-dependent kinase inhibitor 1A (P21) (Cdkn1a), mRNA.
Cdca2	ILMN_212971	1,951175	Mus musculus cell division cycle associated 2 (Cdca2), mRNA.
Mest	ILMN_212378	1,94741	Mus musculus mesoderm specific transcript (Mest), mRNA.
Nedd9	ILMN_211969	1,944938	Mus musculus neural precursor cell expressed, developmentally down-regulated gene 9 (Nedd9), mRNA.
Hist1h2af	ILMN_196733	1,94446	Mus musculus histone cluster 1, H2af (Hist1h2af), mRNA.
Tes	ILMN_216487	1,934849	Mus musculus testis derived transcript (Tes), transcript variant 1, mRNA.
Sox7	ILMN_214899	1,927593	Mus musculus SRY-box containing gene 7 (Sox7), mRNA.
Spag5	ILMN_216733	1,919256	Mus musculus sperm associated antigen 5 (Spag5), mRNA.
Bax	ILMN_211762	1,9184	Mus musculus Bcl2-associated X protein (Bax), mRNA.
Pgk1	ILMN_253862	1,916492	Mus musculus phosphoglycerate kinase 1 (Pgk1), mRNA.
Top2a	ILMN_187810	1,913319	Mus musculus topoisomerase (DNA) II alpha (Top2a), mRNA.
Slc25a25	ILMN_208797	1,912792	Mus musculus solute carrier family 25 (mitochondrial carrier, phosphate carrier), member 25 (Slc25a25), nuclear gene encoding mitochondrial protein, mRNA.
Gins2	ILMN_233873	1,90627	Mus musculus GINS complex subunit 2 (Psf2 homolog) (Gins2), mRNA.
Kif4	ILMN_222148	1,905222	Mus musculus kinesin family member 4 (Kif4), mRNA.
Rgs2	ILMN_191558	1,904425	
Irf8	ILMN_216627	1,904301	Mus musculus interferon regulatory factor 8 (Irf8), mRNA.

Mif	ILMN_207449	1,898614	
Cdkn1a	ILMN_209664	1,892467	Mus musculus cyclin-dependent kinase inhibitor 1A (P21) (Cdkn1a), mRNA.
Pdk1	ILMN_214993	1,889311	Mus musculus pyruvate dehydrogenase kinase, isoenzyme 1 (Pdk1), nuclear gene encoding mitochondrial protein, mRNA.
LOC100045967	ILMN_311952	1,889034	PREDICTED: Mus musculus hypothetical protein LOC100045967 (LOC100045967), misc RNA.
LOC100048169	ILMN_325188	1,888775	PREDICTED: Mus musculus hypothetical protein LOC100048169 (LOC100048169), mRNA.
Hist2h2ab	ILMN_196734	1,886601	Mus musculus histone cluster 2, H2ab (Hist2h2ab), mRNA.
Phlda3	ILMN_212624	1,885486	Mus musculus pleckstrin homology-like domain, family A, member 3 (Phlda3), mRNA.
LOC100047628	ILMN_309869	1,885046	PREDICTED: Mus musculus similar to Chain L, Structural Basis Of Antigen Mimicry In A Clinically Relevant Melanoma Antigen System, transcript variant 3 (LOC100047628), mRNA.
Cdkn1a	ILMN_209664	1,883341	Mus musculus cyclin-dependent kinase inhibitor 1A (P21) (Cdkn1a), mRNA.
Igk-C	ILMN_217531	1,878156	
Kdelr3	ILMN_240560	1,877055	Mus musculus KDEL (Lys-Asp-Glu-Leu) endoplasmic reticulum protein retention receptor 3 (Kdelr3), mRNA.
Rrbp1	ILMN_211061	1,872033	Mus musculus ribosome binding protein 1 (Rrbp1), transcript variant 2, mRNA.
Dusp8	ILMN_215523	1,871792	Mus musculus dual specificity phosphatase 8 (Dusp8), mRNA.
Adamts1	ILMN_241585	1,867905	Mus musculus a disintegrin-like and metallopeptidase (reprolysin type) with thrombospondin type 1 motif, 1 (Adamts1), mRNA.
Frat2	ILMN_213946	1,866603	Mus musculus frequently rearranged in advanced T-cell lymphomas 2 (Frat2), mRNA.
Ly6c1	ILMN_234229	1,862111	Mus musculus lymphocyte antigen 6 complex, locus C1 (Ly6c1), mRNA.
Ccnb1	ILMN_215403	1,859821	Mus musculus cyclin B1 (Ccnb1), mRNA.
AI507611	ILMN_326750	1,855954	PREDICTED: Mus musculus expressed sequence AI507611, transcript variant 1 (AI507611), mRNA.
F2rl3	ILMN_221588	1,855793	Mus musculus coagulation factor II (thrombin) receptor-like 3 (F2rl3), mRNA.
Aebp1	ILMN_216508	1,854866	Mus musculus AE binding protein 1 (Aebp1), mRNA.
LOC384710	ILMN_254399	1,852747	PREDICTED: Mus musculus similar to 60S acidic ribosomal protein P0 (L10E) (LOC384710), mRNA.
Pabpc4	ILMN_211504	1,852323	Mus musculus poly A binding protein, cytoplasmic 4 (Pabpc4), transcript variant 1, mRNA.
Mx2	ILMN_216138	1,847952	
C230098O21Rik	ILMN_184645	1,845616	
Pfkl	ILMN_212064	1,845147	Mus musculus phosphofructokinase, liver, B-type (Pfkl), mRNA.
Ampd1	ILMN_259430	1,843822	Mus musculus adenosine monophosphate deaminase 1 (isoform M) (Ampd1), mRNA. XM_921992
Trim72	ILMN_252980	1,842086	Mus musculus tripartite motif-containing 72 (Trim72), mRNA.
Slc23a3	ILMN_219791	1,840951	Mus musculus solute carrier family 23 (nucleobase transporters), member 3 (Slc23a3), mRNA.
4930502E18Rik	ILMN_226002	1,834912	Mus musculus RIKEN cDNA 4930502E18 gene (4930502E18Rik), mRNA.
LOC100047827	ILMN_317292	1,829545	PREDICTED: Mus musculus similar to Hmgn2 protein (LOC100047827), mRNA.
Hist1h4f	ILMN_196722	1,82853	Mus musculus histone cluster 1, H4f (Hist1h4f), mRNA.
Vegfa	ILMN_192050	1,827819	Mus musculus vascular endothelial growth factor A (Vegfa), transcript variant 2, mRNA.
Sh3bgrl2	ILMN_184915	1,825051	
Slc12a2	ILMN_211631	1,824497	Mus musculus solute carrier family 12, member 2 (Slc12a2), mRNA.
Magi1	ILMN_251405	1,822669	Mus musculus membrane associated guanylate kinase, WW and PDZ domain containing 1 (Magi1), transcript variant 1, mRNA.
D17H6S56E-5	ILMN_196579	1,821756	Mus musculus DNA segment, Chr 17, human D6S56E 5 (D17H6S56E-5), mRNA.
Ctnnbip1	ILMN_218430	1,820859	Mus musculus catenin beta interacting protein 1 (Ctnnbip1), mRNA.
St8sia4	ILMN_216048	1,81894	Mus musculus ST8 alpha-N-acetyl-neuraminide alpha-2,8-sialyltransferase 4 (St8sia4), mRNA.
LOC547380	ILMN_329718	1,818633	PREDICTED: Mus musculus similar to castor homolog 1, zinc finger (LOC547380), misc RNA.
Ccl7	ILMN_241619	1,812026	Mus musculus chemokine (C-C motif) ligand 7 (Ccl7), mRNA.
D0H4S114	ILMN_217188	1,811246	Mus musculus DNA segment, human D4S114 (D0H4S114), mRNA.
2410015N17Rik	ILMN_216980	1,810334	Mus musculus RIKEN cDNA 2410015N17 gene (2410015N17Rik), mRNA.
Cdca7	ILMN_216604	1,808675	Mus musculus cell division cycle associated 7 (Cdca7), mRNA.
Clspn	ILMN_212127	1,806656	Mus musculus claspin homolog (Xenopus laevis) (Clspn), mRNA.
Col18a1	ILMN_221410	1,806252	Mus musculus procollagen, type XVIII, alpha 1 (Col18a1), mRNA.
Crem	ILMN_195874	1,804158	
Sox7	ILMN_214899	1,803069	Mus musculus SRY-box containing gene 7 (Sox7), mRNA.
Asb4	ILMN_213440	1,801736	Mus musculus ankyrin repeat and SOCS box-containing protein 4 (Asb4), mRNA.
Tes	ILMN_216487	1,800039	Mus musculus testis derived transcript (Tes), transcript variant 1, mRNA.
Ctsj	ILMN_210401	1,797486	Mus musculus cathepsin J (Ctsj), mRNA.
Igh-6	ILMN_209827	1,793297	
LOC380927	ILMN_197525	1,792376	

Fosl2	ILMN_220185	1,791363	Mus musculus fos-like antigen 2 (Fosl2), mRNA.
LOC100041504	ILMN_311371	1,78983	PREDICTED: Mus musculus similar to beta chemokine Exodus-2 (LOC100041504), mRNA.
2610510J17Rik	ILMN_210821	1,788937	Mus musculus RIKEN cDNA 2610510J17 gene (2610510J17Rik), mRNA.
Ccl21c	ILMN_213793	1,7837	
B430201A12Rik	ILMN_217270	1,783034	PREDICTED: Mus musculus RIKEN cDNA B430201A12 gene (B430201A12Rik), mRNA.
Tpi1	ILMN_186788	1,780298	Mus musculus triosephosphate isomerase 1 (Tpi1), mRNA.
Mad2l1	ILMN_236446	1,777282	Mus musculus MAD2 (mitotic arrest deficient, homolog)-like 1 (yeast) (Mad2l1), mRNA.
Tyms	ILMN_186319	1,777063	Mus musculus thymidylate synthase (Tyms), mRNA.
6430550H21Rik	ILMN_243248	1,774841	Mus musculus RIKEN cDNA 6430550H21 gene (6430550H21Rik), mRNA.
Tyms-ps	ILMN_230689	1,773771	Mus musculus thymidylate synthase, pseudogene (Tyms-ps) on chromosome 10.
Flrt3	ILMN_210479	1,773377	Mus musculus fibronectin leucine rich transmembrane protein 3 (Flrt3), mRNA.
Rpl13a	ILMN_238011	1,771436	Mus musculus ribosomal protein L13a (Rpl13a), mRNA.
Nedd9	ILMN_211969	1,770004	Mus musculus neural precursor cell expressed, developmentally down-regulated gene 9 (Nedd9), mRNA.
E2f3	ILMN_231647	1,769801	Mus musculus E2F transcription factor 3 (E2f3), mRNA.
Srm	ILMN_211754	1,768492	Mus musculus spermidine synthase (Srm), mRNA.
Pa2g4	ILMN_248345	1,765748	Mus musculus proliferation-associated 2G4 (Pa2g4), mRNA.
Plk1	ILMN_215563	1,764969	Mus musculus polo-like kinase 1 (Drosophila) (Plk1), mRNA.
Chaf1b	ILMN_215876	1,761768	Mus musculus chromatin assembly factor 1, subunit B (p60) (Chaf1b), mRNA.
Ednrb	ILMN_208799	1,761024	Mus musculus endothelin receptor type B (Ednrb), mRNA.
Nola2	ILMN_217099	1,758165	Mus musculus nucleolar protein family A, member 2 (Nola2), mRNA.
Rrm1	ILMN_223960	1,752943	
Mybl2	ILMN_212854	1,749548	Mus musculus myeloblastosis oncogene-like 2 (Mybl2), mRNA.
Cenpq	ILMN_223239	1,749382	Mus musculus centromere protein Q (Cenpq), mRNA.
9430028L06Rik	ILMN_226818	1,748862	Mus musculus RIKEN cDNA 9430028L06 gene (9430028L06Rik), mRNA.
Fignl1	ILMN_215790	1,746986	Mus musculus fidgetin-like 1 (Fignl1), mRNA.
Igl-V1	ILMN_214703	1,74529	
Tfrc	ILMN_211824	1,744264	Mus musculus transferrin receptor (Tfrc), mRNA.
Ppa1	ILMN_215557	1,742715	Mus musculus pyrophosphatase (inorganic) 1 (Ppa1), mRNA.
Hmgn2	ILMN_213625	1,742624	Mus musculus high mobility group nucleosomal binding domain 2 (Hmgn2), mRNA.
Kntc1	ILMN_224984	1,742596	Mus musculus kinetochore associated 1 (Kntc1), mRNA.
Sgol2	ILMN_224737	1,741683	Mus musculus shugoshin-like 2 (S. pombe) (Sgol2), mRNA.
Lig1	ILMN_209408	1,741334	Mus musculus ligase I, DNA, ATP-dependent (Lig1), transcript variant 2, mRNA.
Chaf1a	ILMN_219209	1,738889	Mus musculus chromatin assembly factor 1, subunit A (p150) (Chaf1a), mRNA.
Lonrf3	ILMN_245582	1,738413	Mus musculus LON peptidase N-terminal domain and ring finger 3 (Lonrf3), mRNA.
Zwint	ILMN_186201	1,73491	Mus musculus ZW10 interactor (Zwint), mRNA.
Hist1h4a	ILMN_196739	1,734772	Mus musculus histone cluster 1, H4a (Hist1h4a), mRNA.
Timm8a1	ILMN_223570	1,734477	Mus musculus translocase of inner mitochondrial membrane 8 homolog a1 (yeast) (Timm8a1), mRNA.
Mcm2	ILMN_214921	1,729189	Mus musculus minichromosome maintenance deficient 2 mitotin (S. cerevisiae) (Mcm2), mRNA.
Nasp	ILMN_211691	1,728943	Mus musculus nuclear autoantigenic sperm protein (histone-binding) (Nasp), transcript variant 2, mRNA.
LOC632667	ILMN_229024	1,726661	PREDICTED: Mus musculus similar to PNG protein (LOC632667), mRNA.
Pdgfa	ILMN_185165	1,726603	
Adarb1	ILMN_247455	1,726498	Mus musculus adenosine deaminase, RNA-specific, B1 (Adarb1), transcript variant 3, mRNA.
Adamts4	ILMN_214117	1,726064	
Per1	ILMN_221472	1,725626	Mus musculus period homolog 1 (Drosophila) (Per1), mRNA.
Eif4a1	ILMN_211682	1,725266	Mus musculus eukaryotic translation initiation factor 4A1 (Eif4a1), mRNA.
Trp53	ILMN_190062	1,72415	Mus musculus transformation related protein 53 (Trp53), mRNA.
Incenp	ILMN_219004	1,720737	Mus musculus inner centromere protein (Incenp), mRNA.
Psmd8	ILMN_217006	1,716066	Mus musculus proteasome (prosome, macropain) 26S subunit, non-ATPase, 8 (Psmd8), mRNA. XM_001002011
Plau	ILMN_212726	1,714184	Mus musculus plasminogen activator, urokinase (Plau), mRNA.
5530400B01Rik	ILMN_184143	1,713677	
Samsn1	ILMN_231098	1,711544	Mus musculus SAM domain, SH3 domain and nuclear localization signals, 1 (Samsn1), mRNA.
Clspn	ILMN_212127	1,7111	Mus musculus claspin homolog (Xenopus laevis) (Clspn), mRNA.
Sphk1	ILMN_255350	1,711067	Mus musculus sphingosine kinase 1 (Sphk1), transcript variant 1, mRNA.

Tnfaip3	ILMN_187343	1,708158	Mus musculus tumor necrosis factor, alpha-induced protein 3 (Tnfaip3), mRNA.
Cdt1	ILMN_221053	1,708109	Mus musculus chromatin licensing and DNA replication factor 1 (Cdt1), mRNA.
Sntb2	ILMN_203960	1,70787	
Cdkn3	ILMN_244631	1,703884	PREDICTED: Mus musculus cyclin-dependent kinase inhibitor 3, transcript variant 5 (Cdkn3), mRNA.
Ccl7	ILMN_223895	1,701413	
2010204K13Rik	ILMN_202423	1,700025	
Hist1h1c	ILMN_235246	1,699681	Mus musculus histone cluster 1, H1c (Hist1h1c), mRNA.
Dusp16	ILMN_238688	1,699654	Mus musculus dual specificity phosphatase 16 (Dusp16), transcript variant B1, mRNA.
Aste1	ILMN_212823	1,699502	Mus musculus asteroid homolog 1 (Drosophila) (Aste1), mRNA.
Ccnb1	ILMN_215403	1,699363	Mus musculus cyclin B1 (Ccnb1), mRNA.
Bmp1	ILMN_217705	1,697854	Mus musculus bone morphogenetic protein 1 (Bmp1), mRNA.
Srm	ILMN_211754	1,696849	Mus musculus spermidine synthase (Srm), mRNA.
Tuba6	ILMN_191105	1,695869	
Uck2	ILMN_220523	1,69324	Mus musculus uridine-cytidine kinase 2 (Uck2), mRNA.
Tor1aip2	ILMN_213899	1,690293	Mus musculus torsin A interacting protein 2 (Tor1aip2), mRNA.
2610305D13Rik	ILMN_194398	1,689452	
Igh-6	ILMN_209827	1,689321	
Car11	ILMN_210367	1,687999	Mus musculus carbonic anhydrase 11 (Car11), mRNA.
Mtap1b	ILMN_220448	1,687998	Mus musculus microtubule-associated protein 1 B (Mtap1b), mRNA.
Adm	ILMN_216448	1,686872	Mus musculus adrenomedullin (Adm), mRNA.
EG666756	ILMN_324295	1,685553	PREDICTED: Mus musculus predicted gene, EG666756 (EG666756), misc RNA.
LOC100046232	ILMN_310357	1,684541	PREDICTED: Mus musculus similar to NFIL3/E4BP4 transcription factor (LOC100046232), mRNA.
Col6a1	ILMN_208779	1,681953	Mus musculus procollagen, type VI, alpha 1 (Col6a1), mRNA.
Gnl3	ILMN_250637	1,681835	Mus musculus guanine nucleotide binding protein-like 3 (nucleolar) (Gnl3), transcript variant 2, mRNA.
Mcm4	ILMN_218428	1,681763	Mus musculus minichromosome maintenance deficient 4 homolog (S. cerevisiae) (Mcm4), mRNA.
Steap2	ILMN_261623	1,681037	Mus musculus six transmembrane epithelial antigen of prostate 2 (Steap2), mRNA. XM_900299 XM_905527 XM_919398 XM_919422 XM_919426 XM_919434 XM_919444 XM_979606 XM_979649 XM_979723 XM_979751 XM_979777 XM_979804
Lgals1	ILMN_211746	1,677268	
Jmjd3	ILMN_234631	1,674756	Mus musculus jumonji domain containing 3 (Jmjd3), mRNA.
8430403J19Rik	ILMN_202890	1,672247	
Lmnb1	ILMN_220293	1,668613	Mus musculus lamin B1 (Lmnb1), mRNA.
Pabpc1	ILMN_201529	1,668157	Mus musculus poly A binding protein, cytoplasmic 1 (Pabpc1), mRNA.
Trib3	ILMN_184853	1,667189	Mus musculus tribbles homolog 3 (Drosophila) (Trib3), mRNA.
Hmgb2	ILMN_222466	1,664652	Mus musculus high mobility group box 2 (Hmgb2), mRNA.
Emb	ILMN_208803	1,66241	Mus musculus embigin (Emb), mRNA.
BC003236	ILMN_191936	1,661933	
Shmt1	ILMN_188851	1,661913	
Kif15	ILMN_212864	1,661321	Mus musculus kinesin family member 15 (Kif15), mRNA.
D2Ertd750e	ILMN_216759	1,661064	Mus musculus DNA segment, Chr 2, ERATO Doi 750, expressed (D2Ertd750e), mRNA.
Gramd1b	ILMN_258584	1,657623	Mus musculus GRAM domain containing 1B (Gramd1b), mRNA.
Mcm7	ILMN_212527	1,657459	Mus musculus minichromosome maintenance deficient 7 (S. cerevisiae) (Mcm7), mRNA.
Tipin	ILMN_236940	1,657258	Mus musculus timeless interacting protein (Tipin), mRNA.
Erdr1	ILMN_221931	1,656539	Mus musculus erythroid differentiation regulator 1 (Erdr1), mRNA.
Susd4	ILMN_236294	1,654983	Mus musculus sushi domain containing 4 (Susd4), mRNA.
Mid1ip1	ILMN_217229	1,654229	Mus musculus Mid1 interacting protein 1 (gastrulation specific G12-like (zebrafish)) (Mid1ip1), mRNA.
Aurkb	ILMN_244379	1,653717	Mus musculus aurora kinase B (Aurkb), mRNA.
C130032J12Rik	ILMN_222501	1,653144	Mus musculus RIKEN cDNA C130032J12 gene (C130032J12Rik), mRNA.
Mapk6	ILMN_235220	1,651576	Mus musculus mitogen-activated protein kinase 6 (Mapk6), transcript variant 2, mRNA.
3010031K01Rik	ILMN_196193	1,648686	
Prickle3	ILMN_221714	1,648628	Mus musculus prickle homolog 3 (Drosophila) (Prickle3), mRNA.
LOC100044829	ILMN_310045	1,647515	PREDICTED: Mus musculus similar to Fibrillarin, transcript variant 1 (LOC100044829), mRNA.
Phlda3	ILMN_212624	1,646574	Mus musculus pleckstrin homology-like domain, family A, member 3 (Phlda3), mRNA.
Kif23	ILMN_260615	1,644797	Mus musculus kinesin family member 23 (Kif23), mRNA.

3000004C01Rik	ILMN_208849	1,643941	Mus musculus RIKEN cDNA 3000004C01 gene (3000004C01Rik), mRNA.
Zfp703	ILMN_259956	1,643767	PREDICTED: Mus musculus zinc finger protein 703 (Zfp703), mRNA.
Npy	ILMN_219845	1,643404	Mus musculus neuropeptide Y (Npy), mRNA.
E130012A19Rik	ILMN_212728	1,641949	Mus musculus RIKEN cDNA E130012A19 gene (E130012A19Rik), mRNA.
Ckap2	ILMN_217790	1,641018	
Cirh1a	ILMN_220606	1,639609	Mus musculus cirrhosis, autosomal recessive 1A (human) (Cirh1a), mRNA.
Rrp12	ILMN_220883	1,639161	Mus musculus ribosomal RNA processing 12 homolog (S. cerevisiae) (Rrp12), mRNA.
Prmt5	ILMN_257867	1,638493	Mus musculus protein arginine N-methyltransferase 5 (Prmt5), mRNA.
Hrmt1l2	ILMN_216956	1,638398	
LOC100042405	ILMN_332368	1,637669	PREDICTED: Mus musculus similar to high mobility group nucleosomal binding domain 2 (LOC100042405), mRNA.
6430550H21Rik	ILMN_223944	1,637151	
Eno1	ILMN_228029	1,636743	Mus musculus enolase 1, alpha non-neuron (Eno1), mRNA.
C330023M02Rik	ILMN_244240	1,634796	Mus musculus RIKEN cDNA C330023M02 gene (C330023M02Rik), mRNA.
LOC100042777	ILMN_309878	1,63242	PREDICTED: Mus musculus similar to human protein homologous to DROER protein (LOC100042777), mRNA.
LOC230253	ILMN_197814	1,632041	
Hnrpa1	ILMN_213596	1,630955	
Serpina3b	ILMN_211013	1,630226	Mus musculus serine (or cysteine) peptidase inhibitor, clade A, member 3B (Serpina3b), mRNA.
LOC100047934	ILMN_312047	1,630002	PREDICTED: Mus musculus hypothetical protein LOC100047934 (LOC100047934), mRNA.
Timp1	ILMN_242087	1,626785	Mus musculus tissue inhibitor of metalloproteinase 1 (Timp1), transcript variant 2, mRNA.
Ccl21b	ILMN_208956	1,624764	Mus musculus chemokine (C-C motif) ligand 21b (Ccl21b), mRNA.
Dusp4	ILMN_231310	1,623806	Mus musculus dual specificity phosphatase 4 (Dusp4), mRNA.
LOC245892	ILMN_198932	1,622669	
Arhgap18	ILMN_218009	1,622468	Mus musculus Rho GTPase activating protein 18 (Arhgap18), mRNA.
Dusp16	ILMN_232573	1,621963	Mus musculus dual specificity phosphatase 16 (Dusp16), transcript variant A1, mRNA.
Gapdh	ILMN_207562	1,621905	Mus musculus glyceraldehyde-3-phosphate dehydrogenase (Gapdh), mRNA.
C1qbp	ILMN_211748	1,621454	Mus musculus complement component 1, q subcomponent binding protein (C1qbp), nuclear gene encoding mitochondrial protein, mRNA.
Sox11	ILMN_211466	1,621211	
Ncapd2	ILMN_212377	1,619806	Mus musculus non-SMC condensin I complex, subunit D2 (Ncapd2), mRNA.
Gna13	ILMN_222752	1,618245	
Cdc20	ILMN_211070	1,617341	Mus musculus cell division cycle 20 homolog (S. cerevisiae) (Cdc20), mRNA.
Pgm2	ILMN_223984	1,61468	
H2afx	ILMN_208765	1,614619	Mus musculus H2A histone family, member X (H2afx), mRNA.
A430006M23Rik	ILMN_202970	1,61213	
Enpp2	ILMN_247627	1,610934	Mus musculus ectonucleotide pyrophosphatase/phosphodiesterase 2 (Enpp2), mRNA.
Nasp	ILMN_211691	1,610011	
LOC674912	ILMN_246251	1,609732	PREDICTED: Mus musculus similar to melanoma antigen, transcript variant 1 (LOC674912), mRNA.
Rec8	ILMN_217508	1,609136	Mus musculus REC8 homolog (yeast) (Rec8), mRNA.
Bhlhb2	ILMN_211922	1,608958	Mus musculus basic helix-loop-helix domain containing, class B2 (Bhlhb2), mRNA.
Parp1	ILMN_211978	1,607902	Mus musculus poly (ADP-ribose) polymerase family, member 1 (Parp1), mRNA.
Cttnbp2nl	ILMN_252976	1,607384	Mus musculus CTTNBP2 N-terminal like (Cttnbp2nl), mRNA.
Tfrc	ILMN_211824	1,606591	Mus musculus transferrin receptor (Tfrc), mRNA.
Ptpre	ILMN_215063	1,606508	Mus musculus protein tyrosine phosphatase, receptor type, E (Ptpre), mRNA.
Mex3a	ILMN_249418	1,604941	Mus musculus mex3 homolog A (C. elegans) (Mex3a), mRNA.
Cdc6	ILMN_209589	1,604172	Mus musculus cell division cycle 6 homolog (S. cerevisiae) (Cdc6), transcript variant 1, mRNA.
Cd93	ILMN_219342	1,604117	Mus musculus CD93 antigen (Cd93), mRNA.
LOC269251	ILMN_197210	1,601098	
Hist1h4m	ILMN_196725	1,600218	Mus musculus histone cluster 1, H4m (Hist1h4m), mRNA.
Tpx2	ILMN_184135	1,599864	Mus musculus TPX2, microtubule-associated protein homolog (Xenopus laevis) (Tpx2), mRNA.
2410006H16Rik	ILMN_316697	1,599698	PREDICTED: Mus musculus RIKEN cDNA 2410006H16 gene (2410006H16Rik), mRNA.
8430403M15Rik	ILMN_196333	1,599603	
BC027231	ILMN_244646	1,599325	Mus musculus cDNA sequence BC027231 (BC027231), mRNA.
Rfc4	ILMN_211155	1,595562	
Ppp1r10	ILMN_214471	1,595365	Mus musculus protein phosphatase 1, regulatory subunit 10 (Ppp1r10), mRNA.

EG668300	ILMN_259331	1,593346	PREDICTED: Mus musculus predicted gene, EG668300 (EG668300), mRNA.
Myc	ILMN_210055	1,592727	Mus musculus myelocytomatosis oncogene (Myc), mRNA.
LOC380665	ILMN_199085	1,592623	
Ppp1r9a	ILMN_212965	1,591681	Mus musculus protein phosphatase 1, regulatory (inhibitor) subunit 9A (Ppp1r9a), mRNA.
Fabp9	ILMN_220068	1,59073	Mus musculus fatty acid binding protein 9, testis (Fabp9), mRNA.
Parp1	ILMN_211978	1,590391	Mus musculus poly (ADP-ribose) polymerase family, member 1 (Parp1), mRNA.
Slc20a1	ILMN_208778	1,588589	Mus musculus solute carrier family 20, member 1 (Slc20a1), mRNA.
Sbno2	ILMN_213561	1,588434	Mus musculus strawberry notch homolog 2 (Drosophila) (Sbno2), mRNA.
Timp1	ILMN_223823	1,58762	
LOC270589	ILMN_198037	1,58723	
Adamts1	ILMN_241585	1,586602	Mus musculus a disintegrin-like and metallopeptidase (reprolysin type) with thrombospondin type 1 motif, 1 (Adamts1), mRNA.
Pkm2	ILMN_222874	1,586352	Mus musculus pyruvate kinase, muscle (Pkm2), mRNA. XM_979725 XM_979753 XM_979779 XM_979805 XM_979833 XM_979863 XM_979890 XM_979922 XM_979949
E2f2	ILMN_215692	1,58574	Mus musculus E2F transcription factor 2 (E2f2), mRNA.
Nol10	ILMN_238030	1,581572	Mus musculus nucleolar protein 10 (Nol10), mRNA.
Bub1b	ILMN_217683	1,581572	
Asb4	ILMN_213440	1,57999	
Ddx26	ILMN_205973	1,578478	
LOC100041230	ILMN_318359	1,576115	PREDICTED: Mus musculus similar to histone H4 (LOC100041230), mRNA.
Nnmt	ILMN_215936	1,575293	Mus musculus nicotinamide N-methyltransferase (Nnmt), mRNA.
8430408G22Rik	ILMN_218091	1,574935	Mus musculus RIKEN cDNA 8430408G22 gene (8430408G22Rik), mRNA.
LOC672474	ILMN_240395	1,574768	PREDICTED: Mus musculus similar to 60S ribosomal protein L29 (LOC672474), mRNA.
Map4k4	ILMN_223098	1,57471	Mus musculus mitogen-activated protein kinase kinase kinase kinase 4 (Map4k4), mRNA.
LOC668038	ILMN_316510	1,57468	PREDICTED: Mus musculus similar to ribosomal protein (LOC668038), misc RNA.
Csnk1d	ILMN_218794	1,57392	Mus musculus casein kinase 1, delta (Csnk1d), transcript variant 2, mRNA.
Casp4	ILMN_213344	1,573823	Mus musculus caspase 4, apoptosis-related cysteine peptidase (Casp4), mRNA.
Cldn4	ILMN_209388	1,572954	Mus musculus claudin 4 (Cldn4), mRNA.
Rps6ka3	ILMN_221099	1,572802	Mus musculus ribosomal protein S6 kinase polypeptide 3 (Rps6ka3), mRNA.
Pkm2	ILMN_220567	1,572335	
Crem	ILMN_233527	1,572211	Mus musculus cAMP responsive element modulator (Crem), mRNA.
Rps24	ILMN_237874	1,570606	Mus musculus ribosomal protein S24 (Rps24), transcript variant 2, mRNA.
Bach1	ILMN_221891	1,570117	Mus musculus BTB and CNC homology 1 (Bach1), mRNA.
Psmc3ip	ILMN_219061	1,569885	Mus musculus proteasome (prosome, macropain) 26S subunit, ATPase 3, interacting protein (Psmc3ip), mRNA.
Dcakd	ILMN_218673	1,569836	Mus musculus dephospho-CoA kinase domain containing (Dcakd), mRNA.
Suclg2	ILMN_241062	1,568561	Mus musculus succinate-Coenzyme A ligase, GDP-forming, beta subunit (Suclg2), mRNA.
LOC100045677	ILMN_313349	1,568129	PREDICTED: Mus musculus similar to DNA replication licensing factor MCM3 (DNA polymerase alpha holoenzyme-associated protein P1) (P1-MCM3) (LOC100045677), misc RNA.
Tfdp1	ILMN_218135	1,56755	
Dusp4	ILMN_188216	1,566964	
Lck	ILMN_214719	1,566708	Mus musculus lymphocyte protein tyrosine kinase (Lck), mRNA.
Akr1b8	ILMN_218920	1,566649	Mus musculus aldo-keto reductase family 1, member B8 (Akr1b8), mRNA.
Lonrf1	ILMN_228296	1,566617	Mus musculus LON peptidase N-terminal domain and ring finger 1 (Lonrf1), mRNA.
Thoc4	ILMN_211571	1,566207	Mus musculus THO complex 4 (Thoc4), mRNA.
Eif4el3	ILMN_209247	1,566181	
Slc12a2	ILMN_211631	1,565604	Mus musculus solute carrier family 12, member 2 (Slc12a2), mRNA.
Hist1h2bk	ILMN_215120	1,563854	Mus musculus histone cluster 1, H2bk (Hist1h2bk), mRNA.
A930008A22Rik	ILMN_185047	1,56236	
Cdc45l	ILMN_212085	1,561965	Mus musculus cell division cycle 45 homolog (S. cerevisiae)-like (Cdc45l), mRNA.
Lrrc8c	ILMN_223759	1,561595	Mus musculus leucine rich repeat containing 8 family, member C (Lrrc8c), mRNA.
A330021E22Rik	ILMN_212595	1,559276	Mus musculus RIKEN cDNA A330021E22 gene (A330021E22Rik), mRNA.
LOC633945	ILMN_247247	1,558974	PREDICTED: Mus musculus hypothetical LOC633945 (LOC633945), mRNA.
Tmem55b	ILMN_253733	1,558079	Mus musculus transmembrane protein 55b (Tmem55b), mRNA. XM_919952 XM_919965
Zmat3	ILMN_184413	1,556569	Mus musculus zinc finger matrin type 3 (Zmat3), mRNA.
Ccl21c	ILMN_240017	1,556056	Mus musculus chemokine (C-C motif) ligand 21c (leucine) (Ccl21c), mRNA.
Tnip1	ILMN_184343	1,555718	Mus musculus TNFAIP3 interacting protein 1 (Tnip1), mRNA.

LOC433476	ILMN_255769	1,555213	PREDICTED: Mus musculus similar to ribosomal protein L27a (LOC433476), mRNA.
Steap1	ILMN_210027	1,554794	Mus musculus six transmembrane epithelial antigen of the prostate 1 (Steap1), mRNA.
Fndc8	ILMN_243346	1,552406	Mus musculus fibronectin type III domain containing 8 (Fndc8), mRNA.
Rap2a	ILMN_212297	1,551938	Mus musculus RAS related protein 2a (Rap2a), mRNA.
Slc38a2	ILMN_217242	1,551333	Mus musculus solute carrier family 38, member 2 (Slc38a2), mRNA.
Maged2	ILMN_209932	1,549634	Mus musculus melanoma antigen, family D, 2 (Maged2), mRNA.
Sdcbp2	ILMN_217512	1,548391	Mus musculus syndecan binding protein (syntenin) 2 (Sdcbp2), mRNA.
Shroom2	ILMN_196571	1,547532	Mus musculus shroom family member 2 (Shroom2), mRNA.
Eif4a1	ILMN_211682	1,545877	Mus musculus eukaryotic translation initiation factor 4A1 (Eif4a1), mRNA.
Bcl6b	ILMN_212741	1,544725	Mus musculus B-cell CLL/lymphoma 6, member B (Bcl6b), mRNA.
Per2	ILMN_210764	1,543266	Mus musculus period homolog 2 (Drosophila) (Per2), mRNA.
Cct3	ILMN_223467	1,542337	Mus musculus chaperonin subunit 3 (gamma) (Cct3), mRNA.
LOC100048721	ILMN_317796	1,542274	PREDICTED: Mus musculus similar to fibronectin leucine rich transmembrane protein 3, transcript variant 1 (LOC100048721), mRNA.
Pard6g	ILMN_223284	1,541327	Mus musculus par-6 partitioning defective 6 homolog gamma (C. elegans) (Pard6g), mRNA.
Rg9mtd2	ILMN_214434	1,540788	Mus musculus RNA (guanine-9-) methyltransferase domain containing 2 (Rg9mtd2), mRNA.
LOC100040573	ILMN_312264	1,538715	PREDICTED: Mus musculus similar to putative transcription factor ZNF131, transcript variant 1 (LOC100040573), mRNA.
BC006779	ILMN_251332	1,537924	Mus musculus cDNA sequence BC006779 (BC006779), mRNA. XM_001001098 XM_001003843 XM_001003848 XM_001003853 XM_001003857 XM_994341 XM_994355 XM_994381 XM_994398
Nfkbid	ILMN_223090	1,537114	Mus musculus nuclear factor of kappa light polypeptide gene enhancer in B-cells inhibitor, delta (Nfkbid), mRNA.
Spc25	ILMN_219453	1,536722	Mus musculus SPC25, NDC80 kinetochore complex component, homolog (S. cerevisiae) (Spc25), mRNA.
Rbbp6	ILMN_191626	1,536483	
Pgm2	ILMN_225618	1,536276	Mus musculus phosphoglucomutase 2 (Pgm2), mRNA.
Rpl23	ILMN_214598	1,536257	Mus musculus ribosomal protein L23 (Rpl23), mRNA.
Ung	ILMN_188946	1,535436	Mus musculus uracil DNA glycosylase (Ung), transcript variant 2, mRNA.
Serf1	ILMN_212907	1,534509	Mus musculus small EDRK-rich factor 1 (Serf1), mRNA.
Grb10	ILMN_202038	1,532297	
Cxcl13	ILMN_223155	1,531981	
Diap3	ILMN_238102	1,531467	Mus musculus diaphanous homolog 3 (Drosophila) (Diap3), mRNA.
Tnip1	ILMN_184343	1,530628	Mus musculus TNFAIP3 interacting protein 1 (Tnip1), mRNA.
LOC100042970	ILMN_315266	1,52882	PREDICTED: Mus musculus similar to Kifc1 protein (LOC100042970), mRNA.
Ezh2	ILMN_210518	1,528734	Mus musculus enhancer of zeste homolog 2 (Drosophila) (Ezh2), mRNA.
Gata6	ILMN_209474	1,528477	Mus musculus GATA binding protein 6 (Gata6), mRNA.
Uchl3	ILMN_238798	1,527942	Mus musculus ubiquitin carboxyl-terminal esterase L3 (ubiquitin thiolesterase) (Uchl3), mRNA.
Plekhm3	ILMN_255681	1,527905	Mus musculus pleckstrin homology domain containing, family M, member 3 (Plekhm3), mRNA.
Mpp3	ILMN_215702	1,52778	
Eef1b2	ILMN_212511	1,527704	Mus musculus eukaryotic translation elongation factor 1 beta 2 (Eef1b2), mRNA.
Rhoc	ILMN_222425	1,526111	Mus musculus ras homolog gene family, member C (Rhoc), mRNA.
Ldha	ILMN_210192	1,526102	Mus musculus lactate dehydrogenase A (Ldha), mRNA.
Cdk4	ILMN_209396	1,523668	Mus musculus cyclin-dependent kinase 4 (Cdk4), mRNA.
Npm1	ILMN_252426	1,5234	Mus musculus nucleophosmin 1 (Npm1), mRNA.
LOC381230	ILMN_198449	1,519905	
Dusp16	ILMN_238688	1,51972	Mus musculus dual specificity phosphatase 16 (Dusp16), transcript variant B1, mRNA.
Kcnk5	ILMN_218669	1,519662	Mus musculus potassium channel, subfamily K, member 5 (Kcnk5), mRNA.
Tpp2	ILMN_184733	1,51919	Mus musculus tripeptidyl peptidase II (Tpp2), mRNA.
G430005B15Rik	ILMN_207399	1,519106	
Impdh1	ILMN_214886	1,518458	Mus musculus inosine 5'-phosphate dehydrogenase 1 (Impdh1), mRNA.
Camk2n2	ILMN_234856	1,518297	PREDICTED: Mus musculus calcium/calmodulin-dependent protein kinase II inhibitor 2 (Camk2n2), mRNA.
Nasp	ILMN_211691	1,516894	Mus musculus nuclear autoantigenic sperm protein (histone-binding) (Nasp), transcript variant 2, mRNA.
Vars	ILMN_186885	1,516429	Mus musculus valyl-tRNA synthetase (Vars), mRNA.
EG384525	ILMN_234509	1,515572	PREDICTED: Mus musculus predicted gene, EG384525 (EG384525), mRNA.
2010317E24Rik	ILMN_214147	1,514224	
Blm	ILMN_226979	1,514017	Mus musculus Bloom syndrome homolog (human) (Blm), transcript variant 2, mRNA.

Mdm2	ILMN_220130	1,513744	Mus musculus transformed mouse 3T3 cell double minute 2 (Mdm2), mRNA.
EG433923	ILMN_244170	1,511868	Mus musculus predicted gene, EG433923 (EG433923), mRNA.
Col6a1	ILMN_208779	1,511707	Mus musculus procollagen, type VI, alpha 1 (Col6a1), mRNA.
LOC666403	ILMN_319803	1,511695	PREDICTED: Mus musculus similar to ribosomal protein S2 (LOC666403), misc RNA.
Gm889	ILMN_244144	1,51142	Mus musculus gene model 889, (NCBI) (Gm889), mRNA.
Tcf19	ILMN_212294	1,511262	Mus musculus transcription factor 19 (Tcf19), mRNA.
Chmp4b	ILMN_210939	1,510731	Mus musculus chromatin modifying protein 4B (Chmp4b), mRNA.
Nola1	ILMN_222966	1,509843	Mus musculus nucleolar protein family A, member 1 (H/ACA small nucleolar RNPs) (Nola1), mRNA.
Plp2	ILMN_210163	1,509612	Mus musculus proteolipid protein 2 (Plp2), mRNA.
2610305D13Rik	ILMN_230652	1,508322	Mus musculus RIKEN cDNA 2610305D13 gene (2610305D13Rik), mRNA.
Mrps6	ILMN_219726	1,508099	Mus musculus mitochondrial ribosomal protein S6 (Mrps6), nuclear gene encoding mitochondrial protein, mRNA.
Qtrt1	ILMN_219623	1,506697	Mus musculus queuine tRNA-ribosyltransferase 1 (Qtrt1), mRNA.
Mthfd2	ILMN_208674	1,506219	
Tbrg4	ILMN_208825	1,506114	Mus musculus transforming growth factor beta regulated gene 4 (Tbrg4), mRNA.
Hap1	ILMN_216862	1,506087	Mus musculus huntingtin-associated protein 1 (Hap1), mRNA.
Rrm1	ILMN_231868	1,506024	Mus musculus ribonucleotide reductase M1 (Rrm1), mRNA.
1700025G04Rik	ILMN_216343	1,506001	Mus musculus RIKEN cDNA 1700025G04 gene (1700025G04Rik), mRNA.
LOC382061	ILMN_201187	1,505877	
Mad2l1	ILMN_236446	1,504826	Mus musculus MAD2 (mitotic arrest deficient, homolog)-like 1 (yeast) (Mad2l1), mRNA.
LOC278105	ILMN_197080	1,504817	
Plod1	ILMN_217271	1,504793	Mus musculus procollagen-lysine, 2-oxoglutarate 5-dioxygenase 1 (Plod1), mRNA.
F730003H07Rik	ILMN_207130	1,502591	
Abcb1b	ILMN_212008	1,502448	Mus musculus ATP-binding cassette, sub-family B (MDR/TAP), member 1B (Abcb1b), mRNA.
Map3k6	ILMN_223877	1,502185	
Csnk1d	ILMN_218794	1,501818	Mus musculus casein kinase 1, delta (Csnk1d), transcript variant 2, mRNA.
Esco2	ILMN_208759	1,501756	Mus musculus establishment of cohesion 1 homolog 2 (S. cerevisiae) (Esco2), mRNA.
Kctd17	ILMN_245700	1,500079	Mus musculus potassium channel tetramerisation domain containing 17 (Kctd17), mRNA.
Nrarp	ILMN_209560	0,500884	Mus musculus Notch-regulated ankyrin repeat protein (Nrarp), mRNA.
Plxdc1	ILMN_211971	0,500164	Mus musculus plexin domain containing 1 (Plxdc1), mRNA.
Tha1	ILMN_209329	0,498936	Mus musculus threonine aldolase 1 (Tha1), mRNA.
Nrp	ILMN_203001	0,49721	
Tgfbi	ILMN_259309	0,496894	Mus musculus transforming growth factor, beta induced (Tgfbi), mRNA.
Efnb1	ILMN_218638	0,495811	Mus musculus ephrin B1 (Efnb1), mRNA.
Cyp2d22	ILMN_223233	0,49573	Mus musculus cytochrome P450, family 2, subfamily d, polypeptide 22 (Cyp2d22), mRNA.
Lyzs	ILMN_261574	0,494954	Mus musculus lysozyme (Lyzs), mRNA.
Hbb-b1	ILMN_202035	0,494835	
Lhfpl2	ILMN_220383	0,494033	Mus musculus lipoma HMGIC fusion partner-like 2 (Lhfpl2), mRNA.
Il6st	ILMN_247872	0,490684	Mus musculus interleukin 6 signal transducer (Il6st), mRNA.
Amy2-2	ILMN_234838	0,490115	Mus musculus amylase 2-2, pancreatic (Amy2-2), mRNA.
Inmt	ILMN_246327	0,488066	Mus musculus indolethylamine N-methyltransferase (Inmt), mRNA.
Ltbp4	ILMN_208840	0,487549	Mus musculus latent transforming growth factor beta binding protein 4 (Ltbp4), mRNA.
AU021092	ILMN_234071	0,487541	Mus musculus expressed sequence AU021092 (AU021092), mRNA.
Tgfbi	ILMN_259309	0,486783	Mus musculus transforming growth factor, beta induced (Tgfbi), mRNA.
9330175B01Rik	ILMN_184183	0,48303	
db2	ILMN_202115	0,481806	
Angptl6	ILMN_214036	0,48139	
Dmbt1	ILMN_212691	0,478111	
Cd84	ILMN_222783	0,478022	Mus musculus CD84 antigen (Cd84), mRNA.
AU021092	ILMN_234071	0,475182	Mus musculus expressed sequence AU021092 (AU021092), mRNA.
Gpc1	ILMN_244157	0,475055	Mus musculus glypican 1 (Gpc1), mRNA.
Cxcl12	ILMN_215390	0,474925	
Mup2	ILMN_244952	0,47268	Mus musculus major urinary protein 2 (Mup2), transcript variant 1, mRNA.
Mras	ILMN_216920	0,472586	Mus musculus muscle and microspikes RAS (Mras), mRNA.
Tmcc2	ILMN_209160	0,471389	Mus musculus transmembrane and coiled-coil domains 2 (Tmcc2), mRNA.

Mrg1	ILMN_205923	0,471365	
3230402H02Rik	ILMN_202638	0,468732	
OC620807	ILMN_234960	0,466342	Mus musculus novel member of the major urinary protein (Mup) gene family (LOC620807), mRNA.
LOC100041516	ILMN_311457	0,463591	PREDICTED: Mus musculus similar to 4933409K07Rik protein (LOC100041516), misc RNA.
Fbxw17	ILMN_211369	0,462536	Mus musculus F-box and WD-40 domain protein 17 (Fbxw17), mRNA.
Cbfa2t3h	ILMN_231319	0,461507	Mus musculus core-binding factor, runt domain, alpha subunit 2, translocated to, 3 homolog (human) (Cbfa2t3h), mRNA.
Chst2	ILMN_217756	0,457889	Mus musculus carbohydrate sulfotransferase 2 (Chst2), mRNA.
D630040I23Rik	ILMN_193224	0,457818	
Spon2	ILMN_223108	0,45617	Mus musculus spondin 2, extracellular matrix protein (Spon2), mRNA.
Jam2	ILMN_208960	0,454692	Mus musculus junction adhesion molecule 2 (Jam2), mRNA.
D630014A15Rik	ILMN_234807	0,453767	Mus musculus RIKEN cDNA D630014A15 gene (D630014A15Rik), mRNA.
Hpse	ILMN_216095	0,45113	Mus musculus heparanase (Hpse), mRNA.
Wnt9b	ILMN_191238	0,443867	Mus musculus wingless-type MMTV integration site 9B (Wnt9b), mRNA.
Slc40a1	ILMN_222315	0,442656	Mus musculus solute carrier family 40 (iron-regulated transporter), member 1 (Slc40a1), mRNA.
Jam2	ILMN_208960	0,439153	Mus musculus junction adhesion molecule 2 (Jam2), mRNA.
Galntl2	ILMN_258096	0,432429	Mus musculus UDP-N-acetyl-alpha-D-galactosamine:polypeptide N-acetylgalactosaminyltransferase-like 2 (Galntl2), mRNA.
Cdh13	ILMN_228863	0,431088	Mus musculus cadherin 13 (Cdh13), mRNA.
Ltbp4	ILMN_208840	0,430711	Mus musculus latent transforming growth factor beta binding protein 4 (Ltbp4), mRNA.
D630014A15Rik	ILMN_195707	0,429394	
dh13	ILMN_228863	0,428428	Mus musculus cadherin 13 (Cdh13), mRNA.
Slco2b1	ILMN_211808	0,416566	Mus musculus solute carrier organic anion transporter family, member 2b1 (Slco2b1), mRNA.
Cd209b	ILMN_221151	0,408797	Mus musculus CD209b antigen (Cd209b), transcript variant 1, mRNA.
Prelp	ILMN_221743	0,403352	Mus musculus proline arginine-rich end leucine-rich repeat (Prelp), mRNA.
Wnt9b	ILMN_191238	0,402488	Mus musculus wingless-type MMTV integration site 9B (Wnt9b), mRNA.
Cdh13	ILMN_228863	0,402125	Mus musculus cadherin 13 (Cdh13), mRNA.
5430433G21Rik	ILMN_312765	0,390741	PREDICTED: Mus musculus RIKEN cDNA 5430433G21 gene (5430433G21Rik), mRNA.
4632428N05Rik	ILMN_329956	0,388347	Mus musculus RIKEN cDNA 4632428N05 gene (4632428N05Rik), mRNA.
Darc	ILMN_215205	0,386566	Mus musculus Duffy blood group, chemokine receptor (Darc), mRNA.
2310046K01Rik	ILMN_216823	0,384608	Mus musculus RIKEN cDNA 2310046K01 gene (2310046K01Rik), mRNA.
Ddah1	ILMN_195643	0,378474	
Fcna	ILMN_220175	0,375715	Mus musculus ficolin A (Fcna), mRNA.
Ltbp4	ILMN_208840	0,375101	Mus musculus latent transforming growth factor beta binding protein 4 (Ltbp4), mRNA.
LOC331139	ILMN_197795	0,37196	
Jam2	ILMN_208960	0,370257	Mus musculus junction adhesion molecule 2 (Jam2), mRNA.
Galntl2	ILMN_258096	0,35897	Mus musculus UDP-N-acetyl-alpha-D-galactosamine:polypeptide N-acetylgalactosaminyltransferase-like 2 (Galntl2), mRNA.
Reln	ILMN_252319	0,357487	Mus musculus reelin (Reln), mRNA.
Il33	ILMN_213496	0,35178	Mus musculus interleukin 33 (Il33), mRNA.
Nuak1	ILMN_234029	0,332318	Mus musculus NUAK family, SNF1-like kinase, 1 (Nuak1), mRNA.
Vwf	ILMN_195886	0,325375	Mus musculus Von Willebrand factor homolog (Vwf), mRNA.
Vegfc	ILMN_192275	0,303032	Mus musculus vascular endothelial growth factor C (Vegfc), mRNA.
Thsd2	ILMN_221501	0,29159	
Ntn4	ILMN_250922	0,278944	Mus musculus netrin 4 (Ntn4), mRNA.
Bmp4	ILMN_223427	0,275359	Mus musculus bone morphogenetic protein 4 (Bmp4), mRNA.
9330175B01Rik	ILMN_184183	0,263274	
Rspo3	ILMN_221501	0,233446	Mus musculus R-spondin 3 homolog (Xenopus laevis) (Rspo3), mRNA.
Ntn4	ILMN_223838	0,225324	

List of figures and tables

References

Adams, R. H., Alitalo, K., 2007. Molecular regulation of angiogenesis and lymphangiogenesis. Nat Rev Mol Cell Biol. 8**,** 464-78.

Allenspach, E. J., Maillard, I., Aster, J. C., Pear, W. S., 2002. Notch signaling in cancer. Cancer Biol Ther. 1**,** 466-76.

Ando, M., Sasaki, J., Hua, H., Matsunaga, A., Uchida, K., Jou, K., Oikawa, S., Saito, T., Nihei, H., 1999. A novel 18-amino acid deletion in apolipoprotein E associated with lipoprotein glomerulopathy. Kidney Int. 56**,** 1317-23.

Armulik, A., Abramsson, A., Betsholtz, C., 2005. Endothelial/pericyte interactions. Circ Res. 97**,** 512-23.

Artavanis-Tsakonas, S., Delidakis, C., Fehon, R. G., 1991. The Notch locus and the cell biology of neuroblast segregation. Annu Rev Cell Biol. 7**,** 427-52.

Artavanis-Tsakonas, S., Matsuno, K., Fortini, M. E., 1995. Notch signaling. Science. 268**,** 225-32.

Artavanis-Tsakonas, S., Rand, M. D., Lake, R. J., 1999. Notch signaling: cell fate control and signal integration in development. Science. 284**,** 770-6.

Baladron, V., Ruiz-Hidalgo, M. J., Nueda, M. L., Diaz-Guerra, M. J., Garcia-Ramirez, J. J., Bonvini, E., Gubina, E., Laborda, J., 2005. dlk acts as a negative regulator of Notch1 activation through interactions with specific EGF-like repeats. Exp Cell Res. 303**,** 343-59.

Barthel, A., Schmoll, D., Unterman, T. G., 2005. FoxO proteins in insulin action and metabolism. Trends Endocrinol Metab. 16**,** 183-9.

Becam, I., Fiuza, U. M., Arias, A. M., Milan, M., 2010. A role of receptor Notch in ligand cis-inhibition in Drosophila. Curr Biol. 20**,** 554-60.

Benedito, R., Roca, C., Sorensen, I., Adams, S., Gossler, A., Fruttiger, M., Adams, R. H., 2009. The notch ligands Dll4 and Jagged1 have opposing effects on angiogenesis. Cell. 137**,** 1124-35.

Benedito, R., Rocha, S. F., Woeste, M., Zamykal, M., Radtke, F., Casanovas, O., Duarte, A., Pytowski, B., Adams, R. H., 2012. Notch-dependent VEGFR3 upregulation allows angiogenesis without VEGF-VEGFR2 signalling. Nature. 484**,** 110-4.

Benest, A. V., Augustin, H. G., 2009. Tension in the vasculature. Nat Med. 15**,** 608-10.

Bergers, G., Brekken, R., McMahon, G., Vu, T. H., Itoh, T., Tamaki, K., Tanzawa, K., Thorpe, P., Itohara, S., Werb, Z., Hanahan, D., 2000. Matrix metalloproteinase-9 triggers the angiogenic switch during carcinogenesis. Nat Cell Biol. 2**,** 737-44.

Bergers, G., Hanahan, D., 2008. Modes of resistance to anti-angiogenic therapy. Nat Rev Cancer. 8**,** 592-603.

Bergers, G., Song, S., 2005. The role of pericytes in blood-vessel formation and maintenance. Neuro Oncol. 7**,** 452-64.

Bray, S. J., 2006. Notch signalling: a simple pathway becomes complex. Nat Rev Mol Cell Biol. 7**,** 678-89.

Bray, S. J., Takada, S., Harrison, E., Shen, S. C., Ferguson-Smith, A. C., 2008. The atypical mammalian ligand Delta-like homologue 1 (Dlk1) can regulate Notch signalling in Drosophila. BMC Dev Biol. 8**,** 11.

Brutsaert, D. L., 2003. Cardiac endothelial-myocardial signaling: its role in cardiac growth, contractile performance, and rhythmicity. Physiol Rev. 83**,** 59-115.

Burri, P. H., Hlushchuk, R., Djonov, V., 2004. Intussusceptive angiogenesis: its emergence, its characteristics, and its significance. Dev Dyn. 231**,** 474-88.

Carmeliet, P., 2003. Angiogenesis in health and disease. Nat Med. 9**,** 653-60.

Carmeliet, P., Ferreira, V., Breier, G., Pollefeyt, S., Kieckens, L., Gertsenstein, M., Fahrig, M., Vandenhoeck, A., Harpal, K., Eberhardt, C., Declercq, C., Pawling, J., Moons, L., Collen, D., Risau, W., Nagy, A., 1996. Abnormal blood vessel development and lethality in embryos lacking a single VEGF allele. Nature. 380**,** 435-9.

Carmeliet, P., Jain, R. K., 2011. Principles and mechanisms of vessel normalization for cancer and other angiogenic diseases. Nat Rev Drug Discov. 10**,** 417-27.

Chen, S., Lechleider, R. J., 2004. Transforming growth factor-beta-induced differentiation of smooth muscle from a neural crest stem cell line. Circ Res. 94**,** 1195-202.

Chigurupati, S., Arumugam, T. V., Son, T. G., Lathia, J. D., Jameel, S., Mughal, M. R., Tang, S. C., Jo, D. G., Camandola, S., Giunta, M., Rakova, I., McDonnell, N., Miele, L., Mattson, M. P., Poosala, S., 2007. Involvement of notch signaling in wound healing. PLoS One. 2**,** e1167.

Chillakuri, C. R., Sheppard, D., Lea, S. M., Handford, P. A., 2012. Notch receptor-ligand binding and activation: insights from molecular studies. Semin Cell Dev Biol. 23**,** 421-8.

Chung, A. S., Lee, J., Ferrara, N., 2010. Targeting the tumour vasculature: insights from physiological angiogenesis. Nat Rev Cancer. 10**,** 505-14.

Cleaver, O., Melton, D. A., 2003. Endothelial signaling during development. Nat Med. 9**,** 661-8.

Cole, L. K., Dolinsky, V. W., Dyck, J. R., Vance, D. E., 2011. Impaired phosphatidylcholine biosynthesis reduces atherosclerosis and prevents lipotoxic cardiac dysfunction in ApoE-/- Mice. Circ Res. 108**,** 686-94.

Conway, E. M., Collen, D., Carmeliet, P., 2001. Molecular mechanisms of blood vessel growth. Cardiovasc Res. 49**,** 507-21.

Cordle, J., Johnson, S., Tay, J. Z., Roversi, P., Wilkin, M. B., de Madrid, B. H., Shimizu, H., Jensen, S., Whiteman, P., Jin, B., Redfield, C., Baron, M., Lea, S. M., Handford, P. A., 2008. A conserved face of the Jagged/Serrate DSL domain is involved in Notch trans-activation and cis-inhibition. Nat Struct Mol Biol. 15**,** 849-57.

De Smet, F., Segura, I., De Bock, K., Hohensinner, P. J., Carmeliet, P., 2009. Mechanisms of vessel branching: filopodia on endothelial tip cells lead the way. Arterioscler Thromb Vasc Biol. 29**,** 639-49.

Dejana, E., 2010. The role of wnt signaling in physiological and pathological angiogenesis. Circ Res. 107**,** 943-52.

Dejana, E., Tournier-Lasserve, E., Weinstein, B. M., 2009. The control of vascular integrity by endothelial cell junctions: molecular basis and pathological implications. Dev Cell. 16**,** 209-21.

DeLeve, L. D., 2003. Vascular liver diseases. Curr Gastroenterol Rep. 5**,** 63-70.

Dickson, B. C., Mulligan, A. M., Zhang, H., Lockwood, G., O'Malley, F. P., Egan, S. E., Reedijk, M., 2007. High-level JAG1 mRNA and protein predict poor outcome in breast cancer. Mod Pathol. 20**,** 685-93.

Dixelius, J., Makinen, T., Wirzenius, M., Karkkainen, M. J., Wernstedt, C., Alitalo, K., Claesson-Welsh, L., 2003. Ligand-induced vascular endothelial growth factor receptor-3 (VEGFR-3) heterodimerization with VEGFR-2 in primary lymphatic endothelial cells regulates tyrosine phosphorylation sites. J Biol Chem. 278**,** 40973-9.

Dou, G. R., Wang, Y. C., Hu, X. B., Hou, L. H., Wang, C. M., Xu, J. F., Wang, Y. S., Liang, Y. M., Yao, L. B., Yang, A. G., Han, H., 2008. RBP-J, the transcription factor downstream of Notch receptors, is essential for the maintenance of vascular homeostasis in adult mice. FASEB J. 22**,** 1606-17.

Duarte, A., Hirashima, M., Benedito, R., Trindade, A., Diniz, P., Bekman, E., Costa, L., Henrique, D., Rossant, J., 2004. Dosage-sensitive requirement for mouse Dll4 in artery development. Genes Dev. 18**,** 2474-8.

Ebos, J. M., Bocci, G., Man, S., Thorpe, P. E., Hicklin, D. J., Zhou, D., Jia, X., Kerbel, R. S., 2004. A naturally occurring soluble form of vascular endothelial growth factor receptor 2 detected in mouse and human plasma. Mol Cancer Res. 2**,** 315-26.

Egan, S. E., St-Pierre, B., Leow, C. C., 1998. Notch receptors, partners and regulators: from conserved domains to powerful functions. Curr Top Microbiol Immunol. 228**,** 273-324.

Eiraku, M., Tohgo, A., Ono, K., Kaneko, M., Fujishima, K., Hirano, T., Kengaku, M., 2005. DNER acts as a neuron-specific Notch ligand during Bergmann glial development. Nat Neurosci. 8**,** 873-80.

Eklund, L., Olsen, B. R., 2006. Tie receptors and their angiopoietin ligands are context-dependent regulators of vascular remodeling. Exp Cell Res. 312**,** 630-41.

Eldadah, Z. A., Hamosh, A., Biery, N. J., Montgomery, R. A., Duke, M., Elkins, R., Dietz, H. C., 2001. Familial Tetralogy of Fallot caused by mutation in the jagged1 gene. Hum Mol Genet. 10**,** 163-9.

Fang, D., Wang, L., Zhang, D., 2000. [Correlation study of the longest diameter of gastric cardia cancer and its prognosis]. Zhonghua Zhong Liu Za Zhi. 22**,** 161-3.

Felcht, M., Luck, R., Schering, A., Seidel, P., Srivastava, K., Hu, J., Bartol, A., Kienast, Y., Vettel, C., Loos, E. K., Kutschera, S., Bartels, S., Appak, S., Besemfelder, E., Terhardt, D., Chavakis, E., Wieland, T., Klein, C., Thomas, M., Uemura, A., Goerdt, S., Augustin, H. G., 2012. Angiopoietin-2 differentially regulates angiogenesis through TIE2 and integrin signaling. J Clin Invest. 122**,** 1991-2005.

Feng, F., Wang, Y. C., Hu, X. B., Liu, X. W., Ji, G., Chen, Y. R., Wang, L., He, F., Dou, G. R., Liang, L., Zhang, H. W., Han, H., 2010. The transcription factor RBP-J-mediated signaling is essential for dendritic cells to evoke efficient anti-tumor immune responses in mice. Mol Cancer. 9**,** 90.

Fernandez, L. A., Sanz-Rodriguez, F., Blanco, F. J., Bernabeu, C., Botella, L. M., 2006. Hereditary hemorrhagic telangiectasia, a vascular dysplasia affecting the TGF-beta signaling pathway. Clin Med Res. 4**,** 66-78.

Ferrara, N., Carver-Moore, K., Chen, H., Dowd, M., Lu, L., O'Shea, K. S., Powell-Braxton, L., Hillan, K. J., Moore, M. W., 1996. Heterozygous embryonic lethality induced by targeted inactivation of the VEGF gene. Nature. 380**,** 439-42.

Ferrara, N., Gerber, H. P., LeCouter, J., 2003. The biology of VEGF and its receptors. Nat Med. 9**,** 669-76.

Ferrara, N., Keyt, B., 1997. Vascular endothelial growth factor: basic biology and clinical implications. EXS. 79**,** 209-32.

Fischer, A., Gessler, M., 2003. Hey genes in cardiovascular development. Trends Cardiovasc Med. 13**,** 221-6.

Fischer, A., Schumacher, N., Maier, M., Sendtner, M., Gessler, M., 2004. The Notch target genes Hey1 and Hey2 are required for embryonic vascular development. Genes Dev. 18**,** 901-11.

Fitch, M. J., Campagnolo, L., Kuhnert, F., Stuhlmann, H., 2004. Egfl7, a novel epidermal growth factor-domain gene expressed in endothelial cells. Dev Dyn. 230**,** 316-24.

Fleming, R. J., 1998. Structural conservation of Notch receptors and ligands. Semin Cell Dev Biol. 9**,** 599-607.

Folkman, J., Kalluri, R., 2004. Cancer without disease. Nature. 427**,** 787.

Fraisl, P., Baes, M., Carmeliet, P., 2008. Hungry for blood vessels: linking metabolism and angiogenesis. Dev Cell. 14**,** 313-4.

Fulton, D., Gratton, J. P., McCabe, T. J., Fontana, J., Fujio, Y., Walsh, K., Franke, T. F., Papapetropoulos, A., Sessa, W. C., 1999. Regulation of endothelium-derived nitric oxide production by the protein kinase Akt. Nature. 399**,** 597-601.

Funahashi, Y., Hernandez, S. L., Das, I., Ahn, A., Huang, J., Vorontchikhina, M., Sharma, A., Kanamaru, E., Borisenko, V., Desilva, D. M., Suzuki, A., Wang, X., Shawber, C. J., Kandel, J. J., Yamashiro, D. J., Kitajewski, J., 2008. A notch1 ectodomain construct inhibits endothelial notch signaling, tumor growth, and angiogenesis. Cancer Res. 68**,** 4727-35.

Gaengel, K., Genove, G., Armulik, A., Betsholtz, C., 2009. Endothelial-mural cell signaling in vascular development and angiogenesis. Arterioscler Thromb Vasc Biol. 29**,** 630-8.

Gale, N. W., Dominguez, M. G., Noguera, I., Pan, L., Hughes, V., Valenzuela, D. M., Murphy, A. J., Adams, N. C., Lin, H. C., Holash, J., Thurston, G., Yancopoulos, G. D., 2004. Haploinsufficiency of delta-like 4 ligand results in embryonic lethality due to major defects in arterial and vascular development. Proc Natl Acad Sci U S A. 101**,** 15949-54.

Garg, V., Muth, A. N., Ransom, J. F., Schluterman, M. K., Barnes, R., King, I. N., Grossfeld, P. D., Srivastava, D., 2005. Mutations in NOTCH1 cause aortic valve disease. Nature. 437**,** 270-4.

Gerhardt, H., Betsholtz, C., 2003. Endothelial-pericyte interactions in angiogenesis. Cell Tissue Res. 314**,** 15-23.

Gerhardt, H., Golding, M., Fruttiger, M., Ruhrberg, C., Lundkvist, A., Abramsson, A., Jeltsch, M., Mitchell, C., Alitalo, K., Shima, D., Betsholtz, C., 2003. VEGF guides angiogenic sprouting utilizing endothelial tip cell filopodia. J Cell Biol. 161**,** 1163-77.

Gordon, W. R., Arnett, K. L., Blacklow, S. C., 2008. The molecular logic of Notch signaling--a structural and biochemical perspective. J Cell Sci. 121**,** 3109-19.

Greenwald, I., 1998. LIN-12/Notch signaling: lessons from worms and flies. Genes Dev. 12**,** 1751-62.

Greenway, S. C., Pereira, A. C., Lin, J. C., DePalma, S. R., Israel, S. J., Mesquita, S. M., Ergul, E., Conta, J. H., Korn, J. M., McCarroll, S. A., Gorham, J. M., Gabriel, S., Altshuler, D. M., Quintanilla-Dieck Mde, L., Artunduaga, M. A., Eavey, R. D., Plenge, R. M., Shadick, N. A., Weinblatt, M. E., De Jager, P. L., Hafler, D. A., Breitbart, R. E., Seidman, J. G., Seidman, C. E., 2009. De novo copy number variants identify new genes and loci in isolated sporadic tetralogy of Fallot. Nat Genet. 41**,** 931-5.

Gupta, M. K., Qin, R. Y., 2003. Mechanism and its regulation of tumor-induced angiogenesis. World J Gastroenterol. 9**,** 1144-55.

Hagberg, C. E., Falkevall, A., Wang, X., Larsson, E., Huusko, J., Nilsson, I., van Meeteren, L. A., Samen, E., Lu, L., Vanwildemeersch, M., Klar, J., Genove, G., Pietras, K., Stone-Elander, S., Claesson-Welsh, L., Yla-Herttuala, S., Lindahl, P., Eriksson, U., 2010. Vascular endothelial growth factor B controls endothelial fatty acid uptake. Nature. 464**,** 917-21.

Hagberg, C. E., Mehlem, A., Falkevall, A., Muhl, L., Fam, B. C., Ortsater, H., Scotney, P., Nyqvist, D., Samen, E., Lu, L., Stone-Elander, S., Proietto, J., Andrikopoulos, S., Sjoholm, A., Nash, A., Eriksson, U., 2012. Targeting VEGF-B as a novel treatment for insulin resistance and type 2 diabetes. Nature. 490**,** 426-30.

Haines, N., Irvine, K. D., 2003. Glycosylation regulates Notch signalling. Nat Rev Mol Cell Biol. 4**,** 786-97.

Hambleton, S., Valeyev, N. V., Muranyi, A., Knott, V., Werner, J. M., McMichael, A. J., Handford, P. A., Downing, A. K., 2004. Structural and functional properties of the human notch-1 ligand binding region. Structure. 12**,** 2173-83.

Hanahan, D., Folkman, J., 1996. Patterns and emerging mechanisms of the angiogenic switch during tumorigenesis. Cell. 86**,** 353-64.

Harper, J. A., Yuan, J. S., Tan, J. B., Visan, I., Guidos, C. J., 2003. Notch signaling in development and disease. Clin Genet. 64**,** 461-72.

Harrington, L. S., Sainson, R. C., Williams, C. K., Taylor, J. M., Shi, W., Li, J. L., Harris, A. L., 2008. Regulation of multiple angiogenic pathways by Dll4 and Notch in human umbilical vein endothelial cells. Microvasc Res. 75**,** 144-54.

Hashizume, H., Baluk, P., Morikawa, S., McLean, J. W., Thurston, G., Roberge, S., Jain, R. K., McDonald, D. M., 2000. Openings between defective endothelial cells explain tumor vessel leakiness. Am J Pathol. 156**,** 1363-80.

Hellberg, C., Ostman, A., Heldin, C. H., 2010. PDGF and vessel maturation. Recent Results Cancer Res. 180**,** 103-14.

Hellstrom, M., Gerhardt, H., Kalen, M., Li, X., Eriksson, U., Wolburg, H., Betsholtz, C., 2001. Lack of pericytes leads to endothelial hyperplasia and abnormal vascular morphogenesis. J Cell Biol. 153**,** 543-53.

Hellstrom, M., Phng, L. K., Hofmann, J. J., Wallgard, E., Coultas, L., Lindblom, P., Alva, J., Nilsson, A. K., Karlsson, L., Gaiano, N., Yoon, K., Rossant, J., Iruela-Arispe, M. L., Kalen, M., Gerhardt, H., Betsholtz, C., 2007. Dll4 signalling through Notch1 regulates formation of tip cells during angiogenesis. Nature. 445**,** 776-80.

Herbert, S. P., Huisken, J., Kim, T. N., Feldman, M. E., Houseman, B. T., Wang, R. A., Shokat, K. M., Stainier, D. Y., 2009. Arterial-venous segregation by selective cell sprouting: an alternative mode of blood vessel formation. Science. 326**,** 294-8.

Herranz, H., Stamataki, E., Feiguin, F., Milan, M., 2006. Self-refinement of Notch activity through the transmembrane protein Crumbs: modulation of gamma-secretase activity. EMBO Rep. 7**,** 297-302.

Herwig, L., Blum, Y., Krudewig, A., Ellertsdottir, E., Lenard, A., Belting, H. G., Affolter, M., 2011. Distinct cellular mechanisms of blood vessel fusion in the zebrafish embryo. Curr Biol. 21**,** 1942-8.

Hicks, C., Ladi, E., Lindsell, C., Hsieh, J. J., Hayward, S. D., Collazo, A., Weinmaster, G., 2002. A secreted Delta1-Fc fusion protein functions both as an activator and inhibitor of Notch1 signaling. J Neurosci Res. 68**,** 655-67.

Hoeben, A., Landuyt, B., Highley, M. S., Wildiers, H., Van Oosterom, A. T., De Bruijn, E. A., 2004. Vascular endothelial growth factor and angiogenesis. Pharmacol Rev. 56**,** 549-80.

Hofmann, J. J., Iruela-Arispe, M. L., 2007. Notch signaling in blood vessels: who is talking to whom about what? Circ Res. 100**,** 1556-68.

Holmgren, L., O'Reilly, M. S., Folkman, J., 1995. Dormancy of micrometastases: balanced proliferation and apoptosis in the presence of angiogenesis suppression. Nat Med. 1**,** 149-53.

Hrabe de Angelis, M., McIntyre, J., 2nd, Gossler, A., 1997. Maintenance of somite borders in mice requires the Delta homologue DII1. Nature. 386**,** 717-21.

Hu, W., Lu, C., Dong, H. H., Huang, J., Shen, D. Y., Stone, R. L., Nick, A. M., Shahzad, M. M., Mora, E., Jennings, N. B., Lee, S. J., Roh, J. W., Matsuo, K., Nishimura, M., Goodman, B. W., Jaffe, R. B., Langley, R. R., Deavers, M. T., Lopez-Berestein, G., Coleman, R. L., Sood, A. K., 2011. Biological roles of the Delta family Notch ligand Dll4 in tumor and endothelial cells in ovarian cancer. Cancer Res. 71**,** 6030-9.

Hu, X. B., Feng, F., Wang, Y. C., Wang, L., He, F., Dou, G. R., Liang, L., Zhang, H. W., Liang, Y. M., Han, H., 2009. Blockade of Notch signaling in tumor-bearing mice may lead to tumor regression, progression, or metastasis, depending on tumor cell types. Neoplasia. 11**,** 32-8.

Hurlbut, G. D., Kankel, M. W., Lake, R. J., Artavanis-Tsakonas, S., 2007. Crossing paths with Notch in the hyper-network. Curr Opin Cell Biol. 19**,** 166-75.

Imatani, A., Callahan, R., 2000. Identification of a novel NOTCH-4/INT-3 RNA species encoding an activated gene product in certain human tumor cell lines. Oncogene. 19**,** 223-31.

Iso, T., Hamamori, Y., Kedes, L., 2003. Notch signaling in vascular development. Arterioscler Thromb Vasc Biol. 23**,** 543-53.

Jain, R. K., Booth, M. F., 2003. What brings pericytes to tumor vessels? J Clin Invest. 112**,** 1134-6.

Jefferies, J. L., Towbin, J. A., 2010. Dilated cardiomyopathy. Lancet. 375**,** 752-62.

Joutel, A., Corpechot, C., Ducros, A., Vahedi, K., Chabriat, H., Mouton, P., Alamowitch, S., Domenga, V., Cecillion, M., Marechal, E., Maciazek, J., Vayssiere, C., Cruaud, C., Cabanis, E. A., Ruchoux, M. M., Weissenbach, J., Bach, J. F., Bousser, M. G., Tournier-Lasserve, E., 1996. Notch3 mutations in CADASIL, a hereditary adult-onset condition causing stroke and dementia. Nature. 383**,** 707-10.

Jubb, A. M., Soilleux, E. J., Turley, H., Steers, G., Parker, A., Low, I., Blades, J., Li, J. L., Allen, P., Leek, R., Noguera-Troise, I., Gatter, K. C., Thurston, G., Harris, A. L., 2010. Expression of vascular notch ligand delta-like 4 and inflammatory markers in breast cancer. Am J Pathol. 176**,** 2019-28.

Jurkovicova, D., Goncalvesova, E., Sedlakova, B., Hudecova, S., Fabian, J., Krizanova, O., 2006. Is the ApoE polymorphism associated with dilated cardiomyopathy? Gen Physiol Biophys. 25**,** 3-10.

Karavia, E. A., Papachristou, D. J., Kotsikogianni, I., Giopanou, I., Kypreos, K. E., 2011. Deficiency in apolipoprotein E has a protective effect on diet-induced nonalcoholic fatty liver disease in mice. FEBS J. 278**,** 3119-29.

Kashyap, V. S., Santamarina-Fojo, S., Brown, D. R., Parrott, C. L., Applebaum-Bowden, D., Meyn, S., Talley, G., Paigen, B., Maeda, N., Brewer, H. B., Jr., 1995. Apolipoprotein E deficiency in mice: gene replacement and prevention of atherosclerosis using adenovirus vectors. J Clin Invest. 96**,** 1612-20.

Kendall, R. L., Wang, G., Thomas, K. A., 1996. Identification of a natural soluble form of the vascular endothelial growth factor receptor, FLT-1, and its heterodimerization with KDR. Biochem Biophys Res Commun. 226**,** 324-8.

Kerbel, R. S., 2008. Tumor angiogenesis. N Engl J Med. 358**,** 2039-49.

Kidd, S., Kelley, M. R., Young, M. W., 1986. Sequence of the notch locus of Drosophila melanogaster: relationship of the encoded protein to mammalian clotting and growth factors. Mol Cell Biol. 6**,** 3094-108.

Kilarski, W. W., Samolov, B., Petersson, L., Kvanta, A., Gerwins, P., 2009. Biomechanical regulation of blood vessel growth during tissue vascularization. Nat Med. 15**,** 657-64.

Kim, I. M., Wolf, M. J., Rockman, H. A., 2010. Gene deletion screen for cardiomyopathy in adult Drosophila identifies a new notch ligand. Circ Res. 106**,** 1233-43.

Kohler, C., Bell, A. W., Bowen, W. C., Monga, S. P., Fleig, W., Michalopoulos, G. K., 2004. Expression of Notch-1 and its ligand Jagged-1 in rat liver during liver regeneration. Hepatology. 39**,** 1056-65.

Kola, S., Koneti, N. R., Golla, J. P., Akka, J., Gundimeda, S. D., Mundluru, H. P., 2011. Mutational analysis of JAG1 gene in non-syndromic tetralogy of Fallot children. Clin Chim Acta. 412**,** 2232-6.

Koo, B. K., Lim, H. S., Song, R., Yoon, M. J., Yoon, K. J., Moon, J. S., Kim, Y. W., Kwon, M. C., Yoo, K. W., Kong, M. P., Lee, J., Chitnis, A. B., Kim, C. H., Kong, Y. Y., 2005. Mind bomb 1 is essential for generating functional Notch ligands to activate Notch. Development. 132**,** 3459-70.

Kopan, R., Ilagan, M. X., 2009. The canonical Notch signaling pathway: unfolding the activation mechanism. Cell. 137**,** 216-33.

Korff, T., Augustin, H. G., 1998. Integration of endothelial cells in multicellular spheroids prevents apoptosis and induces differentiation. J Cell Biol. 143**,** 1341-52.

Krebs, L. T., Shutter, J. R., Tanigaki, K., Honjo, T., Stark, K. L., Gridley, T., 2004. Haploinsufficient lethality and formation of arteriovenous malformations in Notch pathway mutants. Genes Dev. 18**,** 2469-73.

Krebs, L. T., Xue, Y., Norton, C. R., Shutter, J. R., Maguire, M., Sundberg, J. P., Gallahan, D., Closson, V., Kitajewski, J., Callahan, R., Smith, G. H., Stark, K. L., Gridley, T., 2000. Notch signaling is essential for vascular morphogenesis in mice. Genes Dev. 14**,** 1343-52.

Kuhn, R., Schwenk, F., Aguet, M., Rajewsky, K., 1995. Inducible gene targeting in mice. Science. 269**,** 1427-9.

Kuhnert, F., Kirshner, J. R., Thurston, G., 2011. Dll4-Notch signaling as a therapeutic target in tumor angiogenesis. Vasc Cell. 3**,** 20.

Kurz, H., Gartner, T., Eggli, P. S., Christ, B., 1996. First blood vessels in the avian neural tube are formed by a combination of dorsal angioblast immigration and ventral sprouting of endothelial cells. Dev Biol. 173**,** 133-47.

Lai, E. C., 2002. Keeping a good pathway down: transcriptional repression of Notch pathway target genes by CSL proteins. EMBO Rep. 3**,** 840-5.

Landor, S. K., Mutvei, A. P., Mamaeva, V., Jin, S., Busk, M., Borra, R., Gronroos, T. J., Kronqvist, P., Lendahl, U., Sahlgren, C. M., 2011. Hypo- and hyperactivated Notch signaling induce a glycolytic switch through distinct mechanisms. Proc Natl Acad Sci U S A. 108**,** 18814-9.

Le Caignec, C., Lefevre, M., Schott, J. J., Chaventre, A., Gayet, M., Calais, C., Moisan, J. P., 2002. Familial deafness, congenital heart defects, and posterior embryotoxon caused by cysteine substitution in the first epidermal-growth-factor-like domain of jagged 1. Am J Hum Genet. 71**,** 180-6.

Lei, L., Xu, A., Panin, V. M., Irvine, K. D., 2003. An O-fucose site in the ligand binding domain inhibits Notch activation. Development. 130**,** 6411-21.

Leslie, J. D., Ariza-McNaughton, L., Bermange, A. L., McAdow, R., Johnson, S. L., Lewis, J., 2007. Endothelial signalling by the Notch ligand Delta-like 4 restricts angiogenesis. Development. 134**,** 839-44.

Leuker, C. E., Labow, M., Muller, W., Wagner, N., 2001. Neonatally induced inactivation of the vascular cell adhesion molecule 1 gene impairs B cell localization and T cell-dependent humoral immune response. J Exp Med. 193**,** 755-68.

Li, J. L., Sainson, R. C., Oon, C. E., Turley, H., Leek, R., Sheldon, H., Bridges, E., Shi, W., Snell, C., Bowden, E. T., Wu, H., Chowdhury, P. S., Russell, A. J., Montgomery, C. P., Poulsom, R., Harris, A. L., 2011. DLL4-Notch signaling mediates tumor resistance to anti-VEGF therapy in vivo. Cancer Res. 71**,** 6073-83.

Limbourg, F. P., Takeshita, K., Radtke, F., Bronson, R. T., Chin, M. T., Liao, J. K., 2005. Essential role of endothelial Notch1 in angiogenesis. Circulation. 111**,** 1826-32.

Lin, L., Mernaugh, R., Yi, F., Blum, D., Carbone, D. P., Dang, T. P., 2010. Targeting specific regions of the Notch3 ligand-binding domain induces apoptosis and inhibits tumor growth in lung cancer. Cancer Res. 70**,** 632-8.

Lindahl, P., Johansson, B. R., Leveen, P., Betsholtz, C., 1997. Pericyte loss and microaneurysm formation in PDGF-B-deficient mice. Science. 277**,** 242-5.

Liu, R., Trindade, A., Sun, Z., Kumar, R., Weaver, F. A., Krasnoperov, V., Naga, K., Duarte, A., Gill, P. S., 2012. Inhibition of Notch signaling by Dll4-Fc promotes reperfusion of acutely ischemic tissues. Biochem Biophys Res Commun. 418**,** 173-9.

Liu, Z., Turkoz, A., Jackson, E. N., Corbo, J. C., Engelbach, J. A., Garbow, J. R., Piwnica-Worms, D. R., Kopan, R., 2011. Notch1 loss of heterozygosity causes vascular tumors and lethal hemorrhage in mice. J Clin Invest. 121**,** 800-8.

Lobov, I. B., Renard, R. A., Papadopoulos, N., Gale, N. W., Thurston, G., Yancopoulos, G. D., Wiegand, S. J., 2007. Delta-like ligand 4 (Dll4) is induced by VEGF as a negative regulator of angiogenic sprouting. Proc Natl Acad Sci U S A. 104**,** 3219-24.

Loges, S., Schmidt, T., Carmeliet, P., 2010. Mechanisms of resistance to anti-angiogenic therapy and development of third-generation anti-angiogenic drug candidates. Genes Cancer. 1**,** 12-25.

Lu, X., Le Noble, F., Yuan, L., Jiang, Q., De Lafarge, B., Sugiyama, D., Breant, C., Claes, F., De Smet, F., Thomas, J. L., Autiero, M., Carmeliet, P., Tessier-Lavigne, M., Eichmann, A., 2004. The netrin receptor UNC5B mediates guidance events controlling morphogenesis of the vascular system. Nature. 432**,** 179-86.

Lubarsky, B., Krasnow, M. A., 2003. Tube morphogenesis: making and shaping biological tubes. Cell. 112**,** 19-28.

MacGrogan, D., Nus, M., de la Pompa, J. L., 2010. Notch signaling in cardiac development and disease. Curr Top Dev Biol. 92**,** 333-65.

Mandarino, L. J., Sundarraj, N., Finlayson, J., Hassell, H. R., 1993. Regulation of fibronectin and laminin synthesis by retinal capillary endothelial cells and pericytes in vitro. Exp Eye Res. 57**,** 609-21.

Mazzone, M., Dettori, D., Leite de Oliveira, R., Loges, S., Schmidt, T., Jonckx, B., Tian, Y. M., Lanahan, A. A., Pollard, P., Ruiz de Almodovar, C., De Smet, F., Vinckier, S., Aragones, J., Debackere, K., Luttun, A., Wyns, S., Jordan, B., Pisacane, A., Gallez, B., Lampugnani, M. G., Dejana, E., Simons, M., Ratcliffe, P., Maxwell, P., Carmeliet, P., 2009. Heterozygous deficiency of PHD2 restores tumor oxygenation and inhibits metastasis via endothelial normalization. Cell. 136**,** 839-51.

McCright, B., Gao, X., Shen, L., Lozier, J., Lan, Y., Maguire, M., Herzlinger, D., Weinmaster, G., Jiang, R., Gridley, T., 2001. Defects in development of the kidney, heart and eye vasculature in mice homozygous for a hypomorphic Notch2 mutation. Development. 128**,** 491-502.

McDonald, D. M., Baluk, P., 2002. Significance of blood vessel leakiness in cancer. Cancer Res. 62**,** 5381-5.

McDonald, D. M., Foss, A. J., 2000. Endothelial cells of tumor vessels: abnormal but not absent. Cancer Metastasis Rev. 19**,** 109-20.

Meloty-Kapella, L., Shergill, B., Kuon, J., Botvinick, E., Weinmaster, G., 2012. Notch ligand endocytosis generates mechanical pulling force dependent on dynamin, epsins, and actin. Dev Cell. 22**,** 1299-312.

Meng, H., Zhang, X., Hankenson, K. D., Wang, M. M., 2009. Thrombospondin 2 potentiates notch3/jagged1 signaling. J Biol Chem. 284**,** 7866-74.

Michiels, C., 2003. Endothelial cell functions. J Cell Physiol. 196**,** 430-43.

Miele, L., Osborne, B., 1999. Arbiter of differentiation and death: Notch signaling meets apoptosis. J Cell Physiol. 181**,** 393-409.

Miller, K., Wang, M., Gralow, J., Dickler, M., Cobleigh, M., Perez, E. A., Shenkier, T., Cella, D., Davidson, N. E., 2007. Paclitaxel plus bevacizumab versus paclitaxel alone for metastatic breast cancer. N Engl J Med. 357**,** 2666-76.

Mishra-Gorur, K., Rand, M. D., Perez-Villamil, B., Artavanis-Tsakonas, S., 2002. Down-regulation of Delta by proteolytic processing. J Cell Biol. 159**,** 313-24.

Mizuhara, E., Nakatani, T., Minaki, Y., Sakamoto, Y., Ono, Y., Takai, Y., 2005. MAGI1 recruits Dll1 to cadherin-based adherens junctions and stabilizes it on the cell surface. J Biol Chem. 280**,** 26499-507.

Moghadasian, M. H., McManus, B. M., Nguyen, L. B., Shefer, S., Nadji, M., Godin, D. V., Green, T. J., Hill, J., Yang, Y., Scudamore, C. H., Frohlich, J. J., 2001. Pathophysiology of apolipoprotein E deficiency in mice: relevance to apo E-related disorders in humans. FASEB J. 15**,** 2623-30.

Murakami, M., Nguyen, L. T., Zhuang, Z. W., Moodie, K. L., Carmeliet, P., Stan, R. V., Simons, M., 2008. The FGF system has a key role in regulating vascular integrity. J Clin Invest. 118**,** 3355-66.

Murphy, P. A., Lam, M. T., Wu, X., Kim, T. N., Vartanian, S. M., Bollen, A. W., Carlson, T. R., Wang, R. A., 2008. Endothelial Notch4 signaling induces hallmarks of brain arteriovenous malformations in mice. Proc Natl Acad Sci U S A. 105**,** 10901-6.

Nakahara, J., Aiso, S., Suzuki, N., 2009. Factors that retard remyelination in multiple sclerosis with a focus on TIP30: a novel therapeutic target. Expert Opin Ther Targets. 13**,** 1375-86.

Nakamura, M., Takii, Y., Ito, M., Komori, A., Yokoyama, T., Shimizu-Yoshida, Y., Koyabu, M., Matsuyama, M., Mori, T., Kamihira, T., Daikoku, M., Migita, K., Yatsuhashi, H., Nozaki, N., Shimoda, S., Ishibashi, H., 2006. Increased expression of nuclear envelope gp210 antigen in small bile ducts in primary biliary cirrhosis. J Autoimmun. 26**,** 138-45.

Nakhai, H., Siveke, J. T., Klein, B., Mendoza-Torres, L., Mazur, P. K., Algul, H., Radtke, F., Strobl, L., Zimber-Strobl, U., Schmid, R. M., 2008. Conditional ablation of Notch signaling in pancreatic development. Development. 135**,** 2757-65.

Nichols, J. T., Miyamoto, A., Olsen, S. L., D'Souza, B., Yao, C., Weinmaster, G., 2007. DSL ligand endocytosis physically dissociates Notch1 heterodimers before activating proteolysis can occur. J Cell Biol. 176**,** 445-58.

Nickoloff, B. J., 1991. The cytokine network in psoriasis. Arch Dermatol. 127**,** 871-84.

Nicolas, M., Wolfer, A., Raj, K., Kummer, J. A., Mill, P., van Noort, M., Hui, C. C., Clevers, H., Dotto, G. P., Radtke, F., 2003. Notch1 functions as a tumor suppressor in mouse skin. Nat Genet. 33**,** 416-21.

Niessen, K., Karsan, A., 2008. Notch signaling in cardiac development. Circ Res. 102**,** 1169-81.

Nofziger, D., Miyamoto, A., Lyons, K. M., Weinmaster, G., 1999. Notch signaling imposes two distinct blocks in the differentiation of C2C12 myoblasts. Development. 126**,** 1689-702.

Noguera-Troise, I., Daly, C., Papadopoulos, N. J., Coetzee, S., Boland, P., Gale, N. W., Lin, H. C., Yancopoulos, G. D., Thurston, G., 2006. Blockade of Dll4 inhibits tumour growth by promoting non-productive angiogenesis. Nature. 444**,** 1032-7.

North, P. E., Waner, M., Mizeracki, A., Mihm, M. C., Jr., 2000. GLUT1: a newly discovered immunohistochemical marker for juvenile hemangiomas. Hum Pathol. 31**,** 11-22.

Nueda, M. L., Baladron, V., Sanchez-Solana, B., Ballesteros, M. A., Laborda, J., 2007. The EGF-like protein dlk1 inhibits notch signaling and potentiates adipogenesis of mesenchymal cells. J Mol Biol. 367**,** 1281-93.

Orlandi, F., Barucca, A., Biagini, G., Pasqui, G., Mottolese, M., Botti, C., Bracalenti, C., Cardarelli, M. A., Concetti, A., Venanzi, F. M., 2002. Molecular stability of DNA typing short tandem repeats in the mammary tree of patients with breast cancer. Diagn Mol Pathol. 11**,** 41-6.

Ozhan, H., Okcun, B., Akdemir, R., 2004. Constrictive pericarditis associated with right atrial and major venous thrombosis. Acta Cardiol. 59**,** 435-7.

Paik, J. H., Kollipara, R., Chu, G., Ji, H., Xiao, Y., Ding, Z., Miao, L., Tothova, Z., Horner, J. W., Carrasco, D. R., Jiang, S., Gilliland, D. G., Chin, L., Wong, W. H., Castrillon, D. H., DePinho, R. A., 2007. FoxOs are lineage-restricted redundant tumor suppressors and regulate endothelial cell homeostasis. Cell. 128**,** 309-23.

Pajvani, U. B., Shawber, C. J., Samuel, V. T., Birkenfeld, A. L., Shulman, G. I., Kitajewski, J., Accili, D., 2011. Inhibition of Notch signaling ameliorates insulin resistance in a FoxO1-dependent manner. Nat Med. 17**,** 961-7.

Parker, L. H., Schmidt, M., Jin, S. W., Gray, A. M., Beis, D., Pham, T., Frantz, G., Palmieri, S., Hillan, K., Stainier, D. Y., De Sauvage, F. J., Ye, W., 2004. The endothelial-cell-derived secreted factor Egfl7 regulates vascular tube formation. Nature. 428**,** 754-8.

Parks, A. L., Klueg, K. M., Stout, J. R., Muskavitch, M. A., 2000. Ligand endocytosis drives receptor dissociation and activation in the Notch pathway. Development. 127**,** 1373-85.

Patel, N. S., Dobbie, M. S., Rochester, M., Steers, G., Poulsom, R., Le Monnier, K., Cranston, D. W., Li, J. L., Harris, A. L., 2006. Up-regulation of endothelial delta-like 4 expression correlates with vessel maturation in bladder cancer. Clin Cancer Res. 12**,** 4836-44.

Penton, A. L., Leonard, L. D., Spinner, N. B., 2012. Notch signaling in human development and disease. Semin Cell Dev Biol. 23**,** 450-7.

Phng, L. K., Gerhardt, H., 2009. Angiogenesis: a team effort coordinated by notch. Dev Cell. 16**,** 196-208.

Piedrahita, J. A., Zhang, S. H., Hagaman, J. R., Oliver, P. M., Maeda, N., 1992. Generation of mice carrying a mutant apolipoprotein E gene inactivated by gene targeting in embryonic stem cells. Proc Natl Acad Sci U S A. 89**,** 4471-5.

Popov, D., Simionescu, M., 2006. Cellular mechanisms and signalling pathways activated by high glucose and AGE-albumin in the aortic endothelium. Arch Physiol Biochem. 112**,** 265-73.

Potente, M., Urbich, C., Sasaki, K., Hofmann, W. K., Heeschen, C., Aicher, A., Kollipara, R., DePinho, R. A., Zeiher, A. M., Dimmeler, S., 2005. Involvement of Foxo transcription factors in angiogenesis and postnatal neovascularization. J Clin Invest. 115**,** 2382-92.

Qi, H., Rand, M. D., Wu, X., Sestan, N., Wang, W., Rakic, P., Xu, T., Artavanis-Tsakonas, S., 1999. Processing of the notch ligand delta by the metalloprotease Kuzbanian. Science. 283**,** 91-4.

Rebay, I., Fleming, R. J., Fehon, R. G., Cherbas, L., Cherbas, P., Artavanis-Tsakonas, S., 1991. Specific EGF repeats of Notch mediate interactions with Delta and Serrate: implications for Notch as a multifunctional receptor. Cell. 67**,** 687-99.

Ridgway, J., Zhang, G., Wu, Y., Stawicki, S., Liang, W. C., Chanthery, Y., Kowalski, J., Watts, R. J., Callahan, C., Kasman, I., Singh, M., Chien, M., Tan, C., Hongo, J. A., de Sauvage, F., Plowman, G., Yan, M., 2006. Inhibition of Dll4 signalling inhibits tumour growth by deregulating angiogenesis. Nature. 444**,** 1083-7.

Risau, W., 1997. Mechanisms of angiogenesis. Nature. 386**,** 671-4.

Roca, C., Adams, R. H., 2007. Regulation of vascular morphogenesis by Notch signaling. Genes Dev. 21**,** 2511-24.

Roodhart, J. M., Langenberg, M. H., Witteveen, E., Voest, E. E., 2008. The molecular basis of class side effects due to treatment with inhibitors of the VEGF/VEGFR pathway. Curr Clin Pharmacol. 3**,** 132-43.

Rosen, E. D., MacDougald, O. A., 2006. Adipocyte differentiation from the inside out. Nat Rev Mol Cell Biol. 7**,** 885-96.

Rucker, H. K., Wynder, H. J., Thomas, W. E., 2000. Cellular mechanisms of CNS pericytes. Brain Res Bull. 51**,** 363-9.

Ruhrberg, C., De Palma, M., 2010. A double agent in cancer: deciphering macrophage roles in human tumors. Nat Med. 16**,** 861-2.

Sainson, R. C., Harris, A. L., 2007. Anti-Dll4 therapy: can we block tumour growth by increasing angiogenesis? Trends Mol Med. 13**,** 389-95.

Salfeld, J. G., 2007. Isotype selection in antibody engineering. Nat Biotechnol. 25**,** 1369-72.

Sawamiphak, S., Seidel, S., Essmann, C. L., Wilkinson, G. A., Pitulescu, M. E., Acker, T., Acker-Palmer, A., 2010. Ephrin-B2 regulates VEGFR2 function in developmental and tumour angiogenesis. Nature. 465**,** 487-91.

Schaper, W., 2009. Collateral circulation: past and present. Basic Res Cardiol. 104**,** 5-21.

Segarra, M., Williams, C. K., Sierra Mde, L., Bernardo, M., McCormick, P. J., Maric, D., Regino, C., Choyke, P., Tosato, G., 2008. Dll4 activation of Notch signaling reduces tumor vascularity and inhibits tumor growth. Blood. 112**,** 1904-11.

Semenza, G. L., 2008. A new weapon for attacking tumor blood vessels. N Engl J Med. 358**,** 2066-7.

Seo, S., Fujita, H., Nakano, A., Kang, M., Duarte, A., Kume, T., 2006. The forkhead transcription factors, Foxc1 and Foxc2, are required for arterial specification and lymphatic sprouting during vascular development. Dev Biol. 294**,** 458-70.

Shutter, J. R., Scully, S., Fan, W., Richards, W. G., Kitajewski, J., Deblandre, G. A., Kintner, C. R., Stark, K. L., 2000. Dll4, a novel Notch ligand expressed in arterial endothelium. Genes Dev. 14**,** 1313-8.

Simpson, M. A., Irving, M. D., Asilmaz, E., Gray, M. J., Dafou, D., Elmslie, F. V., Mansour, S., Holder, S. E., Brain, C. E., Burton, B. K., Kim, K. H., Pauli, R. M., Aftimos, S., Stewart, H., Kim, C. A., Holder-Espinasse, M., Robertson, S. P., Drake, W. M., Trembath, R. C., 2011. Mutations in NOTCH2 cause Hajdu-Cheney syndrome, a disorder of severe and progressive bone loss. Nat Genet. 43**,** 303-5.

Song, R., Koo, B. K., Yoon, K. J., Yoon, M. J., Yoo, K. W., Kim, H. T., Oh, H. J., Kim, Y. Y., Han, J. K., Kim, C. H., Kong, Y. Y., 2006. Neuralized-2 regulates a Notch ligand in cooperation with Mind bomb-1. J Biol Chem. 281**,** 36391-400.

Sorensen, I., Adams, R. H., Gossler, A., 2009. DLL1-mediated Notch activation regulates endothelial identity in mouse fetal arteries. Blood. 113**,** 5680-8.

Staal, F. J., Langerak, A. W., 2008. Signaling pathways involved in the development of T-cell acute lymphoblastic leukemia. Haematologica. 93**,** 493-7.

Strilic, B., Kucera, T., Eglinger, J., Hughes, M. R., McNagny, K. M., Tsukita, S., Dejana, E., Ferrara, N., Lammert, E., 2009. The molecular basis of vascular lumen formation in the developing mouse aorta. Dev Cell. 17**,** 505-15.

Suchting, S., Freitas, C., le Noble, F., Benedito, R., Breant, C., Duarte, A., Eichmann, A., 2007. The Notch ligand Delta-like 4 negatively regulates endothelial tip cell formation and vessel branching. Proc Natl Acad Sci U S A. 104**,** 3225-30.

Sun, X., Artavanis-Tsakonas, S., 1997. Secreted forms of DELTA and SERRATE define antagonists of Notch signaling in Drosophila. Development. 124**,** 3439-48.

Swift, M. R., Weinstein, B. M., 2009. Arterial-venous specification during development. Circ Res. 104**,** 576-88.

Tamura, K., Taniguchi, Y., Minoguchi, S., Sakai, T., Tun, T., Furukawa, T., Honjo, T., 1995. Physical interaction between a novel domain of the receptor Notch and the transcription factor RBP-J kappa/Su(H). Curr Biol. 5**,** 1416-23.

Tanimizu, N., Miyajima, A., 2004. Notch signaling controls hepatoblast differentiation by altering the expression of liver-enriched transcription factors. J Cell Sci. 117**,** 3165-74.

Thelu, J., Rossio, P., Favier, B., 2002. Notch signalling is linked to epidermal cell differentiation level in basal cell carcinoma, psoriasis and wound healing. BMC Dermatol. 2**,** 7.

Thurston, G., 2003. Role of Angiopoietins and Tie receptor tyrosine kinases in angiogenesis and lymphangiogenesis. Cell Tissue Res. 314**,** 61-8.

Torres-Vazquez, J., Kamei, M., Weinstein, B. M., 2003. Molecular distinction between arteries and veins. Cell Tissue Res. 314**,** 43-59.

Urs, S., Roudabush, A., O'Neill, C. F., Pinz, I., Prudovsky, I., Kacer, D., Tang, Y., Liaw, L., Small, D., 2008. Soluble forms of the Notch ligands Delta1 and Jagged1 promote in vivo tumorigenicity in NIH3T3 fibroblasts with distinct phenotypes. Am J Pathol. 173**,** 865-78.

Uyttendaele, H., Ho, J., Rossant, J., Kitajewski, J., 2001. Vascular patterning defects associated with expression of activated Notch4 in embryonic endothelium. Proc Natl Acad Sci U S A. 98**,** 5643-8.

Varnum-Finney, B., Purton, L. E., Yu, M., Brashem-Stein, C., Flowers, D., Staats, S., Moore, K. A., Le Roux, I., Mann, R., Gray, G., Artavanis-Tsakonas, S., Bernstein, I. D., 1998. The Notch ligand, Jagged-1, influences the development of primitive hematopoietic precursor cells. Blood. 91**,** 4084-91.

Vollrath, B., Pudney, J., Asa, S., Leder, P., Fitzgerald, K., 2001. Isolation of a murine homologue of the Drosophila neuralized gene, a gene required for axonemal integrity in spermatozoa and terminal maturation of the mammary gland. Mol Cell Biol. 21**,** 7481-94.

Wang, L., Wang, C. M., Hou, L. H., Dou, G. R., Wang, Y. C., Hu, X. B., He, F., Feng, F., Zhang, H. W., Liang, Y. M., Dou, K. F., Han, H., 2009a. Disruption of the transcription factor recombination signal-binding protein-Jkappa (RBP-J) leads to veno-occlusive disease and interfered liver regeneration in mice. Hepatology. 49**,** 268-77.

Wang, L., Wang, Y. C., Hu, X. B., Zhang, B. F., Dou, G. R., He, F., Gao, F., Feng, F., Liang, Y. M., Dou, K. F., Han, H., 2009b. Notch-RBP-J signaling regulates the mobilization and function of endothelial progenitor cells by dynamic modulation of CXCR4 expression in mice. PLoS One. 4**,** e7572.

Weijzen, S., Velders, M. P., Elmishad, A. G., Bacon, P. E., Panella, J. R., Nickoloff, B. J., Miele, L., Kast, W. M., 2002. The Notch ligand Jagged-1 is able to induce maturation of monocyte-derived human dendritic cells. J Immunol. 169**,** 4273-8.

Weis, S. M., Cheresh, D. A., 2011. alphav Integrins in Angiogenesis and Cancer. Cold Spring Harb Perspect Med. 1**,** a006478.

Weng, A. P., Ferrando, A. A., Lee, W., Morris, J. P. t., Silverman, L. B., Sanchez-Irizarry, C., Blacklow, S. C., Look, A. T., Aster, J. C., 2004. Activating mutations of NOTCH1 in human T cell acute lymphoblastic leukemia. Science. 306**,** 269-71.

Wharton, K. A., Johansen, K. M., Xu, T., Artavanis-Tsakonas, S., 1985. Nucleotide sequence from the neurogenic locus notch implies a gene product that shares homology with proteins containing EGF-like repeats. Cell. 43**,** 567-81.

Xie, G., Zhang, H., Du, G., Huang, Q., Liang, X., Ma, J., Jiao, R., 2012. Uif, a large transmembrane protein with EGF-like repeats, can antagonize Notch signaling in Drosophila. PLoS One. 7**,** e36362.

Xue, Y., Gao, X., Lindsell, C. E., Norton, C. R., Chang, B., Hicks, C., Gendron-Maguire, M., Rand, E. B., Weinmaster, G., Gridley, T., 1999. Embryonic lethality and vascular defects in mice lacking the Notch ligand Jagged1. Hum Mol Genet. 8**,** 723-30.

Yaffe, D., Saxel, O., 1977. Serial passaging and differentiation of myogenic cells isolated from dystrophic mouse muscle. Nature. 270**,** 725-7.

Yan, M., Callahan, C. A., Beyer, J. C., Allamneni, K. P., Zhang, G., Ridgway, J. B., Niessen, K., Plowman, G. D., 2010. Chronic DLL4 blockade induces vascular neoplasms. Nature. 463**,** E6-7.

Yancopoulos, G. D., Davis, S., Gale, N. W., Rudge, J. S., Wiegand, S. J., Holash, J., 2000. Vascular-specific growth factors and blood vessel formation. Nature. 407**,** 242-8.

Yang, Y., Ahn, Y. H., Gibbons, D. L., Zang, Y., Lin, W., Thilaganathan, N., Alvarez, C. A., Moreira, D. C., Creighton, C. J., Gregory, P. A., Goodall, G. J., Kurie, J. M., 2011. The Notch ligand Jagged2 promotes lung adenocarcinoma metastasis through a miR-200-dependent pathway in mice. J Clin Invest. 121**,** 1373-85.

Yang, Z., Stratton, C., Francis, P. J., Kleinman, M. E., Tan, P. L., Gibbs, D., Tong, Z., Chen, H., Constantine, R., Yang, X., Chen, Y., Zeng, J., Davey, L., Ma, X., Hau, V. S., Wang, C., Harmon, J., Buehler, J., Pearson, E., Patel, S., Kaminoh, Y., Watkins, S., Luo, L., Zabriskie, N. A., Bernstein, P. S., Cho, W., Schwager, A., Hinton, D. R., Klein, M. L., Hamon, S. C., Simmons, E., Yu, B., Campochiaro, B., Sunness, J. S., Campochiaro, P., Jorde, L., Parmigiani, G., Zack, D. J., Katsanis, N., Ambati, J., Zhang, K., 2008. Toll-like receptor 3 and geographic atrophy in age-related macular degeneration. N Engl J Med. 359**,** 1456-63.

You, L. R., Lin, F. J., Lee, C. T., DeMayo, F. J., Tsai, M. J., Tsai, S. Y., 2005. Suppression of Notch signalling by the COUP-TFII transcription factor regulates vein identity. Nature. 435**,** 98-104.

Zeng, Q., Li, S., Chepeha, D. B., Giordano, T. J., Li, J., Zhang, H., Polverini, P. J., Nor, J., Kitajewski, J., Wang, C. Y., 2005. Crosstalk between tumor and endothelial cells promotes tumor angiogenesis by MAPK activation of Notch signaling. Cancer Cell. 8**,** 13-23.

Zhang, J. P., Qin, H. Y., Wang, L., Liang, L., Zhao, X. C., Cai, W. X., Wei, Y. N., Wang, C. M., Han, H., 2011. Overexpression of Notch ligand Dll1 in B16 melanoma cells leads to reduced tumor growth due to attenuated vascularization. Cancer Lett. 309**,** 220-7.

Zhang, S. H., Reddick, R. L., Piedrahita, J. A., Maeda, N., 1992. Spontaneous hypercholesterolemia and arterial lesions in mice lacking apolipoprotein E. Science. 258**,** 468-71.

Zhong, T. P., Childs, S., Leu, J. P., Fishman, M. C., 2001. Gridlock signalling pathway fashions the first embryonic artery. Nature. 414**,** 216-20.

ZhuGe, Q., Zhong, M., Zheng, W., Yang, G. Y., Mao, X., Xie, L., Chen, G., Chen, Y., Lawton, M. T., Young, W. L., Greenberg, D. A., Jin, K., 2009. Notch-1 signalling is activated in brain arteriovenous malformations in humans. Brain. 132**,** 3231-41.